



**HAL**  
open science

# Kinetic models, from Kuramoto to Vlasov : bifurcations and experimental analysis of a magneto-optical trap

David Métivier

► **To cite this version:**

David Métivier. Kinetic models, from Kuramoto to Vlasov : bifurcations and experimental analysis of a magneto-optical trap. Other [cond-mat.other]. COMUE Université Côte d'Azur (2015 - 2019), 2017. English. NNT : 2017AZUR4074 . tel-01677847

**HAL Id: tel-01677847**

**<https://theses.hal.science/tel-01677847>**

Submitted on 8 Jan 2018

**HAL** is a multi-disciplinary open access archive for the deposit and dissemination of scientific research documents, whether they are published or not. The documents may come from teaching and research institutions in France or abroad, or from public or private research centers.

L'archive ouverte pluridisciplinaire **HAL**, est destinée au dépôt et à la diffusion de documents scientifiques de niveau recherche, publiés ou non, émanant des établissements d'enseignement et de recherche français ou étrangers, des laboratoires publics ou privés.



# THÈSE DE DOCTORAT

Présentée en vue de l'obtention du grade de

**Docteur en Physique**

d'Université Côte d'Azur

par

David Métivier

---

**MODÈLES CINÉTIQUES, DE KURAMOTO À VLASOV :  
BIFURCATIONS ET ANALYSE EXPÉRIMENTALE D'UN PIÈGE  
MAGNÉTO-OPTIQUE**

**KINETIC MODELS, FROM KURAMOTO TO VLASOV:  
BIFURCATIONS AND EXPERIMENTAL ANALYSIS OF A  
MAGNETO-OPTICAL TRAP**

---

Dirigée par Julien Barré

Soutenue le 22 Septembre 2017

Devant le jury composé de :

---

Bastien Fernandez	DR CNRS, Laboratoire de Probabilités et Modèles	<i>Rapporteur</i>
Philip J. Morrison	Professeur, The University of Texas at Austin	<i>Rapporteur</i>
Médéric Argentina	Professeur, Université Côte d'Azur	<i>Examineur</i>
Caroline Champenois	CR CNRS, Laboratoire PIIM	<i>Examinatrice</i>
Alessandro Torcini	Professeur, Université de Cergy-Pontoise	<i>Examineur</i>
Pascal Viot	Professeur, Université Pierre et Marie Curie	<i>Examineur</i>
Julien Barré	Maitre de Conférence HDR, Université d'Orléans	<i>Directeur</i>

---



*Pour mon Papa*



---

# REMERCIEMENTS

---

Ici commence la déferlante de mercis, néanmoins tout est authentique, sans ces gens ou moments les choses auraient été différentes.

C'est avec plein de joie et de sincérité que je remercie Julien qui depuis le début de mon stage de M2 n'a eu de cesse de montrer patience et enthousiasme et ce jusqu'à l'heure où j'écris ces lignes. Ses conseils avisés et francs m'ont permis d'en arriver là où je suis (c'est-à-dire en fin de thèse). Son encadrement a été super, sa réactivité à toute heure a permis d'effacer la distance. Je crois pouvoir dire qu'il m'a transmis sa passion pour le sujet. Je pense qu'il aurait été difficile d'en trouver un qui me convienne mieux. Je dois au passage remercier Thierry Dauxois qui m'a conseillé d'aller à Nice (c'est aussi lui qui m'avait conseillé mon inoubliable stage de M1) après que je lui ai simplement dit « système autogravitant » (parce que je trouvais que ça sonnait bien). Donc Julien, merci et encore merci !

Je dois évidemment saluer tout le personnel administratif du laboratoire Dieudonné en particulier Jean-Marc et Roland qui m'ont sorti de toutes mes galères numériques ; ainsi que Jean-Louis et les secrétaires qui m'ont aidé à tout moments Angélique, Clara, Julia.

J'ai eu la chance de collaborer avec Guillaume et Robin de l'INLN, je les remercie pour leur patience et pour avoir accepté cette collaboration. Thanks to Yoshi for his comments and ideas always relevant ! Many thanks to Michael always ready to help and for organizing the amazing Trieste conference. I am thankful to T. Rocha for providing his excellent GPU Vlasov-HMF solver.

I would like to thank sincerely every member of my Jury for taking the time to read my work and for their precious advices and suggestions.

Merci aussi à Bruno pour m'avoir initié à CUDA sans qui tout aurait été plus long ! Merci à Shamik pour m'avoir accueilli à Dresde et ensuite m'avoir suggéré de regarder Kuramoto avec retard !

Bien sûr je remercie tous les occupants du bureau 809 : un merci à Bienvenu et Jacques pour leurs nombreuses histoires ; merci à Samira et Ludovick pour m'avoir raconté la saison 3 de Watatatow et d'avoir su travailler la carotte. Merci à Luis pour avoir été toujours jovial et prêt à aider, pour son manoir et tous ses précieux tricks. Merci aussi à Simon qui m'a initié à Python et qui m'a aidé à faire les jolies vidéos ! Merci à Marouane pour sa disponibilité. Merci à Jason, Alyson, Seann, Tara pour avoir été derrière moi tout au long de ces trois ans.

Merci à Pavel pour m'avoir bien facilité la tâche d'enseignement. Merci à Alain Olivetti qui

---

m'avait judicieusement conseillé Julien et à qui j'ai pris ce modèle de thèse ma foi fort bien fait. Merci à David C. d'avoir pris le temps de réfléchir à mes petits problèmes de maths ! Je remercie aussi André pour son éternelle curiosité et son enthousiasme.

Merci à tous les autres doctorants du laboratoire qui ont vraiment contribué à une ambiance géniale ; Charles pour les discussions et m'avoir aidé à trouver mon homonyme ! Merci à Rinel pour les discussions à pas d'heure. Merci aussi à Marcella (pour ton aide), Julie, Arthur, Victor, Bjorn, Giulia et tous les autres, partis ou présents, au GDR goûter ! Merci aussi à Zhiyan. Merci à Reine de m'avoir aidé à répéter MT180s. Je salue aussi les doctorants de l'INLN. Merci à Fernando et tous les Patitos d'avoir toujours été au laboratoire et de m'avoir écouté et fait répéter. Merci à Fernanda pour les bons moments des conférences et pour m'avoir aidé à coder en CUDA !

Merci à tous les Ziggles pour tous ces samedi matin à Vence ! Merci à tous les PhDisc et autres Lyonnais ainsi qu'à la Horde, Grimaud, Paul, Clément, Fred, Timéloan, Guilhem, Hugo, Félix, Victor, Bertrand, La machine, Loïc, Madi, Carpi, Gilles. Le tournoi c'est vraiment une pratique très « marrante » ! Merci aux Counta et bons amis niçois qui m'ont bien fait rigoler : Leslie, Karim, Aude, Mariannick, David R., Jo, Emma, Céline, Steven, Mathilde, Yogi Sarah, LdP,... ! Merci à Loïc (le meilleur *colocorrecteur*) et Grimaud de m'avoir spammé. Merci à Félix d'avoir fait voyager le Ter-Ter et Ludo pour m'avoir dit un jour : « mille » et merci à tous les autres parisiens pour les brèves retrouvailles.

Merci à Michael et George de m'avoir inspiré.

Je remercie ma maman, parce que quand même ! Mon Frère, mon Papi, ma Mami (de m'avoir poussé à finir le plus vite possible) et toute ma famille pour leur « énergie » inspirante !

Leslie, ma fiancée d'aujourd'hui et ma femme de demain, je te dis un grand merci de me supporter depuis le début et vu comme c'est parti jusqu'à la fin.

---

# CONTENTS

---

CONTENTS .....	VII
FOREWORD .....	15
INTRODUCTION .....	17

## PART ONE

### EXPERIMENTAL COLLABORATION: DEBYE LENGTH IN MAGNETO-OPTICAL-TRAPS?

---

#### CHAPTER I FROM MAGNETO-OPTICAL-TRAPS TO PLASMA

---

1	STANDARD MODEL FOR MOT .....	28
1.1	The trapping .....	28
1.1.a	<i>Doppler effect</i> .....	30
1.1.b	<i>Zeeman effect</i> .....	30
1.1.c	<i>Radiation pressure</i> .....	31
1.2	Diffusion .....	34
1.3	Shadow effect: an effective attractive force between atoms .....	35
1.4	Multiple scattering: an effective Coulomb force between atoms .....	36
1.5	Other quantum effects .....	37
2	SUM UP AND QUESTIONS .....	38
2.1	Sum-Up of the model .....	38
2.2	Experimental confirmation? .....	38

3	NON NEUTRAL PLASMA .....	39
3.1	Presentation of NNP model .....	39
3.1.a	<i>Standard NNP model</i> .....	39
3.1.b	<i>NNP model for the MOT</i> .....	40
3.1.c	<i>Debye length</i> .....	42
3.1.d	<i>Plasma parameter</i> .....	43
3.2	Some numerical values for experimental MOT .....	44

---

## CHAPTER II THEORETICAL AND EXPERIMENTAL OBSERVABLES

---

1	DENSITY .....	47
2	PAIR DISTRIBUTION FUNCTION .....	48
3	NUMERICAL EXAMPLES .....	49
3.1	Numerical details .....	49
3.2	Numerics .....	50
4	STRUCTURE FACTOR .....	52
5	COMPARISON WITHOUT CORRELATIONS .....	53
5.1	Random arrangement .....	54
5.2	Turning off the trap and interactions .....	54
6	DIFFRACTION AND STRUCTURE FACTOR: LINK WITH EXPERIMENTS .....	55

---

## CHAPTER III LOOKING FOR DEBYE LENGTH AND OTHER PLASMA PHYSICS EFFECTS

---

1	DIRECT PROBING .....	57
1.1	With a Gaussian probing beam .....	57
1.2	Comparison with experiments .....	58
2	RESPONSE TO AN EXTERNAL POTENTIAL .....	59
2.1	Experiment principle .....	59
2.2	Fluorescence-like density profile .....	60
2.2.a	<i>The Response function</i> .....	60
2.2.b	<i>Numerical Simulations</i> .....	60
2.2.c	<i>Experiments</i> .....	62
2.3	Diffraction .....	62
2.3.a	<i>Expression of the <math>\vec{k}</math> vector</i> .....	62
2.3.b	<i>A simple example: existence of two diffraction regimes Raman-Nath/Bragg</i> ..	64
2.3.c	<i>Diffraction discs</i> .....	65
2.3.d	<i>Comparison theory simulations</i> .....	66

---

2.3.e	<i>Comparison theory/experiments</i> .....	68
3	<b>CONCLUSIONS</b> .....	<b>70</b>

## PART TWO

### BIFURCATIONS FOR VLASOV AND KURAMOTO SYSTEMS

---

#### CHAPTER IV INTRODUCTION TO BIFURCATION

---

1	<b>A BIFURCATION EXAMPLE IN FINITE-DIMENSION</b> .....	<b>79</b>
1.1	Exact solution .....	79
1.2	Center manifold approach .....	80
1.3	Unstable manifold approach .....	81
1.4	Conclusion .....	83
2	<b>INFINITE-DIMENSIONAL SYSTEMS</b> .....	<b>84</b>
2.1	Spectral problem .....	84
2.2	Free transport example .....	85
2.3	Nonlinear analysis for bifurcation .....	87
3	<b>PHYSICAL MOTIVATIONS</b> .....	<b>88</b>

#### CHAPTER V VLASOV SYSTEMS AROUND HOMOGENEOUS EQUILIBRIUM

---

1	<b>INITIAL PROBLEM</b> .....	<b>92</b>
2	<b>SPECTRUM OF THE HOMOGENEOUS VLASOV OPERATOR</b> .....	<b>93</b>
2.1	Eigenvalue problem .....	93
2.2	Continuous spectrum .....	95
3	<b>ADJOINT PROBLEM</b> .....	<b>95</b>
3.1	Adjoint operator construction .....	96
3.2	Eigenvalue problem .....	97
4	<b>LINEAR LANDAU DAMPING</b> .....	<b>97</b>
5	<b>NONLINEAR EXPANSION</b> .....	<b>100</b>
5.1	Symmetries .....	101
5.2	Temporal equations .....	103

---

5.3	Cubic order .....	104
5.4	A note on pinching singularities .....	105
5.5	Higher orders .....	106
6	RESONANCE PHENOMENON .....	107
7	OPEN QUESTIONS .....	109

## CHAPTER VI BIFURCATIONS AROUND NON HOMOGENEOUS STATES

---

1	STEADY STATE .....	112
2	ANGLE-ACTION VARIABLE .....	113
2.1	Angle-action definition .....	113
2.2	Fourier basis of the HMF potential in angle-action variable .....	115
3	LANDAU DAMPING AND RESONANCES .....	116
3.1	Landau damping .....	116
3.2	Resonances .....	117
3.2.a	<i>Non oscillating perturbation</i> $\text{Im } \lambda = 0$ .....	117
3.2.b	<i>Oscillating perturbation</i> $\text{Im } \lambda \neq 0$ .....	117
4	LINEAR PROBLEM .....	118
4.1	Dispersion relation .....	118
4.2	Self-consistent equation for the magnetization .....	120
4.3	Eigenvector and eigenvalue .....	120
4.3.a	<i>Along the sin direction</i> .....	120
4.3.b	<i>Along the cos direction</i> .....	122
4.4	Stability criteria .....	122
4.5	Adjoint problem .....	123
5	NONLINEAR EXPANSION .....	124
6	HIGHER ORDER TERMS .....	126
7	NUMERICS .....	127
8	POSSIBLE APPLICATIONS .....	130
8.1	Radial orbit instability: two possible end states .....	130
8.2	Super Massive Black Hole .....	131
9	TOWARDS AN EXACT DIMENSIONAL REDUCTION? .....	131
9.1	Did we miss something? .....	131

9.2	The Triple Zero bifurcation.....	132
9.2.a	<i>Quick analysis of the reduced equations</i> .....	134
9.2.b	<i>Numerical comparison between reduced system and full Vlasov dynamics</i> ..	134
9.2.c	<i>Questions and puzzles</i> .....	136

---

## CHAPTER VII VLASOV-FOKKER-PLANCK SYSTEM

---

1	SETTINGS.....	<b>139</b>
2	LINEAR PROBLEM.....	<b>140</b>
2.1	Velocity Fourier.....	140
2.2	Eigenvalue problem.....	140
2.3	Spectrum.....	141
2.4	Landau damping.....	142
2.5	Adjoint problem.....	143
2.6	Dispersion relation and normalization check.....	143
3	NONLINEAR EXPANSION.....	<b>144</b>
3.1	Cubic coefficient.....	145
3.2	Higher order terms.....	146
3.3	Critical layers.....	147
4	CONCLUSION AND CONJECTURES.....	<b>147</b>

---

## CHAPTER VIII COUPLED OSCILLATORS SYSTEMS: THE KURAMOTO MODEL

---

1	HISTORICAL REVIEW.....	<b>150</b>
1.1	The model.....	151
1.2	Original result (Kuramoto 1975).....	151
1.3	Large oscillator number limit (Mirollo & Strogatz, 1991).....	153
2	CRAWFORD APPROACH (1993).....	<b>154</b>
3	OTT-ANTONSEN ANSATZ (2008).....	<b>156</b>
3.1	The ansatz.....	156
3.2	Comparison between Ott-Antonsen ansatz and the Unstable manifold.....	158
4	MATHEMATICAL RESULTS.....	<b>160</b>

---

5	EVERYTHING FALLS APART: THE KURAMOTO-DAIDO CASE (1992)!	160
5.1	Crawford result (1994)	161
5.2	Comparison with the Ott-Antonsen ansatz	162
5.3	The Chiba result (2011)	162
5.4	What is the difference?	163

---

## CHAPTER IX KURAMOTO MODEL WITH INERTIA

---

1	THE MODEL	167
2	LINEAR PART	168
2.1	Eigenvalue problem	168
2.2	Adjoint problem	169
3	UNSTABLE MANIFOLD EXPANSION	170
3.1	Computation of $h_{0,0}$	171
3.2	Computation of $h_{2,0}$	171
3.3	Putting everything together	172
4	DISCUSSION	173
4.1	Numerics	175

---

## CHAPTER X KURAMOTO MODEL WITH DELAY

---

1	THEORY OF DELAY DIFFERENTIAL EQUATION	178
1.1	Extended functional space and operator	178
1.2	Dual space	179
1.3	Eigenvalue problem	180
2	OTT-ANTONSEN ANSATZ WITH DELAY	180
2.1	Settings	181
2.2	Ott-Antonsen ansatz	181
2.3	Unstable manifold calculation	182
2.3.a	Linear part	182
2.3.b	Adjoint problem	183
2.3.c	Nonlinear part	183
3	STANDARD KURAMOTO MODEL WITH DELAY	183
3.1	Setting	184
3.2	Eigenvalue problem	184

3.3	Adjoint problem	185
3.4	Unstable manifold calculation	185
3.5	Application	186
3.5.a	Centered distribution $\omega_0 = 0$	186
3.5.b	Lorentzian distribution	187
4	<b>KURAMOTO MODEL WITH INERTIA AND DELAY</b>	<b>187</b>
4.1	Settings	188
4.2	Eigenvalue problem	189
4.3	Unstable manifold	189
4.3.a	Computation of $h_{0,0}$	190
4.3.b	Computation of $h_{2,0}$	190
4.3.c	Putting everything together	191
4.4	Application to a Lorentzian distribution	192

---

## CHAPTER XI REMARKS, CONJECTURES, CONCLUSION & PERSPECTIVES

---

1	CONJECTURES	196
2	FURTHER WORK TO DO	198

---

## APPENDIXES

---

### APPENDIX A MAGNETO-OPTICAL-TRAP COLLABORATION

---

1	STRUCTURE FACTOR AND DIFFRACTED INTENSITY	203
2	THEORETICAL DENSITY PROFILE	205

### APPENDIX B VLASOV NON HOMOGENEOUS

---

1	ANGLE ACTION VARIABLES	207
2	COMPUTATIONS AT HIGHER ORDERS	209
2.1	Structure of the computation for a general potential	209
2.2	Cosine potential - Order of magnitude of $c_3$	210

### APPENDIX C VLASOV-FOKKER-PLANCK

---

1	ZEROth HARMONIC CONTRIBUTION .....	214
1.1	Diverging term .....	214
1.2	Non diverging term .....	216
2	SECOND HARMONIC CONTRIBUTION .....	217

**APPENDIX D THE KURAMOTO MODELS**

---

1	KURAMOTO WITH INERTIA .....	219
1.1	Standard Kuramoto limit, $m \rightarrow 0$ .....	219
1.2	Hamiltonian (Vlasov) limit, $\alpha = 0, m \rightarrow \infty, K \rightarrow \infty, K/m = \text{cst}$ .....	220
2	THE SELF-CONSISTENT MEAN-FIELD METHOD, AND BISTABLE BEHAVIOR .....	220
2.1	Bistable behavior .....	221
2.2	Self-consistent equation .....	221
3	SIGN OF DISPERSION RELATION DERIVATIVE .....	222
3.1	Standard Kuramoto model .....	222
3.2	Kuramoto with inertia .....	224
	BIBLIOGRAPHY .....	225
	RÉSUMÉ & ABSTRACT .....	245

---

# FOREWORD

---

What is this Ph.D. thesis about? At a basic level the answer is: understanding the formation of structures in a particular class of system with a large number of components. This special class concerns systems formed with particles interacting with each other via long-range interactions. The most obvious examples are self-gravitating systems and plasmas but many more systems are concerned. These interactions are opposed to the short-range interactions (e.g. shocks with 0-range or nearest neighbor interactions) and can drive a system out-of-equilibrium. The dynamics of these long-range systems is the primary interest of this Ph.D. thesis. It will be studied through kinetics equations. The difficulty lies in the richness of these equations. The goal of my work is to depict the dynamics around stationary states with simpler equations, this is called dimensional reduction.

The manuscript is composed of two independent parts: one concerning an experimental collaboration on a cold atom system with supposedly long-range interactions and another one which can be considered as the main part on bifurcations in collisionless kinetic systems.

## **Main results of this Ph.D. thesis**

---

In the experimental collaboration part, the main result is the proposition of two experiments that could confirm or not the analogy between Large Magneto Optical Traps and a Non-Neutral Plasma. Preliminary experimental results are discussed with a relatively good matching with theory and simulations. However definitive conclusions remain uncertain.

In the second part, the main achievements are the bifurcation analysis for five different kinetic systems. Numerical simulations were done in some of these systems fully supporting the theoretical claims. These results elucidate partially the dynamics around steady states of out-of-equilibrium systems with long-range interactions and in at least one case predicts a behavior that might be relevant in galactic systems. Our results could prove to be very generic thanks to the universal character of bifurcation analysis. For example, bifurcation regimes found for Vlasov systems with a small dissipation are like the one obtained for two dimensional fluids; we also conjecture a Triple Zero bifurcations around non homogeneous Vlasov states. Moreover, along this Part we raise many questions and observations on the unstable manifold technique used after J.D. Crawford and the possibility of exact dimensional reductions.



---

# INTRODUCTION

---

The Newton's law of universal gravitation describes one of the most fundamental forces, thus since we all experience it directly we will use it as a guiding thread of this introduction. Newton was able to derive planets motions around the sun associating this force with equations of motion he postulated. In other words, he solved a one body problem (since the Sun is considered fixed because of its large mass), meaning he could predict the motion of planets (position and velocity) in time. The natural sequel for this problem is the two-body problem, that we also know exactly how to solve. However, upon increasing the number of bodies  $N$  from two to three the problem incredibly more difficult: no general solutions are known and chaos emerges. A chaotic system can behave very differently for two very close initial conditions, making its analytical description difficult. For even larger systems with a large number  $N$  of self-gravitating bodies, knowing the exact evolution is therefore hopeless.

What can we say about the evolutions of a  $N$ -body systems with gravitational like interactions?

The statistical physics field was actually developed to understand many body systems, not by describing the exact evolution for all bodies but rather by finding the most probable one. The construction of various statistical ensembles such as the Microcanonical/Canonical/Grand Canonical ensemble with quantities such as entropies lead for example to thermodynamics as we teach it nowadays. Laws are essentially known for the non-interacting gas (perfect gas) or for short-range interactions, which is enough to solve a lot of various problems from heat engine to social dynamics. In these problems, a natural assumption is to consider ensemble additivity meaning that if a system is composed of two subsystems 1 and 2, the total energy is approximatively the sum of the individual energies of the subsystems  $E_1 + E_2 = E_{1+2}$ . This turns out to be true for short-range interactions in the large  $N$  limit.

But is this Bachelor statistical physics useful for our self-gravitating problem where long-range interactions are at stake? First let's set our definition<sup>1</sup> of long-range interactions. We will say two bodies are interacting with long-range interactions if their potential of interaction  $V(r)$

---

1. Depending on the field one can find different definitions. For example, one can find that interaction with infinite range are "long-range". That is not our definition.

and more generally their force of interactions  $F(r)$  satisfies

$$V(r) \stackrel{r \rightarrow \infty}{\sim} \frac{\text{cst}}{r^\alpha} \quad \text{or} \quad F(r) \stackrel{r \rightarrow \infty}{\sim} \frac{\text{cst}}{r^{\alpha+1}}, \quad \text{with} \quad \alpha \leq D = \text{spatial dimension.} \quad (1)$$

For example, a Coulomb/Newton interaction is long-range since its  $\alpha = 1 < D = 3$ . From this mathematical definition, we immediately see why this boundary exists<sup>2</sup> at  $\alpha = D$ . Considering the total interaction energy of one particle centered at  $r = 0$  in a constant distribution of particles<sup>3</sup>  $\rho_0$  we get

$$V_{\text{int}} = \rho_0 \int_{r \in \mathbb{R}^D} V(r) d^D r \sim \lim_{L \rightarrow \infty} \rho_0 L^{D-\alpha} = \begin{cases} \text{cst} & \text{if } \alpha > D \\ \infty & \text{if } \alpha \leq D. \end{cases} \quad (2)$$

This phenomenon leads to the non extensivity of long-range systems  $E_1 + E_2 \neq E_{1+2}$ . Long-range systems display other intriguing particularities such as nonequivalence of the different statistical ensembles and negative heat capacity. For review of those systems see [CDR09, DRAW02, CGML08] or the introductory and very understandable talks of J. Barré and H. Touchette [ICT16] at the ICTP of Trieste at the Conference on Long-Range-Interacting Many Body Systems: from Atomic to Astrophysical Scales.

To have a rather broad overview of the different systems displaying long-range forces, one can refer to the program of the ICTP conference program<sup>4</sup> in Trieste, where a lot of different fields were represented. The most obvious example are self-gravitating systems with many astrophysical examples and plasma systems [EE02] with Coulomb forces between electron or ions. Another example that will be presented in this thesis is the large Magneto-Optical Trap (MOT). One also finds examples in hydrodynamics [Mil90, RS91], atomic physics, nuclear physics and for Rydberg gases [DRAW02, CGML08] or spin systems [SJM15]. Characteristic behaviors of long-range systems have been observed in some nonlinear optics experiments [XVF<sup>+</sup>15].

One can argue that we know the fate of any Hamiltonian system (including self-gravitating one) because they should at some point reach Boltzmann-Gibbs statistical equilibrium. Nevertheless, another particularity of long-range systems is that they possess what we call a Quasi Stationary State (QSS) that has a very long relaxation time. Thus, we will need out-of-equilibrium tools. For example, the Large deviation theory [BBDR05] or fluctuation dissipation theorems [Kub66] are precious to give statistical information. Entropy methods with applications closer to our concern are also possible [RTBPL14, LB99, Per06]. Note that non Hamiltonian systems are by nature out-of-equilibrium e.g. system with non-conservative forces and coupled oscillator systems. In this thesis, we are interested in the temporal evolution of out equilibrium system around their stationary states (or QSS). To do so we will use the kinetic description of the system. The kinetic description is often said to be at the mesoscopic scale since it is an intermediate description in between the microscopic scale and macroscopic scale. The microscopic scale describes the evolution of every particle via the different equations of motion. The macroscopic scale describes the evolution of macroscopic observable such as the mean velocity, temperature, pressure, etc. see Figures 1 and 2.

2. In Part Two, in order to simplify the manuscript we will use only a simple all-to-all coupling ( $\alpha = 0 < D$ ), but the main physical phenomena remain. More generic potentials are considered in our publications.

3. In all the manuscript the term particles will refer to the components of the system studied, be it atoms, stars, electrons, oscillators, crickets, etc.

4. <http://indico.ictp.it/event/7612/other-view?view=ictptimetable>

---

## THE VLASOV EQUATION

---

The Vlasov equation is one of the fundamental kinetic equations. It will be the main evolution equation of this thesis (all other equations will be related to it in some way). Here we show formally how the Vlasov equation emerges from the microscopic description of long-range systems. Then, once velocity is integrated, one can obtain macroscopic equations (for observables such as velocity, pressure, etc.). All the reasoning is summarized in Figure 2.

The evolution of a  $N$  bodies Hamiltonian system is governed by  $2N \times D$  first order equations of the form

$$\dot{\vec{r}}_i = \vec{v}_i, \quad (3a)$$

$$m \dot{\vec{v}}_i = \sum_{i \neq j} \vec{F}(\vec{r}_j - \vec{r}_i). \quad (3b)$$

As mentioned earlier, solving this problem analytically is utopian, so a statistical approach of the problem must be developed. The exact position and velocity of each particles is no longer considered but rather the density  $f$  of particles in the phase space  $(\vec{r}, \vec{v})$  is. This forms the mesoscopic approach. Thus, we keep track of both spatial distribution and speed distribution of particles in time. A macroscopic approach would erase the velocity information ; therefore, the kinetic approach can solve more subtle phenomena such as phase mixing and emergence of instabilities due to velocity resonances as we will see later.

There are several ways to construct the Vlasov equation from Eq. (3), here we postulate its form and show that it is the relevant equation to study. The empirical density function is defined as

$$f_E(\vec{r}, \vec{v}, t) = \sum_{i=1}^N \delta(\vec{r} - \vec{r}_i(t)) \delta(\vec{v} - \vec{v}_i(t)), \quad (4a)$$

with

$$\iint f_E(\vec{r}, \vec{v}, t) d^3\vec{r} d^3\vec{v} = N. \quad (4b)$$

This singular distribution still contains all information on the particles. It is possible to show<sup>5</sup> that  $f_E$  is a weak<sup>6</sup> solution of the Vlasov equation,

$$\partial_t f + \vec{v} \cdot \vec{\nabla}_r f + \frac{\vec{F}_{\text{MF}}[f]}{m} \cdot \vec{\nabla}_v f = 0, \quad (5a)$$

$$\vec{F}[f]_{\text{MF}}(\vec{r}) = \iint \vec{F}(\vec{r} - \vec{r}') f(\vec{r}', \vec{v}', t) d^3\vec{r}' d^3\vec{v}', \quad (5b)$$

$$\iint f(\vec{r}, \vec{v}, t) d^3\vec{r} d^3\vec{v} = N. \quad (5c)$$

For a distribution,  $f(\vec{r}, \vec{v}, t) d^3\vec{r} d^3\vec{v}$  gives the number of particles in the phase space volume  $(\vec{r} + d\vec{r}, \vec{v} + d\vec{v})$  at a time  $t$ . In this evolution equation, the distribution evolves through an advection term and a nonlinear term with a self-consistent mean field force  $\vec{F}_{\text{MF}}[f](\vec{r})$ .

---

5. The Vlasov equation can be found writing the density conservation along trajectories  $df_E/dt = 0$ .

6. Weak means that is must be integrated with some test function to make sense.

We just constructed the Vlasov equation from the singular empirical distribution, but is it possible to construct in the large  $N$  limit a smooth distribution describing accurately the particles evolution? How close are the exact dynamics of  $f_E$  to a smoothed version of it  $f$ ? If the two start "closely", how will they evolve through Vlasov dynamics? To measure this, one defines a suitable distance between two distributions  $d(f_1, f_2)$  and look at its time evolution  $d(f(t), f_E(t))$ . It is possible to show [BH77, Dob79, NW80] that this distance is at most exponential:

$$d(f(t), f_E(t)) \leq d(f(0), f_E(0))e^{t/\tau}, \quad (6)$$

where  $\tau$  is a constant independent of the initial condition and  $N$ . So, over a time scale  $O(\tau)$  the two distributions will stay close by. Moreover, the empirical distribution converges toward the smoothed distribution as  $d(f(0), f_E(0)) = O(1/\sqrt{N})$ . So, if  $\tau$  does not depend on  $N$ , we expect the continuous description to be valid over a time scale  $\tau_c = O(\ln N)$ . This estimate can be made sharper for Vlasov steady states as  $\tau_c = O(N^\delta)$ ,  $\delta > 0$ . We name **violent relaxation** the time  $\tau_v$  during which a particles system evolves according to the Vlasov dynamics, after which the **collisional relaxation** dominates. These different time steps are summarized on Figure 1. The demonstration<sup>7</sup> relies heavily on the long-range nature of the interactions to

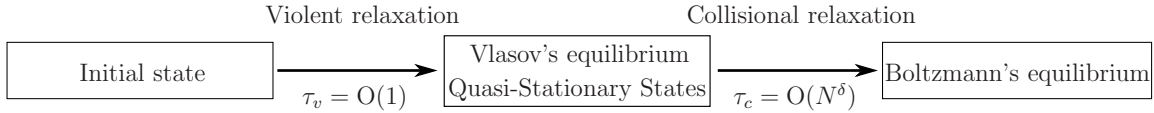


Figure 1 – Schematic representation of the different time scales in a long-range system.

construct the mean field force. This means that the Vlasov equation is not well suited for systems with short-range interactions. In the  $N \rightarrow \infty$  limit, particles only feel the mean force  $\vec{F}_{MF}[f]$  created by the whole distribution of particles, thus correlations vanish. Therefore, the exact interactions between two particles do not matter anymore.

The Vlasov equation has many interesting properties, amongst them, it possesses an infinite number of preserved quantities called the Casimir invariants [Mor00]

$$\mathcal{C}_s[f] = \iint s[f](\vec{r}, \vec{v}, t) d^3\vec{r}d^3\vec{v}, \quad (7)$$

where  $f$  is a Vlasov solution, meaning that  $\dot{\mathcal{C}}_s[f] = 0$  (where the dot denotes  $d/dt$ ) for any generic function  $s$ . Thus, in addition to the energy, entropy, momentum, angular momentum, etc. which are conserved in standard Hamiltonian systems, there are an infinite number of integrals of motion. This gives to the Vlasov equation an infinite number of stationary states. Another very surprising feature associated with the Vlasov flow is that it can relax to its initial state after a perturbation with constant entropy. More precisely, the phase space distribution  $f(\vec{r}, \vec{v}, t)$  oscillates more and more in the velocity variable while the integrated density  $\int f d^3\vec{v}$  does relax (see Section V.4). This phenomenon is the Landau damping (or non-entropic relaxation) and was discovered in the linear case by L.D. Landau [Lan46], a proof for the full nonlinear Vlasov equation has been given recently by C. Mouhot and C. Villani [MV11].

7. To be fair, rigorous mathematical derivation are not yet obtained for Coulomb/Newton potential. Demonstrations without cut off are limited to  $F(r) \sim r^{-\alpha}$  with  $\alpha < 1$  [JH11]. However, in 1D, interaction potential are much more regular and rigorous results exist [Tro86].

**Remark .1**

- The word collision has different meaning here depending on the context. For short-range systems, collision refers to real collision between two particles and in this context, they would be essential, while long-range systems are dominated by mean field. A kinetic description of short-range system leads to the Boltzmann equation. For long-range systems collisions or collisional effects mean finite  $N$  effects, in fact correlations. In the astrophysical community, the Vlasov equation is called the collisionless Boltzmann equation.
- So far, we have used a deterministic approach, meaning that for a given initial distribution  $f_E$  the Vlasov equation gives the deterministic evolution of particles. Another approach is the probabilistic one, considering for example the mean field evolution of particles over different initial conditions distributed along a given  $f_{\text{init}}$  distribution. It uses the propagation of chaos theory [Szn91, Mon16]. Its use led to a recent proof of the mean field limit of the Vlasov equation for Coulomb/Newton potential with a very small cut-off scaling like  $N^{-1/3+\epsilon}$ .

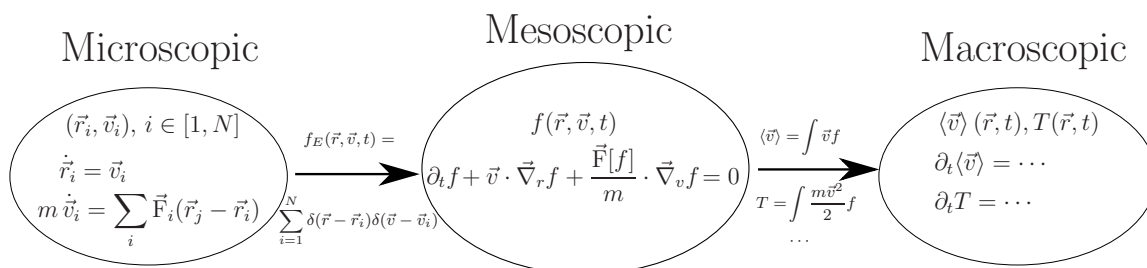


Figure 2 – Schematic representation of the different possible scales of description. On the arrow are the different functions linking two different scales.

With distribution functions, it is easy to construct macroscopic observables such as the mean velocity  $\langle v \rangle(\vec{r}) = \int \vec{v} f d^3v$  and the temperature  $T(\vec{r}) = \int \frac{m \vec{v}^2}{2} f d^3v$ . To obtain the associated evolution equation one must do some approximation valid within some regime; for example fluid equations such as gyrofluid equations can be derived [BH07, SR00] from the Vlasov equation. In this thesis, we do not study this macroscopic behavior. In out-of-equilibrium systems the velocity distribution is in general not simply a Gaussian and leads to counter-intuitive effect like Landau damping (damping without dissipation) that could not be predicted by macroscopic equations.

## GOALS AND OUTLINE OF THE THESIS

The goal of this thesis is to study the behavior of out-of-equilibrium many body systems with long-range interactions. It is divided in two very different parts. In the first Part, we study a real experimental set-up and give theoretical and numerical predictions. In the second Part we focus on the bifurcation technique developed by J.D. Crawford for kinetic equations.

Part **One** is devoted to the study of an experimental Magneto-Optical Trap (MOT). We collaborated with Guillaume Labeyrie and Robin Kaiser of the Non Linear Institute of Nice (INLN) and Bruno Marcos of the Laboratory J.A. Dieudonné. The standard modeling for large MOT

composed of neutral atoms predicts effective Coulomb like interactions between particles (via photon rescattering). Therefore a kinetic description through the Vlasov-Fokker-Planck equation (Vlasov equation with friction and diffusion) is expected to be accurate. The goal of the collaboration is to test experimentally the long-range nature of those effective forces, since the literature still lacks an irrefutable experiment. The main idea was to observe plasma physics effects such as the Debye length as an experimental proof. In Chapter I we present the standard modeling through atomic physics leading to a plasma like description of a large MOT. We introduce then the basics of plasma physics through the Non Neutral Plasma (NNP) model. Chapter II is dedicated to the introduction of the different observables and tools used to analysis and probe a cold atom cloud. In Chapter III we present and discuss different realistic measurements (theoretically and numerically) that could highlight plasma phenomena, and compare them to the preliminary experiments realized by G. Labeyrie.

Part Two is devoted to bifurcations around steady states of kinetic equations. Kinetic equation such as the Vlasov one are nonlinear self-consistent partial differential equations, they have a very rich dynamics such as an infinite number of stationary states, filamentation of the phase space<sup>8</sup>, strong wave/particles resonances, non-entropic relaxation, etc., thus their mathematical and physical understanding is far from being complete. The bifurcation study is a natural strategy to simplify the dynamics in specific cases (e.g. neighboring of stationary states close to an instability threshold). One hope is that these bifurcations might structure the whole dynamics; another motivation is to obtain a classification of these bifurcations (by studying various kinetic equations) as there is for standard (dissipative) systems (saddle-node, pitchfork, Hopf, etc.). However, due to the previously mentioned difficulties standard bifurcation techniques such as multiple-timescale analysis or center manifold fail [CH89, HC89, MH13, HM13].

In Chapter IV we present the unstable manifold technique introduced by J.D. Crawford in the context of kinetic equations [Cra94a, Cra94b, Cra95a, Cra95b] which overcomes some of the difficulties met by standard expansions. The price to pay is that this approach is not well supported mathematically and that the description of the bifurcation is incomplete but qualitatively correct providing precious informations on the bifurcation nature. We shall use this technique for the rest of the manuscript. Chapter V review quickly the standard results for the bifurcation around homogeneous steady states of the Vlasov equation. In Chapter VI we present our results on the bifurcation around inhomogeneous states obtained in collaboration with Y.Y. Yamaguchi. In this case, we also obtain with a center manifold approach a finite three-dimensional reduction agreeing well with the numerical simulations. In Chapter VII, we perform a similar analysis for homogeneous Vlasov-Fokker-Planck states, in particular we show how interplay between a weak instability and weak dissipation gives rise to several regimes.

In Chapter VIII we introduce another kinetic equation based on the Kuramoto model describing coupled oscillator systems. It shares many similarities with the Vlasov equation and was also studied by J.D Crawford. We then once again use in Chapter IX the unstable manifold technique for the Kuramoto model with inertia and in Chapter X with delayed interactions (with and without inertia).

As one can already tell from this outline the work of J.D. Crawford is very important in this thesis since he has laid the foundation of the bifurcation study for both Vlasov and Kuramoto equation. Therefore, the overall procedure will be similar every time but we will see that each specific case has its own physical and technical issues. We will summarize in Chapter XI our results, classifications and conjectures for the bifurcation analysis of the various kinetic

---

8. The filamentation refers to the highly oscillating behavior of the distribution function  $f(\vec{r}, \vec{v}, t)$  with respect to the velocity variable.

equations studied.



**PART ONE**

**EXPERIMENTAL COLLABORATION:  
DEBYE LENGTH IN  
MAGNETO-OPTICAL-TRAPS?**



---

# FROM MAGNETO-OPTICAL-TRAPS TO PLASMA

---

A large part of low energy physics is concerned with set-up at cold temperature  $T \lesssim \text{mK}$ , where lasers are used to manipulate atoms for their useful and interesting classical or quantum properties. To reach weak temperature experiments the radiation pressure exercised by lasers is used. It is the force felt by an atom when it absorbs a photon, possibly decreasing its velocity via momentum transfer. That mechanism is at the origin of the "cold atom" field. A widely used set-up because of its relative simplicity is the Magneto Optical Trap (MOT); its essential components are

- Neutral atoms (such as Rubidium, Strontium)
- Two magnet coils set in anti-Helmholtz configuration (producing a magnetic field gradient),
- Six lasers (one pair for each spatial dimension),
- A vacuum chamber.

At low atom number  $N \lesssim 10^4$ , the physics is relatively well understood. Thanks to radiation pressure of the six lasers the trapping and cooling of atoms is achieved. Moreover, in this regime no interactions between atoms are considered and the particles dynamics is essentially a Brownian motion. In metrology with atomic clocks [KHS<sup>+</sup>16], the low atoms speed is used for high precisions measurements.

However, when  $N \gtrsim 10^5$ , the physics sees several qualitative changes, some effective interactions between atoms appear... Indeed, for MOTs with a large number of particles it has been observed that the cloud size  $L$  increases with the number of atoms  $N$ , whereas for  $N < 10^4$ , the size  $L$  was independent of  $N$ . So, there must be a repulsive process developing. Because of this repulsion, the atom cloud cannot be compressed indefinitely, preventing for example Bose Einstein condensation, that are since its first realization in the 90s [AEM<sup>+</sup>95] a very active topic. With the advent of more powerful laser sources, it is now possible to prepare very large MOTs (VLMOT) with  $10^{11}$  atoms [CKL14], where collective effects are enhanced.

The description of this collective behavior is far from being well understood. Neutral atoms interact with the trap composed of lasers and a magnetic field and with each other through absorption and emission of photons with rules given by the energy levels of atoms of the trap (an exact description should then depend on the atom species and its hyperfine structure). In 1988 Dalibard [Dal88] showed that absorption of the laser light in the cloud results in an effective attracting force between atoms like one dimensional gravity: the so-called Shadow Effect. Dalibard was the first to describe effective interactions between particles and formally his model for VLMOT bears similarities with a galactic model of self-gravitating stars. However, this description didn't explain why in experiments when  $N$  is increased, the cloud  $L$  also increases, in fact it predicts the opposite.

The current "standard model" to describe VLMOTs was then proposed in [WSW90] by T. Walker, D. Sesko and C. Wieman (2001 Nobel prize winner), it includes an effective Coulombian-like force between two level atoms, due to multiple scattering of photons. According to this picture, VLMOTs thus share similarities with a Non Neutral Plasma (NNP). In this plasma physics model electrons are all interacting through Coulomb interactions in a neutralizing background (as large positive ions).

The main question in this part is then can we observe plasma physics phenomenon in VLMOT? Is there any chance to observe Landau damping in a VLMOT? We will quickly answer negatively to this question in the second part Bifurcations of this thesis making a bridge between the two parts. Indeed, the friction range for the experimental MOT is too large to observe Landau damping. So, what else could we seek? Debye length? Instabilities and bifurcations? In this thesis, we will search for the analog of Debye length which is characteristic of plasmas and Coulomb interactions. More generally the goal is to search for evidence of long-range interactions between atoms via direct correlation and response to an external potential measurement.

In this chapter, I will first retrace the standard modeling of VLMOTs. Then I will present the Non Neutral Plasma model, introducing the different characteristic parameters in the MOT units.

---

## 1 STANDARD MODEL FOR MOT

---

All the numerical values given here for the MOT are taken from [CKL14, GPLK10, Ste01]. For the French readers, I recommend the Collège de France lecture by J. Dalibard [Dal14], to get a clear introductory picture of the cold atom field. Also, one can read the review of Cohen-Tannoudji for his 1998 Nobel prize [CT98] on manipulation of atoms with photons.

### 1.1 The trapping

---

The idea behind Magneto-Optical-Trap is to trap atoms in the velocity and position space thanks to one pair of magnet coils and six lasers in all of the six directions of space, as represented in Figure I.1.

For a two energy level atom,  $|g\rangle$  ground state and  $|e\rangle$  excited state trapping occurs via absorption and emission of photons from the Laser (see Figure I.2). Basically, absorbing a photon coming from the left will push the atom to the right (see Section I.1.1.c).

The detuning  $\delta = \omega_L - \omega_{\text{atom}}$  is the quantity that measures the energy difference between a photon with frequency  $\omega_L$  and the excitation energy  $\omega_{\text{atom}}$  of the atoms. In practice, it can

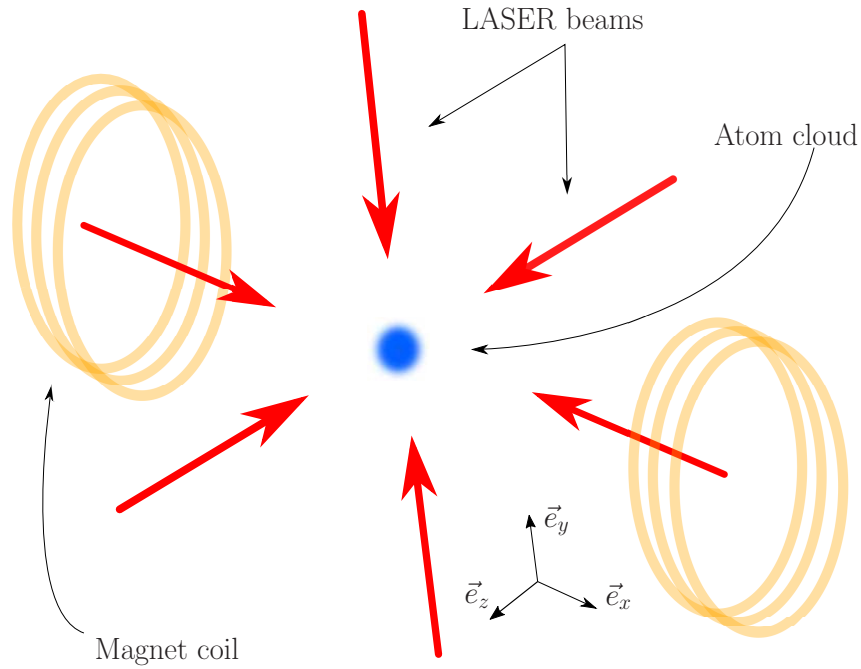


Figure I.1 – Schematic representation of a Magneto-Optical-Trap (MOT) with six Lasers and two magnet coils creating a linear gradient of magnetic field.

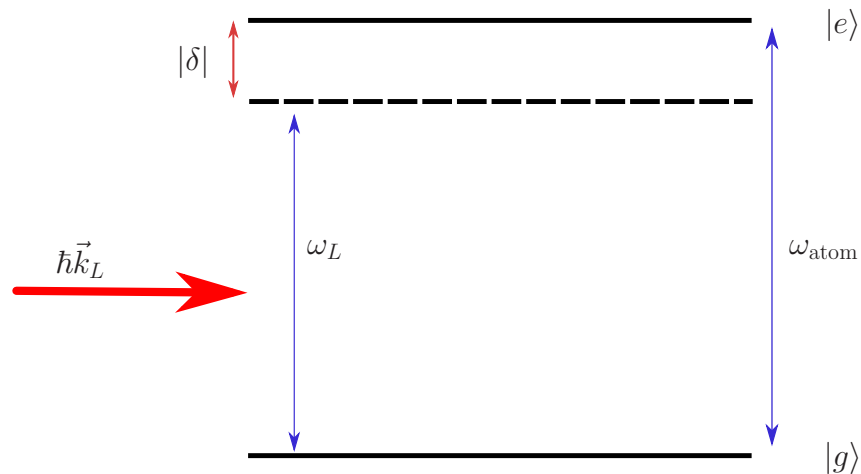


Figure I.2 – Schematic representation of the transition  $|g\rangle \rightarrow |e\rangle$  for an absorbed photon of momentum and frequency  $(\hbar\vec{k}_L, \omega_L)$  with an atomic transition of natural frequency  $\omega_{\text{atom}}$ . The detuning of the lasers  $\delta = \omega_L - \omega_{\text{atom}}$  is negative here.

be tuned<sup>1</sup> very well, in a typical range  $0 \Gamma_d \lesssim |\delta| \leq 8 \Gamma_d$ , where  $\Gamma_d \sim 10$  MHz is the natural width of the transition. For the Rubidium atoms used in experiments  $\Gamma_d = 2\pi \times 6.06$  MHz. In short Doppler and Zeeman effects modify detuning to favor absorption of photon as a function of speed and position for cooling and trapping atoms (see Section I.1.1.a and I.1.1.b).

### 1.1.a Doppler effect

The idea to cool neutral atoms with lasers was first proposed in 1975 by T. Hänsch and A. Schawlow[HS75] (and independently by Wineland and Dehmelt [WD75] for ions). Due to Doppler effect an atom with speed  $v_i > 0$  sees photons coming from the left (in the same direction) with a shifted frequency  $\omega_{\text{left}} = \omega_L - k_L v_i$  and from the right (opposite direction)  $\omega_{\text{right}} = \omega_L + k_L v_i$ . The effective detuning with photon of opposite direction is then  $\tilde{\delta}_{\text{opposite}} = \delta + k_L |v_i|$ . To favor absorption of photons with opposite direction (to reduce the atom velocity after absorption) the detuning  $\delta$  must be negative (redshifted Laser).

### 1.1.b Zeeman effect

Zeeman effect is the energy split of an excited level due to the coupling of an external magnetic field  $\vec{B}$  with the total magnetic dipole moment of electrons  $\vec{\mu}_J = \vec{\mu}_L + \vec{\mu}_S$  ( $J = L + S$  is the total angular momentum,  $L$  is the angular momentum and  $S$  is the spin angular momentum). Let's take the example of a  $J = 0 \rightarrow J' = 1$  transition. Ground state  $|g, J = 0\rangle$  with no magnetic moment is not affected while excited state with  $|e, J = 1\rangle$  sees an energy shift (for weak magnetic field)

$$\Delta E_{\text{Zeeman}} = g_J m_J \mu_B B(\vec{r}),$$

where  $m_J = 0, \pm 1$  is the quantum magnetic number and  $g_J$  is the Landé factor for the atom considered and  $\mu_B$  the Bohr magneton, a universal constant describing the magnetic moment of an electron. Setting two counter propagating lasers with opposite circular polarization  $\sigma^+$  and  $\sigma^-$ , Figure I.3, will then select the transition with the  $m_e = +1$  or  $m_e = -1$  respectively.

The magnetic field created by the two anti-Helmholtz magnetic coils is

$$B(x, y, z) = |\Delta_r B| \left( x \vec{e}_x + \frac{1}{2} (y \vec{e}_y + z \vec{e}_z) \right) \quad (\text{I.1})$$

where  $|\Delta_r B| \simeq 10 \text{ G}\cdot\text{cm}^{-1}$  is the value of the constant gradient imposed. In the end the effective detuning depend on position  $\tilde{\delta} = \delta - m_J g_J \mu_B |\Delta_r B| r_i / \hbar$ , we call  $\mu_i = g_J \mu_B |\Delta_r B| / \hbar$ .

1. The lasers wavelength can be slightly modified with an acoustic-optic modulator.

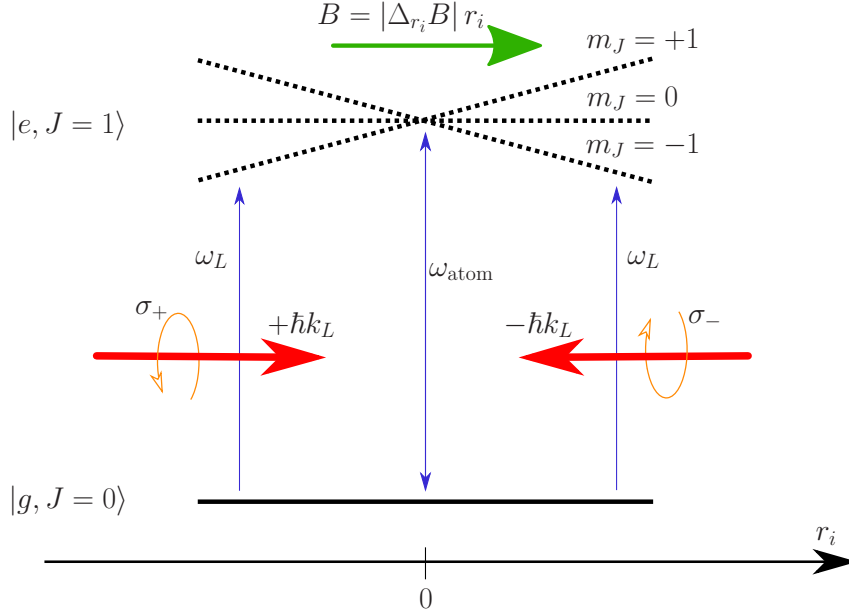


Figure I.3 – Representation of the Zeeman effect in a MOT set up. The energy level 1 is degenerate in three levels  $m_e = +1, 0, -1$  (dotted lines) due to the magnetic field. The constant magnetic gradient insures a linear spatial dependency upon the energy levels  $m_e = +1, -1$ . Two counter propagating lasers (red lines) with opposite polarization  $\sigma_+$  and  $\sigma_-$ , to select absorption of photons with levels  $m_e = +1$  and  $m_e = -1$  respectively.

### 1.1.c Radiation pressure

The first MOT was reported in [RPC<sup>+</sup>87] for Sodium atoms using the radiation pressure of photons on atoms. We describe here the basic mechanisms for two level atoms.

- Absorption: atoms gain  $\hbar\vec{k}_L$
- There are two different mechanism for an atom to relax toward equilibrium
  - Stimulated emission. Emission of the photon in the same direction, so the total momentum gain for the atom is zero, Figure I.4.
  - Spontaneous emission Figure I.4. The atom is reemitted with a random direction. In particular, the probability to be reemitted in direction  $\hbar\vec{k}'_L$  is the same that the probability to be reemitted in  $-\hbar\vec{k}'_L$ , so the momentum gain is on average  $\hbar\langle\vec{k}'_L\rangle = 0$ . In general, this probability is assumed to be isotropic. So, on average the total process absorption+emission gives a gain of  $\hbar\vec{k}_L + \hbar\langle\vec{k}'_L\rangle = \hbar\vec{k}_L$ .

So, the total force in average is

$$\vec{F}_{\text{rad}} = \hbar\vec{k}_L r_e \quad (\text{I.2})$$

where

$$r_e = \Gamma_d P_e \quad (\text{I.3})$$

is the rate of spontaneous emission [Dal14], with  $P_e$  the probability to be in the excited state. This population number is given by optical Bloch equations mixing a coherent process of interaction atom-laser and incoherent process of spontaneous emission. It gives, if the laser is not too powerful (i.e. that the Rabi frequency  $\Omega_r$  of one atom should be very small compared to the optical frequency  $\omega_L \simeq 384 \cdot 10^{12}$  Hz, which can be checked after the fact). The Rabi

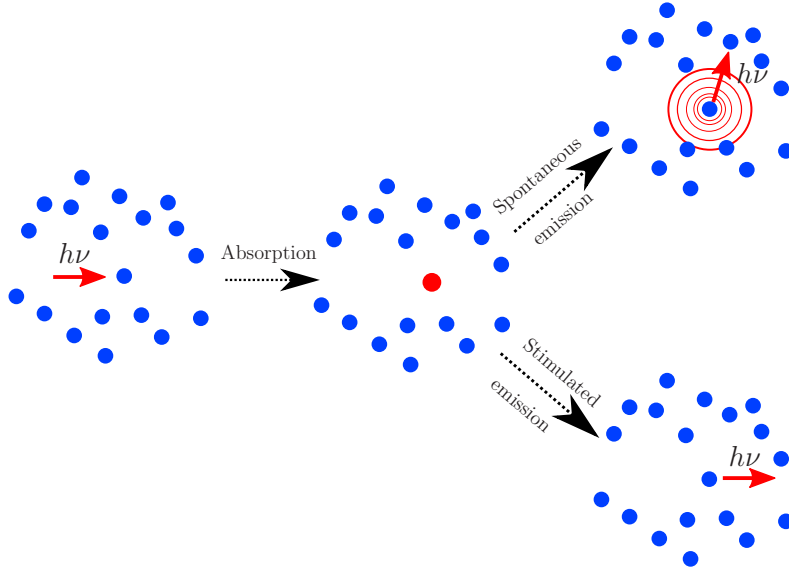


Figure I.4 – Schematic representation of the two different scattering processes stimulated/spontaneous emission. The red color stands for the energy.

frequency<sup>2</sup> is the oscillation frequency between excited and fundamental state due to the laser forcing

$$\Omega_r = \frac{d_p E}{\hbar} = \Gamma_d \sqrt{\frac{I}{2I_{\text{sat}}}} \quad (\text{I.4})$$

where  $E$  is the electric field of amplitude,  $d_p$  the transition dipole moment for the transition  $1 \rightarrow 2$ . In experiments, we use the intensity of the laser  $I$  and the saturation intensity  $I_{\text{sat}}$  (define thought Eq. (I.4)). For our experimental regimes  $I \sim I_{\text{sat}}$  (see Section I.3.2 for typical experimental values), hence we have indeed  $\Omega_r \sim 10^7$  Hz  $\ll \omega_L$ . When  $I/I_{\text{sat}} = 1$  spontaneous and stimulated emission are equally probable.

The saturation parameter

$$s = \frac{I/I_{\text{sat}}}{1 + 4\delta^2/\Gamma_d^2} \quad (\text{I.5})$$

is related to

$$P_e = \frac{1}{2} \frac{s}{1 + s}. \quad (\text{I.6})$$

Hence, the radiation pressure is

$$F_{\text{rad}} = \frac{1}{2} \hbar k_L \Gamma_d \frac{s}{1 + s}. \quad (\text{I.7})$$

Note that this approach, i.e. consider a mean force for all the photon absorptions/emission cycles, is valid for a fixed saturation rate  $s$ . Hence the spatial and velocity dependency of  $s$  (through Zeeman and Doppler effect) must be smooth in order that after a photon hit  $s(\vec{r} + \Delta\vec{r}, \vec{v} + \Delta\vec{v}) \approx s(\vec{r}, \vec{v})$ . The recoil speed after one hit for an atom is

$$\Delta v = \frac{\hbar k_L}{m} \stackrel{\text{Rb}}{\simeq} 5.98 \text{ mm/s}. \quad (\text{I.8})$$

2. Here we are just interested in the modulus of the Rabi frequency, a complex description includes a phase term with the Laser.

The condition is then

$$\omega_r = k_L \Delta v = \frac{\hbar k_L^2}{m} \ll \Gamma_d \quad (\text{I.9})$$

which is known as the **thick band condition**. For Rubidium atoms this condition is satisfied with  $\omega_r = 4.82 \cdot 10^4$  Hz and  $\Gamma_d = 3.80 \cdot 10^7$  Hz.

We will note the lasers propagating in the same direction as the axis  $I_+$  and the opposite one  $I_-$ .

In the weak saturation regime  $s_0 = s(\vec{r} = 0, \vec{v} = 0) \ll 1$ ,

$$F_{\text{rad}} \approx \frac{1}{2} \hbar k_L s(\vec{r}, \vec{v}).$$

Therefore, in one dimension<sup>3</sup> in a weakly saturated regime  $s_0 \ll 1$  adding the Doppler/Zeeman detuning yields the radiation force

$$\vec{F}_{\text{rad}} \cdot \vec{e}_i = \frac{I_0 \hbar k_L \Gamma_d}{I_s 2} \left( \frac{\overbrace{1}^{\text{"left laser"}=I_+}}{1 + 4 \left( \frac{\delta - k_L v_i - \mu_i r_i}{\Gamma_d} \right)^2} - \frac{\overbrace{1}^{\text{"right laser"}=I_-}}{1 + 4 \left( \frac{\delta + k_L v_i + \mu_i r_i}{\Gamma_d} \right)^2} \right). \quad (\text{I.10})$$

Expanding the denominator for small Doppler/Zeeman shifts gives a linearized force with a friction and harmonic trapping term,

$$\vec{F}_{\text{rad}} \cdot \vec{e}_i \simeq -m\gamma v_i - m\omega_0^2 r_i \quad \text{for} \quad \left| \frac{k_L v_i}{\delta} \right| \ll 1, \quad \left| \frac{\mu_i r_i}{\delta} \right| \ll 1, \quad (\text{I.11})$$

where we define the coefficients below.

— The effective friction parameter

$$\gamma = \frac{I_0 8 \hbar k_L^2}{I_s m} \frac{(-\delta)/\Gamma_d}{(1 + 4\delta^2/\Gamma_d^2)^2}.$$

Rough estimation gives  $\gamma \leq 9.6 \times 10^3 \text{ s}^{-1}$  for  $s_0 \leq 0.1$ .

— The effective pulsation of the trap

$$\omega_0^2 = \frac{I_0 8 \hbar k_L \mu}{I_s m} \frac{(-\delta)/\Gamma_d}{(1 + 4\delta^2/\Gamma_d^2)^2} = \frac{\mu}{k_L} \gamma.$$

In this configuration, the cloud is supposed to have cylindrical symmetry because  $\mu_x = 2\mu_y = 2\mu_z$ , but experimentally this asymmetry is compensated via different intensities, so in the following we will consider a spherical symmetry with  $\mu = \mu_x = \mu_y = \mu_z = g_J \mu_B |\Delta_r B| / \hbar$ . Since  $g_J \sim 1$ ,  $\mu = 8.8 \times 10^9 \text{ m}^{-1} \text{ s}^{-1}$  so  $\omega_0 \leq 3 \times 10^3$  Hz.

From this force modeling one can define a quality factor  $Q = \omega_0/\gamma$  as for damped oscillators. Here  $Q \approx 0.3$  lower than  $\frac{1}{2}$  meaning that atoms act like over damped oscillators.

From the small velocity expansion one can see that in this limit the lasers act as "optical molasses" inducing friction for atoms. Similarly, the magnetic field will act as harmonic trapping on atoms.

3. In principle interference terms should be added when summing the effect of the six lasers. A rigorous treatment [Dal14] shows that for  $s_0 \ll 1$  they can be neglected.

Another important parameter of the model is the on resonant cross section

$$\sigma_0 = \frac{\hbar\omega_L\Gamma_d}{2I_{\text{sat}}}, \quad (\text{I.12})$$

it is related to the probability of an incident photon to be absorbed by an atom. For nonzero detuning the cross section is

$$\sigma_L = \frac{\sigma_0}{(1 + 4\delta^2/\Gamma_d^2)^2}.$$

For circular polarization  $\sigma^\pm$ , [Ste01] gives  $\sigma_0 \simeq 2.9 \times 10^{-9} \text{cm}^2$ .

## 1.2 Diffusion

---

The previous Doppler effect would in principle cool atoms to zero temperature. But there are of course fluctuations setting a lower bound to the minimal temperature. The origin of those fluctuations is the random speed due to the large number of absorption/emission cycle giving to the atoms a random recoil force. It is natural to assume that atoms undergo a Brownian motion, allowing us to define a diffusion coefficient  $D_p$  [GA80, Dal14],

$$D_p = \hbar^2 k_L^2 \Gamma_d s_0 \quad (\text{I.13})$$

so, at equilibrium, after a short time of equilibration<sup>4</sup>  $\sim 1/\gamma$  (remember  $Q < 1$ ) the temperature is given by

$$k_B T = \frac{D_p}{m\gamma} = \frac{\hbar \delta^2 + \Gamma_d^2/4}{2|\delta|}. \quad (\text{I.14})$$

The temperature diverges at very small detuning, which of course is nonphysical since in this regime the linear assumption of Eq. (I.10) is not valid.

The minimal possible temperature (in the Doppler limit)  $T_{\text{min}}$  is for  $\delta = -\Gamma_d/2$ ,

$$k_B T_{\text{min}} = \frac{\hbar\Gamma_d}{2}. \quad (\text{I.15})$$

For Rubidium atoms,  $T_{\text{min}} \simeq 145 \mu\text{K}$ , which gives an order of magnitude for the real MOT temperature and for the speed  $v_0 = \sqrt{k_B T/m} \simeq 11.9 \text{cm/s}$  with this speed we can check self consistently<sup>5</sup> the Brownian motion assumption and the development made in Eq. (I.10). Due to more complex structure than two energy levels, there exists systems with sub-Doppler temperatures [MYMB10, CHB<sup>+</sup>14].

---

4.  $1/\gamma = \frac{m}{\hbar k_L^2} \frac{1}{2s_0} \gtrsim 100 \mu\text{s}$  for  $s_0 = 0.1$  (which we can consider to be the largest acceptable saturation parameter in the small  $s_0$  limit).

5. The speed recoil is small in front of the mean speed  $\frac{\Delta v}{v_0} = 2\sqrt{\omega_r/\Gamma_d} \ll 1$  validating the Brownian approach.  $\frac{k_L v_0}{\Gamma_d} = \sqrt{\omega_r/\Gamma_d} \ll 1$  so the linearization is valid.

### 1.3 Shadow effect: an effective attractive force between atoms

In 1988 Dalibard proposed the first model to describe effective interaction between atoms [Dal88]. Indeed, for atoms trapped in a harmonic potential. He considers the fact that the laser is absorbed as it crosses the cloud, so its entrance intensity  $I_0$  will be reduced at the cloud exit. This position dependence of the laser intensity for a laser propagating on the  $z^+$ -axis (other direction lead to similar expressions) can be written as:

$$I_+(x, y, z + dz) - I_+(x, y, z) = \text{absorption} \\ = - \left( I_+[f](x, y, z) \underbrace{\int_{\mathbb{R}} \sigma(z, v'_z) f(x', y', z', v'_z) \delta(x - x') \delta(y - y') dv'_x dv'_y dv'_z}_{\text{portion of absorbed photons}} \right) dz \quad (\text{I.16})$$

with  $I_+(-\infty) = I_0$  and the absorption section (depending on the detuning and thus on position and velocity via the Doppler/Zeman effect)

$$\sigma_{\pm}(z, v_z) = \frac{\sigma_0}{1 + 4 \left( \frac{\delta \mp k_L v_z \mp \mu z}{\Gamma_d} \right)^2}. \quad (\text{I.17})$$

So

$$\frac{dI_{\pm}}{dz}(z) = - \left( I_{\pm}[f](z) \int_{\mathbb{R}} \sigma_{\pm}(z, v') f(z, v'_z) dv'_z \right) \quad (\text{I.18})$$

and

$$\vec{F}_{\text{rad}} \cdot \vec{e}_i = \frac{\hbar k_L \Gamma_d}{2} \left( \frac{I_+[f](r_i)/I_s}{1 + 4 \left( \frac{\delta - k_L v_i - \mu_i r_i}{\Gamma_d} \right)^2} - \frac{I_-[f](r_i)/I_s}{1 + 4 \left( \frac{\delta + k_L v_i + \mu_i r_i}{\Gamma_d} \right)^2} \right). \quad (\text{I.19})$$

with the formal solutions of Eq. (I.18),

$$I_+[f](z) = I_0 \exp \left( - \int_{-\infty}^z \int_{\mathbb{R}} \sigma_+(z', v') f(z', v'_z) dv'_z dz' \right) \quad (\text{I.20a})$$

$$I_-[f](z) = I_0 \exp \left( - \int_z^{+\infty} \int_{\mathbb{R}} \sigma_-(z', v') f(z', v'_z) dv'_z dz' \right). \quad (\text{I.20b})$$

To quantify absorption in the cloud we use an experimentally rather accessible quantity: the optical density (or optical thickness)  $b(\delta)$  defined as

$$e^{-b} = \exp \left( - \int_{-\infty}^{\infty} \int_{\mathbb{R}} \sigma_+(z', v') f(z', v'_z) dv'_z dz' \right). \quad (\text{I.21})$$

For the VLMOT used at INLN its value it typically  $b(\delta = 0) \simeq 100$ .

If we suppose the absorption to be small for working regime  $-\delta/\Gamma_d \simeq 4$ , we can expand the exponential terms<sup>6</sup> to get a total radiation force of the form

$$\vec{F}_{\text{rad}} = -m\gamma\vec{v} - m\omega_0^2\vec{r} + \vec{F}_s[f](\vec{r}) + o \left( \left| \frac{k_L v_i}{\delta} \right|, \left| \frac{\mu_i r_i}{\delta} \right|, b \right), \quad (\text{I.22})$$

6. Note that in fact even for  $\delta = -4\Gamma_d$ ,  $b \sim 1$  which is not small, so the expansion might not be valid. But since there is no better theory available in this regime we keep the expansion.

where

$$\vec{F}_s[f](\vec{r}) = \frac{-\frac{I_0}{I_{\text{sat}}} \frac{\hbar k_L \Gamma_d}{2} \sigma_L}{(1 + 4(\delta/\Gamma_d)^2)^2} \left[ \begin{aligned} & \left\{ \left( \int_{-\infty}^x - \int_x^{+\infty} \right) \rho(x', y', z') \delta(y - y') \delta(z - z') dx' dy' dz' \right\} \vec{e}_x \\ & \left\{ \left( \int_{-\infty}^x - \int_x^{+\infty} \right) \rho(x', y', z') \delta(x - x') \delta(z - z') dx' dy' dz' \right\} \vec{e}_y \\ & \left\{ \left( \int_{-\infty}^z - \int_z^{+\infty} \right) \rho(x', y', z') \delta(x - x') \delta(y - y') dx' dy' dz' \right\} \vec{e}_z \end{aligned} \right]. \quad (\text{I.23})$$

The corresponding two body force is

$$(\vec{F}_s)_{\text{int}}(x, y, z) \cdot \vec{e}_x = I_0 \frac{\sigma_L^2}{c} \text{sign}(x) \delta(y) \delta(z), \quad (\text{I.24})$$

where  $\text{sign}(x < 0) = -1$  and  $\text{sign}(x > 0) = +1$ . Note that numerically one must introduce some spatial extent to the Dirac functions as in [BMW14]. Writing the divergence of this new force gives,

$$\vec{\nabla} \cdot \vec{F}_s = -6I_0 \frac{\sigma_L^2}{c} \rho(x, y, z). \quad (\text{I.25})$$

The computation of the divergence of a Newtonian force would give the same result! Explaining the analogy between gravitational systems and MOT. Nevertheless, this force is different from Newton force because it does not derive from a potential, indeed it is rotational,  $\vec{\nabla} \times \vec{F}_s \neq 0$ , and  $\vec{F}_s \neq \vec{\nabla} V_s$  for a  $V_s(\vec{r})$ . Therefore  $\vec{F}_s = \vec{\nabla} \times \vec{A}_s + \vec{\nabla} V_s$  for some couple  $(\vec{A}_s, V_s)$ . Physically the system is driven out-of-equilibrium by the six laser, this non-potential force is the mathematical translation of this fact, it induces particle flux in the system [BMW14] and complicates the mathematical analysis (a Hamiltonian is not defined for these cases).

### Remark I.1

Note that  $\partial_x |x| = \text{sign}(x) \propto (\vec{F}_s)_{\text{int}}(x)$  which shows that in one dimension the shadow effect is a conservative force (it is exactly one-dimensional gravity). It is the additional spatial dimensions that make the force non conservative.

## 1.4 Multiple scattering: an effective Coulomb force between atoms

---

The shadow effect is a first step for an effective interaction model between atoms, nevertheless this attractive force does not explain satisfactorily experimental observations that shows incompressibility of the MOT that results in a growing cloud size  $L$  [CKL14, GPLK10, WSW90]. This naturally leads one to think that in a VLMOT there is non-negligible repulsive interactions between atoms. Two years after Dalibard's paper, Walker et al. proposed the hypothesis in [WSW90] that this repulsion comes from a multiple scattering effect; indeed, so far, we have not considered what happened to a rescattered photon. There are two different possibilities for a reemitted photon

- Stimulated emission. This process is forgotten since it does not contribute to the total momentum change of atoms.
- Spontaneous emission. The atom is reemitted with a random direction. So, its probability to encounter an atom at distance  $r$  is proportional to  $1/(4\pi r^2)$  which is the inverse

surface of a  $r$ -radius sphere. The bumped atom is then pushed by this incident photon. Considering the large number of spontaneous emission cycles between two atoms, one can justify<sup>7</sup> an effective repulsive force between atoms to be  $\vec{F}_c \propto 1/r^2$ . So, if we assume **isotropic spontaneous emission**, remembering the absorption rate  $\vec{r}_e$  Eq. (I.3) (emission rate should be equal), the average force  $\vec{F}_c$  between atoms is

$$\vec{F}_c(\vec{r}) = \frac{\hbar k_L \Gamma_d I_0}{2 I_s} \frac{s}{1+s} \frac{\langle \sigma_R \rangle}{4\pi} \frac{\vec{r}}{r^3} \stackrel{s \ll 1}{\approx} I_0 \frac{\sigma_L \langle \sigma_R \rangle}{4\pi c} \frac{\vec{r}}{r^3}, \quad (\text{I.26})$$

where  $\langle \sigma_R \rangle$  is the average cross-section of rescattered photon. It is expected that  $\langle \sigma_R \rangle > \sigma_L$  since some reemitted photons are very close to resonance, so their probability of absorption is increased. In fact, the reemission spectrum is quite involved to determine and several photon frequencies are possible [Mol69]. Photons divide in to two contributions: elastic scattering with a reemitted frequency centered in  $\omega_R = \omega_L$  and inelastic scattering with  $\Omega_R = \omega_L \pm \Omega_R$ , with  $\Omega_R$  a frequency shift that can be computed in some regimes. The photons with  $\omega_L + \Omega_R$  have a detuning closer to zeros and a high absorption probability resulting in a high  $\sigma_R$  that is the dominant contribution. The ratio of elastic scattering over the total scattering is [Mol69, SCF92]  $\frac{1}{1+s}$ .

## 1.5 Other quantum effects

Rubidium atoms or other atoms used in MOT are in general more complex than a two energy level description, with hyperfine level leading to other cooling/trapping mechanism such as the Sisyphus effect [DLN<sup>+</sup>94, DCT89]. Nevertheless, in general these effects are forgotten because in regimes studied they are small (in general for small saturation parameter  $s_0$ ).

For Rubidium [DAC<sup>+</sup>00, Ste01] due to the coupling of total angular momentum of the electron  $J$  and nuclear magnetic momentum  $I$  which is much smaller, another energy splitting occurs with a new quantum number  $F = J + I$ , describing the hyperfine structure of atoms. The magnetic field  $B$  splits each  $F$  level into  $2F + 1$  levels which has a linear dependence for small  $B$  (more precisely if the shift induced by  $B$  is small in front of the hyperfine splitting). So, the actual Landé factor for Rb<sup>87</sup> should satisfy  $g_F \neq g_J$ . For example, the two-level transition used for trapping with Rubidium is  $F_g = 2 \rightarrow F_e = 3$ .

In parallel to the hyperfine structure effects, there is the "dressed atom" approach that computes the rescattering cross section  $\langle \sigma_R \rangle$  [RHV11] and deals with the physics at large saturation  $s_0$  [MS79, LPR<sup>+</sup>89]. For example, in [MYMB10] and [CHB<sup>+</sup>14] the effect of  $I_0/I_{\text{sat}}$  (small or not) is clearly measured and compared with the Doppler prediction, leading to sub-Doppler measurements.

7. A similar argument for writing the radiation pressure Eq. (I.7) should be used, verifying that the thick band approximation is enough to write an average force between two atoms.

## 2 SUM UP AND QUESTIONS

### 2.1 Sum-Up of the model

The standard model describing a MOT is then

- Radiation pressure of laser  $\rightarrow$  Doppler effect favors cooling of atoms  $\rightarrow$  friction force  $\vec{F}_{\text{fr}} = -m\gamma\vec{v}$
- Magnet coils  $\rightarrow$  splitting of energy levels  $\rightarrow$  favor absorption of confining photons  $\rightarrow$  position trapping (Zeeman effect)  $\rightarrow \vec{F}_{\text{tr}} = -m\omega_0^2\vec{r}$
- The effective repulsive interaction between atoms (due to multiple scattering) is given by a potential satisfying a Poisson equation  $\vec{F}_c \propto \langle\sigma_R\rangle \sigma_L\vec{r}/r^3$
- Due to attenuation of the lasers in the cloud, there is an effective attractive force  $\vec{\nabla} \cdot \vec{F}_s \propto -\sigma_L^2\rho$ .

One expects for VLMOT  $\langle\sigma_R\rangle > \sigma_L$ , so the Coulomb like force is the dominant interaction force. This mean that the Walker et al. model does indeed predict a cloud size growing with the number of particles since the repulsion dominated. It means that up to some modification (trapping, friction diffusion, shadow force) a VLMOT behave like a plasma of charged particles. Of course, this conclusion is appealing as plasma physics is very rich and well investigated. But due to the relative complexity of the various effects considered for the model it is also legitimate to question this "to good to be true" vision of VLMOT. In the next Section, we review some experiments linked with those questions.

### 2.2 Experimental confirmation?

The Doppler/Zeeman cooling and trapping have been observed since the beginning of MOTs with for example temperature measurements and cloud size (e.g. [RPC<sup>+</sup>87, SF91, MYMB10]). The shadow effect has also been observed in 1D or 2D MOTs (meaning the magnetic field is very strong in two or one dimension leading to consider only the other(s) remaining dimension) with respectively cigar or disc shapes. Indeed, in those asymmetric setting multiple scattering is expected to be much weaker, the reason being that most of the rescattered photons escape the trap in another dimension of the MOT.

A list of the experimental clues in favor of this form of long-range Coulomb force is the following

- Scaling experiments [CKL14, GPLK10, Gat08] where  $L \sim N^{1/3}$ . A skeptic would say as a disclaimer that other types of non long-range interactions can give the same scaling e.g. imagine a set of tennis balls (hard spheres) bound together also have  $L \sim N^{1/3}$ .
- Coulomb explosion. [PSDJ00, Pru12] tested the expansion speed of a cloud when the Zeeman trapping is turned off The result shows a good agreement with what is predicted for a similar Coulomb gas.
- MOT instabilities. In the works [TMK10, LMK06], the authors tested some instability threshold for the MOT due to the non linearity in the radiation pressure. If the instability criterion is found using the Coulomb force for the multiple scattering, it is also not a direct test of the force.

To the author's knowledge these are the only experimental evidences agreeing quantitatively

with the Coulomb nature of the repulsion. Of course, finding the Debye length in a MOT would incontestably highlight the plasma like nature of VLMOT. That is what we will seek.

### 3 NON NEUTRAL PLASMA

We have seen in previous Section that if one forgets about the shadow effect, the VLMOT description in term of forces is equivalent to a plasma formed by electrons pushing each other via Coulomb force and trapped by a harmonic trap. This model is known as the Non Neutral Plasma (NNP) model. NNP experiments are done with a Penning trap [DMF88, MDB<sup>+</sup>88] that traps one charged species (e.g. electrons) with a magnetic and electric field. Another similar model, that we will also refer to is the One Component Plasma (OCP). It is a plasma composed with electrons embedded in a uniform neutralizing background of large positive ions (see [DO99, Ich82, TLB99] for reviews on the subject).

The primary goal of the collaboration and this work is to highlight the similitudes between VLMOT "standard model" and NNP with observables unilaterally characteristic of Coulomb interactions (more selective than the scaling law  $L \sim N^{1/3}$ ). At this point we had two ideas, one was to look directly at the correlations in the system and compare them with those of the NNP model. The other idea was to force the system with an external sinusoidal potential and look at the response of the cloud, a dependence on the force nature (attractive/repulsive and short/long-range) is then expected depending on the sinusoidal modulation.

After defining precisely NNP model and giving its essential parameters and features such as the Debye length we will do a recap of the different expected experimental values for the VLMOT comparing it with some true plasma in Table I.1.

Then we will present different relevant observables of an NNP adapted to a VLMOT.

#### 3.1 Presentation of NNP model

##### 3.1.a Standard NNP model

The NNP model is formed with a single charged species, in general electrons, trapped with a harmonic force. The  $N$  electrons interact through long-range Coulomb force

$$\vec{F}_c = \frac{C}{r^3} \vec{r} \quad (\text{I.27})$$

where here  $C = I_0 \frac{\sigma_L \langle \sigma_R \rangle}{4\pi c} \approx 10^{-34} \text{ N}\cdot\text{m}^2$ . For electrons  $C_{\text{elec}} = q^2 / (4\pi\epsilon_0) \simeq 2 \cdot 10^{-28} \text{ N}\cdot\text{m}^2$  ( $q$  the electron charge and  $\epsilon_0$  the vacuum permittivity). So, there is an order  $10^6$  difference and the effective repulsion between MOT's atoms coupling is very weak.

The Poisson equation satisfied by the associated potential  $V_c$  is

$$\Delta V_c = -4\pi C \delta(\vec{r}). \quad (\text{I.28})$$

The  $N$  evolution equations for the standard NNP systems are

$$\dot{\vec{r}}_i = \vec{v}_i, \quad (\text{I.29a})$$

$$m \dot{\vec{v}}_i = \vec{F}_{\text{trap}}(\vec{r}) + \sum_{i \neq j} \vec{F}_c(\vec{r}_j - \vec{r}_i) \quad (\text{I.29b})$$

where  $\vec{F}_{\text{trap}}(\vec{r}) = -m\omega_0^2\vec{r}$ . When  $N \rightarrow \infty$ , as we have seen in the Introduction we can write in the mean field approximation the Vlasov equation

$$\partial_t f + \vec{v} \cdot \vec{\nabla}_r f + \frac{(\vec{F}_c[f] + \vec{F}_{\text{trap}})}{m} \cdot \vec{\nabla}_v f = 0. \quad (\text{I.30})$$

### 3.1.b NNP model for the MOT

When adding the other forces present in a MOT to the NNP model, such as friction, diffusion and shadow effect we get

$$\dot{\vec{r}}_i = \vec{v}_i, \quad (\text{I.31a})$$

$$m \dot{\vec{v}}_i = -\gamma \vec{v}_i - m\omega_0^2 \vec{r}_i + \sum_{i \neq j} \vec{F}_{\text{int}}(\vec{r}_j - \vec{r}_i) + \vec{\xi}(t), \quad (\text{I.31b})$$

where  $\vec{F}_{\text{int}} = \vec{F}_c + \vec{F}_s$ ,  $\xi$  is a stochastic Gaussian variable accounting for the random noise<sup>8</sup>

$$\langle \xi(t) \rangle = 0 \quad (\text{I.32a})$$

$$\langle \xi(t_1) \xi(t_2) \rangle = 2\gamma k_B T \delta(t_2 - t_1) \quad (\text{I.32b})$$

Then again in the large  $N$  limit one gets the Vlasov-Fokker-Planck equation

$$\partial_t f + \vec{v} \cdot \vec{\nabla}_r f + \frac{(\vec{F}_{\text{trap}} + \vec{F}_c[f] + \vec{F}_s)}{m} \cdot \vec{\nabla}_v f = \gamma \vec{\nabla}_v \cdot \left( \vec{v} f + \frac{k_B T}{m} \vec{\nabla}_v f \right) \quad (\text{I.33a})$$

and the associated Poisson equations

$$\vec{\nabla} \cdot \vec{F}_c = -\Delta \phi_c = 4\pi C \rho, \quad (\text{I.33b})$$

$$\vec{\nabla} \cdot \vec{F}_s = -6\sigma d\rho. \quad (\text{I.33c})$$

The friction and diffusion model possess a return toward thermal equilibrium that the original Vlasov equation does not have. In [RHV11] is considered the Fokker-Planck equation without expanding the radiation pressure force, leading to a position and velocity dependent diffusion coefficient and drift term. In our regime of low saturation and thick band, their model reduces to our equation Eq. (I.33a).

After a fast time<sup>9</sup>  $1/\gamma$ , the velocity distribution relaxes to a Gaussian equilibrium leading for the spatial density evolution to a Fokker-Planck equation (also called nonlinear Smoluchowski equation)

$$\gamma \partial_t \rho(\vec{r}) = \vec{\nabla} \cdot \left( \omega_0^2 \vec{r} \rho + \frac{1}{m} (\vec{F}_c + \vec{F}_s) [\rho] \rho + \frac{k_B T}{m} \vec{\nabla} \rho \right). \quad (\text{I.34})$$

**From now on we will formally forget about the Shadow effect.** Indeed since it has the same divergence as the Coulomb force (with an opposite sign) it suffices to rescale the Coulomb parameter  $C$  to include its effect. The non potential part effects of the Shadow force will be then neglected. Actually, simulations with the full Shadow effect were performed and in the regimes relevant for the experiment, it did not add significant changes, justifying our assumption for a first exploration of the long-range effects.

8. A Gaussian noise is motivated by the discussion Section I.1.2.

9. Indeed in standard experiments the quality factor  $Q = \omega_0/\gamma$  is in the over-damped regime  $Q < \frac{1}{2}$ .

### Density profile for zero temperature

The most natural observable is the density profile of the cloud. Without correlation at zero temperature, the density solution of Eq. (I.34) is expected to have "rigid" boundaries  $\rho(\vec{r}) = \rho_0(\vec{r})\Theta(L - r)$  where  $L$  is the cloud radius<sup>10</sup>.

From Eq. (I.34) at  $T = 0$  K one possible solution satisfies for  $\rho \neq 0$

$$m\omega_0^2\vec{r} + \vec{F}_c[\rho] = 0.$$

Applying the divergence operator  $\vec{\nabla} \cdot$  gives a constant density profile for  $r < L$ ,

$$\rho(\vec{r}) = \frac{3m\omega_0^2}{4\pi C}\Theta(L - r) \quad (\text{I.35a})$$

with the inside density

$$\rho^0 = \frac{3m\omega_0^2}{4\pi C}. \quad (\text{I.35b})$$

The cloud radius  $L$  can be computed from the normalization condition

$$\int_{\mathbb{R}^3} \rho(\vec{r}) d^3r = 4\pi \int_0^\infty r^2 \rho(r) dr = \frac{4\pi L^3 \rho_0}{3} = N; \quad (\text{I.36})$$

thus,

$$L = \left( \frac{NC}{m\omega_0^2} \right)^{1/3}. \quad (\text{I.37})$$

So  $L \propto N^{1/3}$  for the NNP model. This was more or less observed in [CKL14].

### Density profile for non-interacting cloud

The in this case analytically tractable limit of the model is when particles do not interact with each other; they just feel the trapping due to the Zeeman/Doppler effect and the thermal motion.

From Eq. (I.34), one possible solution satisfies for each direction

$$m\omega_0^2 r_i \rho + k_B T \partial_{r_i} \rho = 0,$$

giving (with the normalization condition)

$$\rho_T(\vec{r}) = \frac{N}{2\pi^{3/2}} \left( \frac{m\omega_0^2}{k_B T} \right)^{3/2} \exp\left( -\frac{m\omega_0^2}{k_B T} \frac{\vec{r}^2}{2} \right), \quad (\text{I.38})$$

which does not display any  $N$ -scaling size. We can define the characteristic length (sometime called Gaussian length or one particle length) for this system as

$$l_g = \sqrt{\frac{k_B T}{m\omega_0^2}}.$$

10. For non-zero temperature, this rigid boundary is softened and one expects  $\rho(r) \rightarrow 0$  for  $r \rightarrow \infty$ .

### 3.1.c Debye length

In the OCP model, the classic computation made by Debye and Hückel [HD23] shows the existence of a typical correlation length between particles. This is the famous Debye length. In the context of a plasma with electron and large positive ions, there is a simple interpretation. The positive ions screen the long-range interactions between electrons for long distance, see Figure I.5, so the effective sphere of influence for one electron is given by the Debye radius.

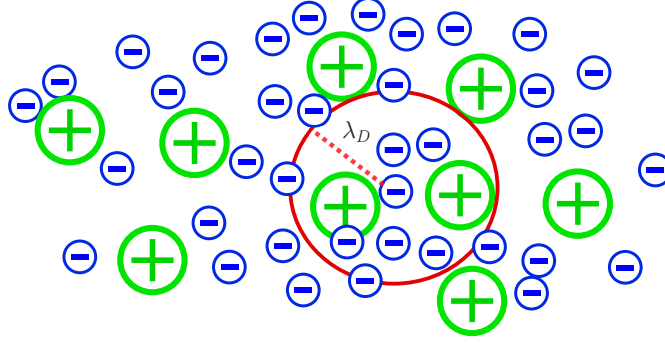


Figure I.5 – Schematic representation of a neutral plasma (OCP model) exhibiting a Debye length of effective interaction.

In the VLMOT model, the neutralizing background of positive ions (OCP model) is replaced by the trapping potential (NNP model). Formally a Debye length is also expected. We will only show the Debye-Hückel computation for this case.

Imagine the system is at statistical equilibrium with a constant density profile  $\rho^0$  and you add a small perturbation, one particle at  $\vec{r} = 0$ . The perturbed profile is given by the Boltzmann factor

$$\rho(\vec{r}) = \rho^0 e^{-\phi_{\text{tot}}(\vec{r})/(k_B T)}, \quad (\text{I.39})$$

and the associated Poisson equation for the total potential is

$$\Delta\phi_{\text{tot}}[\rho(\vec{r})] = \Delta\phi_c[\rho(\vec{r})] + \Delta\phi_{\text{tr}}(\vec{r}) = -4\pi C\rho(\vec{r}) - m\omega_0^2 - 4\pi C\delta(\vec{r}). \quad (\text{I.40})$$

When the temperature is large with respect to the potential created (typically  $\frac{\phi_{\text{tot}}}{k_B T} \ll 1$ ), it is legitimated to expand

$$\Delta\phi_{\text{tot}} = -4\pi C\rho_0 + \frac{4\pi C}{k_B T}\rho^0\phi_{\text{tot}} + 3m\omega_0^2 - 4\pi C\delta(\vec{r}). \quad (\text{I.41})$$

Defining the Debye length <sup>11</sup> as

$$\lambda_D = \sqrt{\frac{k_B T}{3m\omega_0^2}}, \quad (\text{I.42})$$

we get a total potential of the form

$$\left(\Delta - \frac{1}{\lambda_D^2}\right)\phi_{\text{tot}} = -4\pi C\delta(\vec{r}), \quad (\text{I.43})$$

11. Note that  $l_g = \sqrt{3}\lambda_D$

and solution is known as the Yukawa potential

$$\phi_{\text{tot}}(r) = C \frac{e^{-r/\lambda_D}}{r}. \quad (\text{I.44})$$

So, the typical potential created by a particle is screened (strongly attenuated) for distance larger than the Debye length. For  $\lambda_D \rightarrow \infty$ , this potential is again the Coulomb potential as expected.

### 3.1.d Plasma parameter

The experimental set up is believed to be in a 'gas like phase' quantified by the plasma parameter  $\Gamma$  which is the ratio of the typical potential energy between two particles to the typical kinetic energy of a particle

$$\Gamma = \frac{C/a}{k_B T} = \frac{C}{k_B T} \left( \frac{m\omega_0^2}{C} \right)^{1/3} = \frac{a^2}{3\lambda_D^2} \quad (\text{I.45})$$

where  $a$  is the mean distance between particles

$$a = \frac{L}{N^{1/3}} = \left( \frac{C}{m\omega_0^2} \right)^{1/3}. \quad (\text{I.46})$$

Note that in  $\Gamma \ll 1$  regime we justify the derivation made for the Debye length in Eq. (I.43), which means that for other regime  $\Gamma > 1$  the Debye length is not physically relevant any more. It becomes smaller than the inter-particles distance Eq. (I.45).

This is the unique parameter determining the system state for the NNP model (when the system size is infinite or with periodic boundary conditions), it measures the correlation in the system. For the standard OCP model, there is one phase transition from liquid phase to solid phase (see the Los Alamos National Laboratory Plasma group [website](#)<sup>12</sup> for nice illustrations),

Fluid	Solid
Gas-like   Liquid-like	
$\Gamma \ll 1$   $\Gamma \sim 1 - 100$	$\Gamma > 175$

For the finite sized MOT, we also consider

$$h = l_g/L \quad (\text{I.47})$$

which quantifies in a way the finite size and temperature effects.

To have a gas like phase and a quasi-step function density profile we need

$$\Gamma = \frac{a^2}{l_g^2} \ll 1 \quad (\text{I.48})$$

$$h = \frac{l_g}{L} \ll 1 \quad (\text{I.49})$$

this regime is believed to be the one of the VLMOT of INLN.

12. <http://www.lanl.gov/projects/dense-plasma-theory/research/one-component-plasma.php>

A last characteristic plasma parameter is the plasma frequency (also called Langmuir frequency) defined for a MOT as

$$\omega_p = \sqrt{\frac{4\pi\rho^0 C}{m}} = \sqrt{3}\omega_0. \quad (\text{I.50})$$

It characterizes the fast oscillation of the atoms when small perturbations move aside a plasma from a homogeneous distribution. In fact, those oscillations can be related to the Landau damping mechanism that we will study in details in Section V.4.

### 3.2 Some numerical values for experimental MOT

In our MOT, the plasma parameter is weak  $\Gamma \sim 10^{-4}$ , which means that the interactions are weak in comparison with kinetic energy. Thus, one does not expect a liquid or crystal structure in the atomic cloud but rather a gas like medium. This is the weak correlations regime.

Small MOTs size has been measured (e.g. [RPC<sup>+</sup>87]) to be of the order of  $100 \mu\text{m}$ . In these MOTs we expect no Coulomb interactions between atoms. Hence the particles follow a Gaussian distribution Eq. (I.38) with  $l_g \sim 100 \mu\text{m}$ . Since  $l_g = \sqrt{3}\lambda_D$ , we have an expectation value for the Debye length, that in principle should remain true for very large MOTS with repulsive interactions.

In Table I.1 we present some typical value for known weakly coupled ( $\Gamma \ll 1$ ) plasma and compare them with the VLMOT. Despite that the INLN MOT is far from known a regime of plasma it shares some parameters with magnetic fusion plasma.

	$T$ (K)	$\rho^0$ (cm <sup>-3</sup> )	$L$ (cm)	$\Gamma$	$h$	$a$ (cm)	$\lambda_D$ (cm)	$\omega_p$ (rad/s)
Magnetic Fusion	$10^8$	$10^{14}$	100	$10^{-7}$	$10^{-4}$	$10^{-5}$	$10^{-2}$	$6 \cdot 10^{11}$
Solar Wind	$10^5$	10	$6 \cdot 10^5$	$10^{-8}$	$10^{-3}$	0.1	$2 \cdot 10^5$	$7 \cdot 10^3$
Galactic center	$10^7$	$10^2$	$10^{17}$	$10^{-10}$	$10^{-14}$	0.08	$3 \cdot 10^3$	$6 \cdot 10^5$
VLMOT	$10^{-4}$	$10^{11}$	1	$10^{-4}$	0.01	$10^{-4}$	$10^{-2}$	$10^3$

Table I.1 – Some typical parameters for weakly coupled plasma.

So far we have gathered a number of parameters to characterize the system. Here we try to give an overview of them with some typical experimental values.

The number of atoms can be varied over several orders of magnitudes from  $N = 10^6$  to  $10^{11}$  for the INLN MOT. For  $N \sim 10^{11}$  one has  $L \simeq 1 \text{ cm}$  with a density  $\rho_0 \sim 10^{11} \text{ atoms/cm}^3$ . The on resonance optical thickness is computed with the measured maximal density (which is assumed constant along the cloud) and the cloud size  $L$  Eq. (I.21),

$$b_0 = 2L\sigma_0\rho^0 \sim 100.$$

It might seem large and completely invalidate the small  $b$  hypothesis needed to express the shadow effect but it decreases quickly with the detuning since

$$b(\delta) = \frac{b_0}{1 + 4\delta^2/\Gamma_d^2}, \quad (\text{I.51})$$

insuring that experimental working detuning  $b(|\delta|) \sim 1$ .

Here is a list of several other values

- 
- $k_L = \frac{2\pi}{780} \text{ nm}^{-1}$  is the wavenumber of the laser
  - $m = m_{\text{Rd}} = 1.443 \times 10^{-25} \text{ kg}$  is the atom mass (while  $m_{\text{electron}} = 9.1 \cdot 10^{-31} \text{ kg}$ )
  - Two energy level rubidium atoms  $\Delta E = \hbar\omega_{\text{atom}} \simeq 1.589 \text{ eV}$ , with the corresponding wavelength  $\lambda_{\text{atom}} = 780.241 \text{ nm}$  (in vacuum)
  - Temperature  $\sim 150 \mu\text{K}$
  - $I_0 \approx 1.2 \text{ mW/cm}^{-2}$  lasers intensity
  - $I_s = 1.67 \text{ mW/cm}^{-2}$  [Ste01].
  - $\Gamma_d = 2\pi \times 6.06 \text{ MHz}$  natural width of the atomic transition for Rubidium atoms at resonance at  $\omega_{\text{atom}}$
  - $\sigma_0 \simeq 2.9 \times 10^{-9} \text{ cm}^2$
  - $C = I_0 \frac{\sigma_L \langle \sigma_R \rangle}{4\pi c} \approx 2 \cdot 10^{-34} \text{ N}\cdot\text{m}^2$  (while  $C_{\text{electron}} = 2 \cdot 10^{-28} \text{ N}\cdot\text{m}^2$ )
- Also, to be useful the probing of the Debye length by a laser must satisfy  $\lambda_D/\lambda_L \gg 1$



---

# THEORETICAL AND EXPERIMENTAL OBSERVABLES

---

The analogy between the MOT and NNP model is now established. The aim of this Chapter is to define the characteristic observable of the NNP model (and in general long-range systems) that could be use in a real experiment. We will also introduce our numerical simulations to illustrate those observable. In next Chapter, all those tools will serve the experimental proposal to see long-range effects.

## 1 DENSITY

---

The most obvious observable is the one point density function  $\rho(\vec{r})$  that depends directly on the interactions. Due to the supposed isotropy of the system one can in general consider only  $\rho(\vec{r}) = \rho(r)$ . However experimentally, one cannot<sup>1</sup> access this 3D profile and only an integrated profile  $\rho_x(x)$ ,

$$\rho_x(x) = \int_{-\epsilon}^L \int_{-\epsilon}^L \rho(\sqrt{x^2 + y'^2 + z'^2}) dy' dz'. \quad (\text{II.1})$$

It corresponds to what is seen when the cloud is observed with fluorescence on a slice  $-\epsilon < y = 0 < \epsilon$ .

The fluorescence technique consists in changing brutally the detuning of the confining lasers from the working experimental value to the largest detuning possible  $|\delta| = 8\Gamma_d$  and observing the photon emitted. The switch and measurement are fast enough so that the atom positions do not change much. If single scattering events are diminished " $\propto \sigma_L \downarrow$ " at large detuning,

---

1. In principle a tomography, which gives  $\rho(r)$ , is doable but experimentally somehow painful to set up.

scattering followed by rescattering on another atom  $\propto \sigma_L \sigma_R \downarrow \downarrow$  is furthermore diminished. Therefore, photons on the CCD camera mainly come from single scattering events and so are linked with the position of atoms. The resulting profile is more accurate than directly looking at the emitted light from the cloud at smaller detuning [CKL14] where both types of scattering are mixed.

So experimentally we will compare two things with the Coulomb model

- The shape of  $\rho_x(r)$
- The scaling of the cloud radius with various quantities. Practically it is easy to change
  - The detuning  $\delta$  with the disadvantage that it changes both interactions and temperature.
  - The number of particles  $N$ , that should be a well-controlled and predicted quantity.

The cloud size is experimentally measured as the Full Width at Half Maximum (FWHM) of the fluorescence profile. Per the standard model Eq. (I.35),

$$\rho_x(x) \propto \sqrt{L^2 - x^2} \Theta(L - r)$$

and  $L \sim N^{1/3}$ . [CKL14] gives

- approximatively the good  $N$ -scaling
- a density profile  $\rho_x(x)$  which is not very well fitted by the theory.

## 2 PAIR DISTRIBUTION FUNCTION

---

The pair distribution function  $g^{(2)}$  is a direct measure of correlation in the system, it is defined through the one and two point density function,

$$\rho^{(2)}(\vec{r}_2, \vec{r}_1) = g^{(2)}(\vec{r}_2, \vec{r}_1) \rho(\vec{r}_1) \rho(\vec{r}_2), \quad (\text{II.2})$$

where  $\rho^{(2)}(\vec{r}_2, \vec{r}_1)$  measures the probability of two atoms being at  $\vec{r}_2$  and  $\vec{r}_1$ . If  $g^{(2)} = 1$ , it means there are no correlations, thus a particle at  $\vec{r}_1$  will see a homogeneous density around it with no particular exclusion zone. For a weakly correlated plasma  $\Gamma \ll 1$  the pair correlation function can be found by the Debye-Hückel theory (similar calculation to that of Section I.3.1.c) as

$$g^{(2)}(\vec{r}_1, \vec{r}_2 - \vec{r}_1) \simeq g^{(2)}(r) \simeq 1 - \frac{a\Gamma}{r} e^{-r/\lambda_D} \simeq \exp\left(-\frac{a\Gamma}{r} e^{-r/\lambda_D}\right) \quad (\text{II.3})$$

where we assumed the isotropy; the last equality an interpolation between  $g^{(2)}(r=0) = 0$  and the Debye-Hückel theory, its validity is discussed in [BH80]. For small  $r \ll \lambda_D$  it is very close to zero, meaning two particles cannot collide (because of the interaction), then it goes quickly to 1, meaning for  $r > \lambda_D$  one particle "sees" a homogeneous repartition of particles.

Theoretically and numerically this quantity is very interesting and accessible, but experimentally it is not directly accessible. It would require position tracking for particles. Note that for some "dusty" plasma experiment with heavy ions it is feasible [SVH<sup>+</sup>04].

## 3 NUMERICAL EXAMPLES

---

The major issue with the simulation of a VLMOT is the number of particles. Due to the machine limitations, the simulated particle number cannot be higher than about  $N \sim 10^5$ . Thus, obtaining both low  $h$  of Eq. (I.47) and  $\Gamma$  of Eq. (I.45) is difficult. The only way to decrease one without increasing the other is to have a large  $N$ . In fact, to get  $h \sim 10^2$  and  $\Gamma \sim 10^{-4}$  as in the experiment we would need about  $N \sim 10^9$  particles...!

Nevertheless, we expect the main features we seek to remain. Thus, in Part [One](#) we will perform molecular dynamics simulations with  $N = 16384$ <sup>2</sup>.

The inter-particles distance  $a$  of Eq. (I.46) is relatively well known in experiments since both the number of particles and the size of the cloud are controlled. It is thus natural to use  $a$  to define dimensionless distances.

### 3.1 Numerical details

---

All MOT numerical simulations are performed via a 3D molecular dynamics (MD) code with a parallel implementation on a Graphical Processing Units (GPU). I gratefully acknowledge Bruno Marcos who provided the code in its original structure (for pure self-gravitating systems). I added to the code friction, diffusion<sup>3</sup> and trapping. For some tests I also coded the Shadow Force. The code performs a time integration for the  $N$  particles evolving through Eq. (I.31).

- The interaction force is coded in parallel: thanks to the block structure of GPUs the force  $F_i$  felt by an atom  $i$  can be computed simultaneously for many  $is$ . Compared with a standard Central Processing Unit (CPU) computation the number of operations is still proportional to  $N(N - 1)$  but with a coefficient greatly diminished. The speed-up depends on the number of particles, the problem and the GPU used, but here it is at least 100 times.
- The whole Langevin dynamics (with friction and diffusion) is coded according to a second order Leapfrog algorithm [[ISP10](#)].

The advantage of this code is that it computes exactly all force terms. Indeed, other codes such as GADGET [[Spr05](#)], make approximations using the long-range nature of the force to gain in computation time. It is also a disadvantage because GADGET codes are much faster. In our simulations we find a compromise between a large particle number and a reasonable simulation time with  $N = 16384$ .

---

2. This number was chosen because it is a power of two and it is optimal for GPU computing.

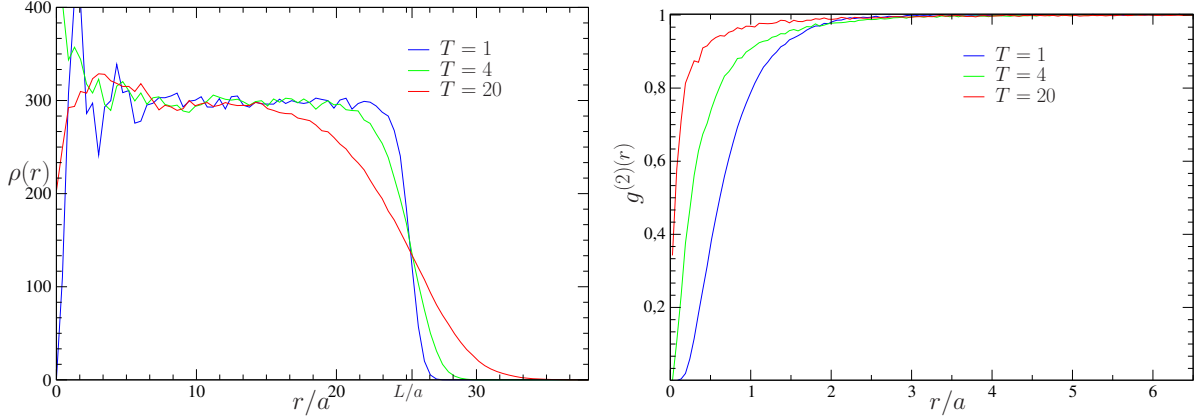
3. The cuRAND library [[CGM14](#)] allows fast random Gaussian number generation on GPU.

### 3.2 Numerics

For one snapshot the density is computed as

$$\rho(r) = \sum_{\vec{r}_1} \frac{\delta_{\Delta r}(|\vec{r}_1| - r)}{V_{\odot}(r)}, \quad (\text{II.4})$$

where  $V_{\odot} = 4\pi(r^3 - (r - \Delta r)^3)/3$  is the volume of a 3D ring between  $r$  and  $r + dr$ . Then it is averaged over at least 50 snapshots. Simulations are shown in Figure II.1(a), for different



(a) Density profile  $\rho(r)$ . We noted the theoretical length  $L$  given by Eq. (I.37).

(b) Pair correlation function  $g^{(2)}(r)$ .

Figure II.1 – Density and pair correlation functions from MD simulations for three different temperatures (see Table II.1 for parameters value).

dimensionless temperatures  $T$ . For  $h \ll 1$  the profile is a step function while for  $h \gg 1$  it has a Gaussian shape. The length of the cloud  $L$  indicated on the Figure is well recovered in simulation as well as the density  $\rho_0 = 298$ . The pair correlation function  $g^{(2)}$  is computed as follows:

$$g^{(2)}(r) = \frac{1}{N_z} \sum_{r_1 < \epsilon} \frac{\rho^{(2)}(r, \vec{r}_1)}{\rho(r_1)} = \sum_{r_1 < z} \sum_{\vec{r}_2 \neq \vec{r}_1} \frac{\delta_{\Delta r}(|\vec{r}_2 - \vec{r}_1| - r)}{V_{\odot}(r)\rho(r_1)} \quad (\text{II.5})$$

where

$$\delta_{\Delta r}(r' - r) = \begin{cases} 1, & |r' - r| < \Delta r \\ 0, & \text{elsewhere.} \end{cases} \quad (\text{II.6})$$

Here  $\epsilon$  is a parameter that should be smaller than the cloud radius but large enough to sample many particles. Just a note, the large  $r$  limit of  $g^{(2)}$  is supposed to be 1, but obviously for a finite system it will go to 0. It does not matter since the correlation effects we seek are found for small  $r$ .

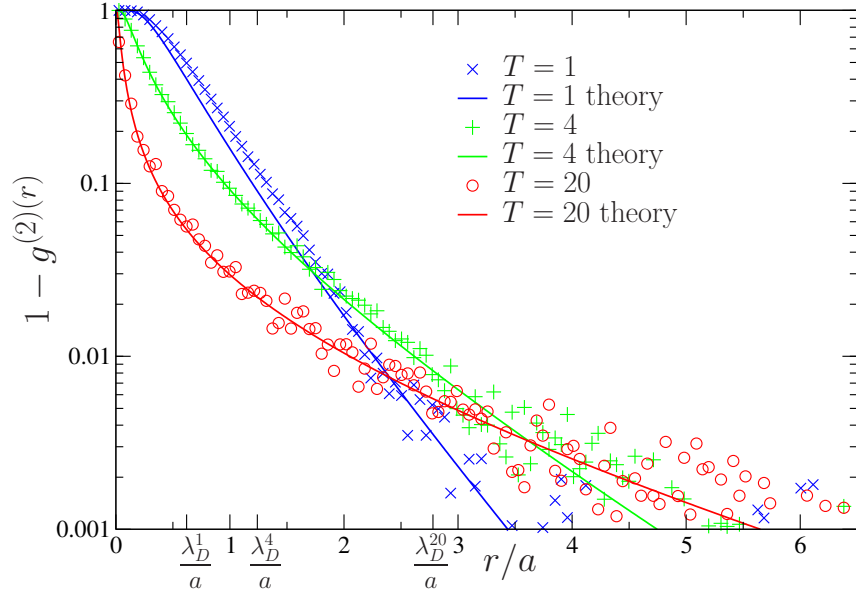


Figure II.2 –  $1 - g^{(2)}(r)$  for three different temperatures in a simulation with standard Coulombian interaction. Also, plotted is the analytical expression of  $g^{(2)}(r)$  with the computed values of  $\lambda_D$ ,  $a$  and  $\Gamma$  (see Table II.1 for parameter values)

#### Numerical test

To see these correlation effects (i.e. when  $g^{(2)}(r) \neq g_{\text{MF}}^{(2)}(r) = 1$ ) we look at  $1 - g^{(2)}(r)$  in Figure II.2. We compare the simulations with the theory of Eq. (II.3) with the theoretical parameters (hence it is not a fit). The effect of temperature is clear: on one hand for high correlations (low temperature) the theory is less accurate. On the other hand for high temperature, fluctuations are higher which may also damage the precision.

	$T = 1$	$T = 4$	$T = 20$
$\lambda_D$	0.0577	0.115	0.258
$h$	0.0245	0.0490	0.110
$\Gamma$	0.862	0.215	0.0431

Table II.1 – Parameters used in the MD simulations for different temperatures. We also have temperature independent parameters:  $\gamma = 100$ ,  $mC = 0.08$ ,  $N = 16384$ ,  $\omega_0 = 10$  so  $L = 2.36$ ,  $a = 0.093$ ,  $\rho^0 = 298$  for the three different temperatures.

## 4 STRUCTURE FACTOR

If the pair correlation function was clear to interpret and density independent, it could not be directly observed in experiment<sup>4</sup>. However, the static structure factor  $S(\vec{k})$  has the advantage that it can be directly linked to the experimental diffraction profile (see Appendix A.1). Following [HM06], we define the structure factor as

$$S(\vec{k}) = \left\langle \frac{1}{N} \rho(\vec{k}) \rho(-\vec{k}) \right\rangle = \left\langle \frac{1}{N} \left| \sum_i e^{-i\vec{k} \cdot \vec{r}_i} \right|^2 \right\rangle \quad (\text{II.7})$$

where the bracket stands for an ensemble average and we have used the empirical density Eq. (4a) to obtain the last expression

$$\rho(\vec{k}) = \int \rho(\vec{r}) e^{-i\vec{k} \cdot \vec{r}} d\vec{r} = \int \sum_{i=1}^N \delta(\vec{r} - \vec{r}_i) e^{-i\vec{k} \cdot \vec{r}} d\vec{r} = \sum_{i=1}^N e^{-i\vec{k} \cdot \vec{r}_i}. \quad (\text{II.8})$$

The ensemble average is crucial to see correlations, removing it carelessly would erase them. Another formulation of the structure factor highlights their role

$$\begin{aligned} S(\vec{k}) &= \left\langle \frac{1}{N} \left| \sum_i e^{-i\vec{k} \cdot \vec{r}_i} \right|^2 \right\rangle = \left\langle \frac{1}{N} \sum_{i=1}^N \sum_{j=1}^N e^{-i\vec{k} \cdot (\vec{r}_i - \vec{r}_j)} \right\rangle = 1 + \left\langle \frac{1}{N} \sum_{i=1}^N \sum_{j \neq i}^N e^{-i\vec{k} \cdot (\vec{r}_i - \vec{r}_j)} \right\rangle \\ &= 1 + \left\langle \frac{1}{N} \sum_{i=1}^N \sum_{j \neq i}^N \int \int e^{-i\vec{k} \cdot (\vec{r}_1 - \vec{r}_2)} \delta(\vec{r} - \vec{r}_i) \delta(\vec{r} - \vec{r}_j) d\vec{r}_1 d\vec{r}_2 \right\rangle \\ &= 1 + \frac{1}{N} \iint e^{-i\vec{k} \cdot (\vec{r}_1 - \vec{r}_2)} \rho^{(2)}(\vec{r}_1, \vec{r}_2) d\vec{r}_1 d\vec{r}_2 \end{aligned} \quad (\text{II.9})$$

where we used the definition of the empirical two point density function. So, neglecting correlations would correspond to considering  $\rho^{(2)} = \rho(\vec{r}_1) \rho(\vec{r}_2)$ . For an isotropic infinite homogeneous media ( $N \rightarrow \infty$ ), one can write

$$\begin{aligned} S(k) &= 1 + \rho_0 \int e^{-i\vec{k} \cdot \vec{r}} d\vec{r} + \rho_0 \int (g^{(2)} - 1) e^{-i\vec{k} \cdot \vec{r}} d\vec{r} = 1 + \rho_0 V_{\text{tot}} \delta(k) - 4\pi \rho_0 \int \frac{a\Gamma}{r} e^{-r/\lambda_D} e^{-i\vec{k} \cdot \vec{r}} d\vec{r} \\ &= N\delta(k) + 1 - \frac{4\pi a\Gamma \rho_0}{k^2 + 1/\lambda_D^2} = N\delta(k) + 1 - \frac{\lambda_D^{-2}}{k^2 + 1/\lambda_D^2} \\ &= N\delta(k) + \frac{k^2}{k^2 + 1/\lambda_D^2} \end{aligned} \quad (\text{II.10})$$

where the 3D Fourier transform was directly obtained from the modified Poisson equation Eq. (I.43) that is satisfied by the Yukawa potential. The Dirac function corresponds to the unscattered radiation. Without interactions  $g^{(1)} = 1$ , so one would expect

$$S_{\text{MF}} = N\delta(k) + 1.$$

In our problem, the structure factor will be modified for large wavelength due to the finite size effect, resulting in a spread peak reflecting the Fourier transform of the density profile, not just a Dirac peak.

4. However if the media is infinite, homogeneous, and isotropic it can be computed via the structure factor.

*Numerical test*

- Computing  $S(|\vec{k}| = k)$  for a MD simulation of a trapped Coulomb cloud gives Figure II.3,
- The main peak in  $S(k = 0) = N$  correspond to the unscattered radiation.
  - For small  $k \sim 1/L$ , a large peak with many bump, reflecting the step function profile of the cloud
  - For large  $k$ , the structure factor goes to 1. This contribution is always present and stands for a background noise.
  - For intermediate  $k \sim 1/\lambda_D$ , a small gap is formed and is deeper when the temperature is smaller (thus it depends on  $\lambda_D$ ). This is characteristic of the Coulomb correlations.

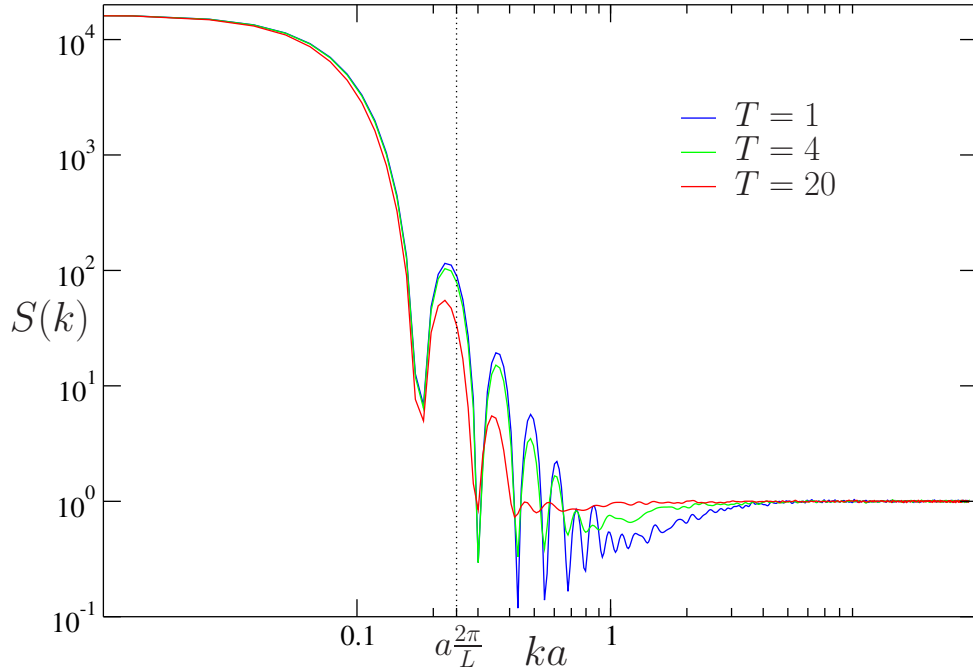


Figure II.3 – Structure factor  $S(k)$  from MD simulations averaged in all  $\vec{k}$  directions at a fixed  $|\vec{k}| = k$  for three different temperatures. We indicated the position of the peak corresponding to the cloud size  $2\pi a/L$ . For other parameters see Table II.1.

We compare these simulations with the exact overcritical expression Eq. (II.10) for  $k \gg 1/L$  in Figure II.4. Once again, the simulation/theory agreement is very good.

## 5 COMPARISON WITHOUT CORRELATIONS

We have a clear prediction for an experimental measurement of correlations: a "dip" in the structure factor characteristic of Coulomb interactions with a functional dependence that leads directly to the Debye length. Nevertheless, to be sure that this "dip" corresponds to correlations we can compare it with the structure factor of a cloud with no correlations (see Figure III.1). We propose two different ways to achieve this, one that will be useful for numerics and one that shall be used in experiments.

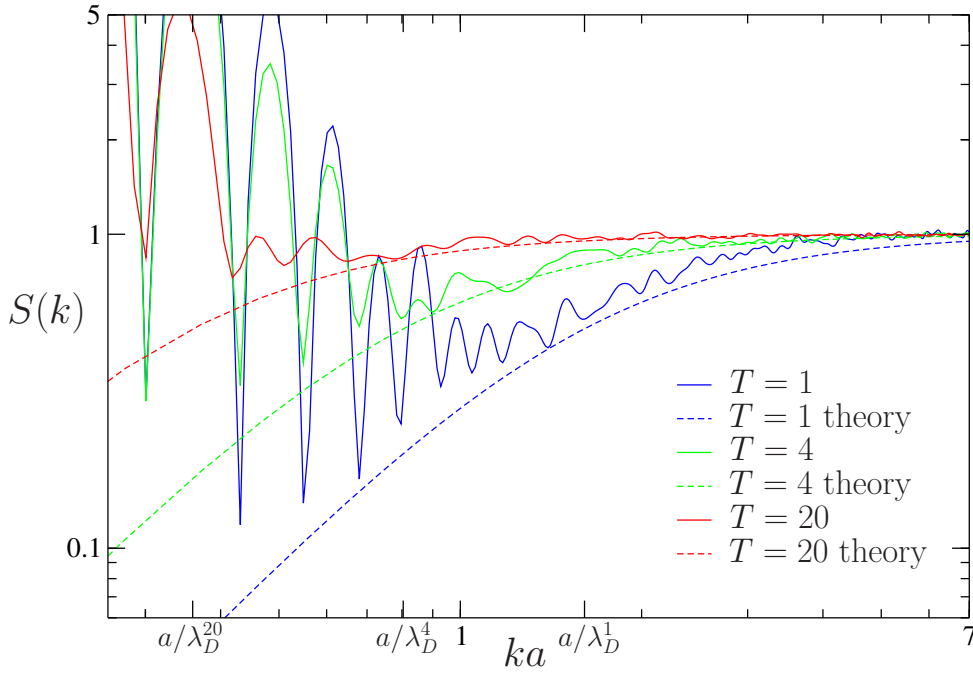


Figure II.4 – Structure factor  $S(k)$  from MD simulations averaged in all  $\vec{k}$  directions at a fixed  $|\vec{k}| = k$  for three different temperatures. We plot the non fitted theoretical expression Eq. (II.10). We indicated the position of the different Debye length. Theoretical values used are given in Table II.1.

## 5.1 Random arrangement

Numerically we know the density profile, it is then easy to draw random particle positions according to this profile. With this procedure, we have a cloud with the exact same density profile but without any correlation between particles, in particular we expect  $g^{(2)}(r) = 1$ . This method is also very useful for the structure factor since the density profile plays an important role, so keeping it constant allows us to distinguish the correlation effects without assuming an ideal profile. This will be very useful when we study different interaction models (with a priori different density shapes). However, we cannot apply this procedure in experiments.

## 5.2 Turning off the trap and interactions

In the experiment one cannot turn off interaction without turning off the lasers and thus the whole trap. When it is done, particles evolve freely with constant speed and direction. After a time  $t_D = \lambda_D / \langle |v| \rangle$  (typical time to "escape" the Debye radius), we expect correlations to have diminished greatly. Plotting the new structure factor<sup>5</sup> (Figure II.5) gives as expected a "closing

5. From now on we normalize the structure factor by  $S(0)$ .

of the dip". Note that  $t_D$  is estimated as

$$t_D = \frac{\lambda_D}{\langle |v| \rangle} = \frac{\sqrt{\frac{k_B T}{3m\omega_0^2}}}{\sqrt{\frac{8k_B T}{\pi m}}} = \sqrt{\frac{\pi}{24\omega_0^2}} \approx 1 \text{ ms.}$$

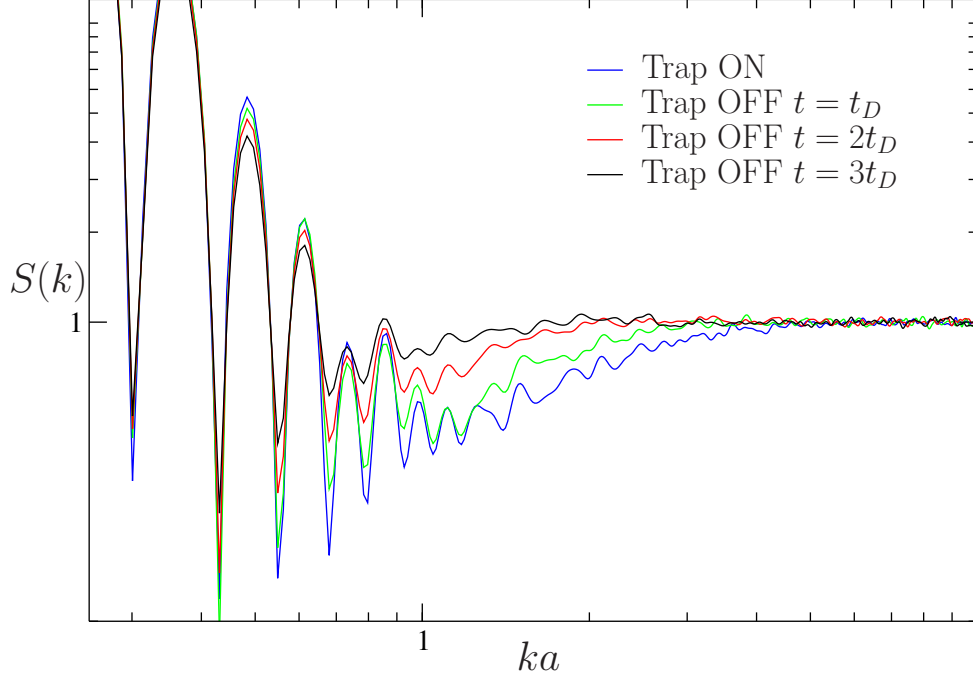


Figure II.5 – Structure factor  $S(k)$  from MD simulations with the trap ON (interaction force + friction/diffusion + harmonic force) and after turning OFF the trap (evolution at constant velocity  $\vec{v}$ ). We wait respectively  $t_D$ ,  $2t_D$ ,  $3t_D$  and plot the associate structure factor to observe the correlations disappearing.

Experimentally this method is well controlled. The escape time has  $t_D$  small enough so the density profile doesn't change too much (and so the structure factor). However, an issue of this method is that it cannot be simply transposed for the modulations experiment we will propose Section III.2.

## 6 DIFFRACTION AND STRUCTURE FACTOR: LINK WITH EXPERIMENTS

As explained in Appendix A.1, there is a simple link between the structure factor  $S(\vec{k})$  and the experimental diffracted intensity. However, the real diffracted intensity contains multiple scattering (which is not contained in  $S(k)$ ) events that can screen the effect we seek. These events are typically measured by the optical thickness  $b(\delta)$  Eq. (I.51). For large  $b$ , multiple

scattering is very important, while for very small  $b$  the diffraction is mainly composed of single scattering. We show in Figure A.1 that for  $b \sim 1$  these effects are small and thus can be forgotten for this first exploration. A laser emits a wave  $\vec{E}_{\text{in}} \propto e^{ik_L z} \vec{e}_z$ . The wave is diffracted in direction

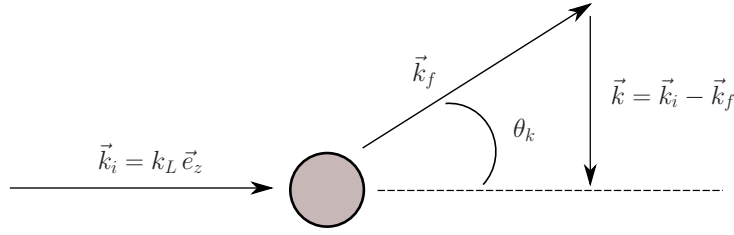


Figure II.6 – Sketch of an incident beam  $\vec{k}_i$  diffracted on an atom with an angle  $\theta$ .

$\vec{k}_f = k_L(\cos \varphi_k \sin \theta_k, \sin \varphi_k \sin \theta_k, \cos \theta_k)$ , see Figure II.6. In our regimes, it is natural to consider elastic scattering ( $|\vec{k}_f| = |\vec{k}_i| = k_L|\vec{e}_z|$ ). The difference vector  $\vec{k} = \vec{k}_i - \vec{k}_f$  appears naturally (see Eq. (A.4)) in computation of the diffracted light, thus we will study  $S(\vec{k}) = S(\theta_k, \varphi_k)$ .

---

# LOOKING FOR DEBYE LENGTH AND OTHER PLASMA PHYSICS EFFECTS

---

The goal of the experimental collaboration is to highlight the repulsive long-range nature of the effective forces between atoms as it was predicted by [WSW90]. As we have seen no experimental measurement has yet confirmed with no ambiguities these forces.

In this Chapter, we come to what is the result of Part [One](#): experimental proposals to measure the Debye length or at least stress the long-range nature of the forces. We first briefly review the direct diffraction response method with a more realistic Laser shape. However, in real experiment this method might give a signal way too weak to be observed. The other experiment idea is to force the MOT with an external potential and look at its response. This latter should be characteristic of the nature of the effective interaction forces. The numerics and theoretical prediction are compared to the preliminary experiment done by the INLN team. **The theoretical and experimental data are consistent nevertheless it remains difficult to draw conclusion on the presence or not of long-range forces.** Indeed, the effect sought might be cover by density effects due to the existence of two diffraction regimes that crossover about where the experiment probed.

## 1 DIRECT PROBING

---

### 1.1 With a Gaussian probing beam

---

In real experiments the probing Laser (in the  $z$  direction) is not an ideal plane waves  $E_G \propto e^{ik_L z}$  but has a Gaussian envelope. Thus, we consider following expression for the probing

Laser

$$E_{\text{Laser}} \propto e^{ik_L z} e^{-2\frac{x^2+y^2}{w^2}},$$

where  $w$  is the Laser waist<sup>1</sup>. If the Laser waist  $w$  is smaller than the cloud's size (typically in experiments  $L \simeq 8$  mm and  $w \simeq 2$  mm) it has the advantage to soften borders. Figure III.1 clearly shows how in the diffraction response border effects are suppressed with a Gaussian beam. We also compare this profile with an another one without correlations. This uncorrelated cloud was obtained via the procedure explained in Section II.5.1 (we randomly drawn particles along the density of the correlated cloud). Clearly the small dip disappears with correlations.

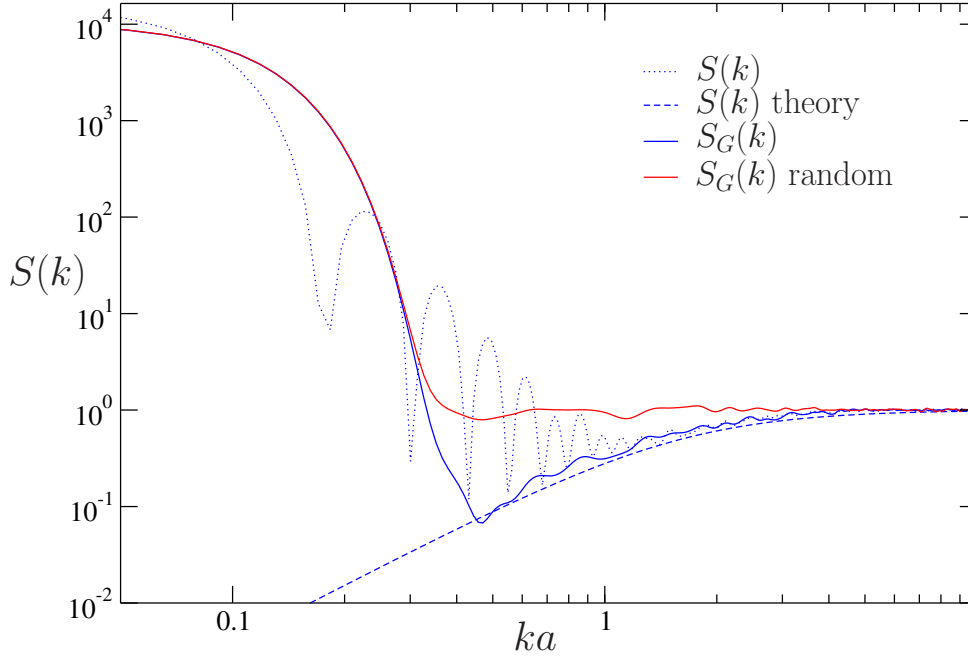


Figure III.1 – Structure factor with a Gaussian probing beam  $S_G(k)$  and with a plane wave  $S(k)$ . The "random" curve is obtained for a random drawing of particles as suggested in Section II.5.1. We plot the non fitted theoretical expression Eq. (II.10) of the Structure factor. Theoretical values used are given in Table II.1, here  $T = 4$ .

## 1.2 Comparison with experiments

The correlations of the Coulomb forces are characterized by a small dip in the diffracted intensity as explained in Section II.5. We expect the background intensity to be of the order  $1/N_d$ , where  $N_d$  is the number of diffracting atoms. If the probing beam is larger than the cloud all atoms diffract so  $N_d = N$  and  $S(k \rightarrow \infty)/S(0) = 1/N \sim 10^{-10}$ ! Such contrast leaves no hope to observe any dip near  $k = 1/\lambda_D$  (even with a Gaussian beam where  $N_d$  is smaller the contrast would be too large). The best experimental resolution is about five orders of magnitudes...

A mask was used to hide the central peak in order diminish the contrast but preliminary experiments were pessimistic. Thus, this experiment was abandoned.

1. There is in principle also a dependence of the waist dependence on the longitudinal direction  $w(z)$  but for the Laser used, this effect is very small since  $z < z_R = 41$  m, where  $z_R$  is the Rayleigh length.

---

## 2 RESPONSE TO AN EXTERNAL POTENTIAL

---

Since the dip characterizing the Debye correlation is very hard to detect in experiments, we must change strategy. Going from a static measurement, to a response to an external forcing measurement, increasing the signal to measure. Note that not only the measurement principle is different but also the effect sought. In previous experiments, we wanted to analyze the position of particles to find some special arrangement between them: correlations, characteristic of Coulomb interactions. Here we no longer look directly for correlations between particles, but rather for a response characteristic of Coulomb forces (or more generally long-range interactions).

### 2.1 Experiment principle

---

We apply a modulation in one direction  $\vec{e}_x$  of the cloud and measure the response depending on the modulation length. The modulating potential is made experimentally by focusing two interfering laser beam on the cloud. Its shape is

$$\phi_{\text{ext}} = A \sin(k_e x)$$

where the angle between the two modulating Lasers determines the wavelength  $k_e$  and  $A$  is the modulation amplitude. The Fokker-Planck equation predicts the density response in stationary regime

$$\vec{\nabla} \cdot \left[ (\vec{F}_{\text{tr}} + \vec{F}_c[\rho])\rho - k_B T \vec{\nabla} \rho - \rho \vec{\nabla} \phi_{\text{ext}} \right] = 0, \quad (\text{III.1})$$

so around the constant profile  $\rho(\vec{r}) = \rho_0 + \delta\rho(\vec{r})$ , the linear response in  $A$  is (neglecting border effects of the cloud)

$$\Delta\delta\rho - \kappa_D^2 \delta\rho = -\frac{A}{k_B T} k_e^2 \rho_0 \sin(k_e x), \quad (\text{III.2a})$$

so

$$\delta\rho(x, y, z) = \frac{A}{k_B T} \rho_0 \frac{k_e^2}{k_e^2 + \kappa_D^2} \sin(k_e x) \quad (\text{III.2b})$$

with  $\kappa_D = 1/\lambda_D$ , where we used that  $\vec{F}_c[\rho] + \vec{F}_{\text{tr}} = 0$ . Hence the modulated profile has a clear amplitude dependence on the modulation number  $k_e$  and it is characteristic of Coulomb interactions (another force would have given a different result). Hence if we measure this shape it will prove the experimentally the Coulomb-like model of VLMOT [WSW90]. In next Section, we will discuss this dependence in terms of long-range interactions.

#### Remark III.1

Here we have done a 3D computations assuming an infinite homogeneous unmodulated density. Of course, the border effects (as finite size and temperature) might modify slightly the profile and response, but it seems quite safe to assume that at first order and for  $k \gg 1/L$  they can be neglected

## 2.2 Fluorescence-like density profile

---

### 2.2.a The Response function

A direct observation of the modulation effects consists in looking directly at the density profile  $\rho_x(x)$  via the fluorescence technique. In the Fourier spectrum, we expect a peak at  $k_x = k_e$  with height proportional to the response function

$$B(k) = \frac{k^2}{k^2 + \kappa_D^2}, \quad (\text{III.3})$$

there are also some density effects for  $k \lesssim 1/L$  since  $\rho^0$  is not a perfect infinite constant density profile. Without interactions between particles (thus with no Debye length), the response function is  $B(k_e) = 1$ . For other type of interaction forces this response function changes. The interpretation here can be put this way

- For large scale  $k < \kappa_D$ , moving atoms on large distance will cost much (so the response will diminish) since particles interact via long-range forces, moving on large scale will imply moving a lot of particles and modify  $(N - 1)$  terms in their potential energy.
- On the contrary for large  $k > \kappa_D$  (small modulations), it will cost less to move on small scale involving less.

For short range repulsion, the response has an opposite profile  $B(k_e \rightarrow 0) = \text{cst}$  (a particle sees only its neighbors, hence for modulation larger than a given scale the response is constant) while  $B(k_e)$  will decrease for large  $k_e$ .

For attractive long-range forces, we also expect  $B(\text{large } k_e) \rightarrow \text{cst}$ , but for large scale perturbation, we expect an instability to develop at a certain scale  $k_J$ , where  $k_J$  is the Jeans wavenumber. This is the Jeans instability [Jea02, BT11] well known for galactic systems: when a self-gravitating system is too large its kinetic pressure cannot compensate the gravitational force and the system collapses.

### 2.2.b Numerical Simulations

In Figure III.2 we plot a simulation of the modulated density profile  $\rho_x(x)$  (for a fixed temperature) for two different modulations. As expected the amplitude grows with  $k_e$ . In Figure III.3 we plot the response to modulation (peak of the Fourier transform at  $k = k_e$ ) for several  $k_e$  and different temperatures and compare the result with the response function  $B(k_e)$ . The ratio between the amplitude response for different temperatures agrees with the factor  $(k_B T)^{-1}$  in Eq. (III.2b). For small temperature, the simulations do not match perfectly the theory, this is because in the regime  $A/T > 1$  the linear theory is expected to fail. Nevertheless, we see that the essential features of  $B(k_e)$  remain, just the effective  $1/\lambda_D$  seems shifted to the left, thus there is a larger effective  $\lambda_D$  outside linear regime. Effective  $(\lambda_D^1)_{\text{eff}}$  and  $\lambda_D^4$  seems to be about the same.

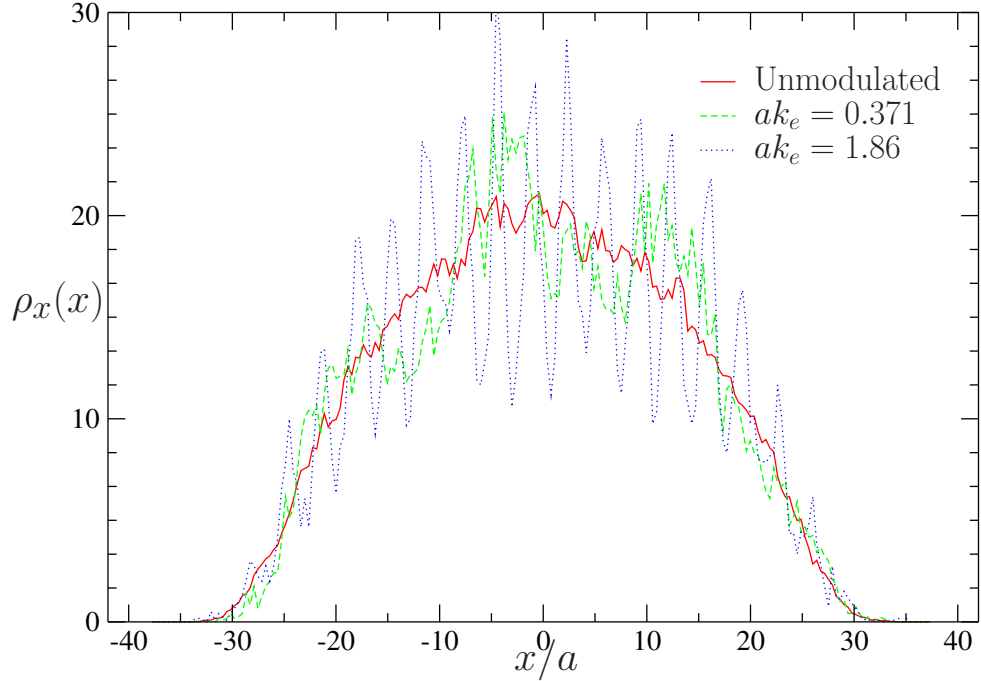


Figure III.2 – Integrated density profile  $\rho_x(x)$  with and without an external potential with amplitude  $A = 8$  and wavenumber  $k_e$ . When  $k_e$  increases the response also increases. Here  $T = 20$  and other theoretical values used are given in Table II.1.

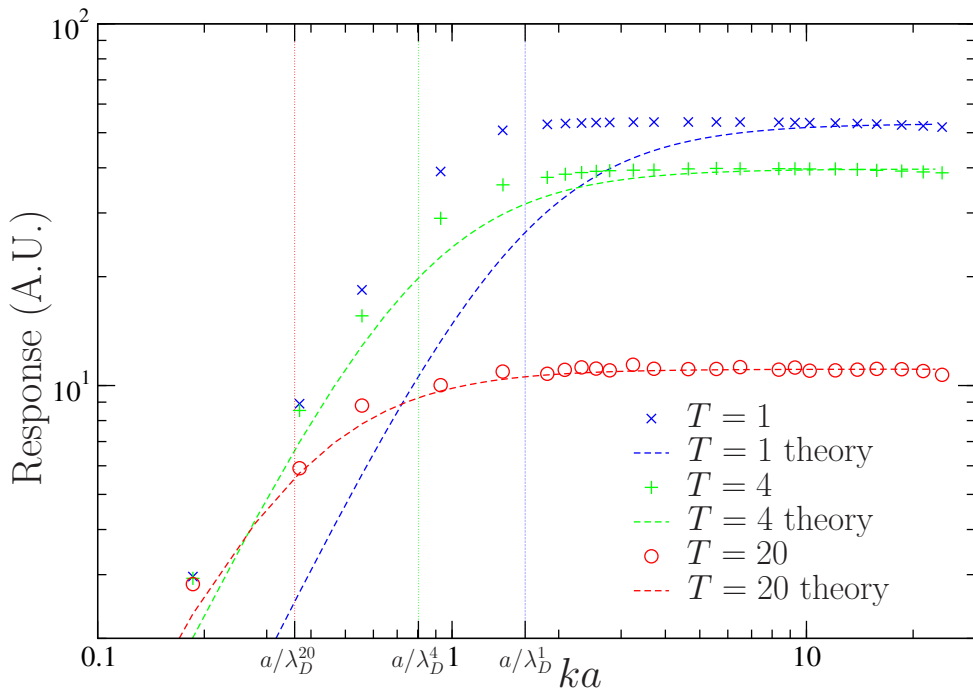


Figure III.3 – Amplitude of the Fourier transform  $\text{FT}|\rho_x|(k_e)$ . We plot the theoretical expression of the response  $B(k_e) = \text{Eq. (III.3)}$  for the theoretical parameters given in Table II.1. The external amplitude is  $A = 8$ . The linear theory works better for  $A/T$  small.

### 2.2.c Experiments

This method requires experimentally to be able to see the modulations in the fluorescence profile and then deduce its Fourier spectrum. This set up can be seen more generally as testing the long-range character of the interaction; an increasing response with  $k_e$  would be a signature of a long-range repulsion.

Unfortunately, it seems that fluorescence techniques are not accurate enough, less than 10% changes are in the noise of the density profile. Our small modulations are thus not observed at all. Also, larger modulation intensity seems not possible without completely destabilizing the MOT.

## 2.3 Diffraction

---

Since the fluorescence technique is not accurate enough, an alternative way to measure the density modulation is diffraction. It is very accurate, but interpreting the results is not straightforward, as we will now explain.

As explained in Sections II.4 and III.1, to predict the diffraction profile we must study the perturbed structure factor

$$S(\vec{k}) = S^0(\vec{k}) + \left\langle \frac{1}{N} \delta\rho(\vec{k}) \rho^0(-\vec{k}) \right\rangle + \left\langle \frac{1}{N} \delta\rho(-\vec{k}) \rho^0(\vec{k}) \right\rangle + \left\langle \frac{1}{N} \delta\rho(\vec{k}) \delta\rho(-\vec{k}) \right\rangle \quad (\text{III.4})$$

where  $S^0$  is the unmodulated structure factor (without external potential  $A = 0$ ).

In this modulation experiment it is legitimate to neglect the correlations because here they are very small as we have already painfully experimented, Section III.1. So, we can write for a symmetric density profile

$$S(\vec{k}) = S^0(\vec{k}) + \frac{2}{N} \delta\rho(\vec{k}) \rho^0(\vec{k}) + \delta\rho(\vec{k})^2 + \text{O}(\text{correlation}). \quad (\text{III.5})$$

The perturbed density Fourier transform can be easily related to the unperturbed Fourier transform thanks to the shift in  $\vec{k}$  induced by the sin function

$$\text{FT}[\rho(x) \sin(k_e x)](k_x) = \frac{1}{2} (\rho(k_x - k_e) - \rho(k_x + k_e)),$$

where  $\text{FT}[\rho](k_x)$  stands for the Fourier Transform of the density  $\rho$ .

### 2.3.a Expression of the $\vec{k}$ vector

The goal of this subsection is to introduce some effects that may not be intuitive for reader concerning 1D and 3D diffraction calculus. For example,  $|\vec{k} - \vec{k}_e| \neq |k - k_e|$  in 3D while it is true in 1D. The diffracted wavenumber vector is (see Figure II.6)

$$\vec{k} = (k_x, k_y, k_z) = (-\cos \phi_k \sin \theta_k, -\sin \phi_k \sin \theta_k, 1 - \cos \theta_k),$$

and its norm is

$$k = 2k_L \sin(\theta_k/2), \quad (\text{III.6})$$

so  $\theta_k = 2 \arcsin(k/(2k_L))$ . A simple calculus shows that

$$\vec{k} = \left( -k\sqrt{1 - \left(\frac{k}{2k_L}\right)^2} \cos \varphi_k, -k\sqrt{1 - \left(\frac{k}{2k_L}\right)^2} \sin \varphi_k, \frac{k^2}{2k_L} \right). \quad (\text{III.7})$$

In experiments, we observe  $S(\theta_k, \phi_k)$ . Two modulated density produces two diffraction peaks in  $\varphi_k = 0$  and  $\pi$ . The angle  $\theta_k$  is directly linked with  $|\vec{k}|$ . Due to the modulation, we expect a peak in  $S(\vec{k})$  around  $k \sim k_e$ . The perturbed wave vector expression after the shift due to the modulation is

$$|\vec{k} \pm \vec{k}_e| = \sqrt{k_x^2 + k_y^2 + k_z^2 + k_e^2 \pm 2k_x k_e} = \sqrt{k^2 + k_e^2 \mp 2k k_e \sqrt{1 - \left(\frac{k}{2k_L}\right)^2} \cos \phi_k}. \quad (\text{III.8})$$

The minimum of this norm is reached around  $k = k_e$  with  $\phi_k = 0$  or  $\pi$  (those will correspond experimentally to the two-diffraction discs observed).

We expect the Debye length to be around  $100 \mu\text{m}$  so  $k \sim 10^4 \text{ m}^{-1}$ , with  $k_L = \frac{10^6}{0.78} \text{ m}^{-1}$ , so  $k_e/k_L \ll 1$ . Hence, we can safely expand the square root in Eq. (III.8), to get with  $|k| \simeq k_e$  and  $\phi_k = 0$  (for example)

$$\begin{aligned} |k_e \vec{e}_k - k_e \vec{e}_x| &= \frac{k_e^2}{2k_L} + k_e \times O\left(\left(\frac{k_e}{2k_L}\right)^2\right) \\ &\simeq k_z \neq 0. \end{aligned} \quad (\text{III.9})$$

This computation shows that due to the 3D nature of the system, one must not a priori forget about the longitudinal direction  $\vec{e}_z$  in the diffraction. It will be the origin of two regimes of diffraction.

Therefore, the perturbed Fourier transform is at the peak  $k \simeq k_e$

$$\rho(k_e) \simeq \rho^0(k_e) + \frac{A}{2k_B T} B(k_e) \left( \rho^0\left(\frac{k_e^2}{2k_L}\right) - \rho^0(2k_e) \right). \quad (\text{III.10})$$

Here remember that  $\rho(k=0) = N$  and also that the Fourier transform of the profile decrease very quickly to 0 with  $k$  increasing (the more regular  $\rho(r)$  is the faster its Fourier transform tends to 0). The dominant term in the structure factor<sup>2</sup> is for  $NA/(k_B T) \gg 1$  (for 10% modulation and  $N \sim 10^{10}$  the approximation is safe) and  $k_e \gtrsim 1/L$  (for smaller  $k_e$  the unperturbed term becomes of the same order),

$$S(k_e) \simeq 1 + \frac{1}{N} \left( \frac{A}{2k_B T} \right)^2 B^2(k_e) \left( \rho^0\left(\frac{k_e^2}{2k_L}\right) \right)^2, \quad (\text{III.11})$$

where we have neglected terms with large argument in  $\rho(k)$ . Due to its fast variation around  $k \sim 1/L$  it is dangerous to replace the last term by  $\rho^0(k=0) = N$ . In next Section, we give a simple illustration of this fact.

2. We keep the +1 background term which for large  $k$  is dominant.

### 2.3.b A simple example: existence of two diffraction regimes Raman-Nath/Bragg

In this Section, I will give a simple example where two different regimes are easily observed in the diffraction response.

Let's take a 3D cube of atoms  $\rho^0(x, y, z) = \rho^0 \Theta(L - x) \Theta(L - y) \Theta(L - z)$ , modulated such that  $\delta\rho = \tilde{A} \rho^0 \sin(k_e x)$  where we set a constant  $\tilde{A} = AB(k_e)$  (for example with a trapped non-interacting cloud). It means that here we do not seek interaction effects just the regimes of diffraction. The diffraction  $S(k)$  response is maximum (forgetting of course the undiffracted peak in  $k = 0$ ) for  $k \simeq k_e$ . Standard calculation gives

$$\delta\rho(\vec{k}) = 4\rho^0 \tilde{A} \frac{\sin(k_z L_z)}{k_z} \frac{\sin(k_y L_y)}{k_y} \left( \frac{\sin((k_x - k_e)L_x)}{(k_x - k_e)} - \frac{\sin((k_x + k_e)L_x)}{(k_x + k_e)} \right). \quad (\text{III.12})$$

so, with Eq. (III.11) we have

$$S(\vec{k}) - S^0(\vec{k}) \simeq \frac{1}{N} \left( \frac{4\rho^0 \tilde{A}}{2k_B T} \right)^2 \left( \frac{\sin(k_z L_z)}{k_z} \frac{\sin(k_y L_y)}{k_y} \frac{\sin((k_x - k_e)L_x)}{(k_x - k_e)} \right)^2 \quad (\text{III.13})$$

where we have neglected correlation terms and cross-termed terms in Eq. (III.5) which are negligible for  $k > 1/L$ .

- If  $k_z L_z \ll 1$  (thin media) then the diffraction is independent of the density along the longitudinal direction  $\vec{e}_z$ . The max of this function is reached for  $k_x = k_e$  and  $k_y = 0$ . So, the peak response is constant with  $k_e$  and its amplitude is constant

$$S(k_e) \sim \frac{1}{N} \left( \rho_0^2 \tilde{A} L_z L_y L_x \right)^2.$$

- Now if  $k_z L_z \gg 1$ , the peaks of diffraction are still situated around  $k \simeq k_e$ . We can still set  $k_y = 0$ , but this time we must also consider the additional dependence on  $k_z \neq 0$ .

The peak response is now, remembering  $k_z \simeq \frac{k_e^2}{2k_L}$ ,

$$S(k_e) \sim \frac{1}{N} \left( \frac{4\rho_0 \tilde{A} L_y L_x \sin\left(\frac{k_e^2}{2k_L} L_z\right)}{k_e^2 / (2k_L)} \right)^2.$$

So, in this simple example we have seen the existence of two diffraction regimes:

- $k_z L_z \ll 1$ , response is constant with the modulation  $k_e$   
**No density effects: Raman-Nath regime of diffraction.**
- $k_z L_z \gtrsim 1$ , response has a  $k_e^{-4}$  dependence with the modulation

**Strong longitudinal density effects: Bragg regime of diffraction.**

It shows clearly that the diffraction response to modulation displays a slope change due only to density effects without any link with the response function  $B(\vec{k}_e)$ . Of course, it is problematic, because it will interfere with the slope change effect expected from the long-range interactions!

The criteria for these two regimes is in terms of a critical wavelength  $\lambda_e^{(c)}$  (or wavenumber  $k_e^{(c)}$ ) of modulation

$$\lambda_e^{(c)} = 2\pi \sqrt{\frac{L_z}{2k_L}} = \sqrt{\pi L_z \lambda_L} \quad \text{or} \quad k_e^{(c)} = \sqrt{\frac{2k_L}{L_z}}. \quad (\text{III.14})$$

So, for a cloud of radius  $L \approx 6$  mm and a laser  $\lambda_L = 780$  nm, the regime change is expected at  $\lambda_e^{(c)} \approx 120 \mu\text{m}$ ... which is the worst case scenario since the Debye length is also expected around  $100 \mu\text{m}$ !

**Thus in the following, we will need to distinguish/separate the "density effects" from the "long-range effects".** To do so theoretically, we will often set  $B(k_e) = 1$ , which corresponds to a response without interaction, to compare with a case with interactions.

### Remark III.2

One physical picture for those regimes is: considers at the cloud entrance a series of Gaussian beams with a waist given by the size of diffracted object, which is here the density modulation of size  $\lambda_e = 2\pi/k_e$ . That beam will propagate and spread in perpendicular plane, Raman-Nath regime corresponds to the situation where two adjacent beams do not superpose which is to say the Rayleigh length

$$z_R = \pi \frac{\lambda_e^2}{\lambda_L}$$

is smaller than the longitudinal size of the cloud  $L_z$ . When  $z_R > L_z$  beams overlap: it is the Bragg regime. In the context of ultrasonic light diffraction this criteria Eq. (III.14) between Raman-Nath/Bragg is also known [KC67].

### 2.3.c Diffraction discs

In the previous Section, we have seen on a simple example that we expect for a homogeneous distribution of particles with no interactions a diffraction profile with

- $\lambda_e \ll \lambda_e^{(c)}$ ,  $S(\lambda_e) \propto \lambda_e^4$ ,
- $\lambda_e \gg \lambda_e^{(c)}$ ,  $S(\lambda_e) \propto \lambda_e^0$ .

Here we will show how measuring the total intensity of diffraction discs ( $\lambda_e$ ) (and not only its maximum) affects the scaling in adding a linear contribution  $\lambda_e$

- $\lambda_e \ll \lambda_e^{(c)}$ ,  $R(\lambda_e) \propto \lambda_e^5$ ,
- $\lambda_e \gg \lambda_e^{(c)}$ ,  $R(\lambda_e) \propto \lambda_e^1$ .

Indeed, in experiments is measured the total intensity of diffraction discs (to which we remove the unmodulated profile). It is defined as follow

$$R(\lambda_e) = \int_{\theta_e - \epsilon_\theta}^{\theta_e + \epsilon_\theta} \int_{\varphi_e - \epsilon_\varphi}^{\varphi_e + \epsilon_\varphi} (S - S^0)(\theta_e + \epsilon'_\theta, \varphi_e + \epsilon'_\varphi) d\epsilon'_\theta d\epsilon'_\varphi \quad (\text{III.15})$$

where  $\theta_e$  is the associated angle of the modulation Eq. (III.7) and  $(\epsilon_\theta, \epsilon_\varphi)$  are chosen large enough to enclose the diffraction disc.

A simple calculation of the integral of  $(S - S^0)(\vec{k}_e + d\vec{k})$  in two extreme cases (step function and Gaussian) can give an idea of the effect on the response scaling of this computation.

- For the step function density profile Eq. (III.13), we expand around the peak at  $(\theta = \theta_e + \delta\theta, \varphi = 0 + \delta\varphi)$ , which gives a term like

$$\simeq \text{sinc}^2(k_e \delta\varphi).$$

This term integrated give something proportional to  $\frac{1}{k_e} \sim \lambda_e$

- For a peak with Gaussian shape, one expects

$$e^{-w^2|\vec{k}_\perp - k_e \vec{e}_x|^2/8} = e^{-w^2(\vec{k}_\perp^2 + k_e^2 - 2k_\perp k_e \cos \phi)/8} \vec{k}_\perp \underset{\sim \vec{k}_e}{\propto} e^{-w^2 k_e^2 \delta\phi^2/4} e^{-w^2 \delta k/8} \quad (\text{III.16})$$

this term integrated gives something proportional to  $1/k_e \propto \lambda_e$ .

In conclusion, it seems rather generic that for  $k_e < k_L$ , the total surface intensity of the diffraction peak  $R$  has an extra linear dependency with  $\lambda_e$  when compared to the peak maximum  $S$ .

### 2.3.d Comparison theory simulations

#### Simulations

The various components of this experiment and associated predictions are now theoretically established with simple examples.

We show on Figure III.4 the result of the diffraction on simulated clouds for three different temperatures. We do **not** plot the surface of the diffraction discs as suggested in Section III.2.3.c, but rather the maximum of this diffraction disc (corresponding to  $k = k_e$  and  $\phi = 0$  or  $\pi$ ). We do so just to get a first illustration of the Bragg/Raman-Nath regimes versus long-range effects without additional "surface effects". Furthermore, we chose an infinite waist (corresponding to a plane wave) to avoid other additional effects. In Section III.2.3.e we will consider both effects.

The Figure III.4 shows indeed a regime change where it is expected at  $\lambda_e = \lambda_e^{(a)}$ . Moreover, the effects of the long-range interactions are clear for  $\lambda_e \gtrsim \lambda_D$ : the response decreases. In between the two crossover the response is almost constant which is expected. A cloud with no long-range effects would have a constant response for large modulation  $\lambda_e \gg \lambda_D$  (instead of a decreasing one); but for small modulation  $\lambda_e \ll \lambda_e^{(c)}$  the response will be (as with interactions) dominated by "density effects" (Bragg regime).

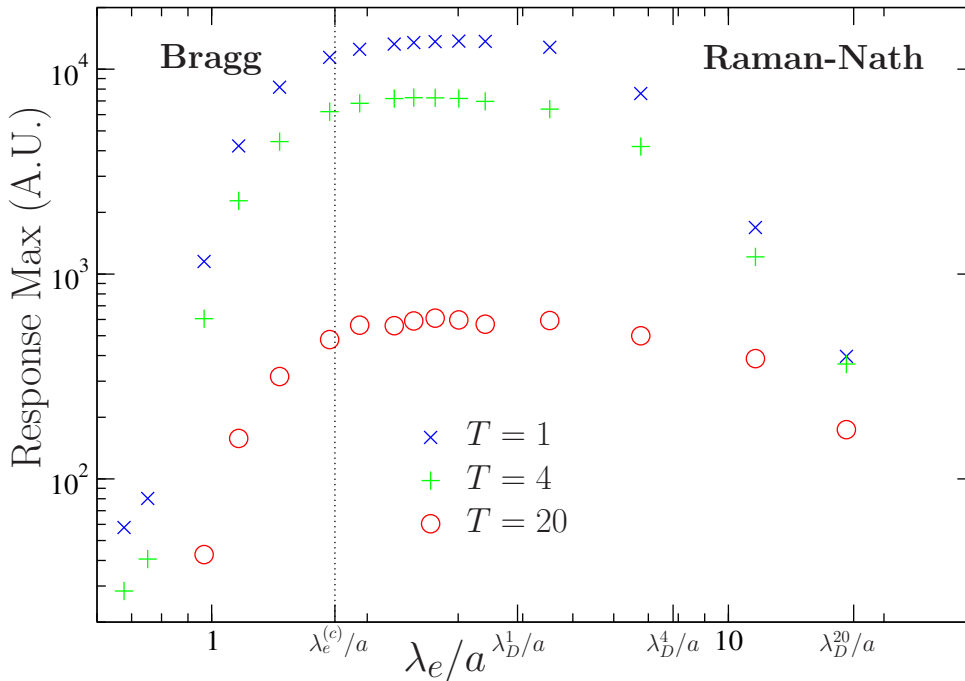


Figure III.4 – Maximum response of the diffraction discs  $S(k)$  for simulated cloud with different temperatures (Table II.1). The waist is infinite here and  $k_L = 1800$ . The amplitude perturbation is  $A = 8$ . We show the two diffraction regimes Bragg and Raman-Nath predicted by theory and well observed here.

### Removing density effects

Here we have chosen this example so the crossover for diffraction does not occur where long-range effects happen. But in the experimental set up both might happen at the same place obscuring the result.

Thus, how could we see without ambiguities the long-range effects without any of these density effects, keeping just the response function  $B(k_e)$ .

In equation Eq. (III.11) we can rewrite the density term to get

$$S(k_e) - S^0(k_e) \simeq \left( \frac{AB(k_e)}{2k_B T} \right)^2 \left( S^0 \left( \frac{k_e^2}{2k_L} \right) - 1 \right). \quad (\text{III.17})$$

Hence the response is linked with the unmodulated structure factor at small angles  $k_e^2/(2k_L)$ . So, in principle measuring these small angles for the unmodulated structure factor  $S^0$  of the same cloud would give the density contribution. Then dividing by this same term

$$\frac{S(k_e) - S^0(k_e)}{S^0 \left( \frac{k_e^2}{2k_L} \right) - 1} \simeq \left( \frac{AB(k_e)}{2k_B T} \right)^2, \quad (\text{III.18})$$

just leaves the response function  $B(k_e)$ <sup>3</sup>.

To test this prediction, for the same simulations than in Figure III.4, we plot in Figure III.5 the height of the diffracted peak  $S(\lambda_e)$ <sup>4</sup> by a probing beam larger than the cloud (so not a Gaussian beam) divided by the corresponding diffraction response at small angles  $S(\lambda_e^2/(\pi\lambda_L))$ . Finally, we plot (with no fit) the remaining term predicted theoretically  $\left( \frac{A}{2k_B T} \right)^2 B^2(\lambda_e)$  for  $A = 8$  and  $T = 20$  (where the linear regime is valid), with the simulation parameters, and it fits very well the simulations! For other regimes where the response is nonlinear ( $A/k_B T > 1$ ), our method still work to highlight long-range effects but the theoretical amplitude (not shown) is different from simulations. The interest to perform such simulations is to check that even with an intense laser the effects sough remain. For very small modulations the denominator of Eq. (III.18) is very close to zero explaining the points out of range.

Once again if there were no long-range interactions  $B(\lambda_e) = 1$ , the response on Figure III.5 would be constant.

It is an excellent means to test our predictions with simulations. Experimentally one may think that measuring the structure factor for small angles would be easy since one expect a large response for small angles. The problem is that the signal might be too strong and varying too much to be well captured. Also, measuring small angles requires to change the experimental set up so that it might be hard to measure both small angles and large angles with one experimental configuration.

3. All the +1 terms can be forgotten for the region of interest.

4. So in principle it is not exactly the disc area experimentally measured.

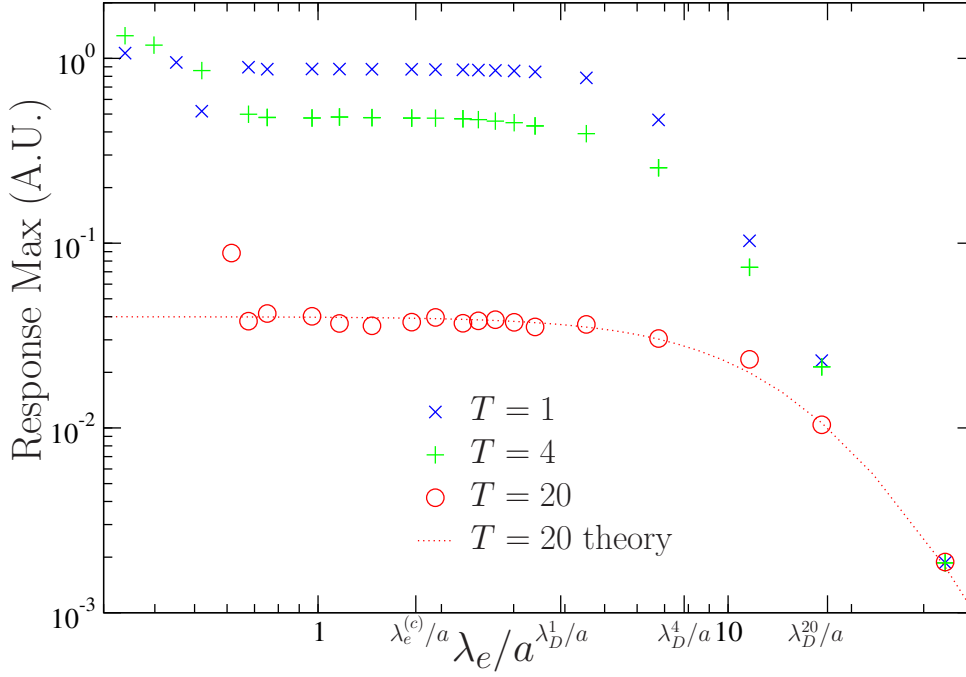


Figure III.5 – Amplitude of diffracted peaks with respect to  $\lambda_e$  without the "density effects" measured as in Eq. (III.18) where  $S^0$  and  $S$  were obtained from simulations for  $T = 1, 4, 20$ . We compare with the theoretical expression of the r.h.s. of Eq. (III.18) for  $T = 20$ . It is the same data that in Figure III.4.

### 2.3.e Comparison theory/experiments

#### Comparison

In order to compare theory and experiments we have to choose a density profile. We chose a simple one that can be tracked analytically in Fourier space. In the perpendicular direction of the probing we know that border effects will be "cut" by the Gaussian beam, while in the  $z$  direction we expect a step like structure. Hence, we chose  $\rho(\vec{r}) = \text{Eq. (A.5)}$  and compute its Fourier transform.

In Figure III.6 is plotted the result of one experiment for two different detuning  $\delta = -4\Gamma_d, -3\Gamma_d$ . We compare these results with the theoretical diffraction response via  $S(\lambda_e) - S^0(\lambda_e)$  of the profile Eq. (A.5). The parameters  $L, w, N$  are chosen to be the same that in the experiment. Indeed, the waist and atom number is well controlled and the length can be easily extracted from a density profile. The only adjusted parameter here is the vertical amplitude of the theoretical response (in arbitrary units), that we set so it coincides with the experimental curves. On the three theoretical curves, we change the value of the Debye length  $\lambda_D$  to observe its effect.

The conclusions of this comparison are

- Experimental crossover coincides with the one predicted Eq. (III.14)
- In the Bragg regime the theoretical prediction has a smaller response. The difference could be explained by the fact that the density profile chosen differs certainly with the real one, and in this region. Exact form of the density might play a role. For example, a sharper density profile decreases slower in this region.
- Theoretically we observe oscillations in Bragg regime (it is to be expected for a step

function). The experimental profile also displays such oscillation (to a lesser extent) around  $\lambda_e = 70 \mu\text{m}$ . We will discuss this next paragraph.

- In the Raman-Nath regime the slopes of experiment and theory are both about 1 as explained in Section III.2.3.c (the response is not constant as in Figure III.4, because this time we consider the whole disc of diffraction). For larger modulation we expect the long-range effects to take place, which we see clearly for  $\lambda_D = 100 \mu\text{m}$ . Unfortunately, the theory agrees well with the experiment only for the non interacting case with  $B(\lambda_e) = 1$  and to some extent with the  $\lambda_D = 300 \mu\text{m}$  case. Hence at this point it is not possible to be conclusive on the presence of long-range interactions.

For a Debye length, larger than  $300 \mu\text{m}$  (blue dashed line), the long-range effects are rather hard to see in the measurement range. Thus, differentiate between the case without interaction (dashed dotted black line) for large Debye length is difficult! One could be tempted to extent the measurement range to conclude but finite size effects of the waist  $k \sim 1/w$  will become dominant.

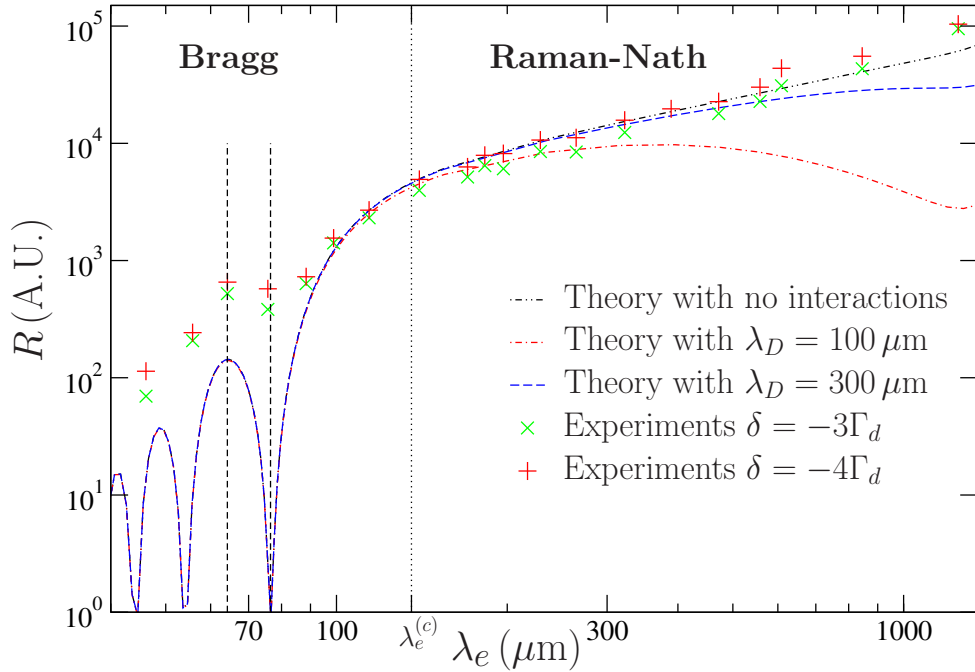


Figure III.6 – Power of the diffracted discs with a Gaussian beam in G. Labeyrie’s experiments (crosses) and in theory (lines). The detuning is  $\delta/\Gamma_d = -3$  and  $-4$ ,  $N \sim 10^{10}$ ,  $L = 7.41 \text{ mm}$ ,  $w = 2.2 \text{ mm}$ . We compare the theoretical model with the same parameters  $L, w$  at various Debye length  $\lambda = 100, 300 \mu\text{m}$ . The "rigidity" of the step function Eq. (A.5) is chosen arbitrary at  $l = 100 \mu\text{m}$  (it does not change much the results). We indicate the theoretical Bragg/Raman-Nath regime change by the tick  $\lambda_e^{(c)} \simeq 135 \mu\text{m}$ . We also show the theoretical extreme case with no interactions  $B(\lambda_e) = 1$ . The vertical dotted line shows the separation of the two diffraction regimes. The vertical dashed lines show at which  $\lambda_e$  the diffracted discs plotted Figure III.7 and III.8 were taken.

### Split bump

In the experiment, some split diffraction discs have been observed, Figure III.7(b), corresponding to the small oscillation in the experimental response near  $\lambda_e \simeq 70 \mu\text{m}$ . Can we explain this observation? To explain simply their origin, one has to remember that the response has a dependence with the longitudinal profile Eq. (III.10), so around a peak  $k = k_e + \delta k$ , the response is

$$S(k) \propto S^0 \left( \frac{k_e^2 + 2k_e \delta k}{2k_L} \right).$$

If this small angle happens to correspond to a "hole" in the Fourier profile (as in Figure II.3 for  $ka < 1$ ), then the diffracted discs can be split in two parts. We illustrate that with our theoretical model with parameters provided by the experiments (thus with no adjustment to fit). We can see in Figure III.6, (dashed lines) that a split bump is also expected around  $\lambda_e = 76.5 \mu\text{m}$ . We show this disc Figure III.8(b). It very close in term of  $\lambda_e$  to the experimental observation!

In Figure III.7(a) we show an experimental diffraction disc at  $\lambda_e = 64.2 \mu\text{m}$  (see the left vertical dashed line of Figure III.6) where no split is expected. There is indeed no particular asymmetry and the disc is circular. The corresponding theoretical expectation is also, Figure III.8(a), not split. It is quite reassuring to have a theory able to explain and describe with

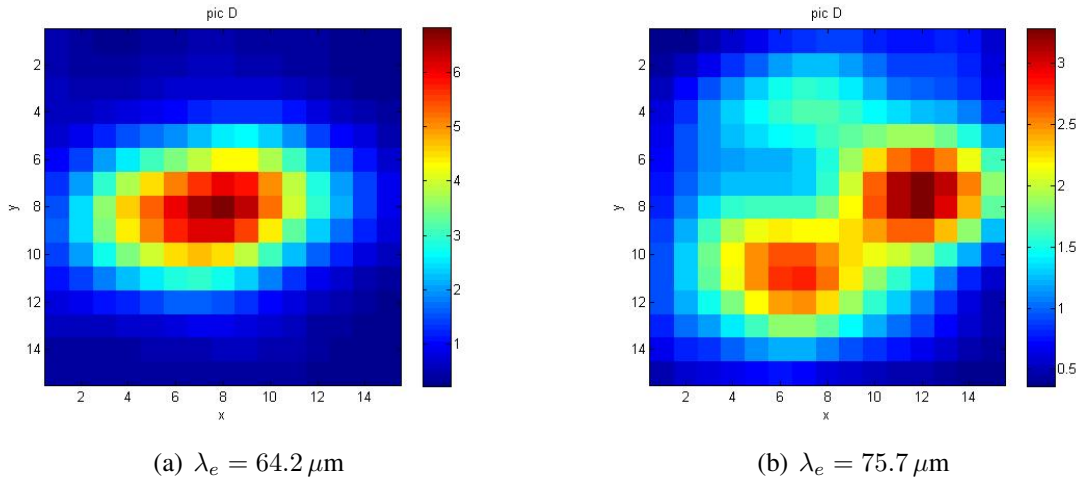


Figure III.7 – Experimental diffraction discs for  $\lambda_e = 75.68 \mu\text{m}$  in the experiment

rather good precision this non trivial/intuitive experimental observations.

## 3 CONCLUSIONS

We suggested different experiments to "see" and measure the Debye length in VLMOT.

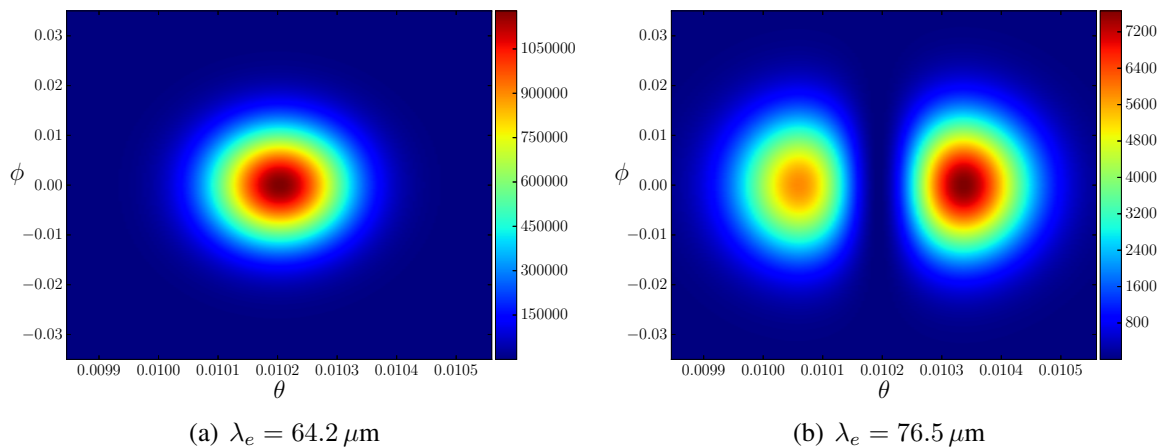


Figure III.8 – Theoretical diffractions discs  $S(\theta, \phi)$ ,  $L = 7.51 \text{ mm}$ .

## Static diffraction experiment

The first experiment (see Section III.1) is a direct diffraction measure on a static MOT. It has the upside of directly measuring the correlations in the system. The downside is that the effect sought is very small and hard to observe. However, with a Gaussian beam, it is possible to "increase" the effect by reducing the contrast between the background and the non-diffracted beam (see Figure III.1). A well-disposed mask should help to reduce the central peak contribution and its tail but so far has not yielded anything.

## Modulation experiments

Modulation experiments (section III.2) have the advantage that the effects foreseen are much bigger than correlations. They do not try to directly measure the correlations of the particles but rather the influence of long-range interaction in the cloud's response.

### *Density response via fluorescence*

The fluorescence experiment (section III.2.2) is well controlled theoretically and numerically. Furthermore, the expected effect is clear: we want to observe a response in the amplitude of the modulated density as  $B(\lambda_e) = \text{Eq. (III.3)}$ . With a precise signal, we could even extract the Debye length value.

A less demanding result would be to simply observe a decreasing response when  $\lambda_e$  grows. This would be enough to conclude on the presence of long-range forces.

However, since the amplitude modulation of the density is small and the fluorescence imaging is mysteriously (of what I have heard) not really accurate, the hope to see any modulation is thin.

*Diffraction response*

The diffraction experiment (Section III.2.3) is more sensitive since experimental signals have been seen and measured. However, the result interpretation is less direct. The measurement is plagued by two regimes of diffraction that cross over near the supposed Debye length. Nevertheless, after simple estimations we believe that we discovered the essential features of this measurement; it seems that the experimental profiles measured are quite well understood.

The remaining problem is that no long-range effects are seen unequivocally since experiments and theoretical predictions for  $\lambda_D = 300 \mu\text{m}$  and  $\lambda_D \rightarrow \infty$  match up to  $\lambda_e \simeq 800 \mu\text{m}$  where the size of the waist could modify the response. Hence several possibilities occur:

- There are no repulsive long-range effects (or they are very weak and not the dominant contribution) thus there is no Debye length in VLMOT. The repulsion mechanism is provided by a non long-range force. An extreme case would be that there are only contact interactions. Note that in this case the scaling  $L \sim N^{1/3}$  observed in [CKL14] would still be valid. Another possibility could be a Yukawa interaction between particles due for example to a very fast reabsorption of rescattered photons. This could be the case of the photon emitted at resonance in the Mollow triplet [Mol69]. Numerical tests of these cases have been started.
- The Debye length is too large for our experimental window (meaning our estimation  $\lambda_D \sim 100 \mu\text{m}$  is wrong). We can either enlarge this window, or reduce the Debye length by increasing for example the trap pulsation  $\omega_0$  or reducing the temperature.
- There are attractive long-range effect dominant for large modulation screening the effect of the repulsive force, which might be of shorter range than expected.
- Another pessimistic possibility is that we did not interpret correctly the theory and thus experimental data, or that we neglected a serious phenomenon (like multiple scattering). Thus, our inconclusive interpretation is wrong.

So far, we did not consider the full Shadow effect (Section I.1.3). In the case where the Coulomb description is false and the true repulsion is of shorter range, the attractive Shadow force could dominate at long-range. Either way (Coulomb forces or not), the first order derivation<sup>5</sup> (at small optical thickness  $b \ll 1$  Eq. (I.21) and Eq. (I.22)) of this effect could be wrong in the experimental regime where  $b \sim 1$ , bringing additional attractive effects that could possibly explain the data.

So, to conclude this Part, a serious theoretical proposal has been made with consistent experimental data. Nevertheless, strong long-range effects as expected with the standard model for MOT do not seem to appear. More experiments should be made with different parameters as well as simulations with various type of interactions. If some more accurate fluorescence technique is developed to observe the modulated density profiles, one could directly measure the amplitude response and compare it with the response function  $B(\lambda_e)$ .

---

5. Even the numerical simulations of this force are considering only the first order expression.

---

**ADDENDUM**


---

Additional comparisons between the experimental data and the Coulomb simulations were done and presented for my Ph.D. defense. I summarize here these results.

We studied experimental static (without modulations) density profiles measured by fluorescence (see Section II.1) for different detuning. The more the detuning is large the more we expect repulsive interactions between atoms to be weak. Hence, for large detuning the cloud size should be smaller and its shape should be Gaussian. We superposed these data with the  $\rho_x(x)$  obtained by Coulomb simulations (see Eq. (II.1)) for well-chosen parameters on Figure III.9. The first thing to notice is that the fits work quite well for the various detuning, meaning the

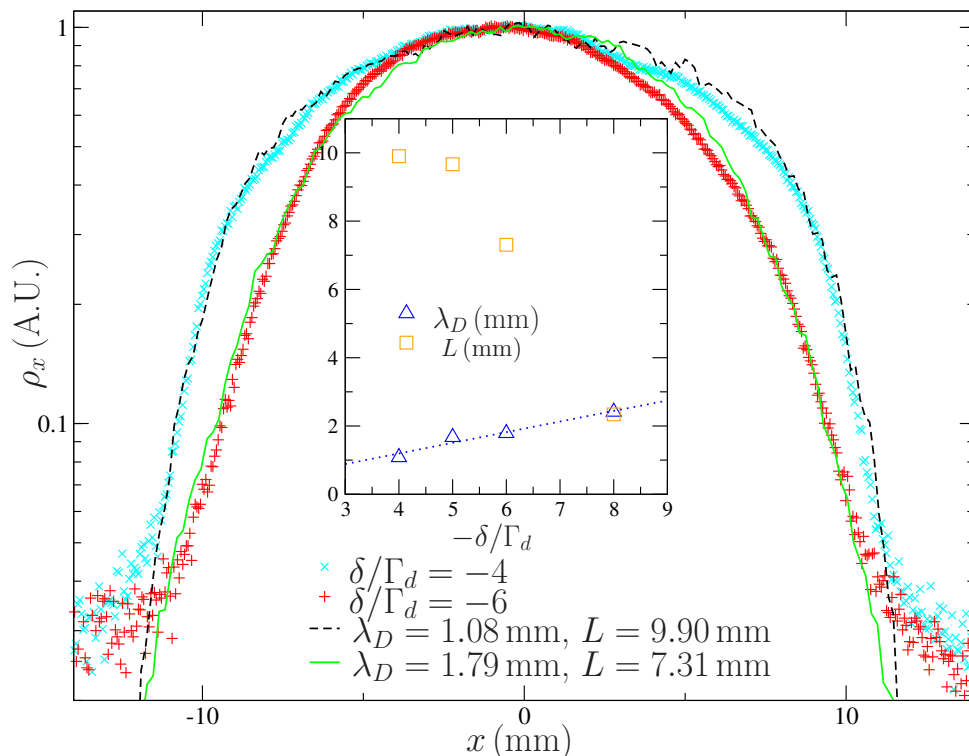


Figure III.9 – Experimental density  $\rho_x(x)$  obtained by fluorescence for  $-\delta/\Gamma_d = 4, 6$  compared with MD simulation (lines) of a tapped Coulomb gas. The inset shows the extrapolated Debye length  $\lambda_D$  and the cloud radius  $L$ . (The density plots for  $-\delta/\Gamma_d = 5, 8$  are not shown here).

trapped Coulomb gas model is coherent with experiments. Knowing the simulation parameters allow us to extrapolate the experimental parameters, in particular the Debye length (which is linked to the size of the distribution tails). However, for the fits to work we have set the Debye length around 1 mm which is much larger than our  $100 \mu\text{m}$  expectation<sup>6</sup>. This "measurement" of a very large Debye length is consistent with the modulation results (see Section III.2) where we did not observe long-range effects around  $100 \mu\text{m}$ . Instead the experimental response profiles were matching the theory uniquely for very large Debye (see Figure III.6).

---

6. Remember that this number is related with the size  $l_g = \sqrt{3}\lambda_D$  of small MOTs. For example see [RPC<sup>+</sup>87] for cloud measurements.

Therefore, these results offer a more conclusive statement than before: the Coulomb model with a Debye of the order of 1 mm are consistent with experiments. We look at the Debye length expression Eq. (I.42) to understand the difference between the "measurements" and the expectation. Either the temperature  $T$  is 100 times larger which is unlikely or either the trap pulsation  $\omega_0$  is ten times weaker. This latter possibility sounds fair since the trapping effect is being attenuated by the cloud thickness. This will be the object of new investigations.

**PART TWO**

**BIFURCATIONS FOR VLASOV AND  
KURAMOTO SYSTEMS**



---

## INTRODUCTION TO BIFURCATION

---

As we have seen in the Introduction the Vlasov equation describes the violent relaxation, i.e. the evolution over timescales  $\tau_v \ll \tau_c = O(N^\delta)$  (see Figure 1) of particle systems interacting with long-range interactions before the collisional relaxation takes over and drives the system toward statistical equilibrium. Thus, this "out-of-equilibrium" process can be arbitrarily long (e.g. galaxies have  $N \approx 10^{11}$  so collisional effects can be ignored over lifetime of  $\sim 10^{10}$  years [BT11]) and their study is relevant by the Vlasov equation. Also for purely out-of-equilibrium systems, such as coupled oscillators, where each oscillator is driven at its own rhythm, there is no defined Boltzmann equilibrium so only the kinetic description can give information on the system state. The dynamics of kinetic equations like the Vlasov is very rich due to advection, nonlinearity and self-consistent mean-field force. It leads to numerous effects such as filamentation of the phase space, strong resonance phenomena, infinite number of stationary states, BGK modes [BGK57], echo plasma effect [MWGO68], etc. We are not going to focus on a specific physical system. Rather we will try to advance the general understanding of bifurcation in the Vlasov equation and other related models, with the hope it may be useful for various situations: tokamaks, galaxies, synchronization, etc.

To study dynamical evolution of those systems a natural starting point is to consider the linear evolution of  $f = f^0 + g$  around a reference state  $f^0$ ,

$$\partial_t g = \mathcal{L} g + \mathcal{N}[g] \tag{IV.1}$$

where  $\mathcal{L}$  and  $\mathcal{N}$  are respectively a linear and nonlinear operators acting on a function space for infinite-dimensional systems or  $\mathbb{R}^n$  for finite-dimensional systems.

The stability of the reference state depends on the spectrum of the linear operator. Eigenvalues  $\lambda$  are defined with their associated eigenspace of eigenvectors  $\Psi_\lambda$ <sup>1</sup> through the equation

$$\mathcal{L} \Psi = \lambda \Psi. \tag{IV.2}$$

---

1. The subscript  $\lambda$  will be dropped in most of the manuscript.

From Eq. (IV.1) the linear evolution of a solution  $g = A(t)\Psi$  parallel to an eigenvector will be determined by the sign of  $\text{Re } \lambda$  (where  $\lambda$  is has the largest real part, which we suppose is simple)

$$\dot{A} = \lambda A \quad \Rightarrow \quad g \propto e^{\lambda t}, \quad (\text{IV.3})$$

- $\text{Re } \lambda < 0$  the system is said to be (spectrally) stable, because small perturbations of the reference states are damped to zero. However even if the system is linearly stable for large initial perturbations nonlinear effects could take over.
- $\text{Re } \lambda > 0$  the system is said to be (spectrally) unstable, after an exponential growth regime, nonlinear effects can
  - Saturate the perturbation. Typically, we have a negative cubic term of the form

$$\dot{A} = \lambda A - |c_3||A|^2 A + O(|A|^4 A) \quad (\text{IV.4})$$

is expected for symmetric systems  $A \longleftrightarrow -A$ .

- Amplify the perturbation which typically yields

$$\dot{A} = \lambda A + |c_3||A|^2 A + O(|A|^4 A). \quad (\text{IV.5})$$

In physical systems, the perturbation eventually saturates with higher order terms at some level  $O(1)$ .

- $\text{Re } \lambda = 0$  the system is said to be neutrally stable. The perturbation is purely oscillating and will neither grow or damp. We say it is a neutral mode.

When the system depends on a parameter  $\mu$ , which could be temperature, coupling, initial velocity distribution width, etc., it can undergo a bifurcation going from a stable state to an unstable state i.e.  $\text{Re } \lambda_{\mu < \mu_c} < 0$  to  $\text{Re } \lambda_{\mu > \mu_c} > 0$ . For a good introduction, quite complete and suitable, to bifurcation theory see [Cra91b]. The goal of bifurcation theory is to describe a qualitative change in a system structure occurring when some parameter is varied. It can be how a homogeneous plasma (with a zero-total electric field) can go unstable, meaning the electron distribution will develop some structure producing an electric field. Biological systems also display bifurcation, e.g. an asynchronous crowd of clapping people synchronizing. As we shall see later to quantify this structure change we will define the concept of order parameter.

A particularity of the kinetic equations we study is that they possess an **"infinite number of neutral modes"**<sup>2</sup> called a **continuous spectrum**. This infinite structure is directly linked with the dimensionality (and difficulty) of the problem. In the simplest bifurcation analysis with one positive mode  $\lambda \ll 1$  and other negative modes  $\nu < 0$ , one can easily separate the two timescales: during time  $|\nu|^{-1} \ll \lambda^{-1}$ , the system goes quickly on the unstable manifold, so a description of the instability will only require one to describe the unstable direction associated with  $\lambda > 0$  and the problem dimension will be reduced from two to one. Here with one neutral mode (or a continuum) one could be tempted to do the same, but removing such modes which are never damped could be very risky. In fact, as we will see, these modes are responsible for stronger nonlinear effects.

We provide a detailed example of such neutral mode effects on a simple tractable example of finite dimension, following [Cra91a]. We will introduce the unstable manifold reduction technique used later and which already exhibits its limitations, and compare it with the more standard central manifold technique. **The goal of the center/unstable manifold technique is always to reduce the dimension of the problem to get a simpler expression of the dynamics close to the bifurcation. Thus one obtains the nonlinear generalization of the eigenvector**

---

2. Strictly speaking this denomination is abusive.

**associated with neutral/unstable eigenvalue.** Of course, in finite dimension we know how to deal with neutral modes and their effect is known; it suffices to include them in the center manifold (which for many neutral mode might be not satisfactory), but their effect on the unstable manifold is less known. In the following finite-dimensional example, we aim to show the features of such unstable expansion with one neutral mode. Because bifurcations are in general classified in "universal categories" (e.g. saddle-node, transcritical, pitchfork, Hopf bifurcation), it makes sense to study a simpler case hoping to gather a general understanding.

Then we introduce the formalism for the infinite-dimensional case, present a rigorous definition for the spectral problem and provide a tractable example where the continuous spectrum leads to damping.

---

## 1 A BIFURCATION EXAMPLE IN FINITE-DIMENSION

---

This example is taken from [GH13, Cra91b]. Let's consider a system that can be reduced to a two-dimensional system of o.d.e.

$$\dot{r} = \lambda r + a_1 z r + a_2 r^3 \tag{IV.6a}$$

$$\dot{z} = \nu z + b_1 r^2 + b_2 z^2 \tag{IV.6b}$$

with an eigenvalue  $\lambda \in \mathbb{R}$  associated with the amplitude  $r(t)$  and  $\nu \in \mathbb{R}$  associated with the mode  $z(t)$ .  $\nu \leq 0$  will be fixed while  $\lambda$  will be crossing 0 to become unstable.

### 1.1 Exact solution

---

We want to study the behavior of the system when  $\lambda > 0$  and  $\nu \leq 0$ . One question is, what is the dependence of the bifurcated solutions around  $(r_0, z_0) = (0, 0)$  on the instability parameter  $\lambda$ ? A set of stationary solutions close to the origin can be found to be

$$\begin{cases} r_\infty^2 = \frac{\lambda(\nu a_1 - \lambda b_2)}{b_1 a_1^2} (1 + O(\lambda, \nu)), \\ z_\infty = -\frac{\lambda + a_2 r_\infty^2}{a_1}. \end{cases} \tag{IV.7}$$

- First we see that to exist the solution needs  $b_1 a_1 < 0$  or if  $\nu = 0$   $b_1 b_2 < 0$  ("saturating conditions"). In practice, we want both  $b_1 a_1 < 0$  and  $b_1 b_2 < 0$  to study  $(r_\infty, z_\infty)$  with fixed parameters and varying  $\nu$ .
- The solution scaling is

$$r_\infty^2 \sim \frac{\nu}{b_1 a_1} \lambda, \quad \text{when } \lambda \rightarrow 0 \text{ and } \nu < 0 \tag{IV.8}$$

- The solution scaling is

$$r_\infty^2 \sim -\frac{b_2}{b_1 a_1^2} \lambda^2, \quad \text{when } \lambda \rightarrow 0 \text{ and } \nu = 0 \tag{IV.9}$$

This latter scaling is different from the usual "pitchfork scaling" (also called here Hopf scaling)  $r_\infty \neq O(\sqrt{\lambda})$ .

The modification provoked by the presence of a neutral mode on the imaginary axis is clear- it changes the final scaling of the solution. The solution with neutral mode is much smaller than without one. Therefore, when neutral modes couple with unstable modes one expect nonlinearities to be much stronger (saturating the perturbation at much weaker amplitudes).

## 1.2 Center manifold approach

---

Now imagine that we cannot guess directly solutions, what can we say about the evolution of the systems and the scaling of its steady states near the origin? The center manifold approach is a dynamical expansion around a stationary point of the full model Eq. (IV.7). For this example, we have  $(r_0, z_0) = (0, 0)$ . We separate the contributions of fast and slow modes. The fast manifold will regroup the contribution of eigenvalues with a finite negative real part. These modes will be quickly damped and thus will not contribute to the "slow" dynamics. On the slow manifold, we consider modes around the imaginary axis (with  $\text{Re } \lambda \approx 0$ ). For example, here  $\nu < 0$  is on the fast manifold and the  $\lambda \approx 0$  is on the slow manifold. The center manifold treats the  $\lambda$  mode as a perturbation of a neutral mode. It is described by writing Eq. (IV.6) as

$$\begin{pmatrix} \dot{r} \\ \dot{z} \end{pmatrix} = \underbrace{\begin{pmatrix} 0 & 0 \\ 0 & \nu \end{pmatrix}}_{\mathcal{L}_0} \begin{pmatrix} r \\ z \end{pmatrix} + \underbrace{\begin{pmatrix} \lambda r + a_1 z r + a_2 r^3 \\ b_1 r^2 + b_2 z^2 \end{pmatrix}}_{\mathcal{N}_\lambda}. \quad (\text{IV.10})$$

- If  $\nu < 0$ , the dynamics will go quickly (as  $\sim 1/|\nu|$ ) close to the center manifold  $W^c$ , so it is legitimate for small  $\lambda$  to parametrize this center manifold as

$$(r, z) \in W^c \text{ then } (r, z) = (r, h_\lambda(r)), \quad (\text{IV.11})$$

with  $h_\lambda(r)$  a regular function for  $r$  close to  $r_0$ . Actually, rigorous mathematical results [HI10] exist to justify that indeed for any initial condition sufficiently close to  $(r_0, z_0)$ , the dynamics will be well described by this  $\lambda$ -dependent manifold. The center manifold is the nonlinear extension of the eigenspace associated with neutral modes. The expansion of  $h_\lambda(r)$  in a series of  $r$ , gives then an expression of the dynamics  $\dot{r} = \dots$  at every order. The saturation scaling also gives

$$r_\infty^2 \sim \frac{\nu}{b_1 a_1} \lambda, \quad \lambda \rightarrow 0 \text{ and } \nu < 0$$

as in the exact asymptotic solution. So, we have successfully reduced the dimensionality from 2 to 1.

- If  $\nu = 0$ , Eq. (IV.11) is no longer the center manifold and thus has no reason to describe well the dynamics. Actually, in this case, the center manifold is of dimension 2 at criticality. So, no further reduction is possible now! The system dimension is still 2 and the scaling is not clear.

### 1.3 Unstable manifold approach

The unstable manifold is based on the idea that only unstable modes  $\text{Re } \lambda > 0$  are important. It does not consider eventual slow modes (e.g.  $\nu = 0$  or modes close to the imaginary axis). Of course these slow modes can be important to describe the full dynamics, hence leaving them aside could lead to an incomplete or wrong reduction. In our example the linear operator has a positive eigenvalue  $\lambda$  and the  $\nu$  mode,

$$\begin{pmatrix} \dot{r} \\ \dot{z} \end{pmatrix} = \underbrace{\begin{pmatrix} \lambda & 0 \\ 0 & \nu \end{pmatrix}}_{\mathcal{L}_\lambda} \begin{pmatrix} r \\ z \end{pmatrix} + \underbrace{\begin{pmatrix} a_1 z r + a_2 r^3 \\ b_1 r^2 + b_2 z^2 \end{pmatrix}}_{\mathcal{N}}. \quad (\text{IV.12})$$

In the unstable manifold picture modes different from  $\lambda$  quickly relax and thus the remaining "slow" dynamics is one-dimensional. The unstable manifold  $W^u$  in Eq. (IV.6) appears then as a one-dimensional manifold tangent to the  $r$  direction near  $(r, z) = (0, 0)$ :

$$(r, z) \in W^u \text{ then } (r, z) = (r, h(r)) \quad (\text{IV.13})$$

with  $h(0) = h'(0) = 0$  (deduced by symmetry  $r \rightarrow -r$ ). We can build as previously the unstable manifold for  $\lambda \neq 0$  and then takes  $\lambda \rightarrow 0$ . In the  $\nu < 0$  case similar mathematical results as for the center manifold hold, while for  $\nu = 0$  there is no result insuring that this manifold is attractive and thus that it describes well the dynamics close to it.

Let's construct it! From  $\dot{z} = h'(r)\dot{r}$  and Eq. (IV.6b) we get

$$h'(r) (\lambda r + a_1 h(r)r + a_2 r^3) = \nu h(r) + b_1 r^2 + b_2 h(r)^2. \quad (\text{IV.14})$$

The following expansion holds for regular maps<sup>3</sup> (which is assumed to be true near the origin)

$$h_n(r) = \sum_{j \geq 1}^n \alpha_j r^{2j}, \quad (\text{IV.15})$$

with

$$\begin{cases} \alpha_1 = \frac{b_1}{2\lambda - \nu} \\ \alpha_n = \frac{-2a_2(n-1)\alpha_{n-1} + \sum_{j=1}^{n-1} (b_2 - 2ja_1)\alpha_j \alpha_{n-j}}{2n\lambda - \nu} \quad n \geq 2. \end{cases} \quad (\text{IV.16})$$

The one-dimensional equation is then

$$\dot{r} = \lambda r + \underbrace{(a_1 \alpha_1 + a_2)}_{c_3} r^3 + \underbrace{\alpha_2}_{c_5} r^5 + \mathcal{O}(r^7). \quad (\text{IV.17})$$

So, at leading order

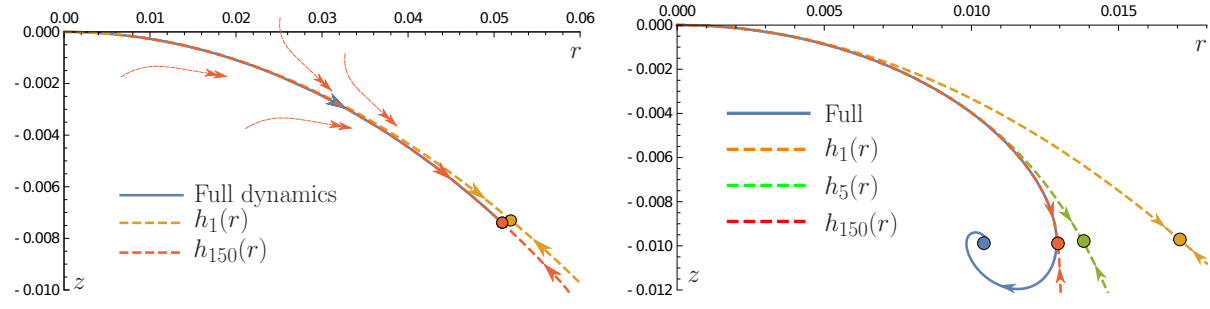
$$r_\infty^2 \sim \frac{\lambda(\nu - 2\lambda)}{a_1 b_1 + a_2(2\lambda - \nu)} \quad (\text{IV.18})$$

$$r_\infty^2 \sim \frac{\nu}{b_1 a_1} \lambda, \quad \lambda \rightarrow 0 \text{ with } \nu < 0 \quad (\text{IV.19})$$

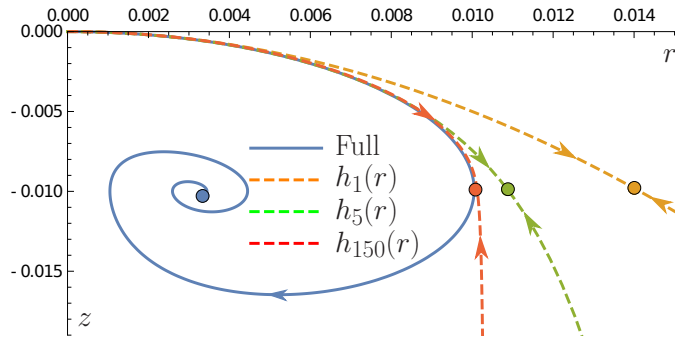
which is the same scaling as the exact asymptotic solution.

---

3. The even symmetry can be demonstrate using the  $r \rightarrow -r$  transformation or by computing every odd coefficients of  $h(r)$  and finding zero.



(a)  $\nu = -0.35$ . The double arrows show that the dynamics is quickly attracted on the unstable manifold. It follows a slow one-dimensional dynamics on this manifold.  
 (b)  $\nu = -0.01 = -\lambda$ . The unstable manifold is no longer attractive and does not describe completely the full dynamics.



(c)  $\nu = 0$ . The unstable manifold is no longer attractive and does not describe completely the full dynamics.

Figure IV.1 – Phase space  $(r, z)$ , for  $\lambda = 0.01$ ,  $a_1 = 1$ ,  $a_2 = -1$ ,  $b_1 = 0.1$ ,  $b_2 = 0.1$  with  $(r(0), z(0)) = (10^{-5}, 10^{-6})$ . The full line is the exact trajectory computed through the full dynamics Eq. (3). Dashed lines are the unstable manifold  $h_n(r)$  computed at orders  $O(r^{2n})$ . The points represent the equilibrium.

— For  $\nu = 0$ , the unstable manifold still exists and we can look at the limit  $\lambda \rightarrow 0$  as it should tend toward the previous two-dimensional center manifold. It gives

$$r_\infty^2 \sim -\frac{2}{b_1 a_1} \lambda^2, \quad \lambda \rightarrow 0 \text{ with } \nu = 0 \quad (\text{IV.20})$$

which is different from the exact asymptotic solution, but still possesses the same scaling and sign. A first observation is that higher orders are not negligible. Indeed when  $\nu = 0$ , at the saturation level is  $r_\infty \propto \lambda$ , furthermore  $\alpha_n \propto 1/\lambda^{2n-1}$ , so

$$O(\lambda r_\infty) = O(c_3 r_\infty^3) = O(c_5 r_\infty^5) = O(c_{2n+1} r_\infty^{2n+1}) = O(\lambda^2), \quad (\text{IV.21})$$

which prevents in principle any truncation!

A crucial remark is that this unstable manifold expansion with neutral modes induces diverging coefficients. Which does not appear in classical dynamical equations (here with  $\nu \leq 0$ ). Nevertheless, the first nonlinear coefficient is enough to obtain the right scaling. To appreciate those assertions, we plot on Figure IV.1 the phase space trajectory for one initial condition and compare it with the result given by the unstable manifold. We compute the unstable manifold  $h_n(r)$  at various orders  $O(r^{2n})$  to see its convergence towards the full dynamics.

- For  $|\nu = -0.35| \gg \lambda = 0.01$ , we are in a regime where the unstable manifold should describe well the dynamics. Indeed, in Figure IV.1(a), we clearly see that the end points are almost the same even at the quadratic order in  $h(r)$ . We can verify numerically that other initial condition close to the origin  $(r_0, z_0)$  are also attracted by the manifold  $h(r)$ .
- For  $|\nu = -0.01| \sim \lambda = 0.01$  Figure IV.1(b) and  $\nu = 0$  Figure IV.1(c), the timescales associated with the  $r$  and  $z$  direction are not dissociable anymore and we don't expect the unstable manifold to be attractive. We see that the effects of the neutral mode are to fold the dynamics and to saturate the end point  $r_\infty$  at a lower level (thus nonlinear effects are stronger). This folding behavior can't be captured by the unstable manifold expansion Eq. (IV.15) which is a function (thus can't have two images). Furthermore, a one-dimensional dynamics can't fold and oscillate. However it is interesting to see that the unstable manifold  $h_n(r)$  converges with  $n$  "as closely as possible" to the "branch point singularities". This phenomenon is the translation of the infinite series Eq. (IV.21).

## 1.4 Conclusion

This simple example highlighted the effect of a neutral mode coupled with an unstable mode on the bifurcation analysis resulting in

- Nonlinear effects are much stronger with a neutral mode.
- The center manifold expansion works when  $\nu < 0$  but for  $\nu = 0$  the dimensional reduction is limited by the number of neutral modes. Hence it is legitimate to think that in general with a continuous spectrum it will not be of any help.
- The unstable manifold expansion predicts the correct scaling but does not describe the effective dynamics e.g. a spiral behavior. Furthermore, no mathematical theorem insures us that it is attractive with respect the dynamics close to the origin.
- The unstable manifold expansion is plagued with a diverging coefficient. At the saturation level, every order  $O(c_{2n+1}r^{2n+1})$  contributes the same.
- It reduces the dimension of the problem.

For a system with a continuous neutral spectrum one expect those effects to be stronger! We will see that it is the case for Vlasov systems but that for the standard Kuramoto system despite the continuous spectrum the nonlinear saturation expansion behaves "normally" and the unstable manifold describes well the dynamics... However, when adding for example a second harmonic coupling, diverging coefficients  $c_{2n+1}$  appear. So, there is more to understand and say than the "continuous spectrum induces singular behavior"<sup>4</sup>....

This example should motivate using unstable manifold expansions for more complex problem where there is not only one neutral mode but an infinity and where exact solutions are hopeless (and thus dimensional reduction more than needed). So, using that expansion will possibly provide us with the right scaling for the bifurcation but one does not expect to get a true dimensional reduction in the sense of going from an infinite-dimensional system to a 1D or 2D unstable manifold. That is to say the expansion won't capture the full dynamic but will tell us if the bifurcation is discontinuous or continuous with its saturation scaling, which is a big qualitative argument.

---

4. This will be the running mystery of my Ph.D.

## 2 INFINITE-DIMENSIONAL SYSTEMS

### 2.1 Spectral problem

In this Section, we briefly review some functional analysis result about spectral analysis of infinite-dimensional operators that are different from the finite-dimensional case.

The mathematical framework to study the spectrum of linear operator for partial differential equation is more involved than the one used to study ordinary differential equation. The first difference is the dimension of the problem which is respectively infinite and finite. To get an easy vision of finite/infinite dimension one can look at the initial conditions for those two problems

- For a system of  $n$  ordinary differential equation (o.d.e.), the initial condition is a vector belonging to  $\mathbb{R}^n$
- For a partial differential equation, the initial condition is a function, for example we can choose initial distributions  $f^0$  such that  $f^0(q, p) \in L^2([-\pi, \pi] \times \mathbb{R}) \cap \mathcal{C}^\infty([-\pi, \pi] \times \mathbb{R})$ .

In this work we choose<sup>5</sup> to use only this following functional space  $\mathcal{B} = L^2([-\pi, \pi] \times \mathbb{R}) \cap \mathcal{C}^\infty([-\pi, \pi] \times \mathbb{R})$ . It corresponds to continuous quadratically integrable functions with regular derivatives. The partial differential equations will be decomposed in a linear  $\mathcal{L}$  and nonlinear  $\mathcal{N}$  operator. These operators will act on the function space e.g.

$$\mathcal{L} : \mathcal{B} \longrightarrow \mathcal{B}. \tag{IV.22}$$

An operator  $\mathcal{L}$  is bounded (continuous) if

$$\forall u \in \mathcal{B}, \|\mathcal{L}u\| \leq Mu,$$

for some norm on  $L^2$  and  $M > 0$ . In our context, we study the spectrum of an unbounded operator  $\mathcal{L}$  acting on a  $f \in \mathcal{B}$ . The choice of the function space  $\mathcal{B}$  is important and can change the spectrum.

The resolvent set of an operator  $\mathcal{L}$  is

$$\rho(\mathcal{L}) = \{\lambda \in \mathbb{C}, (\mathcal{L} - \lambda I) \text{ is bijective and } (\mathcal{L} - \lambda I)^{-1} \text{ is bounded}\},$$

where denote  $I$  the identity operator. For every  $\lambda \in \rho(\mathcal{L})$  we can define the resolvent operator as

$$R_\lambda(\mathcal{L}) = (\mathcal{L} - \lambda I)^{-1}. \tag{IV.23}$$

The complementary set  $\sigma(\mathcal{L}) = \mathbb{C}/\rho(\mathcal{L})$  is called the spectrum of  $\mathcal{L}$ . It is not just the set of its eigenvalues as in finite dimension, it is also composed of two other types of spectrum: the continuous and the residual spectrum that are regrouped in essential spectrum denomination.

- **The point spectrum** is composed of eigenvalues defined as

$$\sigma_P(\mathcal{L}) = \{\lambda \in \mathbb{C}, (\mathcal{L} - \lambda I) \text{ is not injective}\},$$

meaning that there is a non zero vector  $\Psi$  defined on  $\mathcal{B}$  such that

$$\mathcal{L}\Psi = \lambda\Psi. \tag{IV.24}$$

Its physical interpretation as characterizing the modes of a system still holds.

---

5. Some of our results may extend to broader functional spaces.

— **The continuous spectrum** consists of

$$\sigma_C(\mathcal{L}) = \{\lambda \in \mathbb{C}, (\mathcal{L} - \lambda I) \text{ is injective and with a dense image but not surjective}\}.$$

One can show that the densely defined inverse operator  $(\mathcal{L} - \lambda I)^{-1}$  is not bounded (sometime this latter assertion is chosen as the definition for  $\sigma_C(\mathcal{L})$ ). As we will see later when highlighting its physical role this spectrum is a key ingredient in the Vlasov dynamics.

— **The residual spectrum** consists of

$$\sigma_R(\mathcal{L}) = \{\lambda \in \mathbb{C}, (\mathcal{L} - \lambda I) \text{ is injective but has not a dense image}\}.$$

Its physical interpretation is not clear at all<sup>6</sup>. In all of the manuscript, we will forget this type of spectrum.

## 2.2 Free transport example

The continuous spectrum has mixing properties. In the Vlasov context the mixing occurs in the velocity space with oscillations at scale thinner and thinner in time. It is something referred as filamentation of the phase space. Here following [Vil10, BMT13] we show how the continuous spectrum of the advection operator is responsible for this phase mixing and a damping while there is no dissipation mechanism (such as friction), it is sometime referred as non-entropic relaxation. There are other informative examples with continuous spectra like the Baker's transformation [RS80]. Other cases of continuous spectrum and mixing are known in the context of fluid mechanics [SW51, Mie92, PQ02].

The advection equation is

$$\partial_t f(q, p, t) + p \partial_q f(q, p, t) = 0, \quad (\text{IV.25a})$$

$$\mathcal{L} f = -p \partial_q f, \quad (\text{IV.25b})$$

$$\mathcal{L}_k f_k = -ikp f_k, \quad (\text{IV.25c})$$

where we have rewritten its advection term as a linear operator Eq. (IV.25b) and its spatial Fourier transform Eq. (IV.25c). It is one of the simplest partial differential equation one can think of, for example, we know its solutions. Thus this makes a good example to study the effect of a continuous spectrum, indeed the advection operator spectrum is composed exclusively of a continuous part with no "true" eigenvalue.

Trying to solve the eigenvalue problem gives for an eigenvector  $(\Xi_\lambda)_k(q, p) = (\xi_\lambda)_k(p) e^{ikq}$

$$(\lambda + ikp)(\xi_\lambda)_k(p) = 0.$$

For  $\text{Re } \lambda \neq 0$ , this equation has no solutions except the null vector, so  $\sigma_P(\mathcal{L})$  is empty over  $\mathbb{C}/i\mathbb{R}$ . What about  $\text{Re } \lambda = 0$ ? Since the operator

$$(\mathcal{L}_k - \lambda I)^{-1} g(p) = \frac{g(p)}{\lambda + ikp}$$

6. One reason could be that in quantum mechanics where spectral theory of infinite-dimensional operative appeared first in physics, operators are often self-adjoint and one can show that this type of operator has an empty residual spectrum.

is clearly unbounded for  $\lambda \in i\mathbb{R}$ , by definition  $\lambda$  is in the continuous spectrum,  $\lambda \in \sigma_c(\mathcal{L}_k)$ . To every  $\lambda$  on the imaginary axis is associated a generalized eigenvectors

$$(\Xi_\lambda)_k(q, p) = \delta(\lambda + ikp)e^{ikq}.$$

We talk about generalized eigenvectors because they are not defined in the space of solution  $\mathcal{B}$ , but can be defined in a larger functional space that includes distributions like the Dirac Delta function. The conclusion is thus that there is a continuous spectrum on the whole imaginary axis for the advection operator<sup>7</sup>.

In addition, the exact solution of the equation is known as

$$f(q, p, t) = f_i(q - pt, p) = \sum_k (\hat{f}_i)_k(p) e^{-ikpt} e^{ikq} \quad (\text{IV.26})$$

where  $f(q, p, 0) = f_i(q, p)$ . To highlight the role of the continuous spectrum generalized eigenspace we can write

$$f_k = (\hat{f}_i)_k(p) e^{ik(q-pt)} = (\hat{f}_i)_k(p) \int_{\text{Re } \lambda=0} \delta(\lambda + ikp) e^{ikq+\lambda t} d\lambda = (\hat{f}_i)_k(p) \int_{\text{Re } \lambda=0} (\Xi_\lambda)_k(q, p) e^{\lambda t} d\lambda, \quad (\text{IV.27})$$

where we used the Fourier representation of the exponential.

Another way to treat this problem and see the damping due to phase mixing is go to the Fourier transform in both space  $q \rightarrow k$  and velocity  $p \rightarrow \eta$ . It gives

$$\text{FT}_{(q,p)}[f](k, \eta, t) = \text{FT}_{(q,p)}[f_i](k, \eta + kt),$$

where we used the definition of the Fourier transform and indexes change to get this expression. The Riemann-Lebesgue lemma says that the more a function is regular the more its Fourier transform decays quickly. For analytic function in  $p$  the decay is exponential in  $\eta$ , so

$$\text{FT}_{(q,p)}[f_i](k, \eta + kt) = \mathcal{O}(e^{-|\eta+ckt|}) = \begin{cases} \text{cst} & \text{for } k = 0, \text{ fixed } \eta \\ \mathcal{O}(e^{-c|k|t}) & \text{for } k \neq 0, \text{ fixed } \eta \\ \text{cst} & \text{for } \eta = -kt \end{cases} \quad (\text{IV.28})$$

where  $c$  is a constant. It means the zeroth spatial modes is unchanged. All other  $k \neq 0$  modes are damped exponentially fast. The answer to the question where does the initial energy go or why is entropy conserved<sup>8</sup> given the last term of Eq. (IV.28): the energy  $\int p^2 f dp$  is transported in time to higher and higher velocity modes  $\eta = -kt$  (cascade from low to high velocity modes). This is the mixing (filamentation) phenomena: at some point the phase space distribution seems completely homogeneous and the high frequency oscillations in the velocity space become "invisible"<sup>9</sup>. Mathematically,

$$f(q, p, t) \xrightarrow[t \rightarrow \infty]{\text{weakly}} f_\infty(p) = \int f_i(q, p) dq, \quad (\text{IV.29})$$

7. If the velocity variable was confined on a subset of  $\mathbb{R}$ , the spectrum of  $\mathcal{L}_k$  would not fill the whole imaginary axis.

8. It is preserved since it is just advection.

9. In practice even a very small dissipation process (physical or numerical) provides a cut off for those high velocity modes as we will see later in the Vlasov-Fokker-Planck Chapter VII.

meaning the initial distribution will relax to a spatially homogeneous distribution  $f_\infty(p)$ . Here the weak convergence (as opposite to strong convergence) means that to make sense the distribution has to be integrated against some test function. The physical meaning becomes clear with this example, the function converges in time for every  $k \neq 0$  and  $\eta$ , but not for  $\eta = -kt$ . So, the mixing phenomena only can produce damping/relaxation, therefore even though the equation is reversible, the observables (integrated quantities over the velocity) act as if there were dissipation. For example, the space density

$$\text{FT}_{(q,p)}[f_i](k, kt) = \int f_i(q - pt, p) dp$$

converges strongly to its end state. Since  $\eta = 0$  there are no oscillations in velocity space anymore, just the damping, so this velocity integration produces a loss of information over the localization of energy.

### 2.3 Nonlinear analysis for bifurcation

The analysis of linear infinite-dimensional systems relied mainly on their spectrum. We talk about bifurcation when a system goes from spectrally stable (or neutrally stable) to spectrally unstable. In this case, we need to consider the effects of nonlinear terms. To study the nonlinear problem there exists several different methods, like the center manifold [Van89, VI92], the Lyapunov-Schmidt reduction, multiple scale analysis... In finite-dimensional cases or in some infinite-dimensional cases these techniques work fine and provide an accurate reduced description of the full dynamics close to the bifurcation. However in presence of a continuous spectrum these methods are not trivially transposable since the slow manifold (part of the spectrum close to or on the imaginary axis) is of infinite-dimension. In these cases, to the author knowledge there are not many examples where a rigorous bifurcation analysis was performed. For the standard Kuramoto model (that we will examine in Chapter VIII) the first rigorous mathematical treatment was made by H. Chiba [Chi13, CN11] in a quite technical paper. One of his key idea is to use larger function space where the continuous spectrum is no longer on the imaginary axis. Another demonstration more generic and closer to the work of C. Mouhot and V. Villani also using larger function space was provided by H. Dietert [Die16b]. We will come back on those results in Section VIII.4.

However, this standard Kuramoto case may be very unique (because of its nonlinear structure) so that for other systems (e.g. the Vlasov equation) this idea of larger function space might not be enough to deal with the bifurcation analysis. Moreover, in addition to the continuous spectrum difficulty, a wave/particles resonance occurs for Vlasov systems making for example the multiple time scale analysis fails (see discussion in [CH89]).

Hence we will not try to generalize the previously cited, well-established methods to our cases but we will rather stick<sup>10</sup> to one efficient but incomplete method: the unstable manifold technique. It has the advantage to be formally doable even with a continuous spectrum and resonances (that appear as singularities). This method has so far always proven to give qualitatively correct informations (scaling and bifurcation nature). However, as in the finite example case with a neutral mode  $\nu = 0$  (see Figure IV.1(c)) it will not a priori provide the complete dynamics (like oscillations of the order parameter).

In next Chapters we will use the same procedure to deal with the each different case i.e. treat the linear analysis and construct the unstable manifold. However note that each case has its

10. With one exception where the center manifold is doable (see Section VI.9).

own difficulties and solving the eigenvalue/eigenvector problem as well as building the unstable manifold will require different techniques almost every time.

### 3 PHYSICAL MOTIVATIONS

---

---

At the beginning of the 20<sup>th</sup> century the Boltzmann equation was the standard equation used to describe the evolution of particle systems in position-velocity phase space. In 1938 A. Vlasov showed<sup>11</sup> that the Boltzmann equation was not suited to describe plasma and that due to the presence of long-range forces the collisions term should be removed and replaced by a self-consistent term acting as a mean field potential for every particle. The resulting kinetic equation was then studied by Landau [Lan46]. He showed by formal calculus that plasma excitations should be damped (if some stability criterion was satisfied) even though there are no dissipation terms in the equation (energy and entropy are conserved in time). The Landau damping is non intuitive since it is based on the previously seen phase mixing and Landau's demonstration used mathematical tools such as the analytic continuation, obscuring the physical result. Realness of Landau damping has since then been established numerically [CK76, Man97, ZGS01] (I uploaded an example on my [website](#)<sup>12</sup>) and experimentally [CP70, MW64]. Quite recently his result was completed by C. Villani and C. Mouhot [MV11], they showed that Landau damping can also occur when keeping nonlinear terms of the equation, with some mathematical maximum bound for the perturbation. I recommend the lecture notes of C. Villani [Vil10] on this topic compiling a lot of mathematical and physical knowledge on the Vlasov equation. For a discussion on the Landau damping in the Vlasov-gravity case see [Kan98].

Plasma stability was therefore understood, but it has been observed that some cold homogeneous plasma with a bump in their velocity distribution could become unstable and form some small non homogeneous structures resulting in a non zero electric field  $E$ , this is called the bump-on-tail instability. Various plasma instabilities were discovered such as two stream instabilities. The initial instability is caused by the resonant interaction between fluctuation (perturbation) of the initial zero electric field and particles with the same phase velocity. Then at the nonlinear level particles are trapped by the wave created by the now nonzero electric field. Mathematically to understand this process, we consider first the linear instability and the associated exponential growth and then the nonlinear saturating effects. This analysis could provide the final electric field amplitude  $E_\infty$  after a perturbation with respect to some small instability parameter  $|\mu - \mu_c|$ . At this point two contradictory results emerged in the literature: one predicting  $E_\infty \propto \sqrt{|\mu - \mu_c|}$  (called Hopf scaling) [SR76, JR81, BMWZ85, Den85] while the other finding a much smaller amplitude  $E_\infty \propto |\mu - \mu_c|^2$  (called trapping scaling) [OWM71, Dew73]. In the Hopf scaling group for example, Simon and Rosenbluth [SR76] lead a multiple scale expansion producing some singular terms that were regularized with ad hoc prescriptions. In the other group the trapping scaling was found with some adiabatic approximation or introduced as an ansatz. Careful numerical simulations [Den85, SRS88] and even experiments [TDM87] con-

---

11. Although he was not the first one to write it, he correctly recognized that for long-range interaction as mentioned in [PCMM15] the Boltzmann interaction term was inadequate [Vla68] "*or a system of charged particles the kinetic equation method which considers only binary interactions – interactions through collisions – is an approximation which is strictly speaking inadequate, so that in the theory of such systems an essential role must be played by the interaction forces, particularly at large distances and, hence, a system of charged particles is, in essence, not a gas but a distinctive system coupled by long-range forces.*"

12. <http://math.unice.fr/~metivier/video.html>

firming that the correct scaling was the "trapping scaling". J.D. Crawford tried a heavy approach without any approximation on the characteristic time of the nonlinearity  $\tau_{NL}$ ; he developed a theory considering all the eigenvalues and continuous spectrum [CH89], deriving an infinite system of coupled o.d.e. for the amplitude evolution of each mode. Nevertheless, this heavy computation was useless to predict anything. In 1994 he published a paper [Cra94a] where he only considered the unstable mode and the unstable manifold reducing drastically the dimension of the problem. Despite the singularities present in his analysis (like in IV.1) he was able to predict a bifurcation with a scaling consistent with numerics and experiments. His result is very powerful because the method is very generic (as we shall use it for the rest of the manuscript). More recent works by D. del-Castillo-Negrete [dCN98b, dCN98a] later generalized in [BMT13], also confirmed this result by this time finding an infinite dimensional normal form<sup>13</sup> for this bifurcation (in the spirit of T.M. O'Neil, J.H. Malmberg and J.H. Winfrey) called the Single-Wave-Model (SWM). Actually, this SWM proved to describe a lot more systems than bifurcation around homogeneous Vlasov states since it also accounts for bifurcation of a large class of Hamiltonian systems such as Shear flow and the XY model.

In Chapter IV we review in detail the classic results on Landau damping and on the unstable manifold used by J.D. Crawford. Since all other Chapters will be based on this method we will explain the computation in full details.

A natural sequel to this well-known case is to consider bifurcation around steady non homogeneous states with  $E_0 \neq 0$ . To illustrate this we will switch from plasma to astrophysical systems (the formalism is the same) where these non homogeneous situations are more frequent. Consider the self-gravitating system evoked in the introduction with a steady radial distribution of stars, how will it bifurcate? Does Landau damping still exist? Is an unstable manifold expansion or SWM still possible? How does the resonance phenomena survive? In Chapter VI we briefly review the formalism and results used for non homogeneous Landau damping obtained by J. Barré, A. Olivetti and Y.Y. Yamaguchi. Then we present our study of the unstable manifold for the bifurcation around inhomogeneous states obtained in collaboration with J. Barré and Y.Y. Yamaguchi. This work was published in [BMY16] and holds for generic potentials. A potential astrophysical application will be considered. As we will show the effect of wave/particles resonances is weaker, nevertheless we can still talk about Landau damping (with certain modifications) and trapping scaling  $E_\infty - E_0 \propto |\mu - \mu_c|^2$ . However, this time it is not because of a "resonant trapping" thus a SWM is not expected... Moreover we present recent results (not published yet) where a three-dimensional reduction of the bifurcation is achieved without any singularities in the coefficients (contrary to the unstable manifold) as well as a convincing agreement with simulations. This reduced systems known as the Triple Zero bifurcation could be very generic for degenerate<sup>14</sup> Hamiltonian systems (with weak resonances).

In Part One we used the Vlasov-Fokker-Planck equation to describe atom evolution in an optical molasses with Coulomb like interaction. From a theoretical point of view, how the infinite-dimensional properties (continuous spectrum, Landau damping, Casimir invariant, etc.) of the Vlasov equation are modified in the presence of small friction? In Chapter VII we answer these questions and give the different regimes of bifurcation with respect to friction. For small friction, the solution will behave as the pure Vlasov equation with trapping scaling while for large friction we will get a more standard Hopf scaling. This question is very important since in a sense it allows the linking of the different approaches mentioned above (predicting different scaling) and the understanding the role of friction in the nonlinear terms.

13. A normal form can be seen as the simplest way to describe a given bifurcation highlighting its essential features.

14. Degenerate in the sense of the Poisson brackets [MH13, HM13]



---

## VLASOV SYSTEMS AROUND HOMOGENEOUS EQUILIBRIUM

---

In this Chapter, we retrace known results obtained mainly by L.D. Landau and J.D. Crawford on the bifurcation around homogeneous states of the Vlasov equation. Historically in the early 20<sup>th</sup> century the Vlasov equation was used to describe the physics of plasmas where the interaction potential is the Coulomb one  $V_{\text{Coulomb}}(r) = C_3/|r|$  or astrophysical systems using Newton interactions. In this Part, we restrict to the one dimensional Vlasov equation referred with the abbreviation 1D (one spatial dimension + one velocity dimension). A lot of essential features survive in 2D or 3D systems such as Landau damping while 1D has the advantage of keeping the analysis rather simple. Despite this, in 3D new types of bifurcation might appear but the essential physical mechanism of the 1D case should remain.

A way to generalize the Coulomb/Newton potential in other dimensions is to use the Poisson equation it satisfies as a definition, for attractive systems this gives

$$V_{3\text{D}}(r) = -G_3/|r|, \tag{V.1a}$$

$$V_{2\text{D}}(q_x, q_y) = G_2 \log(|q_x^2 + q_y^2|), \tag{V.1b}$$

$$V_{1\text{D}}(q) = G_1|q|. \tag{V.1c}$$

To avoid heavy generic computations, we will restrict in this manuscript to a particular interaction potential between particles, the so-called Hamiltonian Mean Field potential [AR95]. It is defined through the first mode of the Fourier series of the 1D potential

$$V_{1\text{D}}(q) = G_1|q| = -2G_1 \sum_{k=1}^{\infty} \frac{\cos(kq)}{k^2}, \tag{V.2}$$

so

$$V_{\text{HMF}}(q) = -\cos q. \tag{V.3}$$

In fact, it is also the potential term of a pendulum and because of its simplicity we will carry out a lot of explicit computations. Here this choice is only motivated by simplifying the formalism. Moreover, this choice allows direct comparison with numerics (we only use a Vlasov-HMF solver) and an easy physical picture. Another motivation is that this potential is also used in the Kuramoto model studied later in Chapters VIII, IX, X so the comparison between the two models will be easier. Lastly, although it was originally used to study toy models some physical systems display HMF interactions [SJM15]. Nevertheless, the following bifurcation problems were also solved for more generic potential with the same results, see [Cra95a, BMY16]. Throughout this Section, we will keep track of what is generic and what is not.

In order to apply the unstable manifold techniques for kinetic equations with a continuous spectrum (after the finite dimensional example of Section IV.1) in different cases, it will be useful to redo Crawford's original calculations [Cra94a, Cra95a] for what will be considered as the "standard-case" of this thesis.

## 1 INITIAL PROBLEM

---

For the HMF interaction potential the microscopic equations for particles on a 1D ring<sup>1</sup>,  $(q, p) \in ]-\pi, \pi] \times \mathbb{R}$  are for the  $i^{\text{th}}$  particles

$$\dot{q}_i = p_i, \quad (\text{V.4a})$$

$$\dot{p}_i = -\frac{1}{N} \sum_{i \neq j} \sin(q_j - q_i), \quad (\text{V.4b})$$

where we set the particles mass  $m_p = 1$ . The associated Vlasov-HMF equation giving the evolution of the density  $F(q, p, t)$  is

$$\partial_t F + p \partial_q F - \partial_q \phi[F] \partial_p F = 0 \quad (\text{V.5a})$$

$$\phi[F](q) = \int_{-\infty}^{\infty} \int_{-\pi}^{\pi} V_{\text{HMF}}(q - q') F(q', p', t) dq' dp' = V_{\text{HMF}} \star_q \int_{-\infty}^{\infty} F dp \quad (\text{V.5b})$$

$$\int_{-\infty}^{\infty} \int_{-\pi}^{\pi} F dq dp = 1 \quad (\text{V.5c})$$

where  $\star_q$  is the convolution in space (this formulation makes easy the Fourier transform). From now on we will omit the integration bounds. For the HMF potential the mean field potential  $\phi[F]$  becomes

$$\phi[F](q) = -M_c[F](t) \cos q - M_s[F](t) \sin q = -|M| \cos(q - \varphi_M) \quad (\text{V.5d})$$

$$M[F] = M_c[F] + i M_s[F] = \iint F e^{iq} dq dp, \quad (\text{V.5e})$$

where  $M$  is in general referred as the magnetization of the system and  $\varphi_M$  the phase of the potential (defined as the phase of the magnetization). Eq. (V.5a) describes the time evolution of the density  $F(q, p, t)$  in the phase space  $(q, p)$ ; Eq. (V.5b) defines the self-consistent mean field potential  $\phi[F](q)$  (for real systems it is a relevant macroscopic observable like the electric field

---

1. Since the potential is periodic it is a natural choice to have periodic boundary conditions.

of a plasma); Eq. (V.5e) defines the HMF order parameter called magnetization and Eq. (V.5c) is the normalization condition, true for all time  $t$ . For  $M = 0$  the system is unmagnetized (spatially homogeneous), for  $|M| = 1$  the particles distribution is a delta Dirac function (fully magnetized). Without loss of generality we choose in the following  $\varphi_M = 0$  so that the energy minimum is situated in  $q = 0$ . In this Section the initial magnetization  $M(t = 0) = M_0 = 0$  is zero which means that the system is spatially homogeneous (unmagnetized).

**The basic question we ask here is what is the fate of a perturbation around a homogeneous stationary state?** We decompose the solution as

$$F(q, p, t) = f^{(0)}(p) + f(q, p, t),$$

where we have the following normalization conditions

$$\iint f^{(0)} dq dp = 1, \quad \iint f dq dp = 0.$$

To perform the unstable manifold analysis we rewrite the problem in terms of a linear  $\mathcal{L}$  and nonlinear  $\mathcal{N}$  operator

$$\partial_t f = \mathcal{L} f + \mathcal{N}[f] \tag{V.6a}$$

$$\mathcal{L} f = -p \partial_q f + \partial_q \phi[f] (f^0)'(p) \tag{V.6b}$$

$$\mathcal{N} f = \partial_q \phi[f] \partial_p f. \tag{V.6c}$$

---

## 2 SPECTRUM OF THE HOMOGENEOUS VLASOV OPERATOR

---

The latter term of Eq. (V.6b) is a compact perturbation of the advection operator Eq. (IV.25b) (because it is of rank two) so it doesn't change the essential spectrum [Kat95] that is the continuous spectrum. Therefore, the mixing phenomenon studied in Section IV.2.2 is expected to remain, the difference is that now there might be some eigenvalues where for the advection the spectrum was only composed of the continuous one. A complete analysis of the spectrum of Eq. (V.6b) is given in [Deg86].

### 2.1 Eigenvalue problem

---

Let's look at the spectral problem for an eigenvalue  $\lambda$  associated with an eigenvector  $\Psi_k$ . From the linear Vlasov operator Eq. (V.6b) we get in the Fourier space

$$\mathcal{L}_k f_k = -ik p f_k + 2\pi i k (V_{\text{HMF}})_k \int f_k dv \times (f^0)'(p) \tag{V.7}$$

where  $(V_{\text{HMF}})_k = -(\delta_{1,k} + \delta_{-1,k})/2$ .

For  $k = 0$  it is direct to see that  $\mathcal{L}_0 = 0$  so  $\lambda = 0$  is an eigenvalue and any function  $\Psi_n = \psi(p) \neq 0$  is an associated eigenvector. So, there is always an 0 mode with an eigenspace of infinite-dimension. It is related to the infinite number of possible stationary states. Without spatial structure the mean field force is zero. As we shall see later, adding dissipation breaks this structure.

For  $k \neq 0$  we take  $\Psi_k = \psi_k(p)e^{ikq}$ , we find

$$(\lambda + ikp)\psi_k = -ik\pi(f^0)'(\delta_{1,k} + \delta_{-1,k}) \int \psi_k dp. \quad (\text{V.8})$$

It gives for  $\text{Re } \lambda \neq 0$

$$\psi_k(p) = -ik\pi \frac{(f^0)'(p)}{\lambda + ikp}, \quad (\text{V.9})$$

where we have chosen the normalization

$$\int \psi_k dp = 1. \quad (\text{V.10})$$

The normalization condition gives us the dispersion relations<sup>2</sup>  $\Lambda_k(\lambda)$  whose roots are the eigenvalues

$$\Lambda_k(\lambda) = 1 + ik\pi \int \frac{(f^0)'(p)}{\lambda + ikp} dp, \quad (\text{V.11})$$

for  $k = \pm 1$ . For generic potential, each  $k \neq 0$  has its dispersion relation but it just changes the prefactor in front of the integral. It is easy to observe by taking the complex conjugate  $(\Lambda_k(\lambda))^*$  that if  $\lambda$  is an eigenvalue for  $\Lambda_k$  so is  $\lambda^*$  for  $\Lambda_{-k}$ . Similarly, if  $\lambda$  is an eigenvalue for  $\Lambda_k$  so is  $-\lambda$  for  $\Lambda_{-k}$ . It already gives precious information which is that if there is one stable eigenvalue there is also one unstable. Therefore, a marginally stable equilibrium requires that there are no solutions to Eq. (V.11), which says that only the continuous spectrum relaxes the system with no additional damping of a negative eigenvalue. The stability criterion is obtained by taking the limit  $\lambda_r = \text{Re } \lambda \rightarrow 0^+$ , one has to be careful performing this limit and use the Plemelj formula

$$\lim_{\epsilon \rightarrow 0} \int \frac{g(p)}{p - i\epsilon} dp = \text{PV} \int \frac{g(p)}{p} dp + i\pi g(0). \quad (\text{V.12})$$

This formula is counter intuitive since it gives a finite imaginary part to the limit while one could have expected that it should go to zero. In fact, this formula can be obtained by deforming the integration path in the complex plane as in Figure V.4(a) to avoid the singularities as  $\epsilon \rightarrow 0$ . Thus, we get the following stability criteria

$$\mathcal{I}[f^0] = \Lambda(0^+ + i\lambda_i) = 1 + \pi \left( \text{PV} \int \frac{(f^0)'(p)}{p + \lambda_i/k} dp + i\pi(f^0)'(-\lambda_i/k) \right). \quad (\text{V.13})$$

For  $\mathcal{I}[f^0] > 0$ ,  $f^0$  is spectrally stable [Oga13] meaning that there is no eigenvalues (neither positive nor negative). At criticality, both  $\text{Re}(\text{V.13}) = \text{Im}(\text{V.13}) = 0$  which implies that  $(f^0)'(-\lambda_i/k) = 0$ . Hence for an initial Gaussian distribution  $\lambda_i = 0$  and the eigenvalue is real. For a Coulomb repulsive potential one can obtain a similar criterion, the difference being that due to the change of sign in front of the integral Gaussian distributions are always stable. Unstable distributions have bump(s) on their tail(s) and are associated with a complex pair of eigenvalues.

### Remark V.1

Unless specified we will always assume that the eigenvalues of  $\mathcal{L}_k$  are simple  $\Lambda_k'(\lambda) \neq 0$  in all the manuscript. However there might be some confusion here indeed the full dispersion relation

2. This denomination is abusive since the dispersion relation is strictly defined by the relation  $\Lambda_k(\lambda) = 0$ .

of  $\mathcal{L}$  is given by  $\Lambda(\lambda) = \Lambda_1(\lambda)\Lambda_{-1}(\lambda)$ , so a real eigenvalue will be of multiplicity two for the full operator  $\mathcal{L}$ ,

$$\Lambda'(\lambda) = \Lambda_1'(\lambda) \underbrace{\Lambda_{-1}(\lambda)}_{=0} + \underbrace{\Lambda_1(\lambda)}_{=0} \Lambda_{-1}'(\lambda) = 0$$

but simple with respect to  $\mathcal{L}_k$  and the dispersion relation  $\Lambda_k'(\lambda) \neq 0$ . However, in [CH89] with spectral deformation technique is shown that at criticality  $\lambda_c \in i\mathbb{R}$  is simple.

## 2.2 Continuous spectrum

Now that we know the eigenvalues we want to characterize the continuous spectrum over the imaginary axis, see Figure V.1, finding its associated generalized eigenvectors. Looking for  $\Xi_k(q, p) = \xi_k(p)e^{ikq}$  associated with  $\lambda \in i\mathbb{R}$  gives

$$(\lambda + ikp)\xi_k = -ik\pi(f^0)'(\delta_{1,k} + \delta_{-1,k}) \int \xi_k dp. \quad (\text{V.14})$$

Dividing by  $(\lambda + ikp)$  gives a singular contribution (in the distribution sense) [VK55, Cas59],

$$\xi_k(p) = -ik\pi \text{PV} \frac{(f^0)'(p)}{\lambda + ikp} + \delta(\lambda + ikp)A(\lambda), \quad (\text{V.15})$$

for some function  $A_k(\lambda)$  and  $k = \pm 1$  where we have imposed

$$\int \xi_k dp = 1.$$

These are the van Kampen modes are all excited during phase mixing [Bra98, BMT13]. The normalization condition gives

$$A(\lambda \in i\mathbb{R}) = 1 + ik\pi \text{PV} \int \frac{(f^0)'(p)}{\lambda + ikp} dp. \quad (\text{V.16})$$

## 3 ADJOINT PROBLEM

In linear algebra, the notion of scalar product with projection and basis is crucial. It allows for example to decompose a vector in the basis formed by eigenfunctions. What about infinite-dimensional systems with a continuous spectrum? Does such decomposition still hold? In [Cas59], K.M. Case shows the completeness of the basis formed by the eigenvector and generalized eigenvector. We first need to define a scalar product and what is called a dual (adjoint) space of functions upon which to project (as the bra and ket in quantum mechanics or line and column vector in finite-dimensional systems).

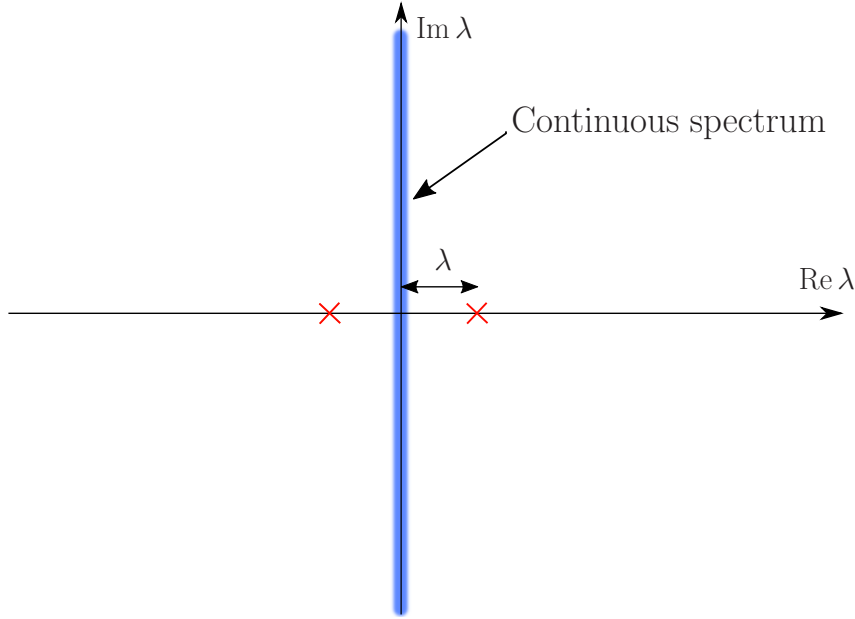


Figure V.1 – Spectrum of the linear homogeneous Vlasov operator with one continuous spectrum on the imaginary axis. Here we show an unstable case with two eigenvalues  $\lambda, -\lambda$  real (in a stable case these two would disappear but not the continuous spectrum).

### 3.1 Adjoint operator construction

---

We denote  $\mathcal{B}^*$  the dual functional space of our space  $\mathcal{B}$  (which is different in general). We define the "scalar product" over the two space for  $f \in \mathcal{B}$  and  $g \in \mathcal{B}^*$  as

$$(g, f) = \int \langle g, f \rangle dq \quad (\text{V.17a})$$

where

$$\langle g, f \rangle = \int g^* f dp. \quad (\text{V.17b})$$

The dual (adjoint) operator  $\mathcal{L}^\dagger$  is then defined by the relation

$$(g, \mathcal{L} f) = (\mathcal{L}^\dagger g, f). \quad (\text{V.18})$$

Similarly, to what has been done previously, we can look for the eigenvalues and eigenvectors for this operator. Let's make explicit the derivation of  $\mathcal{L}^\dagger$ ,

$$\begin{aligned} (g, \mathcal{L} f) &= - \iint g^* p \partial_q f dq dp - \iint g^*(q, p) f^0(p) \left( \iint \partial_q \cos(q - q') f(q', p') dq' dp' \right) dq dp \\ &= \iint (p \partial_q g^* + \phi[g^*(f^0)']) f dq dp = (\mathcal{L}^\dagger g, f) \end{aligned} \quad (\text{V.19})$$

where we have use integration by part in the first member and integral exchange in the second

one to write the second line. So

$$\mathcal{L}^\dagger g = p\partial_q g + \phi[\partial_q g(f^0)'] \quad (\text{V.20a})$$

$$\mathcal{L}_k^\dagger g_k = ikpg_k + \phi_k[\partial_q g(f^0)']. \quad (\text{V.20b})$$

### 3.2 Eigenvalue problem

---

We denote by a tilde the adjoint eigenvectors (not to be mistaken with the  $*$  for the complex conjugate). We have to solve

$$\mathcal{L}^\dagger \tilde{\Psi}_k = \lambda^* \tilde{\Psi}_k \quad (\text{V.21})$$

which gives for  $\tilde{\Psi}_k = \tilde{\psi}_k(p)e^{ikq}/(2\pi)$  and  $\text{Re } \lambda \neq 0$

$$\tilde{\psi}_k(p) = \frac{1}{(\Lambda'_k(\lambda))^* \lambda^* - ikv}, \quad (\text{V.22})$$

where we have chosen the normalization factor so that

$$\left( \tilde{\Psi}_k, \Psi_k \right) = \left\langle \tilde{\psi}_k, \psi_k \right\rangle = 1. \quad (\text{V.23})$$

Indeed, the derivative with respect to  $\lambda$  of the relation dispersion  $\Lambda'_k(\lambda)$  appears naturally in the normalization, one can check that

$$\left\langle \tilde{\psi}_k, \psi_k \right\rangle = -\frac{ik\pi}{\Lambda'_k(\lambda)} \int \frac{(f^0)'(p)}{(\lambda + ikp)^2} dp = \frac{\Lambda'_k(\lambda)}{\Lambda'_k(\lambda)} = 1. \quad (\text{V.24})$$

#### Remark V.2

This "functional" link between scalar product of an eigenvector with its adjoint  $\left\langle \tilde{\psi}_k, \psi_k \right\rangle(\lambda)$  and the first derivative of the dispersion relation  $\Lambda'_k(\lambda)$  is something apparently very generic, similar relations were found for every linear problem treated in this manuscript and eventually "proven" for very generic linear operator in a quite surprising way (see Chapter X). I am not aware of similar results, such result can for example predict directly the right normalization choice.

It can be proven that the eigenvalues associated with  $\tilde{\Psi}$  satisfy the dispersion relation Eq. (V.11) thus the point spectrum of  $\mathcal{L}^\dagger$  is the same than  $\mathcal{L}$ .

[Cas59, CH89, HC89]

## 4 LINEAR LANDAU DAMPING

---

The Landau damping (sometime called resonant relaxation in the astrophysics community or non-entropic relaxation) of stable equilibrium is a phenomenon directly linked with the phase mixing seen previously, IV.2.2. The standard historical way to derive it is to study the linear initial value problem, solve the problem with the Laplace transform in time and then get back to the real problem with the inverse Laplace transform. At this point to evaluate the integral one has to deform the integration contour and the damping is given by the roots of the analytics

continuation of the dispersion relation, these are called **resonances**. The term resonance here has not the usual physical sense (of two components with the same frequency), here it really just denotes a root of the analytical continuation of the dispersion relation.

There exists simpler and stronger ways to show Landau damping via Volterra equation, see the well explained thesis of H. Dietert [Die16a], here we focus on the Landau approach to highlight among other things the analytical continuation method for the dispersion relation that will serve us in Section VII.2.3.

To observe the Landau damping as L.D. Landau found it, we solve the initial value problem considering  $F(x, v, 0) = f^0(v) + f(x, v, 0) = f^0(v) + f^i(x, v)$ . We set ourselves in the stable case so  $\Lambda(\lambda)$  does not have any roots. The Laplace transform is defined by

$$\hat{f}(\omega) = \int_0^\infty f(t)e^{-\omega t} dt \quad (\text{V.25})$$

where  $\text{Re } \omega > 0$  for the integral to be well defined. The inverse Laplace transform is defined through

$$f(t) = \frac{1}{2\pi i} \int_{-i\infty+\sigma_0}^{+i\infty+\sigma_0} \hat{f}(\omega)e^{\omega t} d\omega \quad (\text{V.26})$$

where  $\sigma_0 \in \mathbb{R}$  is large enough to be at the right of every singularity of  $\hat{f}(p)$ .

Inserting the Laplace transform directly in

$$\partial_t f_k = \mathcal{L}_k f_k \quad (\text{V.27})$$

gives for  $k = \pm 1$

$$(\omega + ikp)\hat{f} = -ik\pi(f^0)'(p) \int \hat{f}_k(p', \omega) dp' + (f^i)_k(p) \quad (\text{V.28})$$

since  $\text{Re } \omega > 0$  we can safely divide. We get eventually

$$2\hat{\phi}_k[f](\omega) = - \int \hat{f}_k dp' = \frac{-1}{\Lambda(\omega)} \int \frac{(f^i)_k}{\omega + ikp} dp = \frac{1}{\Lambda(\omega)} \varphi_k^i(\omega) \quad (\text{V.29})$$

where again the division by  $\Lambda(\omega)$  is safe since we have assumed to be in the stable case. Now we want to get back to the real time  $\omega \rightarrow t$ , taking the inverse Laplace transform gives

$$\phi_k[f](t) = \frac{1}{4\pi i} \int_{-i\infty+\sigma_0}^{+i\infty+\sigma_0} \frac{\varphi_k^i(\omega)}{\Lambda(\omega)} e^{\omega t} d\omega. \quad (\text{V.30})$$

When ending up with such integral one wants to use complex analysis results to deform the integration contour toward the left part of the complex plane (so that  $e^{-\omega t}$  goes to zero with  $\text{Re } \omega \rightarrow -\infty$ ) and just look for the pole contribution. That was the strategy of Landau when facing this integral. We assume that the initial condition  $f_i$  is regular enough to be analytically continued in the left part of the plane then so is  $\varphi_k^i$  (with Plemelj formula). Moreover, we assume that the continuation of  $f^i$  has no pole in the left plane. Now what about  $\Lambda(\omega)$ ? We know it is not continuous from the right plane to the left, but we can construct an analytic continuation  $\epsilon(\omega)$  analytic on the all complex plane as follow

$$\epsilon(\lambda) = \begin{cases} \Lambda(\lambda), & \text{Re } \lambda > 0 \\ 1 + k\pi \text{PV} \int_{-\infty}^{\infty} \frac{(f^0)'(p)}{p - i\lambda} dp + i\pi^2 (f^0)'(i\lambda), & \text{Re } \lambda = 0 \\ 1 + k\pi \int_{-\infty}^{\infty} \frac{(f^0)'(p)}{p - i\lambda} dp + 2i\pi^2 (f^0)'(i\lambda), & \text{Re } \lambda < 0. \end{cases} \quad (\text{V.31})$$

This is continuous by construction see Eq. (V.13). Another method is to write

$$\frac{1}{\lambda + ip} = \int_0^\infty e^{-(\lambda+ip)p} dp, \quad \text{Re } \lambda > 0$$

so, that

$$\epsilon(\lambda) = 1 + i\pi \int_{-\infty}^\infty \int_0^\infty e^{-(\lambda+ip)p} (f^0)'(p) dp, \quad \forall \lambda \in \mathbb{C}. \quad (\text{V.32})$$

This new function can have roots  $\omega_d$  on the left plane, they are called **resonances** (but they do not have the traditional physical sense of resonance, see Section V.6).

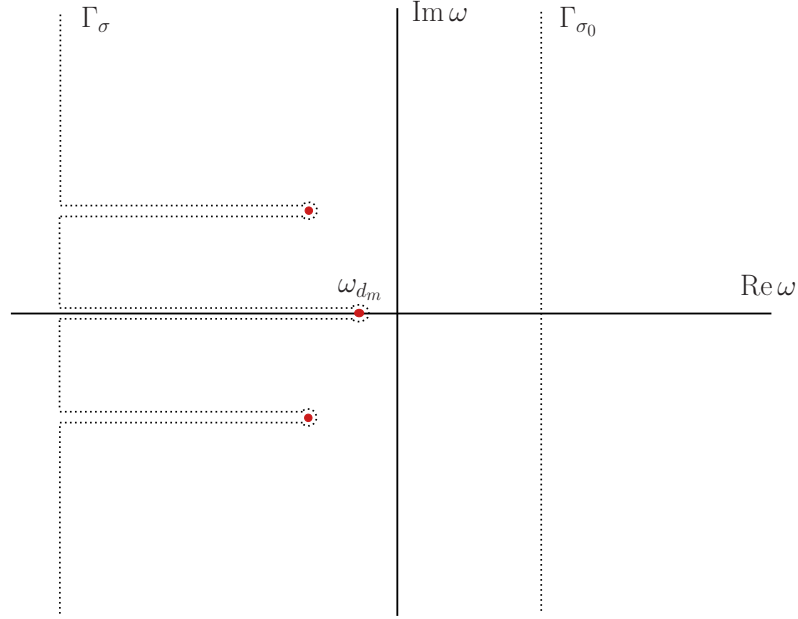


Figure V.2 – Deformation of the contour of integration  $\Gamma_{\sigma_0} \rightarrow \Gamma_\sigma$  in the left plane avoiding the resonances.  $\omega_{d_m}$  has is the resonances with the largest real part.

We know that deforming the integral contour does not change the result of the integral, so we have

$$\phi_k[f](t) = \frac{1}{4\pi i} \int_{-i\infty+\sigma_0}^{+i\infty+\sigma_0} \frac{\varphi_k^i(\omega)}{\Lambda(\omega)} e^{\omega t} d\omega = \lim_{\sigma \rightarrow -\infty} \int_{\Gamma_\sigma} \frac{\varphi_k^i(\omega)}{\epsilon(\omega)} e^{\omega t} d\omega \quad (\text{V.33})$$

where  $\Gamma_{\sigma_0}$  is the deformed contour as in Figure V.2, that avoid the poles of  $1/\epsilon(\omega)$  produced by the root of  $\epsilon(\omega)$ . According to the residue theorem we have

$$\phi_k[f](t) = \frac{1}{2\pi i} \sum_d R_d(\omega) e^{\omega_d t} \underset{\infty}{\overset{t \rightarrow \infty}{\rightarrow}} e^{-|\text{Re } \omega_{d_m}| t} \rightarrow 0 \quad (\text{V.34})$$

where  $R_d$  are the residues and  $\text{Re } \omega_{d_m} < 0$  is the resonance with the largest real part that will dominate for large times the damping. This is the Landau damping, the perturbation is damped in time with no dissipation mechanism. Note that once again as in IV.2.2 the full distribution  $f(q, p, t)$  will be highly oscillating and will only converge to zero in a weak sense. In fact, we could have looked as in Section IV.2.2 at the velocity Fourier transform and get similar result, with the advantage of keeping the information over velocity (here we just look at the integrated density). That is the direction taken in [MV11] to prove nonlinear Landau

damping, that we have no time to develop here. Another method would have been to decompose a function over the basis formed by the generalized eigenvectors observe the linear Landau damping, see [VK55, Cas59].

The classical physical picture for this damping is that the perturbing wave  $\phi_k[f]e^{ikq} + \text{c.c.}$  which has a frequency  $\omega_i = \text{Im} \omega_{d_m}$ , loses energy to the resonant particles  $p \sim \omega_i$ . On my [personal website](#)<sup>3</sup> one can find a Vlasov-HMF simulation of Landau damping, see "[Landau\\_Damping.mp4](#)". The filamentation of the velocity space is clearly visible thanks to the good resolution.

## 5 NONLINEAR EXPANSION

---

Now that we have reviewed the case where a homogeneous state is stable and small perturbation are damped thanks to Landau damping, we will review the case treated by J.D. Crawford [Cra94b, Cra95a] for unstable steady states. Close to the onset of the bifurcation we suppose that only one eigenvalue  $\lambda$  (or a pair of complex conjugate  $\lambda, \lambda^*$ ) emerges in the right complex plane from the continuous spectrum. That will be our unstable mode. As we have seen also appears a negative eigenvalue  $-\lambda$ .

- In the astrophysical context, instabilities can develop when a distribution of stars have a kinetic energy too weak to support the pressure applied by the potential energy. In terms of distribution for example,

$$f^0(p) = \sqrt{\mu} \frac{e^{-\mu p^2/2}}{(2\pi)^{3/2}},$$

the system goes unstable when the parameter  $\mu$  (related to the inverse of the temperature) is varied over a certain value  $\mu_c$ . In astrophysics, this type of instability leads to a collapse and it is known as the Jeans instability.

- In plasma physics as already mentioned, an unstable distribution could be for example as

$$f^0(p) = \frac{e^{-p^2/2}}{(2\pi)^{3/2}} + \mu \frac{e^{-(p-p_0)^2/2}}{(2\pi)^{3/2}},$$

leading to the bump-on tail-instability for a certain bump size  $\mu > \mu_c$  and frequency  $p_0$ .

The idea is the same as in the example IV.1, we want to construct the unstable manifold associated with the unstable eigenvalue  $\lambda$  (or  $\lambda, \lambda^*$ ) close to the bifurcation  $\text{Re} \lambda \rightarrow 0$ . We hope to get a dimensional reduction from infinite to one or two, which would simplify a lot the description of the bifurcation. But as we have seen in the example due the continuum of neutral modes, the constructed manifold will a priori not be attractive and will not describe for example oscillating behavior. Nevertheless, we hope to get precious qualitative information such as the sub/super-critical nature of the bifurcation and in the latter case the scaling of saturation.

### Remark V.3

In the Fourier space, the unstable modes will be associated with  $k = \pm 1$ , for more generic potential, we should also consider other modes but in practice the mode  $k = \pm 1$  are always the first to be unstable so other  $k$ -modes are not associated with eigenvalues just continuous spectrum.

From now on the subscript  $k$  to  $\Psi_k, \Lambda_k$ , etc. will be dropped (as it is  $k = \pm 1$  and there are not ambiguities).

---

3. <http://math.unice.fr/~metivier/video.html>

## 5.1 Symmetries

Before starting building the unstable manifold it is worth looking at the symmetries of the system. Let's define the rotation  $\mathcal{S}_\theta \in \mathcal{SO}(2) : (q, p) \rightarrow (q + \theta, p)$  and reflexion  $\mathcal{S}_R \in \mathcal{O}(2) : (q, p) \rightarrow (-q, -p)$  symmetries. If  $f^0$  is even (reflexion symmetry) then the eigenvalue  $\lambda$  is real Eq. (V.13) associated with a eigenspace of dimension two  $\Psi, \mathcal{S}_R \Psi = \Psi^*$ . Conversely if  $f^0$  is not even the reflexion symmetry is broken, there are two complex eigenvalues  $\lambda = \lambda_r + i\lambda_i$  and  $\lambda^*$  associated respectively with  $\Psi$  and  $\Psi^*$ . Therefore, in both cases the unstable space is of dimension two.

### Remark V.4

An unstable space of dimension four is possible if reflexion symmetry still holds and eigenvalues  $\lambda, \lambda^*$  are complex (as in the plasma case with the two-stream instability) associated respectively with  $\Psi, \mathcal{S}_R \Psi$  and  $\Psi^*, \mathcal{S}_R \Psi^*$ . We will not study this case in this thesis.

### Remark V.5

In [CH89, HC89] authors studied the spectral properties of the Vlasov linear operator. They highlight another difference between the infinite and finite-dimension system that we will explain. Let consider an unstable plasma composed of two pair of complex conjugate eigenvalues (one pair with  $\text{Re } \lambda = \lambda_r > 0$  the other one with  $\text{Re } \lambda = -\lambda_r < 0$ ). Their real part grows with the instability parameter  $\mu - \mu_c > 0$ .

- In finite-dimensional system at criticality  $\mu = \mu_c$ , both "negative"  $\lambda_r \rightarrow 0^-$  and "positive"  $\lambda_r \rightarrow 0^+$  join on the real axis. Thus both  $\lambda_{\mu_c} = 0 + i\lambda_i$  and  $\lambda_{\mu_c}^* = 0 - i\lambda_i$  are associated with a eigenspace of dimension two [VDMvdM85, CMM90]. Therefore, we shall have a  $2 \times 2$  dimensional description of the bifurcation with a two dimensional center manifold for example; a one dimensional description would lead to singular coefficient in the bifurcation expansion, as in the example Section IV.1. Note that in this case the merging of "positive" and "negative" eigenvalues is translated by  $\Lambda'(0 \pm i\lambda_i) = 0$  at  $\mu = \mu_c$ .
- In infinite-dimension (for the Vlasov equation) J.D. Crawford and P.D. Hislop [CH89] showed that at criticality these eigenvalues were simple. It is related to the fact that the dispersion relation is not analytic<sup>4</sup> and  $\Lambda(0^\pm \pm i\lambda_i) \neq 0$  in general. Therefore, the description of the bifurcation should be only 2 dimensional (for  $\lambda, \lambda^*$ ).

For real eigenvalues, the discussion and conclusion are similar.

We can decompose the perturbation close to  $f^0$  in the direction along the unstable eigenspace (for  $\lambda$  complex or not) and its orthogonal

$$f(q, p, t) = A(t)\Psi(q, p) + A^*(t)\Psi^*(q, p) + S(q, p, t) \quad (\text{V.35})$$

for  $(\tilde{\Psi}, f) = A$  and  $S$  such that  $(\tilde{\Psi}, S) = 0$ .  $A$  plays the role of the order parameter. It is directly proportional to the magnetization  $M(t)$  since

$$M(t) = (e^{iq}, f) = A \underbrace{(e^{iq}, \Psi)}_{=2\pi} + \text{O}(A^2).$$

We can write the time evolution of Eq. (V.35) by projecting the on  $(\tilde{\Psi}, f)$  and  $I - (\Psi, f)\Psi$

$$\dot{A} = \lambda A + \left( \tilde{\Psi}, \mathcal{N}[f] \right) \quad (\text{V.36a})$$

$$\partial_t S = \mathcal{L} S + \mathcal{N} S - \left( \left( \tilde{\Psi}, \mathcal{N}[f] \right) \Psi + \text{c.c.} \right). \quad (\text{V.36b})$$

4. Technically "negative" and "positive" eigenvalues are joining the real axis on different Riemann sheet.

Note that this system is still exact and infinite-dimensional, we have just brought out the unstable mode.

The key point is now to decompose our perturbation density  $f$  not on the infinite variety induced by  $S$  but along the finite-dimensional unstable manifold  $W^u$ . It means that we describe now the evolution of functions belonging to the unstable manifold  $f \in W^u$  where  $(A, A^*, S) = (A, A^*, H(A, A^*))$  as schematically represented on Figure V.3. Note that because the unstable manifold is the nonlinear generalization of the eigenvector we have by construction at least  $H = O((A, A^*)^2)$ .

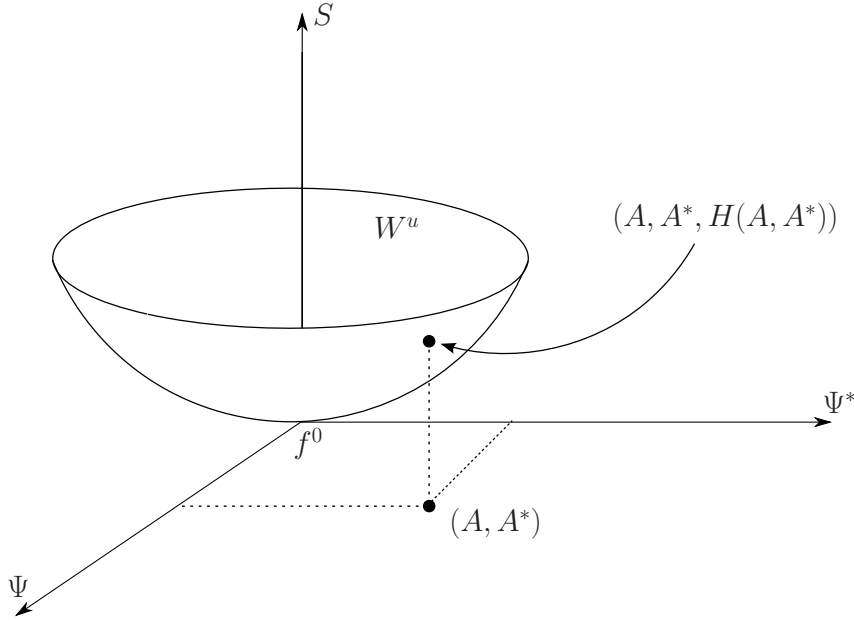


Figure V.3 – Schematic representation of the unstable manifold  $W^u$  near  $f = f^0$  in the infinite-dimensional space.

One can check that the distribution  $f$  is invariant by rotation in the Vlasov equation Eq. (VI.15). Since we want to construct the unstable manifold with a rotational invariance we impose for  $f \in W^u$  Eq. (V.35),  $S_\theta f \in W^u$ . It implies (because of the form of  $\Psi \propto e^{ikq}$ )

$$S_\theta A = A e^{-ik\theta}.$$

Similarly, the Fourier coefficient  $H_k$  of  $H$  will be constrained as  $S_\theta H_k = H_k e^{-ikq}$ , thus

$$H_0 = |A|^2 h_0(p, |A|^2) \quad (\text{V.37a})$$

$$H_1 = A |A|^2 h_1(p, |A|^2), \quad (\text{V.37b})$$

$$H_k = A^k h_k(p, |A|^2), \quad k \geq 2 \quad (\text{V.37c})$$

$$H_{-k} = (H_k)^*, \quad (\text{V.37d})$$

Now our goal is to construct the dominant order of  $H$  in order to get a dynamical equation

$$\dot{A} = \lambda A + c_3(\lambda) |A|^2 A + O(|A|^4 A) \quad (\text{V.38})$$

with potentially a diverging  $c_3(\lambda)$  coefficient as in the example IV.1. Note that the form of the expansion Eq. (V.38) is constrained by the rotational symmetry furthermore terms as  $|A|^{2j}$  have

to be zero because of the rotational symmetry  $A \leftrightarrow -A$ . As we will see in the non homogeneous case this symmetry is not preserved and the quadratic term is non zero.

To summarize the symmetries, constrain a lot the unstable variety and provide precious informations, as that the 0<sup>th</sup> and 2<sup>nd</sup> Fourier mode will be the terms of lowest order  $O(H_0) = O(H_2) = O((A, A^*)^2)$ .

## 5.2 Temporal equations

Now we drop the index  $k = 1$ . The temporal evolution on the unstable manifold is

$$\dot{A} = \lambda A + \left( \tilde{\psi}, \mathcal{N} f \right) \quad (\text{V.39})$$

$$\frac{dH}{dt} = \mathcal{L} H + \mathcal{N}[f] - \left[ \left( \tilde{\psi}, \mathcal{N} f \right) \psi + \text{c.c.} \right]. \quad (\text{V.40})$$

We define  $\dot{A} = A \varrho(\sigma, t)$ . The goal is to get the different order of  $|A|^2$ , by construction  $\varrho_0 = \lambda$ . Since by construction  $H$  is a function, it can be expanded for small  $A$  as

$$h_k(p, \sigma) = \sum_{j=0}^{\infty} h_{k,j}(p) \sigma^j, \quad (\text{V.41})$$

where  $\sigma = |A|^2$ . The task is to evaluate the  $h_{k,j}$  at different order. To remove the temporal evolution, we write on one hand

$$\frac{dH_k}{dt} = \dot{A} \partial_A H_k + \dot{A}^* \partial_{A^*} H_k \quad (\text{V.42})$$

using Eq. (V.37a), Eq. (V.37b), Eq. (V.37c) gives

$$\frac{dH_0}{dt} = A^* \dot{A} (h_{0,0} + O(\sigma)) + A \dot{A}^* (h_{0,0} + O(\sigma)) = \sigma (\varrho + \varrho^*) (h_{0,0} + O(\sigma)). \quad (\text{V.43})$$

So, for  $k \geq 0$ ,

$$\frac{dH_0}{dt} = 2\lambda_r \sigma h_{0,0} + O(\sigma) \quad (\text{V.44a})$$

$$\frac{dH_1}{dt} - \mathcal{L}_1 H_1 = A \sigma [(2\lambda + \lambda^*) - \mathcal{L}_1] h_{1,0} \quad (\text{V.44b})$$

$$\frac{dH_k}{dt} - \mathcal{L}_k H_k = A^k [k\lambda - \mathcal{L}_k] h_{k,0}. \quad (\text{V.44c})$$

On the other hand, from Eq. (V.40),

$$\frac{dH_0}{dt} = \mathcal{N}_0[f] \quad (\text{V.45a})$$

$$\frac{dH_1}{dt} - \mathcal{L}_1 H_1 = \mathcal{N}_1[f] - \left( \tilde{\Psi}_1, \mathcal{N}[f] \right) \psi \quad (\text{V.45b})$$

$$\frac{dH_k}{dt} - \mathcal{L}_k H_k = \mathcal{N}_k[f]. \quad (\text{V.45c})$$

So, by equalizing Eq. (V.44) and Eq. (V.45), we eliminate the temporal dependence allowing us to compute every order of  $H$ .

For the HMF potential

$$\begin{aligned} \mathcal{N}_k f_k = & 2\pi i (A(t)\partial_p\psi\delta_{k-1,1} + A(t)^*\partial_p\psi^*\delta_{k-1,-1} + \partial_p H_{k-1}) \phi_1 [A(t)\psi + H_1] \\ & - 2\pi i (A(t)\partial_p\psi\delta_{k+1,1} + A(t)^*\partial_p\psi^*\delta_{k+1,-1} + \partial_p H_{k+1}) \phi_{-1} [A^*(t)\psi_1^* + H_{-1}]. \end{aligned} \quad (\text{V.46})$$

In particular

$$\mathcal{N}_0[f] = i\pi\sigma (\partial_p\psi^* - \partial_p\psi) + \text{O}(\sigma^2) \quad (\text{V.47a})$$

$$\mathcal{N}_1[f] = i\pi A\sigma (\partial_p h_{0,0} - \partial_p h_{2,0}) + \text{O}(A\sigma^2) \quad (\text{V.47b})$$

$$\mathcal{N}_2[f] = i\pi A^2\partial_p\psi + \text{O}(A^4) \quad (\text{V.47c})$$

where we used the normalization of  $\phi[\psi] = 1/2$ .

### 5.3 Cubic order

---

Combining Eq. (V.45) and Eq. (V.47), gives

$$h_{0,0}(p) = i\pi \frac{(\partial_p\psi^* - \partial_p\psi)}{2\lambda_r} \quad (\text{V.48a})$$

$$h_{2,0}(p) = \frac{i\pi}{2} \frac{\partial_p\psi}{\lambda + ip}. \quad (\text{V.48b})$$

So, with

$$\left(\tilde{\Psi}_1, \mathcal{N}[f]\right) = \left\langle \tilde{\psi}_1, \mathcal{N}_1[f] \right\rangle = A\sigma \underbrace{i\pi \left\langle \tilde{\psi}, \partial_p (h_{0,0} - h_{2,0}) \right\rangle}_{c_3(\lambda)} + \text{O}(A\sigma^2), \quad (\text{V.49})$$

it just remains to compute two scalar products. Let's evaluate the term containing  $h_{2,0}$ ,

$$\begin{aligned} -i\pi \left\langle \tilde{\psi}, \partial_p h_{2,0} \right\rangle &= \frac{\pi^2}{2\Lambda'(\lambda)} \int \frac{\partial_p\psi}{(\lambda + ip)^3} dp = \frac{3i\pi^3}{2\Lambda'(\lambda)} \int \frac{(f^0)'(p)}{(\lambda + ip)^5} dp \\ &= -\frac{3\pi^2}{48} \frac{\Lambda^{(4)}(\lambda)}{\Lambda'(\lambda)}. \end{aligned} \quad (\text{V.50})$$

Let's evaluate the term containing  $h_{0,0}$ ,

$$\begin{aligned} i\pi \left\langle \tilde{\psi}, \partial_p h_{0,0} \right\rangle &= -\frac{\pi^2}{2\lambda_r\Lambda'(\lambda)} \left( \int \frac{\partial_p\psi^*}{(\lambda + ip)^2} dp - \int \frac{\partial_p\psi}{(\lambda + ip)^2} dp \right) = \\ &= -\frac{\pi^2}{\lambda_r\Lambda'(\lambda)} \left( \int \frac{\psi^*}{(\lambda + ip)^3} dp - \int \frac{\psi}{(\lambda + ip)^3} dp \right) \\ &= -\frac{i\pi^3}{\lambda_r\Lambda'(\lambda)} \left( \int \frac{(f^0)'(p)}{(\lambda^* - ip)(\lambda + ip)^3} dp - \int \frac{(f^0)'(p)}{(\lambda + ip)^4} dp \right). \end{aligned} \quad (\text{V.51})$$

At this point of the computation, one can take the limit  $\lambda_r \rightarrow 0$  and look at the scaling. A clever way proposed by J.D. Crawford was to expand the integrand in simple fraction, it has both the

advantages to highlight directly the  $\lambda_r$  dependence and the remaining integral has the form of  $\Lambda^{(n)}(\lambda)$  derivative. The simple fraction is

$$\frac{1}{(\lambda^* - ip)(\lambda + ip)^3} = \frac{1}{8\lambda_r^3(\lambda + ip)} + \frac{1}{4\lambda_r^2(\lambda + ip)^2} + \frac{1}{2\lambda_r(\lambda + ip)^3} + \frac{1}{8\lambda_r^3(\lambda^* - ip)} \quad (\text{V.52})$$

which directly gives

$$c_3 = \frac{-\pi^2}{\lambda_r \Lambda'(\lambda)} \left( \frac{(\Lambda(\lambda))^* - 1 - \Lambda(\lambda) + 1}{8\lambda_r^3} + \frac{\Lambda'(\lambda)}{4\lambda_r^2} - \frac{\Lambda''(\lambda)}{4\lambda_r} - \frac{\Lambda'''(\lambda)}{6} + \frac{\Lambda^{(4)}(\lambda)}{16} \right). \quad (\text{V.53})$$

Since the first  $(\Lambda(\lambda))^* = \Lambda(\lambda) = 0$  ( $\lambda$  is an eigenvalue) we find the asymptotic coefficient as in [Cra94a]

$$c_3 \sim -\frac{\pi^2}{4\lambda_r^3} + O(\gamma^{-2}). \quad (\text{V.54})$$

Note that this result is independent of the initial distribution function  $(f^0)'(p)$ .

Therefore, since  $c_3$  is always negative the bifurcation Eq. (V.38) towards a magnetized system is always supercritical (meaning continuous or to use the equilibrium statistical mechanics term: second order) and the scaling of the saturated states  $A_{\text{sat}}$  is as announced

$$|A_{\text{sat}}| \propto \lambda_r^2,$$

it is the **trapping scaling**.

## 5.4 A note on pinching singularities

To check that the  $\Lambda^{(n)}(\lambda)$  do not bring any additional singularity, one can consider integral of the type

$$\lim_{\epsilon \rightarrow 0} \int \frac{f(p)}{(p - im\epsilon)^k (p + in\epsilon)^l} dp \quad (\text{V.55})$$

for a regular function  $f(p)$ . For  $l = 0$  we have a function proportional to the derivative of the dispersion relation. Once again there are different ways to see the potential divergences

- One could show that the simple fraction expansion leads to divergences in  $1/\epsilon$  only if  $m = n$ .
- Use the Plemelj formula. A graphical interpretation of the result can be seen in Figure V.4. When two poles or more (whatever the order  $k, l$ ) approach the real axis from both side at a different velocity  $p$  one can always deform the integration path to make the limit finite. However, when two singularities approach the real axis at the same velocity  $p$ , the contour cannot be deformed to avoid the singularity. This case is referred to a pinching singularity.

In practice divergence, will come from scalar product containing terms as  $\langle \tilde{\psi}, \psi^* \rangle$ , while terms like  $\langle \tilde{\psi}, \psi \rangle$  will not diverge. This can be interpreted as singular projection over one unstable mode.

Hence, from this calculation the divergence of the coefficient  $c_3$  has its origin from this pinching singularity, but what does it means physically? The divergence occurs for  $p \simeq -\lambda_i$ . It can be physically translated as particles with velocity (frequency) around the frequency  $-\lambda_i$  of the unstable mode have a "singular" behavior. Once again, these particles are called resonant

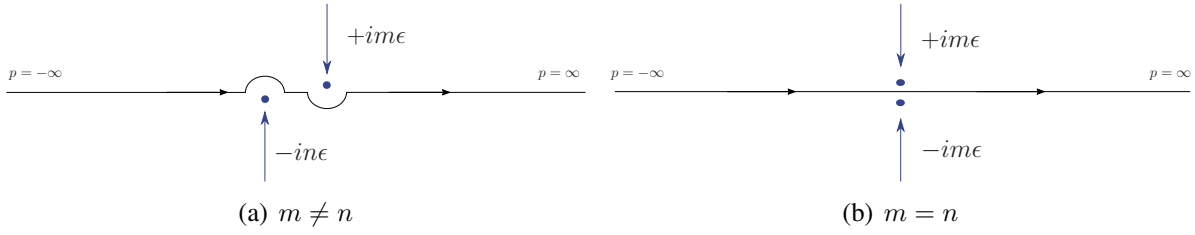


Figure V.4 – Integration path with poles approach the real axis.

particles. As we will see later these particles are in fact trapped with the unstable wave whose amplitude is  $A$ . This singularity is what make the dynamical expansion of the Vlasov bifurcation so "unique", it is not a mathematical artifact and any regularization would lead to a standard Hopf scaling  $\propto \sqrt{\lambda}$ , corresponding to remove the trapping mechanism.

### Remark V.6

These pinching singularities do not appear only in the kinetic context, for example in Perturbative Quantum Chromodynamics such singular integrals with pinching singularities occur. They physically stand for a long-distance sensitivity in the perturbation theory [Ste96]...

## 5.5 Higher orders

For every expansion of the previous type a safety check consist to compute and estimate higher order terms of Eq. (V.38). If they are negligible the dimensional reduction of the system at the bifurcation from the infinite Eq. (V.36) to one dimension Eq. (V.38) becomes exact.

Here we will not detail the computation of higher orders since a more generic treatment was done by J.D. Crawford in [Cra94a]. It brings quite some technicalities and the main insight was already provided by the cubic coefficient. The Crawford result is as follows:

$$c_{2j+1} \propto \frac{1}{\lambda_r^{4j-1}}, \quad j \geq 1. \quad (\text{V.56})$$

What is further more remarkable is that he computed exactly  $c_5 \sim 13/64\lambda_r^{-7}$  which as  $c_3$ , does not depend on the distribution  $f^0$ . It is then natural to conjecture that at leading order the unstable manifold is always the same for the Vlasov dynamics around homogeneous states (so all  $c_{2j+1}$  coefficient have a fixed value).

This result implies that around the saturated solution  $A_{\text{sat}} \propto \lambda^2$ , the series expansion of the one dimensional dynamics becomes singular since as in the example Eq. (IV.21),

$$O(\lambda|A_{\text{sat}}|) = O(c_3|A_{\text{sat}}|^3) = O(c_5|A_{\text{sat}}|^5) = O(c_{2n+1}|A_{\text{sat}}|^{2n+1}) = O(\lambda^3). \quad (\text{V.57})$$

This divergence means once again that the perturbative treatment fails at times larger than  $O(1/\lambda)$ . After this time particles are trapped with the created wave (whose amplitude is  $A$ ) and an oscillation behavior starts (which cannot be described by the one dimensional dynamical equation), see Figure V.6 and V.5.

## 6 RESONANCE PHENOMENON

As we have seen in the computation the damping or growing of stable/unstable perturbation is dominated by the contribution of particles resonating with the wave created self consistently by the perturbed distribution. These particles have a frequency (velocity) close to the frequency of the perturbation.

- In the stable case we observe the Landau damping. The wave is damped according the resonances of the dispersion relation (once again here resonance has the mathematical meaning). Thus, this damping occurs thanks to the particles with a velocity close to frequency of the wave. The Malmberg and Wharton experiment [MW64] showed indeed that a plasma without those particles did not display damping.
- In the unstable case resonances come from pinched singularities of pole. For a perturbation with zero frequency  $\omega = 0$ ,  $M(t) \sin q$ , resonant particles are found around  $v \simeq 0$ . Particles with large velocity  $p$  are not much affected by the perturbation in their phase space trajectories,

$$\begin{cases} \dot{q} = p \\ \dot{p} = -M(t) \sin q \end{cases} \quad (\text{V.58})$$

while resonant particles go from a straight line to a closed orbit in phase space Figure V.5. The period of closed orbit is given by the nonlinear time  $\tau_{NL} \sim \sqrt{M}^{-1} \sim \sqrt{A}^{-1}$ . Hence there is a competition in between trapping time  $\tau_{NL}$  and linear instability  $\tau_\lambda \sim \lambda^{-1}$ . Saturation occurs when both are comparable

$$\tau_{NL} \sim \tau_\lambda \quad \Rightarrow \quad A_{\text{sat}} \sim \lambda^2,$$

this yield the "trapping scaling".

Trapped particles are much more affected by the perturbation since their trajectories change from a straight line to a close orbit. Because the crucial point of the expansion comes from this nonlinear layer where particles are trapped, it was then natural for O'Neil et al. [OWM71] followed by del-Castillo Negrete [dCN98a, dCN98b] to perform an exact asymptotic multiscale expansion of the model considering these two different regions with a third region in between. The region with cycling orbit is called the inner critical layer, it is where the scaling of the expansion is not standard. In the Outer region, the time expansion is regular, then a matching of those two layers is done. It leads to the Single Wave Model (SWM), nicely reviewed in [BMT13]. A normal form is obtained and in fact it is shared with various Hamiltonian systems such as XY model and Euler 2D. The normal form is for our problem (simplified normal form from [BMT13])

$$\partial_t f + p \partial_q f + \partial_q \varphi \partial_p f = 0, \quad (\text{V.59a})$$

$$\varphi(q, t) = A e^{iq} + A^* e^{-iq}, \quad (\text{V.59b})$$

$$i \dot{A}(t) = \int f_1(p, t) dp. \quad (\text{V.59c})$$

It does look as the Vlasov equation with the difference that the perturbing wave  $\varphi$  is only along the unstable Fourier mode  $k = 1$  and it does not depend directly on the distribution as the previous mean field term  $\phi[f]$  did. This description has the advantage to display universality. The drawback of this reduction is that it is still of infinite-dimension, thus the end behavior is not

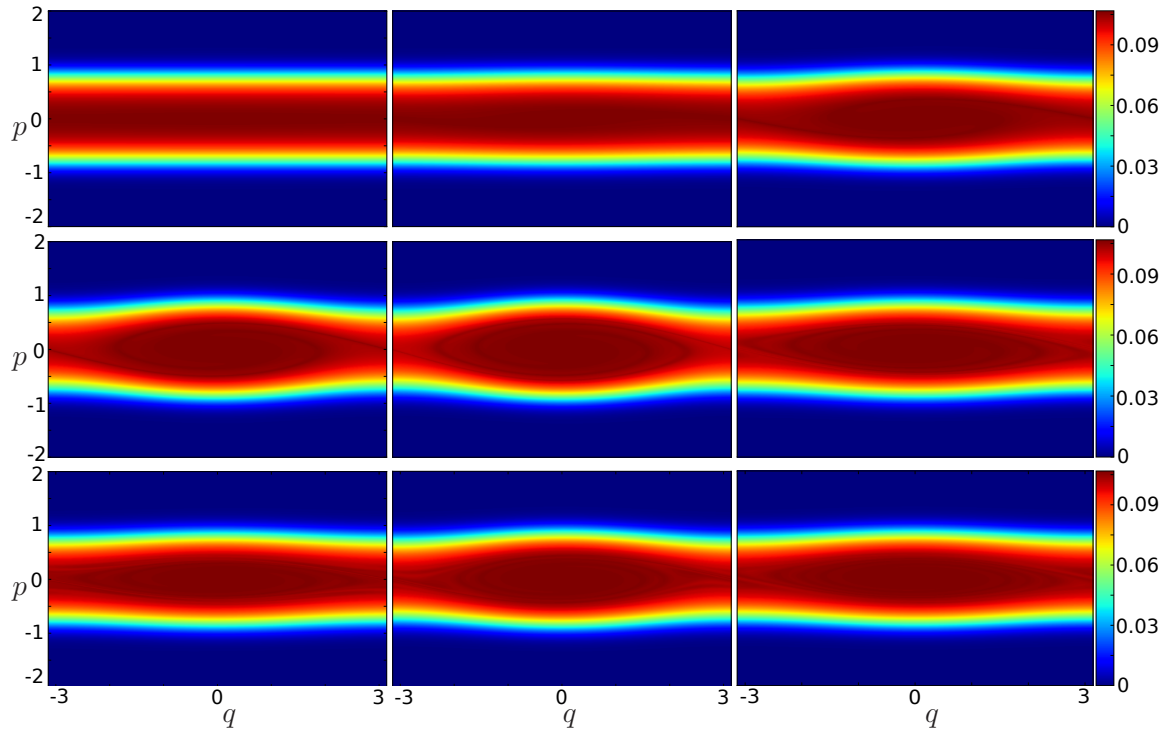


Figure V.5 – Density plot of  $F(q, p, t)$  in the phase space  $(q, p)$  for different times  $t = 0, 30, 50, 60, 70, 90, 110, 130, 170$ . Fermi distribution defined in Eq. (VI.37a) with  $M_0 = 0$ ,  $\beta = 10$ ,  $\mu = 0.277361$ ,  $\epsilon = 10^{-4}$ ,  $\lambda = 0.0729$ . The associated video can be found by clicking here [homogeneous\\_unstable.mp4](#).

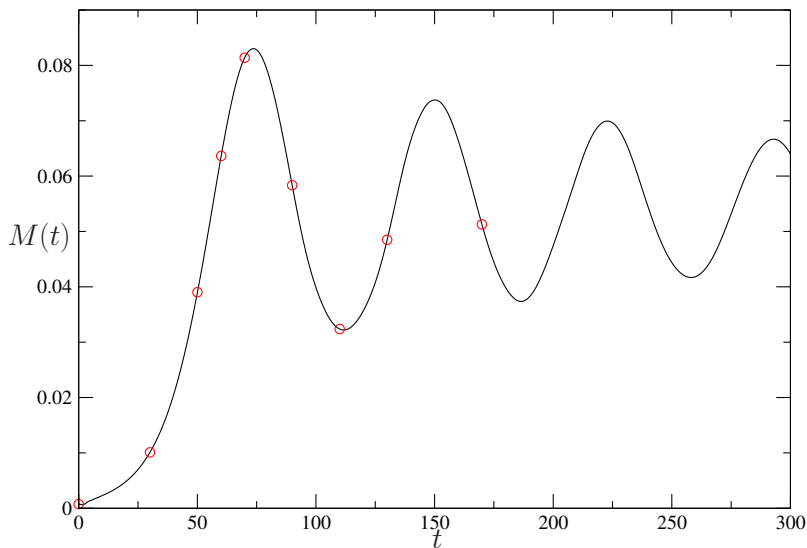


Figure V.6 – Magnetization associated with the Figure V.5. The circles represent the times of the snapshots. Fermi distribution defined in Eq. (VI.37a) with  $M_0 = 0$ ,  $\beta = 10$ ,  $\mu = 0.277361$ ,  $\epsilon = 10^{-4}$ ,  $\lambda = 0.0729$ .

direct. Moreover, in the construction of the model the trapping scaling giving the characteristic size of the critical layer is set as an ansatz that turns out to work (where traditional Hopf scaling would fail) whereas in Crawford method it is found as a result.

## 7 OPEN QUESTIONS

---

---

The partial success of the unstable manifold technique plagued by singularities raise many questions:

- How general is this unstable manifold expansion?
- Can it be applied around non homogeneous systems?
- Are bifurcation around non homogeneous states similar to the homogeneous case
  - Trapping scaling
  - SWM normal form
  - Universal coefficient  $c_n$
  - Singular series expansion at saturation or exact dimensional reduction?
- How with a small dissipation the critical layer is modified to give an exact one dimensional reduction with a  $\sqrt{\lambda}$  scaling as one found in regular expansion.

In the Chapter VI we will perform a similar analysis for the non homogeneous case and answer to some of the previous questions. In Chapter VII we will study the same homogeneous system as here adding a small dissipation. Since for every new Chapter we will use the same methodology we will start each Chapter by highlighting the differences with respect to this homogeneous Crawford model.



---

## BIFURCATIONS AROUND NON HOMOGENEOUS STATES

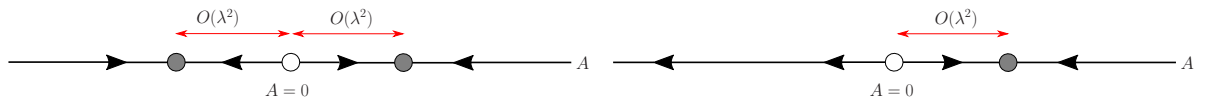
---

Now that we are familiar with the bifurcation problem around a homogeneous state, we consider the same question around an already magnetized (non homogeneous) state and present our original results. We will still consider the HMF model and highlight the differences with generic potential in this Chapter. In [BMY16], we prove that results of the unstable manifold approach remain with generic potentials; we also develop a self-consistent approach in addition to the dynamical one with similar predictions about the final states.

The unstable manifold analysis is then performed for a non oscillating perturbation (the unstable eigenvalue  $\lambda$  is real). The main results and physics of this study reveal that

- The wave particles/resonance is weaker than in the homogeneous case for a non oscillating perturbation since few particles resonate. Thus, the pinching singularities are also weaker.
- Nevertheless a singularity still appears in the bifurcation expansion for another physical reason.
- The bifurcation is now asymmetric with respect to the initial magnetization perturbation (see Figure VI.1) measured by  $A \propto M_\infty - M_0$ ,

$$\dot{A} = \lambda A + c_2 A^2 + O(A^3) \quad \text{with} \quad c_2 \propto \frac{1}{\lambda}.$$



(a) Homogeneous case: symmetric supercritical bifurcation

(b) Inhomogeneous case: asymmetric transcritical bifurcation

Figure VI.1 – Bifurcation diagram for homogeneous and inhomogeneous case

In bifurcation theory, this type of bifurcation is called transcritical (with here an unusual scaling). In one case, we recover the trapping scaling  $A_{\text{sat}} \propto \lambda^2$  while for the opposite initial condition the perturbation grows to be  $A_{\text{sat}} \propto O(1)$ .

- In fact if a singularity arises, it is not as in the homogeneous case because no finite-dimensional reduction is possible (thanks to strong resonances). It is because with the unstable manifold expansion we do not consider all the slow modes that contributes near the critical point i.e.  $-\lambda \rightarrow 0^-$  and 0, as in the finite-dimensional example (see Section IV.1). Hence describing the problem with a three-dimensional<sup>1</sup> manifold yields this time to what seems to be an exact dimensional reduction. The reduction obtained is known as the Triple Zero normal form. Preliminary predictions are compared directly with numerics, providing for example almost exactly the amplitude and frequency of oscillation of the saturated states whereas the unstable manifold just provides "a qualitative" scaling.

Technically the problem is more difficult since the angle-action variable change is necessary. However due to a broken rotational symmetry the nonlinear computation stops at the quadratic order  $c_2$ , which does not require any calculation of the unstable manifold  $H$ .

In the first part, we will introduce the non homogeneous formalism defining the angle-action variable more suited for the problem. Then we will quickly describe the known result for Landau damping in the non homogeneous case.

## 1 STEADY STATE

---

The particles motion in the mean field limit is associated with the following Hamiltonian (also called one particles Hamiltonian),

$$\mathcal{H}[F](q, p) = \frac{p^2}{2} + \phi[F](q) + M_c[F] = \frac{p^2}{2} + M_c[F](1 - \cos q) - M_s[F] \sin q, \quad (\text{VI.1})$$

where we use the same definitions of the magnetization  $M$  and mean field potential  $\phi[f]$  that in Eq. (V.5). We shifted the energy so that its minimum is zero. Hamilton's equations are

$$\frac{dq}{dt} = \partial_p \mathcal{H}, \quad (\text{VI.2a})$$

$$\frac{dp}{dt} = -\partial_q \mathcal{H}. \quad (\text{VI.2b})$$

Following the temporal evolution of the trajectories in the phase space gives the Vlasov equation for the distribution of particles

$$\frac{dF}{dt} = \partial_t F + \partial_p \mathcal{H} \partial_q F - \partial_q \mathcal{H} \partial_p F = 0 = \partial_t F + \{\mathcal{H}[f], F\}, \quad (\text{VI.3})$$

where we used the Poisson bracket

$$\{u, v\} = \partial_p u \partial_q v - \partial_q u \partial_p v. \quad (\text{VI.4})$$

For the homogeneous state finding a time independent solution was direct, here thanks to this Hamiltonian structure one can verify that any function of the one particle Hamiltonian

---

1. Originally we thought that a two dimensional reduction was enough but it led to inconsistencies.

$f^0(H(q, p))$  is a solution of the Vlasov equation. This fact is related to the Jeans [BT11] theorem that states that:

"Any steady-state solution of the Vlasov equation depends on the phase-space coordinates only through integrals of motion in the given potential, and any function of the integrals yields a steady-state solution of the Vlasov equation". To recover homogeneous stationary state one has to set  $M_c = M_s = 0$ .

Here the energy is an obvious integral of motion, in higher dimensions other integral of motion must be considered to describe steady states.

## 2 ANGLE-ACTION VARIABLE

---

If we want to proceed further in the unstable manifold analysis and solve the linear problem we are quickly stopped since the linear operator is here

$$\mathcal{L}f = -v\partial_p f + \partial_q \phi[f](q)\partial_p f^0(q, p) + \partial_q \phi[f^0](q)\partial_p f(q, p) \quad (\text{VI.5})$$

where the last term was previously zero. So, the spatial Fourier transform of  $\mathcal{L}f$  already involves different Fourier modes  $f_k, f_{k-1}, f_{k+1}$ . In other terms the spatial modes are mixed at the linear level, the problem is not diagonal which make it difficult to solve. We will thus have to change basis to diagonalize the problem.

From now on we choose a symmetric initial distribution  $f^0(q, v) = f^0(-q, v)$  so  $(M_0)_y[f^0] = 0$ . As we will explain later this choice should not affect any of our results, moreover we have done some simulation with  $(M_0)_y[f^0] \neq 0$  without any of our conclusion affected. So, the initial potential writes

$$\phi[f^0] = -(M_0)_c \cos q = -M_0 \cos q, \quad (\text{VI.6})$$

where we choose in the following (without loss of generality due to the symmetry of the problem)  $(M_0)_c = M_0 > 0$ .

### 2.1 Angle-action definition

---

The natural change of variable to diagonalize is to go from position-velocity  $(q, p)$  to the angle-action  $(\theta, J)$  variable. Their definition is

$$J = \frac{1}{2\pi} \oint p dq \quad (\text{VI.7a})$$

and the angles variable are obtained through a generator  $W(\theta, J)$  of the canonical transformation  $(q, p) \rightarrow (\theta, J)$

$$W(\theta, J) = \int p(\theta_1, J) d\theta_1 \quad (\text{VI.7b})$$

$$\theta = \partial_J W(\theta, J) \quad (\text{VI.7c})$$

In what follows it will be useful to define the parameter  $\kappa$ ,

$$\kappa = \sqrt{\frac{\mathcal{H}}{2M_0}}, \quad (\text{VI.8})$$

where  $\mathcal{H} = \mathcal{H}(J)$  is the energy of one trajectory of action  $J$ . We define its complementary  $\kappa' = \sqrt{1 - \kappa^2}$ . This parameter is useful since it separated the two different types of orbit. For  $\kappa < 1$  particles have elliptic orbit (blue zone in VI.2). For  $\kappa > 1$  particles have librating orbit (with  $p < 0$  or  $p > 0$ ). The separatrix is the limit orbit with  $\kappa = 1$ . To avoid confusion between the different variable we designated  $f^0(q, p) = \mathcal{F}^0(\mathcal{H}) = F^0(J) = \bar{f}^0(k)$ .

For HMF potential it is possible to obtain an explicit expression for these variables, the starting point is to write

$$p = \pm \sqrt{2(\mathcal{H} + M_0(\cos q - 1))} = \pm 2\sqrt{M_0} \sqrt{\kappa^2 - \sin^2(q/2)} \quad (\text{VI.9})$$

and to compute the integral Eq. (VI.7) in the three different cases  $\kappa < 1, = 1, > 1$ . Therefore, the definition of the angle-action variables is a priori different for three regions of space [BOY10] as show in Figure VI.2.  $J = J_c$  is the action associated with particles on the separatrix. It is easy to understand the different zones for angle-action variable with a pendulum:

- For small initial energy ( $J < J_c$ ) a pendulum oscillates. For very small oscillations it is well known that the period is isochronous.
- At the separatrix  $J = J_c$ , it takes an infinite time to travel cycle.
- For large initial energy ( $J > J_c$ ) the pendulum describes a complete circle

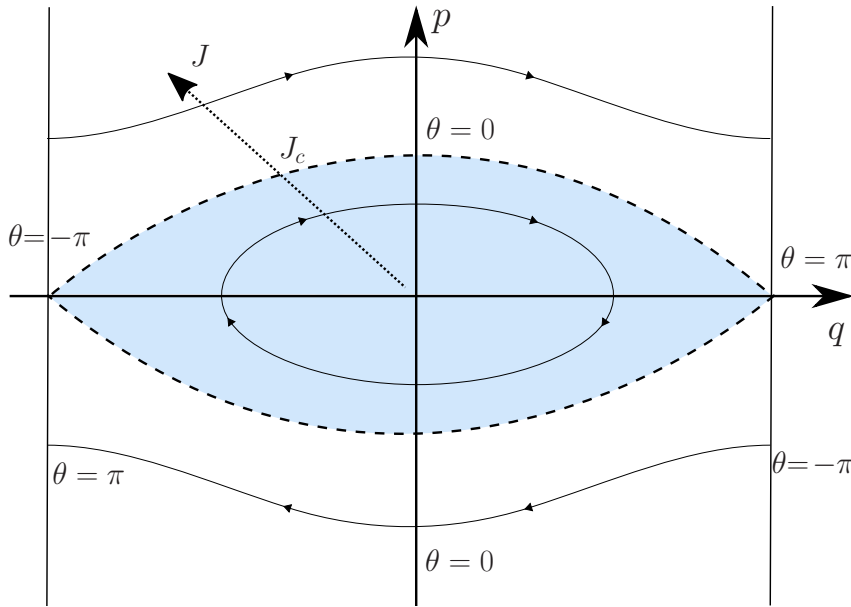


Figure VI.2 – Angle-action variables  $(\theta, J)$  representation in the phase space  $(q, p)$ . Three trajectories (arrows show the stream direction) are shown with associated angle variables. The action variable is increased along the dotted lined. The blue zone is bounded by the separatrix curve which separates close orbit from librating orbits.

These considerations lead naturally to the "analog" of the velocity  $p$  in angle-action variable which is the frequency defined by

$$\Omega(J) = \frac{d\mathcal{H}}{dJ}. \quad (\text{VI.10})$$

As previously mentioned with the pendulum analogy we can already guess without any computations that

- $\Omega(J \rightarrow 0) = \Omega_0 \neq 0$  (isochronicity)

- $\Omega(J = J_c) = 0$  (infinite period)
- $\Omega(J \gg J_c) \propto J$  (orbits no very different from straight lines so frequency is proportional to the momentum).

One can find

$$J(\kappa) = \frac{8\sqrt{M_0}}{\pi} (E(\kappa) - (\kappa')^2 K(\kappa)), \quad \kappa < 1 \quad (\text{VI.11a})$$

$$J(\kappa) = \frac{4\sqrt{M_0}\kappa}{\pi} E(1/\kappa), \quad \kappa > 1 \quad (\text{VI.11b})$$

$$\Omega(\kappa) = \frac{\pi\sqrt{M_0}}{2K(\kappa)}, \quad \kappa < 1 \quad (\text{VI.11c})$$

$$\Omega(\kappa) = \frac{\pi\sqrt{M_0}\kappa}{K(1/\kappa)}, \quad \kappa > 1 \quad (\text{VI.11d})$$

where  $K(\kappa)$  and  $E(\kappa)$  are respectively the complete elliptic integral of the first and second kind, defined in the Appendix B.1. In particular,  $\Omega_0 = \sqrt{M_0}$  and around the separatrix  $\Omega(J \rightarrow J_c) \propto$

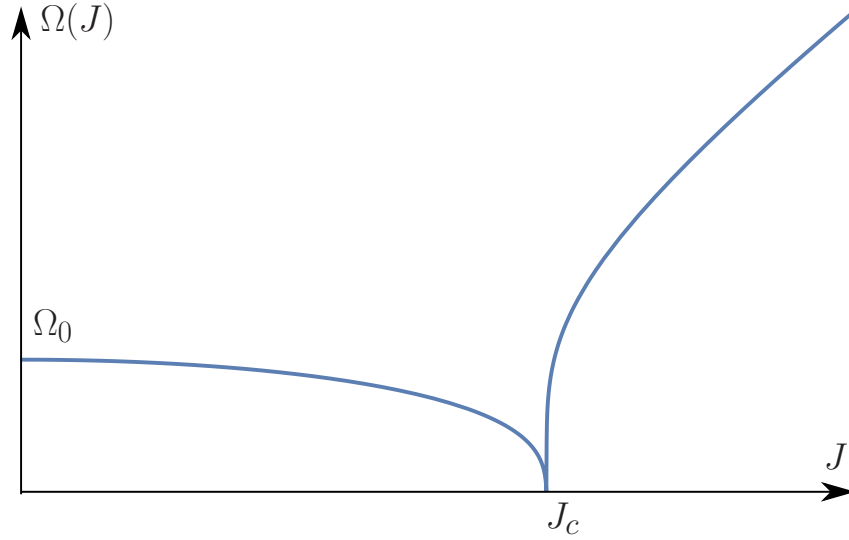


Figure VI.3 – Frequency's orbit  $\Omega(J)$ .

$|\ln^{-1}(|J - J_c|)|$  so the convergence towards zero is logarithmically slow, see Figure VI.3.

## 2.2 Fourier basis of the HMF potential in angle-action variable

Before moving on solving the linear problem we define the Fourier transform according to the angle variable of the potential basis  $(\cos(q(\theta, J)), \sin(q(\theta, J))) \xrightarrow{TF_\theta} (\mathfrak{C}_m(J), \mathfrak{S}_m(J))$ . Indeed, the cost of the diagonalization is that the potential will not have a simple form in the angle Fourier space, in particular it will have component for every angle mode  $m$  (while in  $q$ -Fourier it had components only on  $k = \pm 1$ ). The Fourier coefficients are defined through

$$\mathfrak{C}_m(k) = \frac{1}{2\pi} \int_{-\pi}^{\pi} \cos(q(\theta, \kappa)) e^{-im\theta} \quad (\text{VI.12a})$$

$$\mathfrak{S}_m(\kappa) = \frac{1}{2\pi} \int_{-\pi}^{\pi} \sin(q(\theta, \kappa)) e^{-im\theta}. \quad (\text{VI.12b})$$

A convenient result of this thesis was to explicitly compute these coefficients for every  $m$ . So far only  $c_0$  was known and for  $m \neq 0$  they had to be computed numerically<sup>2</sup>. The details are given in Appendix B.1, we had to use results of S. C. Milne<sup>3</sup> [Mil02], where he derives explicitly a lot of series expansion of Jacobi Elliptic Functions (and associated), in particular the Fourier expansion of  $\text{sn}^2$ ,  $\text{sn} \times \text{cn}$ ,  $\text{sn} \times \text{dn}$ .

In [BM17b] authors used those explicit expressions to compare simulations to a semi analytical theory.

## 3 LANDAU DAMPING AND RESONANCES

---

### 3.1 Landau damping

---

The Landau damping around inhomogeneous states has been studied for generic and HMF potential by my predecessor<sup>4</sup>, my advisor J. Barré and Y.Y Yamaguchi in [BOY10, BOY11]. The result of the study showed Landau damping with an algebraic damping for long times

$$\delta M_c \propto \begin{cases} e^{-|\omega_{dm}|t}, & \text{for } t \ll \nu^{-1} \\ e^{-2i\Omega_0 t}/t^3, & \text{for } t \rightarrow \infty. \end{cases}$$

#### Remark VI.1

The spectrum of the inhomogeneous linear operator is modified with respect to the homogeneous case. Indeed, one can look at its expression in  $(q, p)$  variables Eq. (VI.5) and see that the "perturbation" added to the advection operator are not compact since they are spanned by an infinite-dimensional operator<sup>5</sup>. So a priori the essential spectrum is modified and it depends on both the initial distribution  $f^0(q, p)$  and the interaction potential  $V(q)$ .

In the homogeneous case the spectrum did not depend on the initial distribution  $f^0(v)$  and interaction potential  $V(q)$ . The result found by Crawford [Cra95a] on the nonlinear expansion and by Balmforth et al. [BMT13] on the single wave model also exhibited some universality. Despite that it might be unrelated, we might expect not to find universal coefficient  $c_3, c_5$  for the bifurcation analysis as in the homogeneous case due to this new sensibility of the continuous spectrum. Moreover, we will not expect a universal reduction as the single wave model.

---

2. With a great numerical cost around  $\kappa \simeq 1$ .

3. In what seems to be a colossal work, we see that some number theory in the spirit of Ramanujan is used to finally serve our physical problem!

4. Alain Olivetti was the previous PhD student of Julien Barré.

5. It depends on a function  $f^0(q, p)$  where previously it was a constant w.r.t. to the position variable  $f^0(v)$ .

## 3.2 Resonances

### 3.2.a Non oscillating perturbation $\text{Im } \lambda = 0$

Previously the number of resonant particles  $\mathfrak{R}$  was given by the number of particles with a velocity around the frequency of the perturbing wave. This is for a non oscillating wave  $p = 0$ ,

$$\mathfrak{R}_H = \int_{-\epsilon}^{\epsilon} \int f^0(p) dq dp \sim 4\pi\epsilon f^0(v = 0)$$

for a homogeneous initial distribution regular in velocity. For inhomogeneous case, for non oscillating perturbation, resonant particles will have a frequency  $\Omega(J) < \epsilon$ . For small  $\epsilon$ , the frequency around the separatrix is

$$\Omega(J) \sim -\frac{\pi\sqrt{M_0}}{2\ln(J_c - J)} < \epsilon, \quad \text{for } J < J_c.$$

So

$$\mathfrak{R}_{\text{NH}} = \int_{\Omega(J) < \epsilon} \int F^0(J) d\theta dJ = 2\pi \left( \int_{\substack{J < J_c \\ \Omega(J) < \epsilon}} + 2 \int_{\substack{J > J_c \\ \Omega(J) < \epsilon}} \right) F^0(J) dJ$$

where we supposed that  $F^0$  is regular in  $J = J_c$  and we have separated the different region of integration (the two outside the separatrix regions contribute the same). Going to the  $\kappa$  variable gives at leading order in  $\epsilon$ ,

$$\mathfrak{R}_{\text{NH}} = 2\pi \left( \int_{\substack{\kappa < 1 \\ \Omega(\kappa) < \epsilon}} + 2 \int_{\substack{\kappa > 1 \\ \Omega(\kappa) < \epsilon}} \right) \bar{f}^0(\kappa) \frac{dJ}{d\kappa}(\kappa) d\kappa \propto M_0 \frac{e^{-\pi\sqrt{M_0}/\epsilon}}{\epsilon} \bar{f}^0(\kappa = 1). \quad (\text{VI.13})$$

Therefore, there are a lot less particles resonating around the separatrix

$$\mathfrak{R}_H \propto \epsilon \quad \text{and} \quad \mathfrak{R}_{\text{NH}} \propto \frac{e^{-\pi\sqrt{M_0}/\epsilon}}{\epsilon} \ll \mathfrak{R}_H,$$

thus we expect the resonant phenomena leading to pinching singularities to be a lot weaker. Moreover, if that resonant trapping of particles in a critical layer was the cause to the impossibility of a finite-dimensional description of the bifurcation (see Single Wave Model [BMT13]), maybe here we can achieve some reduction.

### 3.2.b Oscillating perturbation $\text{Im } \lambda \neq 0$

If we seek the number of resonant particles for oscillating wave we find that for both homogeneous and inhomogeneous cases

$$\mathfrak{R}_H \propto \mathfrak{R}_{\text{NH}} \propto \epsilon,$$

because the frequency distribution  $\Omega(J)$  is regular in all region  $J \neq J_c$ .

This contrast leads us to conjecture that there for stable inhomogeneous distribution, the damping always oscillates because there are no resonances with non oscillating modes. In other words, if there is an analytic continuation to the dispersion relation  $\Lambda(\lambda \in \mathbb{R}^+)$  in for  $\lambda < 0$  it has no root. An argument that goes with this reasoning is that for  $\lambda \in \mathbb{R}$ ,  $\Lambda(\lambda)$  is continuous (see later Eq. (VI.25) and Eq. (VI.43)) and infinitely differentiable in  $\lambda = 0$  with  $\partial_\lambda^{2n} \Lambda_s(0) = \partial_\lambda^{2n+1} \Lambda_c(0) = 0$ . So, a conjecture could state that since there is no need for analytic continuation in this case non oscillating damping will never happen.

## 4 LINEAR PROBLEM

### 4.1 Dispersion relation

Since the variable change from  $(q, p) \rightarrow (\theta, J)$  is canonical (in the three regions), the Vlasov equation in these variables is straightforward

$$\frac{dF}{dt} = \partial_t F + \{H[F](J), F(\theta, J)\} = 0, \quad (\text{VI.14})$$

where the Poisson bracket is written here for the angle-action variable.

Around the stationary solution  $F^0(J) = f^0(q, p)$  the linear operator is with  $F = F^0(J) + f(\theta, J)$ :

$$\partial_t f = \mathcal{L} f + \mathcal{N} f \quad (\text{VI.15a})$$

$$\mathcal{L} f = \{f, H[F^0]\} + \{F^0, \phi[f]\} \quad (\text{VI.15b})$$

$$\mathcal{N} f = \{f, \phi[f]\} \quad (\text{VI.15c})$$

The eigenvalue problem for  $\lambda \notin i\mathbb{R}$  and  $\Psi$  is

$$\lambda \Psi(\theta, J) = \mathcal{L} \Psi = -\Omega(J) \partial_\theta \Psi(\theta, J) + \partial_\theta \phi[\Psi](q(\theta, J)) \partial_J F^0(J) \quad (\text{VI.16})$$

going to angle Fourier transform gives

$$\lambda \psi_m(J) = -im\Omega(J)\psi_m + im\phi_m[\Psi] \partial_J F^0(J). \quad (\text{VI.17})$$

we have

$$\psi_m(J) = im \frac{\phi_m[\Psi] \partial_J F^0}{\lambda + im\Omega(J)}, \quad \psi_0 = 0 \quad (\text{VI.18})$$

where

$$\phi_m = -M_c[\Psi] \mathbf{c}_m - M_s[\Psi] \mathbf{s}_m. \quad (\text{VI.19})$$

The dispersion relation is less trivial to obtain than before where eigenvectors had only one non zero Fourier component (the normalization was enough to deduce  $\Lambda(\lambda)$ ). Here to get a closure we have to project the eigenvector Eq. (VI.18) along  $\cos q$  and  $\sin q$

$$\frac{M_c[\Psi]}{2\pi} = \left( \frac{\cos q}{2\pi}, \Psi \right) = -M_c[\Psi] \sum_m \int \frac{im|\mathbf{c}_m|^2 \partial_J F^0}{\lambda + im\Omega(J)} dJ - M_s[\Psi] \sum_m \int \frac{im\mathbf{c}_m^* \mathbf{s}_m \partial_J F^0}{\lambda + im\Omega(J)} dJ \quad (\text{VI.20a})$$

$$\frac{M_s[\Psi]}{2\pi} = \left( \frac{\sin q}{2\pi}, \Psi \right) = -M_c[\Psi] \sum_m \int \frac{im\mathbf{s}_m^* \mathbf{c}_m \partial_J F^0}{\lambda + im\Omega(J)} dJ - M_s[\Psi] \sum_m \int \frac{im|\mathbf{s}_m|^2 \partial_J F^0}{\lambda + im\Omega(J)} dJ \quad (\text{VI.20b})$$

were we used for the projection (scalar product) the Parseval theorem that allows to write the angle integral as a Fourier sum. This last equality can be written in a matrix form as

$$\Lambda(\lambda) \begin{pmatrix} M_c[\Psi] \\ M_s[\Psi] \end{pmatrix} = \begin{pmatrix} \Lambda_c(\lambda) & 0 \\ 0 & \Lambda_s(\lambda) \end{pmatrix} \begin{pmatrix} M_c[\Psi] \\ M_s[\Psi] \end{pmatrix} = 0 \quad (\text{VI.21})$$

where we have eliminated the diagonal terms due to the symmetries (see Eq. (B.4) and Eq. (B.6))

$$\mathfrak{C}_{2m+1}(\kappa < 1) = 0, \quad (\text{VI.22a})$$

$$\mathfrak{S}_{2m}(\kappa < 1) = 0, \quad (\text{VI.22b})$$

$$\mathfrak{S}_m(\kappa > 1, p < 0) = -\mathfrak{S}_m(\kappa > 1, p > 0), \quad (\text{VI.22c})$$

$$\mathfrak{C}_m(\kappa > 1, p < 0) = \mathfrak{C}_m(\kappa > 1, p > 0). \quad (\text{VI.22d})$$

These relations gives for any generic  $G_m(J)$  function that has the same definition on the two outer regions ( $J > J_c, p \leq 0$ ) a zero contribution when integrated,

$$\begin{aligned} \int G_m(J) \mathfrak{C}_m \mathfrak{S}_m^*(J) dJ &= \int_0^{J_c} G_m^<(J) \underbrace{\mathfrak{S}_m^* \mathfrak{C}_m}_{=0 \text{ for } m \text{ odd and even}}(J) dJ + \int_{J_c}^{\infty} G_m^>(J) \mathfrak{S}_m^* \mathfrak{C}_m(J) dJ \\ &\quad - \int_{J_c}^{\infty} G_m^>(J) \mathfrak{S}_m^* \mathfrak{C}_m(J) dJ = 0. \end{aligned} \quad (\text{VI.23})$$

The dispersion function  $\Lambda(\lambda)$  is given by the two dispersion relations

$$\det \Lambda(\lambda) = 0 = \Lambda_c(\lambda) \Lambda_s(\lambda) \quad (\text{VI.24})$$

with

$$\Lambda_c(\lambda) = 1 + 2\pi \sum_{m \neq 0} \int \frac{im \partial_J F^0(J)}{\lambda + im \Omega(J)} |\mathfrak{C}_m|^2(J) dJ \quad (\text{VI.25a})$$

$$\Lambda_s(\lambda) = 1 + 2\pi \sum_{m \neq 0} \int \frac{im \partial_J F^0(J)}{\lambda + im \Omega(J)} |\mathfrak{S}_m|^2(J) dJ. \quad (\text{VI.25b})$$

If  $\lambda$  is a root of  $\Lambda_c(\lambda)$  or  $\Lambda_s(\lambda)$  is an eigenvalue of the whole system. Since the system is diagonal these two type of eigenvalues are associate with different eigenspaces. One can prove using  $m \rightarrow -m$  in Eq. (VI.25), that if  $\lambda$  is a complex eigenvalue  $\Lambda(\lambda) = \Lambda(\lambda^*) = 0$ . Moreover if  $\lambda$  is a complex eigenvalue  $\Lambda(\lambda) = \Lambda(-\lambda) = 0$ . So as before if the system has a stable eigenvalue it has automatically an unstable one, meaning that once again relaxation in stable case will be due to the continuous spectrum (Landau damping).

### Remark VI.2

- For generic potential e.g. for full 1D gravity  $V_{1D} = |q|$ , the potential basis has an infinite number of non zero components. The dispersion matrix can be derived formally the same way, but in general it is an infinite matrix with no zero elements. So manipulating it, is only formal and one cannot explicitly compute the roots  $\lambda$  of its determinant. One has to truncate at some large  $m_M$ .
- For the homogeneous case  $M_0 = 0$ , even for generic potential, the matrix  $\Lambda(\lambda) = \text{diag}(\Lambda_k)$  is diagonal since there are no spatial modes mixing. Thus, the dispersion relation can be explicitly computed in this case (since we are interested in the first Fourier mode to go unstable  $k = 1$ ).
- From Eq. (VI.21), we can find back Eq. (V.14) with  $M_0 \rightarrow 0$ . One can check that  $\kappa \sim p/(2M_0)$ ,  $\Omega(\kappa) \xrightarrow{M_0 \rightarrow 0} v$ , etc., in particular  $\mathfrak{C}_m = (\delta_{m,1} + \delta_{m,-1})/2$ .

- In the homogeneous case we had an eigenvalue associated with an infinite-dimensional eigenspace. Here in Eq. (VI.17) this phenomenon still occurs. Indeed for  $\lambda = 0$  we can find two types of eigenvectors

$$\Psi_n = \begin{pmatrix} \psi_0(J) \\ \frac{\phi_m[\Psi_n]F^0}{\Omega(J)} \end{pmatrix} \quad \text{and} \quad \Psi_n = \begin{pmatrix} \psi_0(J) \\ 0 \end{pmatrix}. \quad (\text{VI.26})$$

It means that for any  $\psi_0(J)$ ,  $\Psi_n$  is an eigenvector associated with  $\lambda = 0$ .

## 4.2 Self-consistent equation for the magnetization

---

To find a steady state solution a function  $f^0(q, p) = F^0(J) = \mathcal{F}^0(\mathcal{H}) = \bar{f}^0(k)$  has to satisfy the normalization condition and a self-consistent equation for the magnetization

$$1 = \iint \mathcal{F}^0 \left( \frac{p^2}{2} - M_0(1 - \cos q) \right) dqdp, \quad (\text{VI.27a})$$

$$M_0 = \iint \mathcal{F}^0 \left( \frac{p^2}{2} - M_0(1 - \cos q) \right) \cos q dqdp. \quad (\text{VI.27b})$$

In practice, to find numerically  $M_0$  and the normalization, we use the transformation  $dqdp \rightarrow d\theta dJ$  and then integration over angle and the change of variable  $J \rightarrow \kappa$  giving

$$1 = 4\pi M_0 \left( \int_0^1 + 2 \int_1^\infty \right) \left( \kappa \frac{\bar{f}^0(\kappa)}{\Omega(\kappa)} \right) d\kappa, \quad (\text{VI.27c})$$

$$M_0 = 4\pi M_0 \left( \int_0^1 + 2 \int_1^\infty \right) \left( \kappa \frac{\bar{f}^0(\kappa)}{\Omega(\kappa)} c_0(\kappa) \right) d\kappa. \quad (\text{VI.27d})$$

## 4.3 Eigenvector and eigenvalue

---

### 4.3.a Along the $\sin$ direction

The problem is spatially invariant, so that if  $F(q, p, t)$  is a solution of the full non homogeneous Vlasov equation then so is  $F(q + q_0, p, t)$ . The generator of this spatial translation is  $\partial_q$ , so we expect to always have an eigenvector as

$$\Psi_s(q, p) = \partial_q f^0(q, p), \quad (\text{VI.28})$$

associated with an eigenvalue  $\lambda_s = \lambda = 0$  which corresponds to the Goldstone mode. Let's check that assertion. In Eq. (VI.25b), with  $\lambda = \text{Re } \lambda \rightarrow 0$  we obtain

$$\Lambda_s(\lambda = 0) = 1 + 2\pi \int \frac{\partial_J F^0(J)}{\Omega(J)} \sum_{m \neq 0} |\mathfrak{s}_m|^2(J) dJ. \quad (\text{VI.29})$$

The Parseval identity here gives [Oga13],

$$2\pi \sum_{m \neq 0} \mathfrak{s}_m^2 = \int \sin(q(\theta, J))^2 d\theta \quad (\text{VI.30})$$

where we used  $\mathfrak{s}_0 = 0$ .

**Remark VI.3**

Here we have replaced  $\lambda = 0$  in all integral at the limit. It might be very dangerous and bring singularities. In fact, in homogeneous case this limit was obtained with the Plemej formula because

$$\int \frac{(f^0)'(p)}{p} dp \quad (\text{VI.31})$$

is not integrable in general. Here because the logarithmic divergence induced by the resonating particles is integrable, the limit is well defined and we can replace  $\lambda$  by 0.

However, if  $\lambda$  is complex, this statement is no longer true since

$$\int \frac{\partial_J F^0}{\lambda_i + m\Omega(J)} dJ$$

is no longer integrable, indeed for every  $J_m^{(i)} \neq J_c$  root of the denominator, we can expand  $\lambda_i + m\Omega(J) = m(J - J_m^{(i)})\Omega(J_m^{(i)})$  that has the same divergence as Eq. (VI.31).

Using that  $\mathcal{H} = p^2/2 + M_0(1 - \cos q)$  and  $d\mathcal{H} = pdp + M_0 \sin q dq$  (since  $q$  and  $p$  are independent variable  $dq/dp = 0$ ) we have

$$\frac{\partial_p f^0(v)}{p} = \frac{d\mathcal{F}^0}{d\mathcal{H}} = \frac{\partial_J F^0(J)}{\Omega(J)} = \frac{\partial_q f^0}{M_0 \sin q}. \quad (\text{VI.32})$$

We may write angle-action integral as a space velocity integral (remember the canonic transformation insure  $d\theta dJ = dq dp$ ) to have

$$\begin{aligned} \Lambda_s(\lambda_s) &= 1 + \iint \frac{1}{p} \partial_p f^0 \sin^2 q dq dp \\ &= 1 + \iint \frac{d\mathcal{F}^0(\mathcal{H}(q, p))}{d\mathcal{H}} \sin^2 q dq dp \\ &= 1 + \frac{1}{M_0} \iint \partial_q f^0 \sin q dq dp = 1 - \frac{1}{M_0} \iint f^0 \cos q dq dp \\ &= 1 - \frac{M_0}{M_0} = 0 \end{aligned} \quad (\text{VI.33})$$

where we have used the definition of the magnetization, integration by part and the different expressions of the energy derivative.

From Eq. (VI.18) we get the eigenvector associated with the neutral mode  $\lambda_s = 0$ ,

$$\Psi_s = \sum_{m \neq 0} \frac{\partial_J F^0}{\Omega(J)} \mathbb{s}_m e^{im\theta} = \frac{\partial_J F^0}{\Omega(J)} \sin q = M_0 \partial_q f^0(q, p) \quad (\text{VI.34})$$

which correspond to what was expected from the symmetry of the problem.

Therefore, there is always a neutral mode along  $\Psi_s$ , whatever the parameters and the function  $f^0$ . Since it is associated with a translation we don't expect it to play any role in the instability in the weakly nonlinear regime. However, we cannot exclude that it couples with the instability for strongly nonlinear regimes (which is not the case studied here). Hence we always suppose that  $M_s[F] = 0$  (which is supported by numerics) moreover we always choose perturbation along the  $\cos$  direction.

### 4.3.b Along the $\cos$ direction

From Eq. (VI.20), we find the eigenvector associated with the eigenvalue root of  $\Lambda_c(\lambda)$ ,

$$\Psi_c = \sum_{m \neq 0} \frac{im \partial_J F^0}{\lambda + im \Omega(J)} \mathbb{C}_m e^{im\theta}. \quad (\text{VI.35})$$

Eigenvectors are defined up to a multiplicative non zero constant, here we choose 1, so

$$M_c[\Psi_c] = (\cos q, \Psi_c) = -1 \quad (\text{VI.36})$$

thanks to the relation dispersion Eq. (VI.25a). The reverse reasoning is possible, set a normalization for the eigenvector and find the associated dispersion relation. Moreover, we have  $M_s[\Psi_c] = 0 = M_c[\Psi_s]$ .

## 4.4 Stability criteria

We introduce as before the parameter  $\mu$  that corresponds to a tunable parameter of the initial distribution  $f^0 = f_\mu^0$ . For example, one can have

$$\mathcal{F}_\mu^0(\mathcal{H}) = N_F^{-1} / [1 + e^{\beta(\mathcal{H}-\mu)}] \quad (\text{Fermi distribution}), \quad (\text{VI.37a})$$

$$\mathcal{G}_\mu^0(\mathcal{H}) = N_G^{-1} \mathcal{H}^2 e^{-\mu\mathcal{H}}, \quad (\text{VI.37b})$$

$N_F$  and  $N_G$  are the normalization factors. The Eq. (VI.37a) is a Fermi distribution of energy (looking like a step function), its stiffness is controlled by the  $\beta$ -parameter. It is a decreasing function of energy. The  $G$ -function Eq. (VI.37b) has an energy minimum in  $\mathcal{H} = 0$  and then reach a maximum for  $\mathcal{H}^* = 2/\mu$ , thus it a non-monotonic function of energy.

We define  $\mu_c$  to be the value for which the system goes unstable i.e.  $(\Lambda_c)_\mu(\lambda = 0) = 0$ . For example, for the function  $\mathcal{F}_\mu^0(\mathcal{E})$  we plot, in Figure VI.4, the phase diagram of the Fermi distribution  $(\mu, M_0)$ . The line corresponds to a steady state solution satisfying the self-consistent equation Eq. (VI.27c). The transition stable/unstable occurs at points  $a = (\mu_c = 0.669, 0.336)$  and  $l = (\mu_c = 0.254, 0)$ . In this thesis, we will numerically test the neighborhood of point  $a$ , where a solution becomes unstable. In principle, we could also test what happens for weakly inhomogeneous and unstable solution, dashed black line around  $l$ . We can establish as in [Oga13], the stability criteria. As mentioned earlier the  $\Psi_s$  direction is always neutrally stable. For a monotonic function of energy S. Ogawa showed that the eigenvalue associated with Eq. (VI.25a) is always real. In this Section, we focus on non oscillating perturbation  $\lambda \in \mathbb{R}$ . However, we let the initial distribution be monotonic or not. In our numerical tests, we use  $\mathcal{F}_\mu^0(\mathcal{H})$  which is monotonic and  $\mathcal{G}_\mu^0(\mathcal{H})$  which is not Eq. (VI.37). As we motivated earlier in Section VI.3.2 and remark VI.3, the choice  $\lambda \in \mathbb{R}$  has important consequence on the number of resonant particles and how the limit  $\lambda \rightarrow 0$  is computed. By replacing  $\lambda$  by zero in Eq. (VI.25a), Ogawa shows that the system is spectrally stable if and only if

$$\mathcal{I}[F^0] = 1 + 2\pi \int \frac{\partial_J F^0}{\Omega(J)} (g_0(J) - \mathbb{C}_0(J)^2) dJ \geq 0 \quad (\text{VI.38})$$

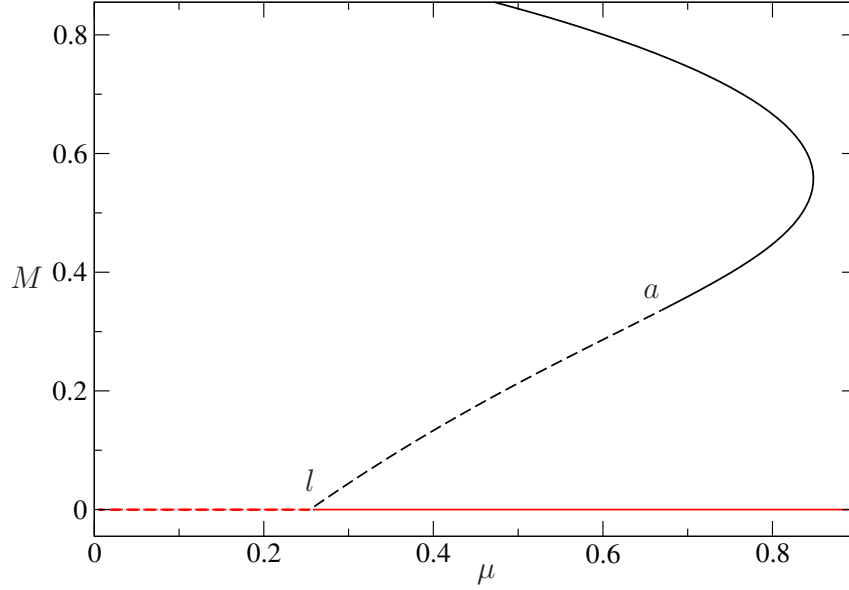


Figure VI.4 – Phase diagram of the Fermi distribution  $\mathcal{F}_\mu^0$  with  $\beta = 40$ . Dotted lines correspond to unstable stationary solutions and solid lines to stable ones. In the neighborhood of point  $a$ , a branch of stable inhomogeneous  $M_0 \neq 0$  stationary solutions becomes unstable. At point  $l$ , a branch of stable homogeneous stationary solutions ( $M_0 = 0$ , red solid line) becomes unstable; the unstable homogeneous case was treated in Chapter V.

where we defined and computed  $g_0$ <sup>6</sup> thanks again to [Mil02] and Eq. (B.2b),

$$g_0(\kappa) = \frac{1}{2\pi} \int \cos^2(q(\theta, J(\kappa))) d\theta = \begin{cases} \frac{1}{3} \left( \frac{4(1-2\kappa^2)E(\kappa)}{K(\kappa)} + 4\kappa^2 - 1 \right), & \kappa < 1 \\ \frac{1}{3} \left( \frac{4(1-2\kappa^2)\kappa^2 E(1/\kappa)}{K(1/\kappa)} + 8\kappa^4 - 8\kappa^2 + 3 \right), & \kappa > 1 \end{cases} \quad (\text{VI.39})$$

The transition occurs at  $\mathcal{S}[F^0] = 0$ .

## 4.5 Adjoint problem

The adjoint linear operator is obtained with respect to the scalar products Eq. (V.19) as,

$$\mathcal{L}^\dagger \tilde{\Psi}_c = \Omega(J) \partial_\theta \tilde{\Psi}_c - K^\dagger(q(\theta, J)) \quad (\text{VI.40})$$

where

$$K^\dagger(q(\theta, J)) = \int \int \left( \partial_\theta \tilde{\Psi}_c \partial_J F^0 \right) (q', p') V_{\text{HMF}}(q' - q) dq' dp'. \quad (\text{VI.41a})$$

$$K_m^\dagger(J) = -M_c[\partial_\theta \tilde{\Psi}_c \partial_J F^0]_{\mathbb{C}_m}(J) - M_s[\partial_\theta \tilde{\Psi}_c \partial_J F^0]_{\mathbb{S}_m}(J). \quad (\text{VI.41b})$$

6. Thanks to the Parseval theorem, we were able to explicit compute a  $q$ -elliptic series  $\sum_{n>0} n^2 \text{csch}^2 \left( n\pi \frac{K(k')}{K(k)} \right) = \frac{8K(k)^2}{3(2\pi^2)^2} \left( (k^2 - 1) K(k)^2 - 2(k^2 - 2) K(k)E(k) - 3E(k)^2 \right)$ . It was unknown (and surely not sought too) to my knowledge.

The adjoint eigenvector of  $\Psi_c$  is thus:

$$\tilde{\Psi}_c(\theta, J) = -\frac{1}{(\Lambda'(\lambda))^*} \sum_m \frac{\mathfrak{c}_m(J)}{\lambda^* - im\Omega(J)} e^{im\theta} \quad (\text{VI.42})$$

where we have set the normalization such that  $(\tilde{\Psi}_c, \Psi_c) = 1$ . So once again we find a relation between this scalar product and the derivative of the dispersion relation. Keeping the  $M_c[\partial_\theta \tilde{\Psi}_c \partial_J F^0]$  term would have led self consistently to a dispersion relation. Let's compute  $\Lambda'_c(\lambda)$  to check our normalizations choice. On one hand, we have

$$\begin{aligned} \Lambda'_c(\lambda) &= -2\pi \sum_{m \neq 0} \int \frac{im \partial_J F^0(J)}{(\lambda + im\Omega(J))^2} |\mathfrak{c}_m|^2(J) dJ \\ &= -8\pi\lambda \sum_{m > 0} \int \frac{m^2 \Omega(J) \partial_J F^0(J)}{(\lambda^2 + (m\Omega(J))^2)^2} |\mathfrak{c}_m|^2(J) dJ \end{aligned} \quad (\text{VI.43})$$

on the other hand

$$(\tilde{\Psi}_c, \Psi_c) = -\frac{1}{\Lambda'_c(\lambda)} \sum_{m \neq 0} \int \frac{im(f^0)'(J)}{(\lambda + im\Omega(J))^2} |\mathfrak{c}_m|^2(J) dJ = 1. \quad (\text{VI.44})$$

For monotonic function of energy  $\partial_J F^0(J) \leq 0$ , it is clear that  $\Lambda'_c(\lambda \in \mathbb{R}) \geq 0$ .

#### Remark VI.4

We notice that because of the spatial mode mixing ( $m$  positive and negative)  $\Lambda_c(\lambda) \propto \lambda \rightarrow 0$  with  $\lambda \rightarrow 0$ . In fact, it is expected because the two roots  $\lambda, -\lambda$  merge in 0, and  $\Lambda(\lambda)$  is differentiable in 0. However, that was not the case for the homogeneous case, where  $\Lambda'(0^+)$  was a non zero constant and  $\Lambda(\lambda)$  was in general not continuous in 0 (because of the singular behavior of  $1/p$ ).

In [BMY16], we give a proof that this normalization factor diverges as  $1/\lambda$  for generic a potential.

## 5 NONLINEAR EXPANSION

---

Now that the linear theory is clear we move on to what happens to a perturbation when unstable. The basic idea is the same that for homogeneous case, decomposing the solution along unstable vector and the unstable manifold. But as we will see due to symmetries the computation will be in fact easier.

Regarding the symmetries of the problem the  $\mathcal{O}(2)$  (rotation/reflexion) symmetry is broken, so for a real eigenvalue the associated unstable manifold will be of dimension one (instead of two for the homogeneous case).

We decompose the  $f$  function on the unstable direction  $\Psi_c$  associated to the eigenvalue  $\lambda > 0$  and its orthogonal direction.

$$f(\theta, J, t) = A(t)\Psi_c(\theta, J) + S(\theta, J, t) \quad (\text{VI.45})$$

with  $A = (\tilde{\Psi}_c, f)$  and  $(\tilde{\Psi}_c, S) = 0$ .  $S$  is assumed to be at least of order  $A^2$  because it is associated with the nonlinear part. The order parameter  $A$  is related to the magnetization perturbation

$\delta M = M(t) - M_0$ , indeed by definition

$$(\tilde{\Psi}_c, f) = A + O(A^2) \quad \text{and} \quad \delta M = M - M_0 = (\cos q, f) = A \underbrace{(\cos q, \Psi_c)}_{=-1} + O(A^2) \quad (\text{VI.46})$$

so  $A \propto \delta M$  for small  $A$  (which is the weakly nonlinear regime we study).

Applying the projection  $(\tilde{\psi}, \cdot)$  on Vlasov equation Eq. (VI.15), we get

$$\dot{A} = \lambda A + (\tilde{\Psi}_c, \mathcal{N} f) = A \varrho(\lambda, A) \quad (\text{VI.47})$$

So, the goal is now to get the first order in  $A$  of  $\varrho(A, \lambda)$ . While for homogeneous case the  $\mathcal{SO}(2)$ -symmetry insured  $A \rightarrow -A \Rightarrow c_2 = 0$ , here we have to consider  $c_2 \neq 0$ . This yield

$$\begin{aligned} \dot{A} &= \lambda A + \left( \tilde{\Psi}_c, \mathcal{N} (A\Psi + O(A^2)) \right) \\ &= \lambda A + c_2 A^2 + A^3 c_3 + O(A^4). \end{aligned} \quad (\text{VI.48})$$

From Eq. (VI.15c),

$$\mathcal{N} f = A^2 \{ \Psi_c, \phi[\Psi_c] \} + O(A^3). \quad (\text{VI.49})$$

In the homogeneous case, this term was zero, so we had to jump to the cubic order and construct the unstable manifold  $H$ . Here the quadratic order is directly given by the eigenvector.

Let's define  $c_2$  the coefficient associated with the quadratic term in  $A$ ,

$$\begin{aligned} c_2(\lambda) &= \left( \tilde{\Psi}_c, \{ \Psi_c, \phi[\Psi_c] \} \right) = \sum_m \int (\tilde{\Psi}_c)_m^* \{ \Psi_c, \phi[\Psi_c] \}_m \, dJ \\ &= \frac{-2\pi}{\Lambda'_c(\lambda)} \int \sum_{m,n \in \mathbb{Z}} \frac{\mathfrak{c}_{m+n}^* \varphi_{m,n}(J)}{\lambda + i(m+n)\Omega} \, dJ \end{aligned} \quad (\text{VI.50})$$

where we have re-indexed the sum to have

$$\varphi_{m,n}(J) = m \left[ n \frac{\partial}{\partial J} \left( \frac{\partial_J F^0 \mathfrak{c}_m}{\lambda + im\Omega} \right) \mathfrak{c}_n - m \frac{\partial_J F^0 \mathfrak{c}_m}{\lambda + im\Omega} \mathfrak{c}'_n \right]. \quad (\text{VI.51})$$

The first thing we want to extract from  $c_2$  is its limit when  $\lambda \rightarrow 0$ . Once again thanks to the logarithmic divergence of the frequency  $\Omega(J)$ , we can safely replace denominator of the form  $\lambda + im\Omega(J)$  by  $im\Omega(J)$  when  $m \neq 0$ . It leaves us with

- the normalization factor  $1/\Lambda'_c(\lambda) \propto 1/\lambda$ ,
- $m = 0$  terms are canceled since  $\varphi_{0,n} = 0$ ,
- $m = -n$  terms bring a supplementary divergence at first sight, but a careful calculation shows that it is not the case. Indeed for  $n = -m$ , we have in the  $J$  integral

$$\begin{aligned} \frac{\mathfrak{c}_0^*}{\lambda} \sum_m \varphi_{m,-m}(J) &= -\frac{\mathfrak{c}_0^*}{\lambda} \partial_J \left( \partial_J F^0 \left( \sum_m \frac{m^2 \mathfrak{c}_m^2}{\lambda + im\Omega} \right) \right) \\ &= -2\mathfrak{c}_0^* \partial_J \left( \partial_J F^0 \left( \sum_{m>0} \frac{m^2 \mathfrak{c}_m^2}{\lambda^2 + (m\Omega)^2} \right) \right) \\ &\xrightarrow{\lambda \rightarrow 0} -2\mathfrak{c}_0^* \partial_J \left( \frac{\partial_J F^0}{\Omega^2} \sum_{m>0} \mathfrak{c}_m^2 \right) = \mathfrak{c}_0^* \partial_J \left( \frac{\partial_J F^0(J)}{\Omega^2(J)} (\mathfrak{c}_0^2 - g_0)(J) \right) \end{aligned} \quad (\text{VI.52})$$

where we have exchanged sum and derivative thanks to the regularity of the  $\mathfrak{c}_m$  function.

Thus, the total divergence is exclusively given by the normalization factor and

$$c_2(\lambda) \propto 1/\lambda.$$

An exact estimation of the  $c_2$  coefficient in particular its sign is probably out of reach but as we will see now it does not matter. Hence the result yields

$$\dot{A} = \lambda A + c_2 A^2 + O(A^3) \quad \text{with} \quad c_2 \propto \frac{1}{\lambda}. \quad (\text{VI.53})$$

which is a transcritical bifurcation whatever the sign of  $c_2$ . This behavior is illustrated and compared with the homogeneous supercritical transition on Figure VI.1. It means for example that if  $c_2 > 0$ , we will have a subcritical (resp. supercritical) bifurcation for  $A(0) > 0$  (resp.  $A(0) < 0$ ). In the supercritical case  $A_{\text{sat}} \propto \lambda^2$  which is the trapping scaling. The numerics (discussed later) Figure VI.5 confirm perfectly this result. Here this origin of this scaling is very different from the homogeneous case since it comes from the normalization factor and not from pinching singularities (associate with resonances). It could be a sign that no Single Wave reduction is possible here.

**Remark VI.5**

- The symmetry of the inhomogeneous system holds for generic potential hence the bifurcation equation is always transcritical

$$\dot{A} = \lambda A + c_2 A^2 + O(A^3).$$

Similarly, even for a generic interaction potential, the divergence of the coefficient  $c_2 \propto 1/\lambda$  will only come from the normalization factor. Other terms are regular if we assume the frequency  $\Omega = dH/dJ$  associated with the generic potential either to not vanish at finite  $J$  or does so only logarithmically. This includes the cases where the stationary potential  $\phi[f^0](q)$  has a single minimum and is infinite for  $|q|$  infinite (such as for 1D gravity), and the generic situation with periodic boundary conditions; indeed, in the latter situation, local minima of the stationary potential give rise to separatrices, on which the action is constant. At these specific values of the action  $\Omega$  vanishes, but generically it does so only logarithmically. These arguments make this result very generic.

- Because  $\Lambda'_c(\lambda) \propto \lambda$ , we have  $|\mu - \mu_c| \propto \lambda^2 \propto A_{\text{sat}}$ . In homogeneous case since  $\Lambda'(0) \neq 0$  we had  $|\mu - \mu_c|^2 \propto \lambda^2 \propto A_{\text{sat}}$ .

## 6 HIGHER ORDER TERMS

---

As before to validate or not the dimensional reduction it is essential to estimate the divergence of higher order terms. The detailed computation does not bring any particular insight so we will present it only in Appendix B.2. This time we cannot escape the computation of the first order of the unstable manifold  $H(A) \in W^u$ . We find for the higher order terms

$$c_3 \propto \frac{1}{\lambda^3} \quad (\text{VI.54})$$

which means that at saturation  $A_{\text{sat}} \propto \lambda^2$ , quadratic and cubic terms are of the same order. It means that some mechanism occurs at the saturation level, this mechanism could be similar or not to the trapping of the SWM.

Note that numerics tends to confirm the failure of this one dimensional reduction since we can see oscillation on inset of Figure VI.1(b). Is this failure related to the nature of the unstable manifold expansion where even for a two dimensional model (Section IV.1) it fails when forgetting the neutral modes? In this case a two (or larger) dimensional reduction could works. Or does it mean as it seems to be the case in the homogeneous model that no finite-dimensional reduction is possible?

**Remark VI.6**

As stated before, remark V.5, in finite-dimensional systems with two eigenvalues  $\lambda, -\lambda$  it is natural to obtain a singular behavior near the criticality if one forget about the  $-\lambda$  mode. In the homogeneous case, we have safely forgotten this mode since the criticality is of dimension 1 with  $(\Lambda^{(H)})'(O^+) \neq 0$ . Here we have seen that  $\Lambda'(0) = 0$ . Hence in principle here we should be able to derive a non singular two dimensional reduction of the bifurcation. In Section VI.9 we will pursue further this discussion...

## 7 NUMERICS

---

Our analytical description of the bifurcation can be accurately tested in the HMF case. The time-evolved distribution function is obtained via a GPU parallel implementation of a semi-Lagrangian scheme for the Vlasov HMF equation with periodic boundary conditions [RF13]. I gratefully acknowledge Tarcisio Rocha Filho who provided the code in its original structure (I just did some modifications in order to choose the initial conditions and to be able to do videos of the density evolution). We use a  $2^n \times 2^n$  grid in position momentum phase space truncated at  $|p| = 2$  with  $n$  up to 12; the time step is usually  $10^{-2}$ . We use the two families of reference stationary Eq. (VI.37). For both families, a real positive eigenvalue appears at a critical value of  $\mu$ : for  $F_\mu^0$ , this is at point  $a$ , see Figure VI.4. The initial perturbation is

$$\epsilon T(q, p) = \epsilon \cos(q) \exp(-\beta_T p^2 / 2). \quad (\text{VI.55})$$

Note that this is not proportional to the unstable eigenvector  $\Psi_c$ : this allows us to test the robustness of our unstable manifold analysis with respect to the initial condition. For all simulation results presented in Figure VI.5, the size of the perturbation  $\epsilon$  was chosen small enough such that the saturated solution reached for  $\epsilon > 0$  does not depend on  $\epsilon$ . On the other hand, the smaller  $\epsilon$ , the more accurate computations are required to avoid numerical errors. In particular, we have observed that numerical errors may drive the system far away from the reference stationary solution, following a dynamics similar to the one with  $\epsilon < 0$ . In such cases, we have used a finer phase space grid: GPU computational power was crucial to reach very fine grids. For example the initial Fermi distribution  $F_\mu^0$  was very sensitive to numerical errors and to  $\epsilon$ : we took  $\epsilon = 1.8 \cdot 10^{-6}$  with a  $4096 \times 4096$  grid; for  $G_\mu^0$  distribution, which is much smoother,  $\epsilon = 10^{-5}$  and a  $1024 \times 1024$  grid was enough (except for the point corresponding to  $\lambda = 0.032$  where more precision was needed, and we took  $\epsilon = 3 \cdot 10^{-6}$ ).

Typical evolutions for the order parameter  $M(t)$  are shown in Figure VI.5 (insets), for positive and negative  $\epsilon$ . The asymmetry is clear: for one perturbation the change in  $\delta M = M(t) - M_0$  remains small, for the other it is  $O(1)$ . In the case where  $\delta M$  remains small, we compute its saturated value by averaging the small oscillations; the result is plotted as a function of  $\lambda$  on Figure VI.5: the  $\delta M \propto \lambda^2$  behavior is clear, for both families. The fact that numerical simulations are able to reach this stationary state suggests that it is a genuine stationary

state, indeed stable with respect to the whole dynamics, and not only on the unstable manifold. However, longer simulations, or with smaller grid sizes (not shown), indicate it is also easily destabilized by numerical noise. We conclude that the  $O(\lambda^2)$  state is thus probably close to the instability threshold. Notice that for the initial unstable reference state  $|\Lambda_\mu(0)| = O(\lambda^2)$  is very small; hence the very close nearby stationary state with  $\delta M \propto \lambda^2$  may have a different stability, although (in)stability of non homogeneous stationary states is rather robust comparing with the homogeneous case (see [BY15] for a discussion).

The precise computations of all the parameters and functions  $\lambda, M_0, \mu, \mathfrak{c}(J), \Omega(J), \dots$  were carefully done via the software Mathematica [Inc].

To better illustrate the phase space dynamics of  $f(q, p)$  in time, one can check online simulations on my [personal website](#)<sup>7</sup>. The colors represent the density of particles (blue: no particles; red a lot of particles). The video "[Fermi\\_eps\\_+.mp4](#)" shows the time evolution of the distribution function in phase space with initial condition  $F_\mu^0(\mathcal{H}(q, p)) + \epsilon T(q, p)$ , for  $\epsilon = +1.8 \cdot 10^{-6}$ ,  $\beta = \beta_T = 40$ ,  $(M_0 = 0.328, \mu = 0.658)$  (it corresponds to the dashed blue curve in the upper inset of Figure VI.5) from  $t = 0$  to  $t = 600$ . For the  $G_\mu^0$  initial distribution the perturbation is similar, the critical parameters are  $(M_0 = 0.243, \mu = 9.59)$ . Since the system reaches a new stationary state close to the original one, we observe almost no change in the distribution function. It is important to notice however that this picture is very different from that of the saturation of an instability over a homogeneous background: in that case, resonances would create small "cat's eyes" structures, which do not appear here. To better appreciate the dynamics in this case, we also provide the video "[Fermi\\_eps\\_+diff.mp4](#)", which is the same as the previous one, except that the reference state  $F_\mu^0$  has been subtracted; hence the evolution of the perturbation is more clearly shown.

The video "[Fermi\\_eps\\_-.mp4](#)" shows the time evolution of the distribution function with the same parameter values except that  $\epsilon = -1.8 \cdot 10^{-6}$  (it corresponds to the green curve in the upper inset of Figure VI.5). This time the distribution changes completely its shape and seems to approach a periodic solution, far away from the original stationary distribution. In all simulations, the relative error between the total energy of the system at a given time and the total initial energy is at most of the order of  $10^{-7}$ . The video "[Torr\\_G\\_eps\\_-.mp4](#)" is also provided corresponding to simulation with the  $G_\mu^0$  function with  $\epsilon = -10^{-5}$  (magenta curve in the lower inset of Figure VI.5).

Testing the predicted scaling  $A_\infty \propto \lambda^2$ , requires computing  $\lambda$  with a good accuracy. To compute the eigenvalue  $\lambda$  for each  $(M, \mu)$  associated with an initial distribution  $\mathcal{F}^0(\mathcal{H})$ , one has to find a positive root of the dispersion function Eq. (VI.25a). The two main numerical obstacles are to compute efficiently the functions  $\mathfrak{c}_m(J)$ , and the infinite sum in  $m$ . The first obstacle is suppressed by our explicit expression Eq. (B.4). It follows from their expression that the convergence of  $\mathfrak{c}_m(J)$  toward 0 with  $m$  is very fast except for  $J = J_c$  where it has a finite value (which will not contribute once integrated). Then we can choose a good truncation for the sum and estimate the precision over  $\lambda$ .

---

7. <http://math.unice.fr/~metivier/video.html>

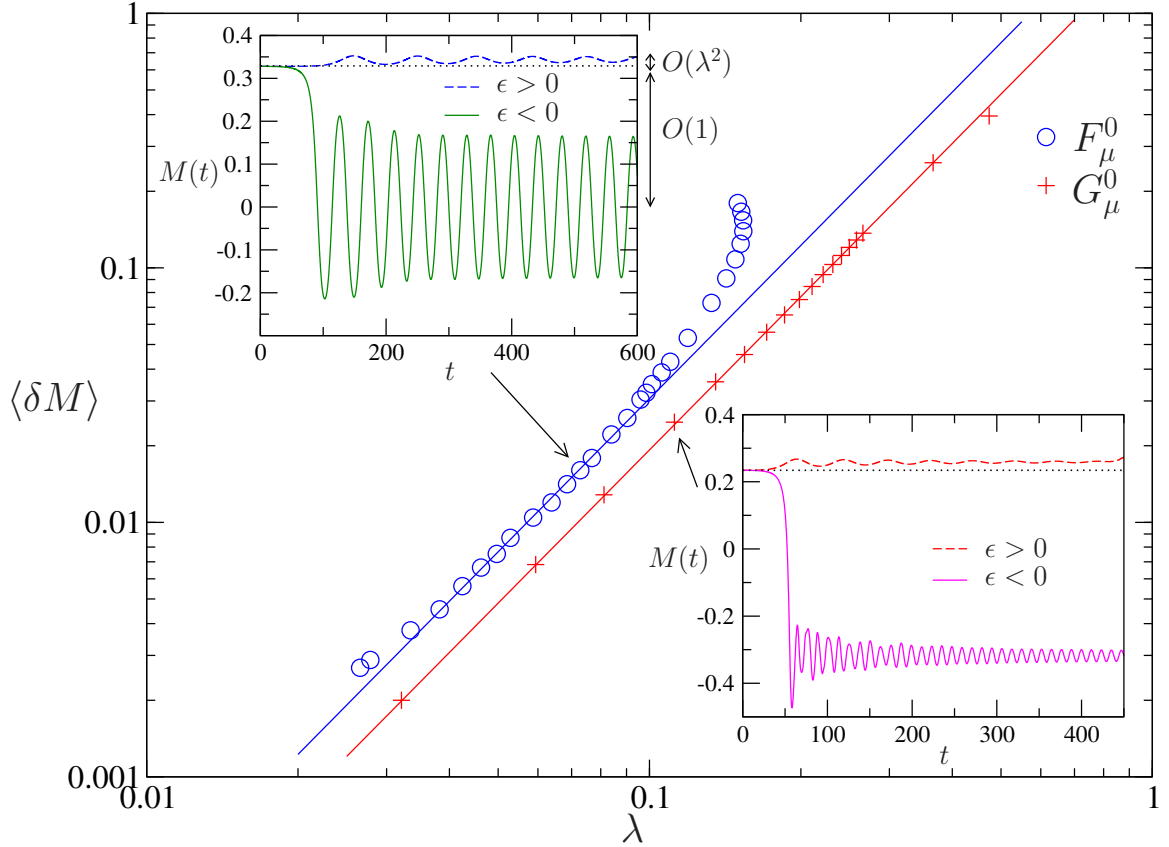


Figure VI.5 –  $\langle \delta M \rangle (\lambda)$  for distributions  $F_\mu^0$  Eq. (VI.37a) (circles) and  $G_\mu^0$  Eq. (VI.37b) (crosses) with associated quadratic fit;  $\beta = \beta_T = 40$ . For each function we show two runs of  $M_c(t) = M(t)$  (here  $M_s(t) = 0$ ) with positive and negative  $\epsilon$ .  $\langle \delta M \rangle$  in the main diagram is computed as a long time average for  $\epsilon > 0$ . For  $F_\mu^0$ ,  $|\epsilon| = 1.8 \cdot 10^{-6}$ ; for  $G_\mu^0$ ,  $|\epsilon| = 10^{-5}$ , except for  $\lambda = 0.032$  where  $|\epsilon| = 3 \cdot 10^{-6}$ . Note that the reference stationary states  $F_\mu^0$  follow the curve from point  $a$  towards point  $l$  on Figure VI.4. Along this curve,  $\lambda$  starts from 0 at point  $a$ , then grows and reaches an upper limit, about 0.15, before decreasing and reaching 0 again at point  $l$ . This is why two values of  $\mu$  may correspond to the same value of  $\lambda$  (but different values of  $\langle \delta M \rangle$ ), as can be seen around  $\lambda = 0.15$ .

## 8 POSSIBLE APPLICATIONS

As detailed in [BMT13], the instability pattern around homogeneous state is shared in many Hamiltonian systems, with applications from plasmas to fluids. Here we have seen that the saturation process seems really different possibly preventing a single-wave-model like description of the instability. So, a natural question is to what correspond that new type of bifurcation? There are probably examples in plasmas physics but so far we didn't found them.

In the astrophysics community, however, we found what seems to be a striking example of this asymmetric bifurcation.

### 8.1 Radial orbit instability: two possible end states

In [PPA90, Pal94] authors study the nonlinear evolution of the Radial Orbit Instability [BT11]. They start from a weakly unstable spherical state

- Close to this reference state, they find an axisymmetric weakly oblate stationary state
- At finite distance from the reference state (outside the perturbative regime), they find a stable prolate stationary state.

This finding is studied in Section 11.1.1 of [Pal94]. Palmer starts from a weakly unstable 3D spherical equilibrium and perturbs its self-consistent potential

$$\phi = \phi_0(r) + \epsilon \zeta(r) P_2(\cos \vartheta) \quad (\text{VI.56})$$

where  $P_2$  is a Legendre polynomial,  $\zeta(r)$  some function with a constant sign,  $\vartheta$  the standard spherical polar angle and  $\epsilon = \delta M(0)$  is the initial amplitude of the order parameter  $\delta M$  of the perturbation. He deduces that if

- $\epsilon > 0$  the perturbed system is prolate (rugby/American football ball shape),
- $\epsilon < 0$  the perturbed system is oblate (discus/flying saucer).

Then after a 3D static treatment (with some approximation and hypothesis), Palmer ends up in the perturbative regime with a self-consistent equation<sup>8</sup> that has to be satisfied by the order parameter and the instability parameter  $\mu - \mu_c \geq 0$

$$A_3 \delta M_\infty^2 - 2\delta M_\infty A_2 - (\mu - \mu_c) = 0, \quad (\text{VI.57})$$

where  $A_3 > 0$ ,  $A_2 > 0$  and  $\mu - \mu_c > 0$  is small. Solutions of this equation are

$$(\delta M_\infty)_- = \frac{A_2 - \sqrt{A_2^2 + A_3(\mu - \mu_c)}}{A_3} \sim -\frac{\mu - \mu_c}{A_2} = -O(\mu - \mu_c) < 0 \quad (\text{VI.58a})$$

$$(\delta M_\infty)_+ = \frac{\sqrt{A_2^2 + A_3(\mu - \mu_c)} + A_2}{A_3} \sim \frac{2A_2}{A_3} = O(1) > 0. \quad (\text{VI.58b})$$

It means that if the initial perturbation  $\epsilon < 0$  there is an oblate stationary solution close by of order  $O((\mu - \mu_c))$  (which is the same scaling than for our 1D case). If  $\epsilon > 0$ , the solution leaves the perturbative regime with a bar-like shape. It is fully consistent with the asymmetric behavior we predict on the unstable manifold. That is one great motivation for application! Indeed, such dynamical theory could be very useful to study galactic formation where bar-like structure could have been formed from spherical structure that went unstable.

8. We rewrite the equation replacing his  $A_1$  parameter by  $(\mu - \mu_c)$  so that the system is unstable for  $\mu > \mu_c$ . Also, his  $A_2 < 0$  is replaced by  $-A_2 < 0$ .

**Remark VI.7**

An open question regards the stability of the new weakly oblate stationary state: in our numerical examples, it seems stable, but very close to threshold. In [PPA90] they claim it is unstable, but since their numerical simulations are much less precise, this could be a numerical artifact.

**8.2 Super Massive Black Hole**

---

With this result in mind we were very excited to hear at the ICTP conference on long-range<sup>9</sup>, astrophysicist talks.

Amongst other we hear Jihad Touma talking about galactic models of stars orbiting around a super massive black hole (SMBH), which is today the standard picture for galaxy structure. For example following elliptic orbit of stars have allowed [SOG<sup>+</sup>02, GSW<sup>+</sup>08] to deduced the position and mass of the SMBH of the Milky-way. In [ST16], Sridhar and Touma derive a reduced model from this complete system ending up with a Vlasov equation in 3D (or 2D or 1D depending on the symmetry assumption) angle-action variables. Once again, we think that our treatment can be applied without much changes<sup>10</sup>. Of course, stability result on such realistic model would be very important for galactic formation. We contacted J. Touma successfully and started to look at the model. However, since I have started my thesis manuscript, I cannot help much my advisor and Y.Y. Yamaguchi on this problem.

**9 TOWARDS AN EXACT DIMENSIONAL REDUCTION?**

---

---

**9.1 Did we miss something?**

---

This Section relates some later findings (June 2017 and after) that could lead to an exact dimensional reduction of the bifurcation problem around steady states of the non homogeneous Vlasov equation. In Remark V.5 we noted that due to the strong resonances of the homogeneous case we had  $\Lambda'(0 \pm i\lambda_i) \neq 0$  at criticality  $\mu = \mu_c$ . It implied that the "positive" and "negative" eigenvalues<sup>11</sup> did not join on the real axis (they are on different Riemann sheets), hence a  $2 \times 2$  description of the bifurcation with a center manifold technique was not possible [CH89] and we had to use only a 2 dimensional unstable manifold leading to a singular expansion.

In the non homogeneous case with a real eigenvalue we followed the same unstable manifold path describing the bifurcation with a one-dimensional unstable manifold (due to the lack of rotational symmetry). This approach though qualitatively correct (predicting the transcritical bifurcation observed in simulations with the correct trapping scaling) was plagued by singularities at every order. Moreover, its one-dimensional form could not account (which was also the case for the homogeneous Vlasov case) for the "trapping oscillations" observed numerically.

Now, what if we could describe this bifurcation with a finite-dimensional center manifold, as one should in a finite-dimension analog of this problem? Here we indeed have  $\Lambda'(0) = 0$ , so that at criticality  $\lambda_{\mu_c} = 0$  the eigenvalues  $\lambda, -\lambda$  do collide. It only happens because this

---

9. ICTP conference program in Trieste on long-range interaction, July 2016.

10. That assertion is optimistic.

11. Either for four complex eigenvalues  $\lambda, \lambda^*, -\lambda, -\lambda^*$  with each an associated dimension of one, or two real eigenvalues  $\lambda, -\lambda$  with an associated dimension of two each (thanks to rotational symmetry).

time there is no need for analytic continuation of the dispersion relation; physically because of weaker resonances between particles at the separatrix and the perturbing wave. Furthermore, here in addition to these two eigenvalues we might expect another 0 eigenvalue associated with the stationary states. Now how to treat this center manifold problem <sup>12</sup>?

## 9.2 The Triple Zero bifurcation

In the following analysis, we are going to leave aside implicitly the continuous spectrum (assuming that in some functional space it can be moved away from the imaginary axis) and the neutral mode  $\lambda_s = 0$  associated with the  $\sin$  direction that we do not perturb. Hence, we will consider the two colliding eigenvalues  $\lambda, -\lambda$  associated with the  $\cos$  direction plus a 0 eigenvalue (that is needed for the center to be feasible) <sup>13</sup>.

From here we leave the index  $c$  of  $\Psi_c$ . Having a triple zero eigenvalue at  $\mu = \mu_c$  means for a 3-dimensional problem that there is a Jordan block representation of the linear problem as

$$\mathcal{L}_J = \begin{pmatrix} 0 & 1 & 0 \\ 0 & 0 & 1 \\ 0 & 0 & 0 \end{pmatrix}. \quad (\text{VI.59})$$

This type of triple zero problem produces the so call Triple Zero (TZ) bifurcation [GFRL<sup>+</sup>99, FGRLA02]. Here the dimension is infinite but we can still use these ideas. The eigenvalue problem is “unusual” since there is only one eigenvector for three eigenvalues. To form a basis at criticality  $\nu = \mu - \mu_c = 0$ , we have to use the notion of generalized eigenvectors (with not the same sense that for van Kampen generalized eigenvectors of Section V.2.2)

$$\mathcal{L}_0 \psi^{(0)} = 0, \quad \mathcal{L}_0 \psi^{(1)} = \psi^{(0)}, \quad \mathcal{L}_0 \psi^{(2)} = \psi^{(1)}, \quad (\text{VI.60})$$

where  $\psi^{(1)}$  and  $\psi^{(2)}$  are called generalized eigenvectors while  $\psi^{(0)}$  is a usual eigenvector associated with  $\lambda = 0$ .

The corresponding projections are given by the adjoint (generalized) eigenvectors, determined by

$$\mathcal{L}_0^\dagger \tilde{\psi}^{(0)} = 0, \quad \mathcal{L}_0^\dagger \tilde{\psi}^{(1)} = \tilde{\psi}^{(0)}, \quad \mathcal{L}_0^\dagger \tilde{\psi}^{(2)} = \tilde{\psi}^{(1)}. \quad (\text{VI.61})$$

This yields (the first line is the  $m = 0$  Fourier coefficient, the second line is for all  $m \neq 0$ ):

$$\psi^{(0)} = \begin{pmatrix} 0 \\ -\frac{F'_0 c_m}{\Omega} \end{pmatrix}, \quad \psi^{(1)} = \begin{pmatrix} 0 \\ \frac{F'_0 c_m}{im\Omega^2} \end{pmatrix}, \quad \psi^{(2)} = \begin{pmatrix} \frac{\Lambda''(0)}{4\pi \int c_0^2 c_0(J)} \\ \frac{F'_0 c_m}{m^2 \Omega^3} \end{pmatrix}. \quad (\text{VI.62})$$

The associated magnetizations are:

$$M[\psi^{(0)}] = 1, \quad M[\psi^{(1)}] = 0, \quad M[\psi^{(2)}] = 0.$$

There is some freedom in the choice of  $\psi_{m=0}^{(2)}$ . It is chosen here so that  $M[\psi^{(2)}] = 0$ ; this fixes only the scalar product with  $c_0$ ; in addition, it is chosen here proportional to  $c_0$ . Note that there is another infinite family of eigenvectors with 0 eigenvalues

$$\psi = \begin{pmatrix} u(J) \\ 0 \end{pmatrix};$$

12. In fact we had this idea at the early stage of the problem but somehow, we got lost and did not pursue further.

13. This is a modification with respect to what was presented at the Ph.D. defense where we had not noticed the inconsistency.

however, they are not associated with a Jordan block.

The generalized eigenprojections are

$$\tilde{\psi}^{(0)} = \begin{pmatrix} \frac{2}{\Lambda''(0)} \mathfrak{c}_0 \\ 0 \end{pmatrix} \quad \tilde{\psi}^{(1)} = \begin{pmatrix} 0 \\ -\frac{2}{\Lambda''(0)} \frac{\mathfrak{c}_m}{im\Omega} \end{pmatrix} \quad \tilde{\psi}^{(2)} = \begin{pmatrix} -\frac{\Lambda^{(4)}(0)}{6\Lambda''^2(0)} \mathfrak{c}_0 \\ \frac{2}{\Lambda''(0)} \frac{\mathfrak{c}_m}{m^2\Omega^2} \end{pmatrix} \quad (\text{VI.63})$$

Note that  $\Lambda''(0) \neq 0$  and  $\Lambda^{(4)}(0) \neq 0$ . These vectors satisfy

$$\langle \tilde{\psi}^{(i)}, \psi^{(j)} \rangle = \delta_{2-i,j}.$$

These last relations fix the prefactors in front of the eigenprojections, involving the derivatives of  $\Lambda$ ; the prefactors are finite. There is some freedom in the choice of  $\tilde{\psi}_{m=0}^{(2)}$ ; it is chosen here proportional to  $\mathfrak{c}_0$ . Note that it is not possible to obtain such a structure with only one or two vectors neither with more than three vectors. On the subspace  $\text{span}(\psi^{(0)}, \psi^{(1)}, \psi^{(2)})$ , the critical linearized operator  $\mathcal{L}_0$  is indeed a 3D Jordan block, with a 0 diagonal.

We write  $f$  as a point on a 3D manifold tangent to  $\text{span}(\psi^{(0)}, \psi^{(1)}, \psi^{(2)})$  at the origin. It should be possible to construct locally such an invariant manifold:

$$f = A_0\psi^{(0)} + A_1\psi^{(1)} + A_2\psi^{(2)} + H[A_0, A_1, A_2].$$

At leading order (quadratic), we do not need to compute  $H$ . The dynamical equation for the perturbation  $f$  is

$$\partial_t f = \mathcal{L}_0 f + \nu \delta \mathcal{L} f + \mathcal{B}(f, f).$$

At quadratic order, there are a priori 27 terms to compute, the  $\langle \tilde{\psi}^{(i)}, \mathcal{B}(\psi^{(j)}, \psi^{(k)}) \rangle$ , for any  $i, j, k$ . The bilinear form  $\mathcal{B}$  reads

$$\mathcal{B}(g, h)_m = M[h] \sum_{l \neq 0} il (g_l \mathfrak{c}'_{m-l} - g'_{m-l} \mathfrak{c}_l).$$

Hence the only non zero terms at quadratic order are

$$\mathcal{B}(\psi^{(i)}, \psi^{(0)}), \quad i = 0, 1, 2.$$

Then many projections vanish because of symmetries. Finally, only 4 terms remain:

$$\langle \tilde{\psi}^{(0)}, \mathcal{B}(\psi^{(1)}, \psi^{(0)}) \rangle, \quad \langle \tilde{\psi}^{(1)}, \mathcal{B}(\psi^{(0)}, \psi^{(0)}) \rangle, \quad \langle \tilde{\psi}^{(1)}, \mathcal{B}(\psi^{(2)}, \psi^{(0)}) \rangle, \quad \langle \tilde{\psi}^{(2)}, \mathcal{B}(\psi^{(1)}, \psi^{(0)}) \rangle.$$

Close to criticality, we need to compute the contributions of  $\nu \delta \mathcal{L}$ . We have (emphasizing that all terms have leading order  $\nu$ ):

$$\nu \delta \mathcal{L} g = -\nu \delta \Omega \partial_\theta g - M[g] \nu \delta F'_0 \partial_\theta \cos q$$

We have a priori 9 terms to compute, the  $\langle \tilde{\psi}^{(i)}, \nu \delta \mathcal{L} \psi^{(j)} \rangle$ . The non zero ones are

$$\langle \tilde{\psi}^{(1)}, \nu \delta \mathcal{L} \psi^{(0)} \rangle, \quad \langle \tilde{\psi}^{(2)}, \nu \delta \mathcal{L} \psi^{(1)} \rangle, \quad \langle \tilde{\psi}^{(1)}, \nu \delta \mathcal{L} \psi^{(2)} \rangle.$$

The final reduced system is

$$\dot{A}_0 = A_1 + \nu b A_1 + \alpha_{01} A_0 A_1 \quad (\text{VI.64a})$$

$$\dot{A}_1 = (1 + \nu c) A_2 + \nu a A_0 + \beta_{00} A_0^2 + \beta_{02} A_0 A_2 \quad (\text{VI.64b})$$

$$\dot{A}_2 = \gamma_{01} A_0 A_1, \quad (\text{VI.64c})$$

where the coefficients have to be computed numerically. It can be simplified a bit further by changes of variables. However, such a 3D dynamical system is not straightforward to analyze.

### 9.2.a Quick analysis of the reduced equations

At linear order,  $\dot{A}_2 = 0$ , so  $A_2$  is conserved at this order. Notice that  $\psi^{(2)}$  has a non vanishing zero mode; hence it modifies the Casimirs of  $F_\mu$  at linear order. It is thus normal that an initial condition with  $A_2 \neq 0$  cannot be dynamically connected to the reference state  $A_0 = A_1 = A_2 = 0$ . It is also a hint that there may be a nonlinear generalization of this conserved quantity  $A_2$  which would be the trace of the Casimir conservation. Let us try  $G(A_0, A_1, A_2) = A_2 + g(A_0)$ , with  $g(A_0) = O(A_0^2)$ . Taylor expanding  $g$ , computing order by order, and resumming the series, one obtains the conserved quantity

$$G(A_0, A_2) = A_2 - \frac{\gamma_{01}}{\alpha_{01}} A_0 + \frac{\gamma_{01}(1 + \nu b)}{\alpha_{01}^2} \ln \left( 1 + \frac{\alpha_{01}}{1 + \nu b} A_0 \right). \quad (\text{VI.65})$$

Since the dynamics is at best accurate at quadratic order, this exactly conserved quantity should be considered with care: it is probably relevant at quadratic order only. As a first consequence, the dynamics is two-dimensional, and this is the reason why we do not observe chaotic trajectories. We are interested in initial conditions very close to the weakly unstable stationary state, actually infinitely close: hence  $A_i(t = 0)$  can be thought of as very small. Hence the value of the conserved quantity is essentially 0. The reduced dynamics, truncated at order  $A_0^2$  (dropping terms such as  $A_0^k$ ,  $k > 2$ , and  $\nu A_0^2$ ) becomes

$$\begin{aligned} \dot{A}_0 &= (1 + \nu b) A_1 + \alpha_{01} A_0 A_1 \\ \dot{A}_1 &= G(\epsilon)(1 + \beta_{02} A_0) + \nu a A_0 + \left( \beta_{00} - \frac{1}{2} \gamma_{01} \right) A_0^2 \end{aligned}$$

Where we used that  $G$  is constant in time and very small such that  $G(\epsilon) = O(A_2(0)) = O(\epsilon) \ll \nu$  with  $G(\epsilon \rightarrow 0) = 0$ . This last system is similar (up to some variable change) to the Bogdanov-Takens normal form [Tak74, Bog75, HK91, Kuz04, Kuz05]. This dynamical system has two fixed points for  $\epsilon \rightarrow 0$ : the reference one  $(0, 0)$  and a new one  $(-\nu a / (\beta_{00} - \gamma_{01}/2))$ ; the new one is at distance  $O(\nu)$  of the first one, that is  $O(\lambda^2)$ . There is a homoclinic orbit at  $(0, 0)$ , which encircles the new fixed point; this homoclinic orbit is a separatrix: any orbit inside it is bounded, and oscillates around the new fixed point; any orbit outside eventually escapes to infinity. The "angular volume" occupied by the bounded orbits around  $(0, 0)$  is small (of order  $\nu$ ), because the stable and unstable manifolds at  $(0, 0)$  are close one to another. Hence one has to choose well the perturbation to observe a bounded dynamics. Nevertheless, any initial condition with  $A_1(t = 0) = 0$  and a well chosen sign for  $A_0$  is in this "bounded region". All this is strikingly consistent with the HMF numerical simulations, and suggest further possible tests, since the coefficients are computable.

### 9.2.b Numerical comparison between reduced system and full Vlasov dynamics

Our quick analysis already showed that the TZ reduced system predicts a transcritical behavior as the one observed in Vlasov simulations (see Section VI.7). Moreover the saturation scaling  $O(\lambda^2)$  predicted is also the one seen in these simulations. Nevertheless these two features were already predicted with the unstable manifold approach despite its singularities. Hence can the TZ model predic more than that? Like the oscillations around the saturated level? Or can we compare TZ model quantitatively with simulations?

In order to answer these questions, we compute all the coefficients  $\nu a, \nu b, \nu c$  at the initial condition  $(M_0, \mu)$  and the nonlinear coefficients at criticality  $((M_0)_{\mu_c}, \mu_c)$ ,  $\alpha_{01}, \beta_{00}, \beta_{02}, \gamma_{01}$ .

Moreover we need the initial conditions  $A_1(0), A_2(0), A_3(0)$  to be the same in simulations and TZ model. The perturbation is given by Eq. (VI.55) however we change the normalization so that  $A_0(0) = \epsilon$ . By symmetry  $A_1(0) = 0$ , but due to numerical grid error  $A_1(0)$  could be nonzero (but very small).  $A_2(0)$  has to be computed with its full definition. The criticality around where the center manifold is computed, corresponds for the Fermi distribution VI.37a to the point  $a$  on Figure VI.4. Taking  $\nu = \mu - \mu_c \neq 0$  corresponds to move on the dashed line; perturbation  $\epsilon$  of this initial state are perturbation away from this dashed line.

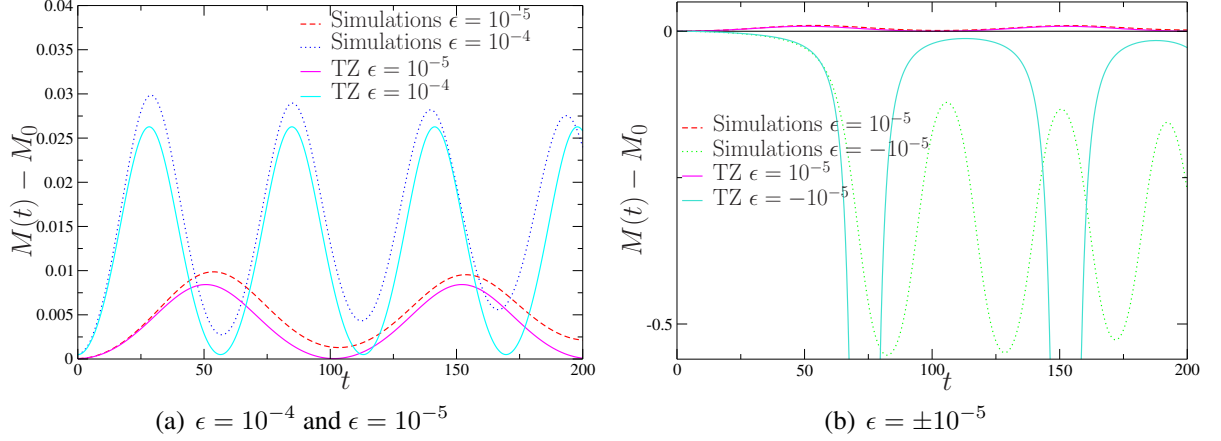


Figure VI.6 – Comparison of the TZ dynamics Eq. (VI.64) versus the full Vlasov-HMF dynamics. We plot the time evolution of the magnetization  $M(t) - M_0$  for a perturbed unstable non homogeneous states of the Fermi distribution Eq. (VI.37a) with  $\beta = 40$  and  $(M_0 = 0.3360, \mu = 0.6691)$  (which correspond to  $\lambda = 8.62 \cdot 10^{-3}$ ). The criticality is  $((M_0)_{\mu_c} = 0.3361, \mu_c = 0.6693)$ . We test different perturbations  $\epsilon$  with  $\beta_T = 10$ . The parameter are (up to three significant digits)  $\nu a = 7.44 \cdot 10^{-5}, \nu b = -3.12 \cdot 10^{-4}, \nu c = \nu b, \alpha_{01} = 0.380, \beta_{00} = -0.181, \beta_{02} = 0.572, \gamma_{01} = -0.602$ . In the simulations the grid is  $4096 \times 4096$  and  $p_{\max} = 3$ .

On Figure VI.6 we show the comparison of the TZ dynamics versus the full Vlasov-HMF simulations by plotting  $M(t) - M_0$ . On Figure VI.6(a) we show the effect of two different  $\epsilon$  on the amplitude and frequency of oscillations. The quantitative agreement between the full simulations and the TZ model is very good: for both  $\epsilon = 10^{-4}$  and  $10^{-5}$  the predicted amplitude match with a error around 10%. Moreover the frequency of oscillations also agrees very well. However we can see on the full dynamics than a small damping occurs while the TZ model conserves the amplitude of orbits (in fact there is no dissipative term in TZ model). This damping could be a manifestation of the weak resonances producing small Landau damping. On Figure VI.6(b) we show that for  $\epsilon$  positive or negative we indeed have a transcritical behavior. The  $O(1)$  curve predicted by TZ matches the simulations up to a time  $\sim 1/\lambda$ , after it undergoes a cycling dynamics but does not match the simulations anymore. It is normal considering that the perturbative approach is no longer valid, nevertheless higher order terms might improve the agreement.

**9.2.c** *Questions and puzzles*

- Can we make further qualitative/quantitative predictions based on the 3D reduced dynamics? Many complicated things happen close to a triple zero bifurcation; here, varying  $\nu$ , we more or less follow a 1D curve in the 3D parameter space close to the bifurcation.
- What happens for a general potential? Computations not shown here show that up to some details the generic reduced system is identical to Eq. (VI.64).
- Pushing the computations to order 3 is likely to produce divergences because of the separatrix. It is not clear how to handle these divergences. Note that models other than HMF may not have any separatrix, and then should not show this type of singularities.
- The "Crawford singularities" have apparently disappeared at order 2, and this is physically not unreasonable, since the resonance with zero velocity particles is now very weak. Does it mean that there is hope for a mathematical conjecture?
- Because of the weak resonances should we couple this TZ system with a kind of single wave model to account for the small Landau damping? Or does it completely disappear in the limit  $\nu, \epsilon \rightarrow 0$  where the center manifold is mathematically defined?
- For a generic degenerate Hamiltonian system (with respect to the Poisson brackets) there are Casimir invariant [MH13, HM13], they are associated with a 0 eigenvalue. In general close to a bifurcation without resonances we expect the two eigenvalue  $\lambda, -\lambda$  to collide in 0. Thus, is the TZ normal form generic for degenerate Hamiltonian systems (without resonances)?

---

## VLASOV-FOKKER-PLANCK SYSTEM

---

Vlasov equation does not possess any mechanism driving the dynamics towards thermal equilibrium, as it neglects collisional effects as well as noise and friction. While the collisionless dynamics can be (and for a given timescale) a very good approximation of the real evolution, small dissipative mechanisms are usually present and slowly drive the system to statistical equilibrium. For plasmas [LLP81] and self-gravitating systems [BT11], discreteness -usually called "collisional"- effects provide this relaxation mechanism; for cold atoms in a magneto-optical trap, there is a rather strong friction and velocity diffusion (see Part One). How do dissipative effects act on the dynamics? How are the two iconic collisionless effects of the Vlasov equation, namely Landau damping and trapping scaling, modified?

In this Chapter, we add to the Vlasov equation a linear Fokker-Planck operator accounting for a friction/diffusion<sup>1</sup> in the system. It forces the equilibrium distribution to be Gaussian in velocity. The first question that arose from our theoretical physicist mind when we started the experimental collaboration (Part One) was "Can we observe Landau damping in a very large Magneto-Optical-Trap?". Since the Vlasov-Fokker-Planck (VFP) equation describes the VLMOT behavior (according to the standard description), it is natural to wonder how Landau damping survives with friction and diffusion. Moreover, the detuning controls the friction and we should then be able to explore different regimes. However, quick estimations of the friction terms showed us that the system was overdamped leaving a thin hope to observe any Landau damping. Nevertheless, the theoretical questions remains, how Landau damping behaves in presence of friction and diffusion? As we will see the spectrum of the linear operator is strongly modified since the continuous spectrum completely disappear [SS02]. Hence we can also wonder how these modifications affect the bifurcation toward instability. Can we construct the unstable manifold for VFP? Do singularities arise? We know that in standard dissipative systems the saturation of the order parameter follows the "Hopf scaling"  $A_{\text{sat}} \propto \sqrt{\lambda}$ , do we recover this regime for large friction? Standard bifurcation methods should work (e.g. center manifold, multiple time scale analysis) for a finite dissipation level, however we know they fail

---

1. That we will often simply denote by friction alone.

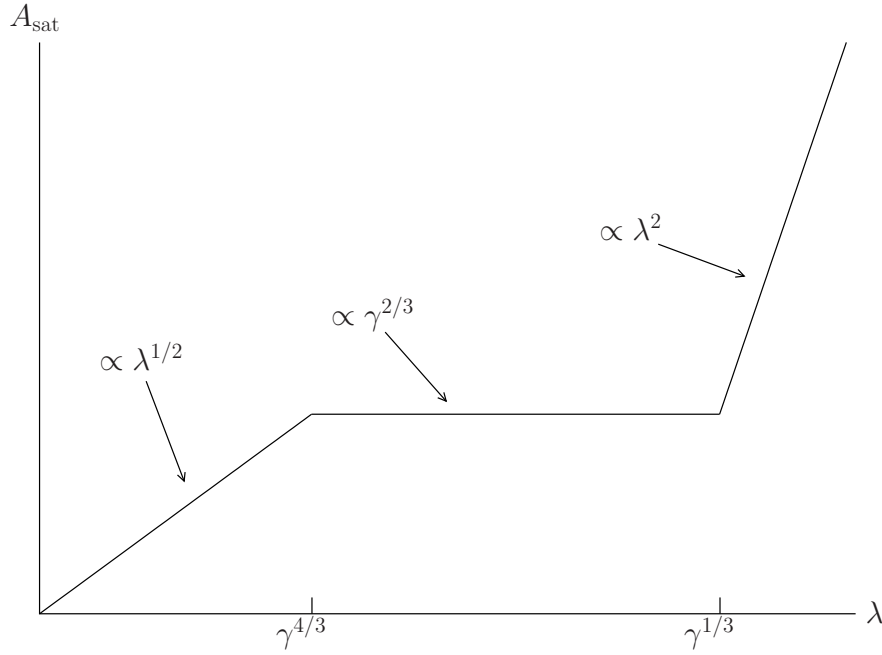


Figure VII.1 – Schematic representation of the main nonlinear results. On the horizontal axis: the linear instability rate  $\lambda$ ; on the vertical axis: the saturation amplitude (ie the amplitude reached by the perturbation over timescales of order  $1/\lambda$ ). The dissipation coefficient  $\gamma$  is fixed. This picture assumes that both  $\gamma$  and  $\lambda$  are small. For  $\lambda \gg \gamma^{1/3}$ , the trapping scaling  $A_{\text{sat}} \propto \lambda^2$ , characteristic of Vlasov regime, appears. For  $\lambda \ll \gamma^{4/3}$ , the normal dissipative scaling  $A_{\text{sat}} \propto \lambda^{1/2}$  is recovered. In between we predict a plateau with saturation amplitude  $A_{\text{sat}} \propto \gamma^{2/3}$ .

at zero dissipation (Vlasov limit), hence using the unstable manifold technique we should be able to observe this "breakdown" when diminishing the dissipation.

In the linear analysis, Section VII.2, we show following [SS02] that the spectrum of the linear operator is drastically modified in presence of friction since the continuous spectrum is removed and the resonances of the dispersion relation become true eigenvalues. Hence in the small friction limit we recover Landau damping because the eigenvalues of the perturbed system converge toward the resonances pure Vlasov equation. However, for larger friction the Landau damping progressively disappears in favor of pure dissipation. Physically the friction/dissipation provides a cut off to the velocity phase mixing. In the nonlinear part, Section VII.3, we manage to perform the nonlinear expansion; the dominating contribution is still provided by the zeroth harmonic of the unstable manifold. Nevertheless, the computations are more involved since we have to express the problem in velocity Fourier space. Eventually we obtain the different scaling of the cubic coefficient  $c_3$  that yield the saturation scaling. We find not two but three different regimes for the saturation amplitude with respect to the instability parameter and friction. We summarize these results on Figure VII.1. Furthermore, these regimes correspond to the ones found for a similar problem on fluid mechanics systems [CS87, CS95]. We can put into perspective this similitude with the fact that Single Wave Model reduction is for both Vlasov and Euler 2D. The interpretation in terms of critical layer (linear, nonlinear, viscous) is done in Section VII.3.3.

Note that we consider here only homogeneous equilibrium contrary at what have been done in the previous Chapter VI. A Vlasov-Fokker-Planck analysis around non homogeneous states is for now out of reach since the system is not Hamiltonian (no action variable could diagonalize

the linear problem).

The method presented here is different from the one used in the article we wrote [BM17a] on this topic. Indeed, in this article to prove rigorous mathematical theorems on the spectrum of the Vlasov-Fokker-Planck operator we used the already existing framework and results of J-M. Bismut and G. Lebeau<sup>2</sup> [BL08] on the perturbed harmonic oscillator operator. We then performed the unstable  $q$  calculation using the Bargman representation. Here in this manuscript we show another way using Fourier velocity calculation as in [LB58, SS02, NBS99]. Of course, the results are the same.

## 1 SETTINGS

Our starting point is the Vlasov-Newton-Fokker-Planck equation [Ris89], Eq. (I.31) and Eq. (I.33a). To keep the following computations as simple as possible, we stick to one dimensional case with HMF interactions. The kinetic equation for the density  $f(q, p, t)$  reads

$$\partial_t F + p \partial_q F - K \partial_q \phi[F] \partial_p F = \gamma \partial_p (pF + \partial_p F), \quad (\text{VII.1a})$$

$$\phi[F] = -M[f] \cos q, \quad (\text{VII.1b})$$

where  $\gamma$  is the friction parameter, we have chosen our units so that  $k_B T = 1$  and introduced a coupling parameter  $K$ . Hence here we change the coupling parameter  $K$  in order to control the (in)stability whereas in the frictionless case in Chapter V the instability coupling was set to  $K = 1$  and the temperature could vary. This change is obtained by rescaling. The distribution

$$f^0(p) = \frac{e^{-p^2/2}}{(2\pi)^{3/2}}$$

is the only velocity stationary solution of this equation. This Gaussian shape is expected since at thermal equilibrium we expect a Gibbs distribution.

### Remark VII.1

In [BM17a] we deal with the Coulomb/Newton case with the same results. The Gaussian equilibrium is always stable for a repulsive interaction; since we are interested in the weakly unstable case we focus on the attractive case.

Furthermore, if we wanted the system to relax towards another equilibrium distribution we could use a more general Fokker-Planck operator

$$\gamma \partial_p \left( f^0 \partial_p \left( \frac{f}{f^0} \right) \right)$$

for which  $f^0(p)$  is a stationary state.

We study the perturbed density  $F(q, p, t) = f_0(p) + f(q, p, t)$  and its evolution. The equation for  $f$  reads:

$$\partial_t f = \mathcal{L} f + \mathcal{N} f \quad (\text{VII.2a})$$

$$\mathcal{L} f = -p \partial_q f + K \partial_q \phi[f] (f^0)'(p) + \gamma \partial_p (p f + \partial_p f) \quad (\text{VII.2b})$$

$$\mathcal{N}[f] = K \partial_q \phi[f] \partial_p f. \quad (\text{VII.2c})$$

Note that the nonlinear operator is the same as in the homogeneous case.

---

2. We are indebted to Gilles Lebeau for this idea.

## 2 LINEAR PROBLEM

### 2.1 Velocity Fourier

In the homogeneous case the eigenvalue problem has been straightforward, in the non homogeneous one we had to change variable. Here at the spatial Fourier level we encounter new terms with first and second order velocity derivatives

$$\mathcal{L}_k f_k = -ikp f_k + ikK\phi_k[f](f^0)' + \gamma\partial_p(p f_k + \partial_p f_k). \quad (\text{VII.3})$$

To simplify further we proceed to the velocity-Fourier transform (denoted by a hat)

$$\hat{f}(\eta) = \text{FT}[f(p)](\eta) = (2\pi)^{-1/2} \int f(p) e^{ip\eta} dp.$$

In velocity Fourier,  $\partial_p \rightarrow -i\eta$  and  $p \rightarrow -i\partial_\eta$ . Moreover for  $k = \pm 1$

$$\phi_k[f] = -\frac{1}{2} \int f_k dp = -\frac{1}{2} (2\pi)^{1/2} \hat{f}_k(\eta = 0). \quad (\text{VII.4})$$

We also have  $\hat{f}^0(\eta) = (2\pi)^{-3/2} e^{-\eta^2/2}$

The Fourier velocity transform of the linear operator yields

$$\widehat{\mathcal{L}}_k \hat{f}_k(\eta) = -k\partial_\eta \hat{f}_k - \eta k K \phi_k[f_k](\hat{f}^0) - \gamma\eta\partial_\eta \hat{f}_k - \gamma\eta^2 \hat{f}_k. \quad (\text{VII.5})$$

#### Remark VII.2

Unlike the two previous conservative case (with no dissipation), the 0<sup>th</sup> spatial Fourier mode  $\mathcal{L}_0 f \neq 0$ . Which mean that  $\lambda = 0$  is no longer an eigenvalue associated with an infinite eigenspace. It is now associated with a one dimensional eigenspace spanned by  $f^0$ . That is to say there is no more an infinity of possible steady states but only one (the Gaussian).

### 2.2 Eigenvalue problem

We can now seek an eigenvector of the form  $\Psi_k = \psi_k(p) e^{ikq}$  for  $k = \pm 1$ .

$$\mathcal{L} \Psi_k = \lambda \Psi_k \quad (\text{VII.6})$$

which gives in Fourier velocity

$$\partial_\eta \hat{\psi}_k + \frac{\lambda + \gamma\eta^2}{k + \gamma\eta} \hat{\psi}_k = -K\phi_k[\Psi] \frac{\eta \hat{f}^0}{k + \gamma\eta} = k\sqrt{2\pi} \hat{\psi}_k(\eta = 0) \frac{K}{2} \frac{\eta \hat{f}^0}{k + \gamma\eta}. \quad (\text{VII.7})$$

We impose the normalization such that  $\hat{\psi}(\eta = 0) = 1$ . From now on we drop the spatial Fourier index  $k = 1$ , e.g.  $\psi_1 = \psi$ .

We define  $y = 1/\gamma$ ,  $a = y^2 + \lambda y$ . The homogeneous solutions of Eq. (VII.7) are given by

$$\hat{\psi}_h(\eta) = \text{cst} \cdot e^{-\eta^2/2} e^{y\eta} \left(1 + \frac{\eta}{y}\right)^{-a}. \quad (\text{VII.8})$$

Since there is an unphysical divergence at  $\eta = -1/\gamma$ , this solution has to be removed (by setting the arbitrary constant to 0).

Hence the complete eigenvector is given by a particular solution [SS02, NBS04],

$$\begin{aligned}
 \widehat{\psi}(\eta) = \widehat{\psi}_p(\eta) &= -\frac{K}{4\pi} e^{-\eta^2/2} e^{y\eta} \left(1 + \frac{\eta}{y}\right)^{-a} \int_{-y}^{\eta} t e^{-yt} \left(1 + \frac{t}{y}\right)^{a-1} dt \\
 &= -\frac{K}{4\pi} y e^{-\eta^2/2} e^{y^2+y\eta} (y^2 + y\eta)^{-a} \int_0^{y^2+y\eta} (x/y - y) e^{-x} x^{a-1} dx \\
 &= \frac{K}{4\pi} e^{-\eta^2/2} e^{y^2+y\eta} (y^2 + y\eta)^{-a} (y^2 \gamma(a, y^2 + y\eta) - \gamma(a+1, y^2 + y\eta)) \\
 &= \frac{K}{4\pi} (1 - \lambda y d(a, y^2 + y\eta)) e^{-\eta^2/2}
 \end{aligned} \tag{VII.9}$$

where we have used  $\widehat{\psi}(\eta = -y) = yK e^{-y^2/2} / (4\pi(y - \lambda))$  to choose the lower integration bound. We have introduced the lower incomplete Gamma function [ODL<sup>+</sup>14]

$$\gamma(a, z) = \int_0^z t^{a-1} e^{-t} dt,$$

(not to be confuse with the friction parameter  $\gamma$ ) and used  $\gamma(a+1, x) = a\gamma(a, x) - x^a e^{-x}$  and defined

$$d(a, x) = x^{-a} e^x \int_0^x e^{-t} t^{a-1} dt = x^{-a} e^x \gamma(a, x) = \int_0^1 e^{xs} (1-s)^{a-1} ds. \tag{VII.10}$$

### Remark VII.3

In the limit  $\gamma = 0$ , the divergence of the homogeneous solution is suppressed  $\widehat{\psi}_h(\eta) \propto e^{\lambda\eta}$  which is indeed the Fourier transform of the generalized eigenvector  $\propto \delta(\lambda + iv)$ . So, with friction these solutions are removed and there is no more continuous spectrum (see next Section).

## 2.3 Spectrum

In the previous computation, we did not have to be careful about whether  $\lambda$  was on the imaginary axis or not which is another indication that the continuous spectrum has somehow changed. In terms of operator the Fokker-Planck "perturbation" is unbounded (because of the velocity derivatives) and we expect that even a small perturbation can affect/break the continuous spectrum structure. Indeed, in standard systems there is in general no such spectrum.

The normalization condition  $\widehat{\psi}(0) = 1$  gives us directly the dispersion relation

$$\Lambda(\lambda, \gamma) = 1 - \frac{K}{4\pi} (1 - \lambda/\gamma d(1/\gamma^2 + \lambda/\gamma, 1/\gamma^2)). \tag{VII.11}$$

In [SS02] is performed the limit  $\gamma \rightarrow 0$ , (which can be done expanding in powers of  $1/\gamma$  in the integral terms) yielding

$$\lim_{\gamma \rightarrow 0} \Lambda(\lambda, \gamma) = 1 - \frac{K}{4\pi} \int_0^\infty e^{-s^2/2 - \lambda s} s ds = \epsilon_1^{(0)}(\lambda) \tag{VII.12}$$

where  $\epsilon_1^{(0)}(\lambda)$  was defined in Eq. (V.32) as the analytic continuation of the homogeneous dispersion relation denoted in this Chapter  $\Lambda^{(0)}(\lambda)$ . It means that indeed the dispersion relation

tends to the dispersion relation without friction which is expected. The important implication is that the roots of this analytic continuation (resonances) are even with a small friction  $\gamma \neq 0$ , true eigenvalues of  $\Lambda(\lambda, \gamma)$  and thus of the system. So, when  $\gamma \rightarrow 0$ , the negative eigenvalues approach the resonances of the frictionless Vlasov equation.

In [BM17a] we prove that indeed the continuous spectrum is empty for the Vlasov-Fokker-Planck operator with the help of [BL08]. In mathematics, it is called "stochastic stability" since eigenvalues of the system with a small stochastic perturbation (Fokker-Planck operator with a Gaussian noise) are close to the resonances. This stochastic stability for the resonances of the linearized Vlasov operator is a phenomenon studied in other contexts: in fluid dynamics [Bal99], for Pollicott-Ruelle resonances [Dro16, DZ15], or for a Schrödinger operator [Zwo15].

## 2.4 Landau damping

---

In the gravitational case, we know that the eigenvalues are real for a Gaussian distribution, hence here we focus on a small real eigenvalue. The stability criterion is obtained for  $\lambda = 0$  as

$$\text{The system is stable iff } I_K = 1 - \frac{K}{4\pi} \leq 0, \quad (\text{VII.13})$$

which does not depend on the friction. So here when the system is stable it has eigenvalues with negative real part (that will damp perturbation instead of the continuous spectrum).

Now what does the stochastic stability implies for the relaxation? The Landau damping occurs through the resonances of the dispersion relation. With friction, we have seen that since the dispersion relation is analytic in the whole plane there are no resonance but only true eigenvalues Eq. (VII.12). In the limit  $\gamma \rightarrow 0$  limit these eigenvalues converge to the resonances which means that the damping is the same that the Landau damping one. In terms of mixing for a fixed  $\lambda, \gamma$  the eigenvector  $\hat{\psi}(\eta)$  associated with a damped mode decrease as  $e^{-\eta^2/2+y\eta}$  to zero. It means that its real velocity counterpart  $\psi(v)$  is regular (Riemann-Lebesgue lemma). In the frictionless limit, we have  $\hat{\psi}(\eta) \propto e^{\lambda\eta}$  which produces a n eigenfunction much less regular and is therefore physically translated by a more important phase mixing.

### Remark VII.4

What is the behavior of the eigenvalues for large friction? In [Cha13] is studied the repulsive case where eigenvalues are a priori complex. A transition is predicted for large friction the damping does not oscillate anymore ( $\lambda \in \mathbb{R} < 0$ ). We can see it by using that [Cha13]

$$1 - a d(a + x, x) \underset{x \rightarrow 0}{\sim} \frac{x}{a + a^2}, \quad \text{for fixed } a$$

which means that in the limit  $\lambda \sim \gamma$  for large  $\gamma$ , we have

$$\Lambda_1^\infty(\lambda) = 1 + \frac{K}{4\pi} \frac{1}{\lambda\gamma + \lambda^2} \quad (\text{VII.14})$$

with solution

$$\lambda = -\frac{\gamma}{2} \sim \sqrt{\gamma^2 - \frac{K}{4\pi}} \quad (\text{VII.15})$$

It means that upon a certain level of friction the stable eigenvalue is real and that the dissipation occurs without oscillation. It corresponds in fact to the transition between an underdamped oscillator and an overdamped oscillator. Since the Magneto Optical Trap is probably in the overdamped regime all mixing (Landau damping) effects must have disappeared.

## 2.5 Adjoint problem

The adjoint equation can be obtained as in previous Chapters,

$$\mathcal{L}^\dagger g = p\partial_q g - K\phi[(f^0)'\partial_q f] - \gamma(p\partial_p g - \partial_p^2 g) \quad (\text{VII.16a})$$

$$\mathcal{L}_k^\dagger g_k = ipkg_k - ikK\phi_k[(f^0)'\partial_q f] - \gamma(p\partial_p g_k - \partial_p^2 g_k) \quad (\text{VII.16b})$$

$$\widehat{\mathcal{L}}_k^\dagger \widehat{g}_k = k\partial_\eta \widehat{g}_k - ikK\phi_k[(f^0)'\partial_q f]\delta(\eta) + \gamma(\partial_\eta(\eta\widehat{g}_k) - \eta^2\widehat{g}_k) \quad (\text{VII.16c})$$

Let the adjoint eigenvector be  $\tilde{\Psi} = \frac{\tilde{\psi}(p)e^{iq}}{2\pi}$

$$\partial_\eta \widehat{\psi} - \frac{\lambda^* - \gamma + \gamma\eta^2}{1 + \gamma\eta} \widehat{\psi} = \text{cst} \cdot \frac{\delta(\eta)}{1 + \gamma\eta}. \quad (\text{VII.17})$$

To get the solution we must separate the problem in several domains and seek a homogeneous solution (for  $k = 1$ ):

$$\widehat{\psi}_h(\eta) = Ce^{\eta^2/2} e^{-\eta/\gamma} (1 + \gamma\eta)^{(\lambda\gamma+1)/\gamma^2-1} \quad (\text{VII.18})$$

we know that  $\widehat{\psi}(-1/\gamma) = 0$  also that for  $w < -1/\gamma$  homogeneous solution does not admit real solution so we put the function to zero in this domain. Then combining it with the particular solution [NBS04]

$$\widehat{\psi}(\eta) = \frac{1}{(\Lambda'(\lambda))^*} e^{\eta^2/2} e^{-\eta/\gamma} (1 + \gamma\eta)^{(\lambda\gamma+1)/\gamma^2-1} (\Theta(1/\gamma + \eta) - \Theta(\eta)) \quad (\text{VII.19})$$

where we defined  $\Theta(\eta)$  as the Heaviside function and used  $\Theta'(\eta) = \delta(\eta)$ . The normalization factor will be justified in the next Section. It produces indeed a non zero solution for  $\eta \in ]-1/\gamma, 0[$ . The effect of friction is once again highlighted: it produces a cut-off to the velocity modes.

## 2.6 Dispersion relation and normalization check

To normalize the projection  $(\widehat{\psi}, \widehat{\psi}) = 1$ , we first express

$$\Lambda'(\lambda) = \frac{yK}{4\pi} (d(a, y^2) + \lambda y \partial_a d(a, y^2)) \quad (\text{VII.20})$$

with

$$\partial_a d(a, x) = x^{-a} e^x \int_0^x \ln\left(\frac{t}{x}\right) e^{-t} t^{a-1} dt = -x^{-a} e^x \int_0^x \frac{\gamma(a, t)}{t} dt. \quad (\text{VII.21})$$

On the other hand

$$\begin{aligned} (\tilde{\Psi}, \Psi) = 1 &= \frac{1}{\Lambda'(\lambda)} \frac{K}{4\pi} \int_{-y}^0 e^{-y\eta} (1 + \eta/y)^{a-1} (1 - \lambda y d(a, y^2 + y\eta)) d\eta \\ &= \frac{1}{\Lambda'(\lambda)} \frac{K}{4\pi} \left( y d(a, y^2) - \lambda y^3 e^{y^2} (y^2)^{-a} \int_{-y}^0 \frac{\gamma(a, y^2 + y\eta)}{y^2 + y\eta} d\eta \right) \\ &= \frac{1}{\Lambda'(\lambda)} \frac{K}{4\pi} \left( y d(a, y^2) - \lambda y^2 e^{y^2} (y^2)^{-a} \int_0^{y^2} \frac{\gamma(a, t)}{t} dt \right) \\ &= \frac{1}{\Lambda'(\lambda)} \Lambda'(\lambda) = 1, \end{aligned} \quad (\text{VII.22})$$

which once again links the dispersion relation and the normalization factor in a nontrivial fashion.

### 3 NONLINEAR EXPANSION

Here we perform the nonlinear analysis that will be very similar to the one in Chapter V. The main differences and difficulties are that the unstable manifold will be expressed in Fourier velocity through first order differential equation. Furthermore, the asymptotic regimes in  $\lambda, \gamma$  will require nontrivial integral estimations.

Since the symmetry  $O(2)$  holds for the Vlasov-Fokker-Planck equation with a Gaussian initial distribution  $f^0(p)$  the unstable manifold is of dimension two with one real eigenvalue and we can decompose  $f$  on the unstable manifold  $W^u$  as

$$f = A\Psi + \text{c.c.} + H(A, A^*).$$

The rotational symmetry insures that the form of  $H$  is still constrained by Eq. (V.37), moreover we can still expand the Fourier coefficient of  $H$  in series of  $|A|^2$  and get

$$\dot{A} = \lambda A + (\tilde{\Psi}, Nf) = \lambda A + c_3|A|^2 A + O(|A|^5 A). \quad (\text{VII.23})$$

The nonlinear terms have formally the same expression as before

$$\mathcal{N}_0[f] = -K \sum_l i l \phi[f]_{-l} \partial_v f_l = |A|^2 i K (\phi_1[\Psi] \partial_v \psi^* - \phi_{-1}[\Psi^*] \partial_v \psi) + O(|A|^4) \quad (\text{VII.24a})$$

$$\mathcal{N}_1[f] = K \sum_l i(1-l) \phi[f]_{1-l} \partial_v f_l = A|A|^2 i K (\phi_1[\Psi] \partial_v h_{0,0} - \phi_{-1}[\Psi^*] \partial_v h_{2,0}) + O(A|A|^4) \quad (\text{VII.24b})$$

$$\mathcal{N}_2[f] = K \sum_l i(2-l) \phi[f]_{2-l} \partial_v f_l = A^2 i K \phi_1[\Psi] \partial_v \psi + O(A^4). \quad (\text{VII.24c})$$

From Eq. (VII.24b) we deduce that the expression of the cubic coefficient is formally the same that in the frictionless case Eq. (V.49),

$$c_3(\lambda, \gamma) = -iK\pi\sqrt{2\pi} \left\langle \tilde{\psi}, \partial_p (h_{0,0} - h_{2,0}) \right\rangle = c_3^{(h_0)} + c_3^{(h_2)} \quad (\text{VII.25})$$

where we separated the contribution from the zeroth and second harmonic.

We will derive the expressions of  $h_{0,0}$  and  $h_{2,0}$  with the same method than in frictionless case. Formally we still have (since  $\lambda$  is real in the attractive case)

$$(2\lambda - \mathcal{L}_0)h_0 = \mathcal{N}_0[f] \quad (\text{VII.26a})$$

$$(2\lambda - \mathcal{L}_2)h_2 = \mathcal{N}_2[f], \quad (\text{VII.26b})$$

but here the linear operator  $\mathcal{L}_0 \neq 0$  and we only know the Fourier velocity expression of  $\psi$  which forces us to solve a differential problem

$$\partial_\eta \hat{h}_{0,0} + \frac{2\lambda + \gamma\eta^2}{\gamma\eta} \hat{h}_{0,0} = -\pi \frac{K}{2} \sqrt{2\pi} (\hat{\psi}^* - \hat{\psi}) / \gamma, \quad (\text{VII.27a})$$

$$\partial_\eta \hat{h}_{2,0} + \frac{2\lambda + \gamma\eta^2}{2 + \gamma\eta} \hat{h}_{2,0} = -\pi \frac{K}{2} \sqrt{2\pi} \frac{\eta}{2 + \gamma\eta} \hat{\psi}. \quad (\text{VII.27b})$$

**Remark VII.5**

At first sight the perspective of Fourier velocity computation transform back in real velocity space is not enjoyable at all, but thanks to the Parseval theorem claiming that the Fourier transform is an isometry, the result of the projection (scalar product) will be the same expressed in real or Fourier space,

$$\begin{aligned} \langle \widehat{g}^*(p), f(p) \rangle &= \int g^*(p) f(p) dp = (2\pi)^{-1} \int \left( \int \widehat{g}(\eta) e^{-ip\eta} d\eta' \right)^* \left( \int \widehat{f}(\eta') e^{-ip\eta'} d\eta' \right) dp \\ &= \iint \widehat{g}^*(\eta) \widehat{f}(\eta') \delta(\eta - \eta') d\eta' d\eta = \int \widehat{g}^*(\eta) \widehat{f}(\eta) d\eta. \end{aligned} \quad (\text{VII.28})$$

It is really one of the big advantage of the unstable manifold expansion with its geometrical interpretation, that allows to express the problem in the most convenient basis and still have formally the same quantities to compute. For example, in [BM17a] we express the problem in another basis, the Bargman one but the quantity  $c_3$  is exactly the same in both cases. The Fourier velocity uses integrals while the Bargman representation uses series. In the way, we automatically prove some integral/series equalities.

### 3.1 Cubic coefficient

As in the frictionless case there are two terms to estimate one with  $h_{0,0}$  and one with  $h_{2,0}$ . We will compute the divergence induced by the first term and recover the Crawford one in the frictionless limit. The  $h_{2,0}$  term for  $\gamma = 0$  does not produce any divergence and as shown in Appendix C.2.

**Remark VII.6**

With a more generic potential there would be a third term, easier to compute, that produces a divergence like  $\lambda^{-1}$  for  $\lambda \ll \gamma^{1/3}$  and  $\lambda\gamma^{-2/3}$  for  $\lambda \gg \gamma^{1/3}$ . As we will see this singularity is always weaker than the one produced by the zeroth Fourier term  $h_{0,0}$ .

We seek a particular solution of Eq. (VII.27a)

$$\begin{aligned} \widehat{h}_{0,0}(\eta) &= -\pi \frac{K}{2} \sqrt{2\pi} y e^{-\eta^2/2} \eta^{-2\lambda y} \int_0^\eta e^{t^2/2} t^{2\lambda y} \left( \widehat{\psi}^*(-t) - \widehat{\psi}(t) \right) dt \\ &= \sqrt{2\pi} \frac{K^2}{8} \lambda y^2 e^{-\eta^2/2} \eta^{-2\lambda y} \int_0^\eta t^{2\lambda y} \left( d(a, y^2 - yt) - d(a, y^2 + yt) \right) dt, \end{aligned} \quad (\text{VII.29})$$

so

$$\begin{aligned} c_3^{(h_0)} &= -i\pi K \sqrt{2\pi} (\tilde{\psi}, \partial_p h_{0,0}) = -\pi \frac{K}{2} \sqrt{2\pi} \int \eta \widehat{\psi}^*(\eta) \widehat{h}_{0,0} d\eta \\ &= \frac{\pi^2 K^3}{4\Lambda'(\lambda)} \lambda y^2 \int_{-y}^0 \eta^{1-2\lambda y} (1 + \eta/y)^{a-1} e^{-y\eta} \int_0^\eta t^{2\lambda y} \left( d(a^*, y^2 - yt) - d(a, y^2 + yt) \right) dt d\eta. \end{aligned} \quad (\text{VII.30})$$

The difficulty lies in estimating the asymptotic behavior of this integral. In this Section, we will not present further computations to only highlight the results and leave details for the Appendix C.1. The  $h_{0,0}$  term gives the main contribution to the cubic coefficient. We get in the limit of small instability  $\lambda$  and friction  $\gamma$ , three different regimes,

- i)  $\gamma^{1/3} \ll \lambda$ ,
- ii)  $\gamma^{4/3} \ll \lambda \ll \gamma^{1/3}$ ,
- iii)  $\lambda \ll \gamma^{4/3}$ .

The asymptotic expansion gives for the cubic coefficient

$$c_3 \sim c_3^{(h_0)} \sim \begin{cases} -\pi^2 K^2 / 4 \cdot \lambda^{-3}, & \gamma^{1/3} \ll \lambda \\ -|\text{cst}| \cdot \gamma^{-4/3}, & \gamma^{4/3} \ll \lambda \ll \gamma^{1/3} \\ -|\text{cst}| \cdot O(1), & \lambda \ll \gamma^{4/3}. \end{cases} \quad (\text{VII.31})$$

In regime i) (Vlasov regime) we recover exactly Eq. (V.54) (with  $K = 1$ ). This yields the saturation scaling

$$A_{\text{sat}} \sim \begin{cases} \lambda^2, & \gamma^{1/3} \ll \lambda \\ \gamma^{2/3}, & \gamma^{4/3} \ll \lambda \ll \gamma^{1/3} \\ \lambda^{1/2}, & \lambda \ll \gamma^{4/3}. \end{cases} \quad (\text{VII.32})$$

We indeed recover both trapping and Hopf scaling for small and large friction as well as an intermediate regime. This result is summarized on figure VII.1. We discuss the different regimes in the next Sections.

### Remark VII.7

Once again in the unstable case, the friction acts as a cut-off for divergences: high velocity modes  $\eta$  that were responsible for the pinching singularities are now suppressed at some level  $1/\gamma$ .

## 3.2 Higher order terms

---

The natural step after estimating the cubic term is to check the scaling of higher order terms. Unfortunately, the full consideration of all the different terms have not been done yet (it is quite intricate). Preliminary computations tend to show that

$$\text{i) } O(c_5 |A_{\text{sat}}|^5) = O(c_3 |A_{\text{sat}}|^3), \quad \gamma^{1/3} \ll \lambda \quad (\text{VII.33a})$$

$$\text{ii), iii) } O(c_5 |A_{\text{sat}}|^5) \ll O(c_3 |A_{\text{sat}}|^3), \quad \lambda \ll \gamma^{1/3} \quad (\text{VII.33b})$$

Hence in regime i) where we had the trapping scaling the truncation is not possible while it seems possible to do so in regimes ii) and iii). Therefore, we can conjecture is that in region ii), iii) a local dimensional reduction of the bifurcation is possible and thus would describe well the saturation. In particular, we should expect the characteristic trapping oscillations (see Figure V.6) only in the regime i). A numerical simulation could check that there are no oscillations for  $\lambda \ll \gamma^{1/3}$ . Unfortunately, I do not have a Vlasov-Fokker-Planck solver. A molecular dynamics code could be used but would require a very precise integration scheme and a large particles number.

### 3.3 Critical layers

How to interpret the three different regimes of friction, i), ii), iii) in terms of critical layer?

So far, we have abusively use the term friction to talk about friction AND dissipation. Here we distinguish the two. We denote  $\Delta p$  the typical scale of the critical layer (CL) size in velocity (in space it is of order  $2\pi$ ). The different time scales of the problem are

$$\tau_{\text{dyn}} \sim \lambda^{-1} \quad \text{Dynamical time} \quad (\text{VII.34a})$$

$$\tau_{\gamma} \sim \gamma^{-1} \quad \text{Viscous time} \quad (\text{VII.34b})$$

$$\tau_{\text{NL}} \sim A_{\text{sat}}^{-1/2} \quad \text{Nonlinear time (see Eq. (V.58))} \quad (\text{VII.34c})$$

$$\tau_a \sim \Delta p^{-1} \quad \text{typical time for phase mixing inside the CL} \quad (\text{VII.34d})$$

$$\tau_{\text{diss}} \sim \gamma^{-1} \Delta p^{-2} \quad \text{Dissipation time} \quad (\text{VII.34e})$$

where  $\tau_{\text{diss}}$  was estimated from the dissipation term  $\gamma \partial_p^2 f$ . The friction time scale is always larger than the dissipation timescale thus we shall leave it aside.

Comparing timescales with the advection terms yields the different possible CL

$$\Delta p_{\text{dyn}} \sim \lambda; \quad \Delta p_{\text{diss}} \sim \gamma^{1/3}; \quad \Delta p_{\text{NL}} \sim A^{1/2} \quad (\text{VII.35})$$

- If  $\Delta p_{\text{dyn}} \gg \Delta p_{\text{diss}}$  ( $\lambda \gg \gamma^{1/3}$ ) the dissipation is negligible. Then saturation with the nonlinear term force  $\Delta p_{\text{dyn}} \sim \Delta p_{\text{NL}}$ . Thus  $A_{\text{sat}} \sim \lambda^2$ . So, we indeed expect Vlasov regime for  $\lambda \gg \gamma^{1/3}$ .
- If  $\Delta p_{\text{dyn}} \ll \Delta p_{\text{diss}}$  the CL is viscous. Saturation with the nonlinear terms force  $\Delta p_{\text{diss}} \sim \Delta p_{\text{NL}}$ . Thus  $A_{\text{sat}} \sim \gamma^{2/3}$ . However, this regime is relevant only if  $A_{\text{sat}} \leq \lambda^{1/2}$  (standard scaling for dissipative systems). So, we recover that the intermediate regime yields for  $\gamma^{4/3} \ll \lambda \ll \gamma^{1/3}$ .
- The dissipative (third regime) regime is thus  $A_{\text{sat}} \leq \lambda^{1/2}$  for  $\lambda \ll \gamma^{4/3}$ .

This simple reasoning has the advantage to simply predict all our unstable manifold results (both scaling and regimes) with some qualitative picture on the different critical layers.

## 4 CONCLUSION AND CONJECTURES

We provide here some concluding remarks, and make some conjectures to go beyond the results obtained.

1. In regime i), we recover not only the trapping scaling, but also the universal  $-\pi^2 K_c^2/4$  prefactor, obtained without dissipation in [Cra95a, Cra94b].
2. Notice that in regimes i) and ii), the dominant contribution to  $c_3$  is a diverging integral; this means that large velocity modes  $\eta$ , corresponding to highly oscillating velocity profiles, provide the dominant contribution. In regime ii), the dissipation  $\gamma$  plays a role in the cut-off, contrary to regime i) where the cut-off is not strong enough. In regime iii), there is no more divergence.
3. It is interesting to compare more precisely with the literature on weakly unstable 2D shear flows. In [CS95, CS87, CS96], the regimes i)  $c_3 \propto \lambda^{-3}$  and ii)  $c_3 \propto \lambda \gamma^{-4/3}$  also appear. However, the regime iii)  $c_3 = O(1)$  is different, and the boundary between

regimes ii) and iii) is different too. A possible explanation is that when the dissipative time scale is shorter than the linear instability time scale (i.e.  $\lambda \ll \gamma$ ), it is necessary to add an external force to maintain the background shear flow. By contrast, maintaining the Gaussian velocity distribution in the present Vlasov-Fokker-Planck setting does not require any extra force, since it is stationary for the dissipation operator.

4. The  $\lambda \sim \gamma^{1/3}$  boundary already appeared in the literature on Vlasov or 2D Euler equations: in the derivation of the Single Wave Model, taking  $\gamma \propto \lambda^3$  is the right scaling to ensure that dissipation enters in the equation at the same order as the "Vlasov terms" [GH88, dCN98b, Bal99]. This is consistent with our finding that for  $\gamma \ll \lambda^3$ , the dissipation has no effect at leading order, while for  $\gamma \gg \lambda^3$  it qualitatively modifies the problem.
5. In the pure Vlasov case, it is known that rescaling time and amplitude as  $A(t) = \lambda^2 \alpha(\lambda t)$ , all terms in the expansion in powers of  $A$  contribute at the same order to the equation for  $\alpha$  [Cra95a]; it is thus impossible to safely truncate the series to obtain a simple ordinary differential equation, which is usually understood as a manifestation of the fact that the effective dynamics close to the bifurcation is actually infinite dimensional [BMT13]. Here in regards to the first estimation of Section VII.3.2, we may conjecture that as soon as  $\gamma \gg \lambda^3$  under a rescaling  $A(t) = \gamma^{2/3} \alpha(\lambda t)$ , the series can be safely truncated, yielding an effective ordinary differential equation for the reduced dynamics.
6. It is worth noting that the bifurcation of the standard Kuramoto model [Kur75] (see Chapter VIII), which shares some similarities with Vlasov equation, does not present the same kind of divergences [Cra94a, Cra95b], and has been tackled at a rigorous mathematical level [Chi13, Die16b, FGVG16]. One may then wonder if the regimes ii) and iii) of Vlasov-Fokker-Planck equation may be also amenable to a mathematical treatment. All these conjectures go well beyond the scope of this work.

---

## BIFURCATIONS IN COUPLED OSCILLATORS SYSTEMS: THE KURAMOTO MODEL

---

In the three previous Chapters, we have studied Hamiltonian systems with or without dissipation, with long-range interactions and explored their out of equilibrium dynamics using the unstable manifold method. In finite systems, the out of equilibrium states (QSS) eventually relax to some statistical equilibrium in times  $\tau_c = O(N^\delta)$ . Is the physics of purely out of equilibrium systems different? When we started investigating the bifurcations for the Vlasov equation we became aware at some point of a model displaying a lot of similarities with a non Hamiltonian structure. It was the Kuramoto model. This model had also been studied by J.D. Crawford and had no singularities in its bifurcation expansion. The first thing we wanted to understand was what was the difference.

Hence in this Chapter we introduce the Kuramoto model for Coupled Oscillators that is purely out of equilibrium (and non Hamiltonian). The model is by itself very interesting and rich; it is used in many different fields to understand the synchronization phenomenon in a large population of oscillators which result in a nonlinear cooperative effect. The model originally introduced by Y. Kuramoto to describe circadian rhythm [Kur15]. The model is relevant for many of physical/biological/chemical/social/electrical systems such as crickets chirping in synchrony<sup>1</sup> [Wal69], crowd applause [NRV<sup>+</sup>00, XVS08], pedestrians on bridges [PTA<sup>+</sup>01, OA08], electrochemical [KZH02] and electronic [TZT<sup>+</sup>12] oscillators, laser arrays [HKO<sup>+</sup>13], metronomes [MTFH13], etc. The force of the Kuramoto model relies on its simplicity and yet universality to describe the synchronization phenomenon

As we will see this model in the  $N \rightarrow \infty$  limit displays similarities with Vlasov dynamics, like a continuous spectrum and Landau damping. However, it possesses some major differences

---

1. Characteristic of the South of France.

in its standard form<sup>2</sup> that make some "miracles" possible. In particular, an exact (i.e. non local, for any magnitude of order parameter) dimensional reduction known as the Ott-Antonsen ansatz exists while the unstable manifold expansion does not exhibit any singularities. However, this reduction does not hold if the model is slightly modified. In the final Chapter [XI](#), we will gather our thoughts on the "why" such dimensional reduction is possible or not.

This Chapter will be dedicated to review known results on the Kuramoto model and one simple extension in the light of our previous experience with the Vlasov model. We will expose different methods to solve the bifurcation toward synchronization problem, from Y. Kuramoto early calculations to the most recent mathematical results of H. Dietert through Mirollo & Strogatz, J.D. Crawford's unstable manifold computations, Ott-Antonsen ansatz and H. Chiba reduction. This Chapter also serves as an introduction for Chapter [IX](#) and [X](#) where we present our original results concerning the bifurcation analysis of the Kuramoto modified by inertia and delayed interactions.

---

## 1 HISTORICAL REVIEW

---

In nature, many system displays some rhythm, like the spikes emitted by neurons or the cricket's frequency of singing. In 1665 Dutch physicist C. Huygens (inventor of pendulum clock) - ill in bed - noticed that no matter initial conditions, the two clocks on his wall eventually synchronize. He then led several experiments to understand this phenomenon, it was the first scientific description of synchronization. What is surprising about this phenomenon is that the weak coupling (through vibration on the wall [[OM15](#)] for this example) is sufficient for full synchronization. Other examples Understanding synchronization in large populations of coupled oscillators is a question which arises in many different fields, from physics to neuroscience, chemistry, and biology, see for example the book [[PRK01](#)]. Since this synchronization phenomena seems quite universal, there must be some minimal model describing synchrony all those systems. The first idea to reach such paradigm was to describe the oscillators through their phases only and was proposed by A.T. Winfree [[Win67](#)] (see also his extraordinary book [[Win80](#)]). Therefore, for one oscillator the dynamics is only given by one equation on its phase, so the dynamics is automatically non Hamiltonian (since there is no evolution equation for its velocity) and out of equilibrium. Then Y. Kuramoto proposed an even simpler model where the interaction term that should in principle be model dependent was chosen as a sin function<sup>3</sup>. It means that it is then the first Fourier mode of a generic potential that dictates the dynamics of synchronization. It is consistent with the Vlasov investigation where the first mode is always the first one to be unstable. Such minimal model is then enough to understand qualitatively dynamics of a large number of coupled oscillators.

---

2. What we will refer as the original/standard/first order Kuramoto model.

3. The precise mechanism behind the Huygens clocks was only elucidated recently [[OM15](#)].

## 1.1 The model

The Kuramoto model, which features a sinusoidal coupling and an all-to-all interaction between oscillators, has become a paradigmatic model for synchronization, and its very rich behavior prompted an enormous number of studies. The key ingredients are for  $N$  oscillators

- Evolution of the phase  $\dot{\theta}_i = \dots$  uniquely.
- Each oscillator has its own natural frequency  $\omega_i \in ]-\infty, \infty[$ .
- A weak all-to-all coupling as  $K/N \sum_j \sin(\theta_j - \theta_i)$ .

Putting everything together leads to

$$\dot{\theta}_i = \omega_i + \frac{K}{N} \sum_j \sin(\theta_j - \theta_i) \quad (\text{VIII.1})$$

where the  $\omega_i$  are the natural frequencies of oscillators drawn according to some distribution law  $g(\omega)$ . Through a phase shift it is always possible to center the frequency distribution to zero. The dynamics is made through  $1 \times N$  coupled first order equations (where it is  $2 \times N$  for a Hamiltonian system). Kuramoto introduced an order parameter (now named after him) that measures the synchrony of the system,

$$r(t) = |r| e^{i\varphi_r(t)} = \frac{1}{N} \sum_{j=1}^N e^{i\theta_j(t)}. \quad (\text{VIII.2})$$

In fact,  $r$  is the strict equivalent to the magnetization in the HMF system. For  $r = 0$  the system is homogeneous  $\leftrightarrow$  asynchronous while for  $r \neq 0$  some partial synchrony occurs to reach perfect synchrony at  $r = 1$ .

## 1.2 Original result (Kuramoto 1975)

The Kuramoto model was proposed and "solved" by Y. Kuramoto at the same time [Kur84, Kur75]. We retrace here quickly its early computations. Since

$$\frac{K}{N} \sum_j \sin(\theta_j - \theta_i) = \frac{K}{2} (r e^{-i\theta_i} - \text{c.c.}) = -\frac{K}{2} |r| \sin(\theta_i - \varphi_r),$$

one can study only

$$\dot{\theta} = \omega + K|r| \sin \theta \quad (\text{VIII.3})$$

where the phase  $\varphi_r$  has been set to zero thanks to the rotational symmetry.

The great idea of Y. Kuramoto was to separate two populations of oscillators, one "locked" containing synchronized cluster and the other one "drifting" composed of the oscillators drifting around

$$r = r_{\text{lock}} + r_{\text{drift}}.$$

He could predict the critical coupling parameter  $K = K_c$  and the shape of the bifurcation for  $r_\infty$ . In the locked region, we have for a stationary state  $\dot{\theta} = 0$  and

$$\omega = K r_\infty \sin \theta \quad (\text{VIII.4})$$

which is only possible for  $\omega < Kr_\infty$ . It defines the limit between drifting and locked oscillators. Then he estimated the two contributions in the large  $N \rightarrow \infty$  limit with a symmetric distribution  $g(\omega) = g(-\omega)$ , self consistently as

$$r_{\text{locked}} = Kr_\infty \int_{-\pi/2}^{\pi/2} \cos^2 \theta g(Kr_\infty \sin \theta) d\theta. \quad (\text{VIII.5})$$

The drifting part is more involved:

$$r_{\text{drift}} = \int_{|\omega| > Kr_\infty} \frac{g(\omega)}{T(\omega)} \int_{-\pi}^{\pi} \frac{\cos \theta}{V_\omega(\theta)} d\theta, \quad (\text{VIII.6})$$

where  $(\theta, V_\omega(\theta))$  is the attractive periodic orbit for an oscillator with intrinsic frequency  $\omega$ , and  $T(\omega)$  is the period of this orbit. Here  $V_\omega(\theta) = \omega - Kr_\infty \sin \theta$ , so due to the symmetry the drifting part is zero  $r_{\text{drift}} = 0$ .

Near the onset of synchrony, we have  $r_\infty \ll 1$  so for regular function we can expand the  $g$  distribution

$$\begin{aligned} r_\infty = r_{\text{locked}} &= Kr_\infty \left( g(0) \int_{-\pi/2}^{\pi/2} \cos^2 \theta d\theta + \frac{(Kr_\infty)^2}{2} g''(0) \int_{-\pi/2}^{\pi/2} \sin^2 \theta \cos^2 \theta d\theta + O(r_\infty^4) \right) \\ &= Kr_\infty \left( \frac{\pi g(0)}{2} + \frac{\pi (Kr_\infty)^2}{16} g''(0) \right). \end{aligned} \quad (\text{VIII.7})$$

This only produce non zero solution for  $K > K_c = 2/(\pi g(0))$  when  $g''(0) < 0$  (unimodal function). Moreover in this case, the transition is supercritical with

$$r_\infty \sim \sqrt{\frac{16}{\pi K_c^2 g''(0)} \left( 1 - \frac{K}{K_c} \right)}. \quad (\text{VIII.8})$$

In the event that  $g''(0) > 0$ , higher order terms have to be considered and the transition is subcritical (discontinuous).

An amazing feature of the Kuramoto model is that those simple calculations predict the exact asymptotic results (with the right coefficient and stability criteria)! In figure VIII.1 we plot the exact bifurcation diagram that is in agreement with previous computations. For a Lorentzian distribution  $g''(0) < 0$  we observe a square root bifurcation  $\propto \sqrt{K - K_c^{(1)}}$ . For a bi-Lorentzian distribution Eq. (VIII.28) with  $g''(0) > 0$  the transition is indeed subcritical. We will explain later in Section VIII.3, how this plot was made.

### Remark VIII.1

If those calculations are powerful, there are self-consistent, meaning that we assume the existence of an asymptotic steady state and find it. It does not provide us with the dynamics of how such state is reached. That will be given for example with the following bifurcations techniques.

### 1.3 Large oscillator number limit (Mirollo & Strogatz, 1991)

Thanks to its resemblances with the HMF model, obtaining a kinetic equation of the Kuramoto model in the  $N \rightarrow \infty$  limit is mathematically easier than in for Coulomb like systems. In [SM91], S.H. Strogatz and R.E. Mirollo consider for the first time this coupled oscillators problem with a kinetic equation, studying its linear stability. The evolution equation that we call here the Kuramoto equation is for the one particle density distribution  $f(\theta, \omega, t)$ ,

$$\partial_t F + \omega \partial_\theta F + \frac{K}{2i} \partial_\theta \left( (r_1[F] e^{-i\theta} - r_{-1}[F] e^{i\theta}) F \right) = 0 \quad (\text{VIII.9a})$$

$$r_k[F] = \int F(\theta, \omega, t) e^{ik\theta} d\omega d\theta, \quad (\text{VIII.9b})$$

$$\int F(\theta, \omega, t) d\theta = g(\omega), \quad (\text{VIII.9c})$$

$$\int g(\omega) d\omega = 1. \quad (\text{VIII.9d})$$

As before for the linear and nonlinear study we will need to decompose the equation around the incoherent solution  $f^0(\omega) = g(\omega)/(2\pi)$  as  $F(\theta, \omega, t) = f^0(\omega) + f(\theta, \omega, t)$ ,

$$\partial_t f = \mathcal{L} f + \mathcal{N} f \quad (\text{VIII.10a})$$

$$\mathcal{L} f = -\omega \partial_\theta f - \frac{K}{2i} \frac{g(\omega)}{2\pi} \partial_\theta (r_1[f] e^{-i\theta} - r_{-1}[f] e^{i\theta}), \quad (\text{VIII.10b})$$

$$\mathcal{N} f = -\frac{K}{2i} \partial_\theta \left( (r_1[f] e^{-i\theta} - r_{-1}[f] e^{i\theta}) f \right). \quad (\text{VIII.10c})$$

Let's list the differences and similarities between the Vlasov homogeneous kinetic system and the Kuramoto one, just looking at Eq. (VIII.9) and Eq. (VIII.10).

#### Similarities

- Same HMF interactions (thus same order parameter)
- The presence of an advection term that was previously responsible for the continuous spectrum and Landau damping. Thus, one may expect Landau damping to also occur in the Kuramoto model.
- The 0<sup>th</sup> Fourier mode of the linear operator  $\mathcal{L}_0 = 0$ . In Vlasov equation this was linked directly with the infinite number of possible stationary states. Here it also means that any distribution  $g(\omega)$  (regular enough) is steady state solution. Thus  $\lambda = 0$  is an eigenvalue with an infinite dimensional eigenspace associated. One could define Casimir invariant for this problem as

$$\mathcal{C}_s[f] = \iint s[f](\theta, \omega, t) d\theta, \quad (\text{VIII.11})$$

### Differences

- The first order dynamics induces no derivatives terms  $\partial_\omega$ , only  $\partial_\theta$ .
- The 0<sup>th</sup> Fourier mode of the linear AND nonlinear operator are zero  $\mathcal{N}_0 = \mathcal{L}_0 = 0$ . It means that the spatial Fourier mode  $f_0$  is constant in time (and even zero by normalization). An equivalent statement is given in Eq. (VIII.9c). A direct implication is that the unstable manifold that will be constructed in Section VIII.2 has no zero spatial mode  $H_0 = 0$ . Remember that in the Vlasov case this 0<sup>th</sup> harmonic was responsible of the strongest divergence in the dynamical expansion (its importance in terms of diverging coefficient is also known in fluid mechanics, see [CS87]). Therefore, if any divergence occurs we expect them to be weaker.

Hence since the linear operator is similar (up to one velocity derivative) the linear problem looks very much like the Vlasov-HMF case. The criteria derived in [SM91] holds for generic  $g(\omega)$  function. S.H. Strogatz and R.E. Mirollo also consider a Gaussian noise for the phase  $\theta$  which has for effect to add as with Vlasov-Fokker-Planck equation a  $D\partial_\theta^2 f$  operator (where  $D$  is the diffusion coefficient). In terms of spectrum this noise displaces the continuous spectrum on the left plane on  $\sigma_c = \{\lambda / \text{Re } \lambda = -D\}$

#### Remark VIII.2

If the support of  $g(\omega)$  is finite on  $[-a, a]$  so will be the continuous spectrum  $\sigma_c = \{\text{Im } \lambda \in [-a, a] \cup \text{Re } \lambda = 0\}$ . It is also true in the Vlasov case, but here we restrict to distribution with infinite support. The branch cuts in the continuous spectrum are responsible for other effects as in the non homogeneous case.

## 2 CRAWFORD APPROACH (1993)

---

At this point the linear analysis had been done, it remained to deal with the nonlinear dynamical analysis of the bifurcation with generic  $g$  distribution. Historically at the same time as his paper on the homogeneous Vlasov equation J.D. Crawford performed his unstable calculation for the Kuramoto equation. Its results confirmed the finding of Y. Kuramoto. On this subject a very well written paper by S.H. Strogatz [Str00] (that could serve as a nice introduction to this PhD thesis) highlights the crucial contribution of J.D. Crawford on the topics.

Since the method is very similar to the previous cases we will only gather the most important steps here.

The  $\mathcal{O}(2)$  symmetry predicts as in homogeneous Vlasov, that if  $g$  is even with each eigenvalues  $\lambda$  associated with an eigenspace of dimension two. If  $g$  is not even, there is only the  $\mathcal{SO}(2)$  rotational symmetry and the eigenvalues have an associated eigenspace of dimension one.

$$\Psi_1(\theta, \omega) = \psi_1(\omega) e^{i\theta} = \frac{K}{2} \frac{g(\omega)}{\lambda + i\omega} e^{i\theta} \quad (\text{VIII.12a})$$

$$\tilde{\Psi}_1(\theta, \omega) = \tilde{\psi}_1(\omega) \frac{e^{i\theta}}{2\pi} = \frac{1}{\Lambda_1'(\lambda)} \frac{1}{\lambda^* - i\omega} \frac{e^{i\theta}}{2\pi} \quad (\text{VIII.12b})$$

$$\Lambda_1(\lambda) = 1 - \frac{K}{2} \int \frac{g(\omega)}{\lambda + i\omega} d\omega \quad (\text{VIII.12c})$$

with once again  $(\tilde{\Psi}_1, \Psi_1) = 1$  and  $\int \psi_1 d\omega = 1$  For the nonlinear problem, we have

$$\mathcal{N}_1[f] = 0 \quad (\text{VIII.13a})$$

$$\mathcal{N}_1[f] = -|A|^2 A \frac{K}{2} \left( r_1[\Psi_1^*] h_{2,0} - A r_{-1}[\Psi_1] \underbrace{H_0}_{=0} + O(|A|^2) \right) \quad (\text{VIII.13b})$$

$$\mathcal{N}_2[f] = K (A^2 r_{-1}[\Psi_1] \psi + O(|A|^2)) \quad (\text{VIII.13c})$$

so

$$\dot{A} = \lambda A + \left\langle \tilde{\psi}_1, \mathcal{N}_1[f_t] \right\rangle = \lambda A - \underbrace{2\pi \frac{K}{2} \left\langle \tilde{\psi}_1, h_{2,0} \right\rangle}_{c_3} |A|^2 A + O(|A|^4 A) \quad (\text{VIII.14})$$

Since we can compute

$$h_{2,0}(0) = \frac{\pi K^2}{2} \frac{g(\omega)}{(\lambda + i\omega)^2} \quad (\text{VIII.15})$$

we are left with

$$\begin{aligned} c_3 &= -\frac{\pi^2 K^3}{2} \frac{1}{\Lambda'(\lambda)} \int \frac{g(\omega)}{(\lambda + i\omega)^3} d\omega \\ &= \frac{\pi^2 K^2}{2} \frac{\Lambda''(\lambda)}{\Lambda'(\lambda)}. \end{aligned} \quad (\text{VIII.16})$$

Since we want to deal with an unstable manifold of dimension two let's either assume that  $g$  is even and  $\lambda$  real (which is not automatic, for example bi-Lorentzian distributions exhibit a threshold upon which a real eigenvalue becomes complex.) or  $\lambda$  complex and  $g$  not even.

Here let's assume that  $\lambda$  is real, let's perform the  $\lambda \rightarrow 0$  limit in  $c_3$ . Thanks to integration by part and Plemej formula we obtain

$$c_3(0) = \frac{\pi^3 K_c^2}{4} \frac{g''(0)}{-\text{PV} \int (g'(\omega)/\omega) d\omega} \stackrel{g=g_L}{=} \frac{\pi^3 K_c^2}{4} g''(0). \quad (\text{VIII.17})$$

If we go back to the  $r$  variable with  $r \sim 2\pi A$

$$\dot{r} = \lambda r + \frac{\pi K_c^2}{16} g''(0) |r|^2 r + O(|r|^4 r) \quad (\text{VIII.18})$$

which gives

$$r_\infty \sim \sqrt{\frac{-16\lambda}{\pi K_c^2 g''(0)}} = \sqrt{\frac{16}{\pi K_c^2 g''(0)} \left(1 - \frac{K}{K_c}\right)}, \quad (\text{VIII.19})$$

where we have used that for a Lorentzian distribution  $\lambda = K/K_c - 1$ . It is the original Y. Kuramoto result.

### Remark VIII.3

We notice that to be supercritical we should in principle prove that  $\Lambda''(0^+ + i\lambda_i)/\Lambda'(0^+ + i\lambda_i) < 0$  either with i)  $g$  even and  $\lambda_i = 0$  or ii)  $g$  not even and  $\lambda_i \neq 0$ . To my knowledge nobody has proved such thing or even considered this question. Indeed, in general authors are concerned with even unimodal distribution (where the demonstration is immediate). In Appendix D.3, we prove in the i) case that this is true for bimodal distribution (in particular it says that when  $g$  is even and bimodal, eigenvalues are real iff  $\Lambda''(0) > 0$ ). But the demonstration still resists for more generic functions.

So in this Kuramoto example despite the presence of a continuous spectrum, the cubic coefficient is non singular! Giving rise to a standard "Hopf" scaling as in dissipative systems, while the relaxation process in stable case is still pure Landau damping.

Do the higher orders terms possess some divergences? The answer is no for the standard Kuramoto case, see a generic demonstration given in [Cra95a]. Hence if the higher orders coefficients are regular then, we have close to the bifurcation  $\lambda_r \ll 1$  at saturation,

$$O(\lambda|A|_\infty) = O(c_3|A|_\infty^3) \gg O(c_{2n+1}|A|_\infty^{2n+1}). \quad (\text{VIII.20})$$

Therefore, we expect<sup>4</sup> the one dimensional description Eq. (VIII.18) of the infinite dimensional original system to be accurate for the supercritical bifurcation.

At this point the natural question is "Why does it work here and not with Vlasov"? Is it uniquely linked with the presence of diverging coefficients? What makes a coefficient to diverge or not? Why in the unstable case the continuous spectrum does not seem to play a role? Is there some kind of Single Wave Model associated with trapping of particles ? In [BS00] the authors start a SWM approach for the Kuramoto model, but it seems that they do not pursue further.

### 3 OTT-ANTONSEN ANSATZ (2008)

---

In 2008 while the Kuramoto field was already quite big, with many extension and methods to study them; the "game" was shaken by an astonishing discovery of E. Ott and T.M. Antonsen [OA08] which could be the dream of every theoretical physicist: the discovery of an explicit class of solution to a full partial differential equation... This new solution lead to a large number of papers<sup>5</sup> using this Ott-Antonsen ansatz (OA ansatz). The force of their ansatz is to reduce exactly the dimension of the bifurcation problem in a certain case globally. Here globally is opposed to locally and means that the analysis holds for any  $r$ . In this Section, we will discuss this ansatz.

#### 3.1 The ansatz

---

Let's decompose the real distribution function in its Fourier expansion

$$F(\theta, \omega, t) = \frac{g(\omega)}{2\pi} \left( 1 + \sum_{k>0} (\alpha_k(\omega, t)e^{ik\theta} + c.c.) \right). \quad (\text{VIII.21})$$

We now restrict the dynamics to Fourier modes that satisfies the following ansatz

$$\alpha_k(\omega, t) = \alpha^k(\omega, t), \quad (\text{VIII.22})$$

where  $|\alpha| < 1$  to ensure the convergence of the series. Inserting this in the Kuramoto equation Eq. (VIII.9c) gives after a factorization by  $\alpha^k$  the same equation to satisfy for each Fourier mode:

$$\partial_t \alpha + i\omega \alpha + \frac{K}{2} (\alpha^2 r^* - r) = 0 \quad (\text{VIII.23a})$$

$$r^*(t) = \int \alpha(\omega, t) g(\omega) d\omega. \quad (\text{VIII.23b})$$

---

4. Of course it is not a mathematical theorem saying that this unstable manifold is attractive, but a formal result.  
 5. 372 citations in less than ten years which is quite big for this field I guess.

This equation is still infinite dimensional but less "complex" since we only have to deal with one Fourier coefficient. For example, we have a simple expression for the total distribution function

$$F(\theta, \omega, t) = \frac{g(\omega)}{2\pi} \left( 1 + \left( \frac{\alpha_k(\omega, t)e^{ik\theta}}{1 - \alpha_k(\omega, t)e^{ik\theta}} + \text{c.c.} \right) \right). \quad (\text{VIII.24})$$

One could find some similarities between this reduced model and the Single Wave Model Eq. (V.59).

Another miracle occurs at this step since for a Lorentzian distribution the integrals can be computed explicitly<sup>6</sup> thanks to its poles in  $i, -i$

$$g_L = \frac{\sigma}{\pi} \frac{1}{\sigma^2 + \omega^2}. \quad (\text{VIII.25})$$

For simplicity we take  $\sigma = 1$ . Thus, we have

$$r^*(t) = \int \alpha(\omega, t) g_L(\omega) d\omega = \alpha(-i, t). \quad (\text{VIII.26})$$

The price is of course to assume some analyticity of the  $\alpha(\omega, t)$  functions. So replacing with  $\omega = -i$  in Eq. (VIII.23) gives exactly

$$\dot{r} = \frac{K - K_c}{2} r - \frac{K}{2} |r|^2 r \quad (\text{VIII.27})$$

with  $K_c = 2$ . Here there is no neglected higher order terms and  $r$  does not have to be small. It means that there is an exact global dimensional reduction to the "standard" normal form. The dimension went from infinity to one (for this class a solution satisfying the ansatz Eq. (VIII.22))!

Despite that it is not the purpose to study in details all the possibilities of this ansatz let's mention that it works (with a reduction not necessarily to dimension equal one) for a variety of extensions [OA08]:

— All rational functions. For bi-Lorentzian distribution [MBS<sup>+</sup>09],

$$g_{bL} = \frac{\sigma}{2\pi} \left( \frac{1}{\sigma^2 + (\omega - \omega_0)^2} + \frac{1}{\sigma^2 + (\omega + \omega_0)^2} \right), \quad (\text{VIII.28})$$

one can reduce the system to a set of two coupled o.d.e. In particular, one can plot the exact bifurcation diagram for a Lorentzian and bi Lorentzian, see Figure VIII.1 (the equations of the red plot are not shown here the interested reader can refer to [MBS<sup>+</sup>09]).

- A forcing term
- Delayed coupling, we will come back to this in Chapter X
- Different species of oscillators with different coupling within each species.

---

6. Integrals of rational functions are particularly simple to compute with this trick.

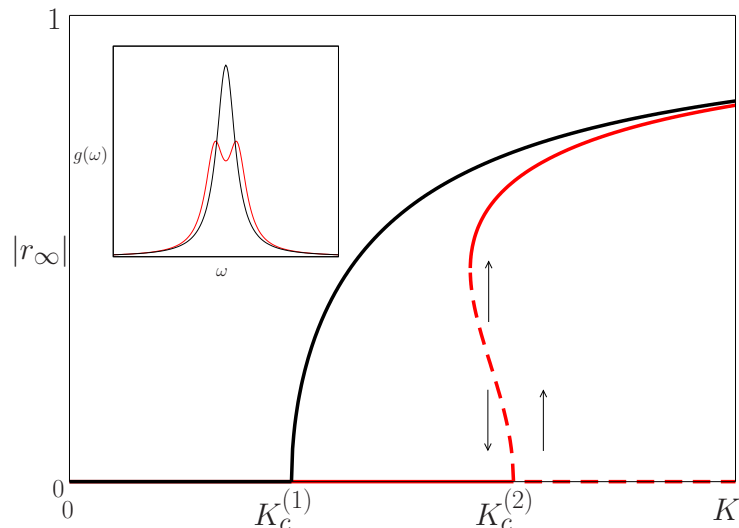


Figure VIII.1 – Bifurcation diagram for the Kuramoto order obtained via the OA ansatz. Dashed line show unstable states while solid line are stable steady states. In black the supercritical bifurcation corresponding to  $\omega_0 = 0$  in Eq. (VIII.28) (associated distribution shown in the inset). In red, the subcritical bifurcation of Eq. (VIII.28) for  $\omega_0 = 0.8$  (associated distribution shown in the inset). Associated OA ansatz for this latter case in [MBS<sup>+</sup>09].

### 3.2 Comparison between Ott-Antonsen ansatz and the Unstable manifold

Now a lot of questions arise

- Why does it work? Some papers have addressed the generality of this reduction for some extensions of the model [PR08, MMS09] as well as the analogy with the Watanabe-Strogatz ansatz [WS93].
- Is this OA manifold representing well the full dynamics? In [OA09, OHA11] the attractiveness of the ansatz for the full dynamics is shown "In particular, for distribution  $g$  with non zero spreading<sup>7</sup>, all attractors of the full system lie on the reduced manifold, and all attractors of the dynamics on the reduced manifold are attractors of the full system". It says that for regular enough distribution  $g(\omega)$  (with no zero width) a phase mixing between the different oscillators occurs so the system eventually relaxes to the OA manifold.
- The physical meaning of this reduction still for us remains unclear. How to interpret that for a Lorentzian distribution we get an exact one dimensional reduction while for a Gaussian distribution we still have an infinite integro-differential problem (still simpler than the full Kuramoto model). Is it just mathematics?
- Can it be applied to the Vlasov case (in which case most of the previous work would be useless!)?
- In the bi-Lorentzian case we know that there must exist an exact two-dimensional reduction, how with the Crawford technique could we end up with this reduction (since it matches in the supercritical case?). How the Crawford approach is local and exactly the same that the global OA reduction? What for the subcritical case where  $O(A_\infty = 1)$ ?

7. Which is always the case we study.

Are higher order terms exactly zero like with the OA ansatz?

One of the obvious limitation of the OA ansatz is that it really fully works only for rational function while techniques as Crawford's one are more generic. This point legitimates the use of such technique. How does the unstable manifold look compared to the OA ansatz? To answer this question let's write the distribution on the unstable manifold, for convenience we define before

$$\psi_1(\omega) = \frac{g(\omega)}{2\pi} \beta_{1,0}(\omega) \quad (\text{VIII.29a})$$

$$h_{1,j}(\omega) = \frac{g(\omega)}{2\pi} \beta_{1,j}(\omega) \quad j \geq 1 \quad (\text{VIII.29b})$$

$$h_{k,j}(\omega) = \frac{g(\omega)}{2\pi} \beta_{k,j}(\omega) \quad j \geq 0, k \geq 2 \quad (\text{VIII.29c})$$

$$h_{0,j} = 0 \quad \forall j \geq 0 \quad (\text{VIII.29d})$$

it gives

$$F(\theta, \omega, t) = \frac{g(\omega)}{2\pi} \left( 1 + \sum_{k>0} (A^k \beta_{k,0}(\omega, t) e^{ik\theta} + \text{c.c.}) + \sum_{j \geq 1} |A|^{2j} \sum_{k>0} (A^k \beta_{k,1}(\omega, t) e^{ik\theta} + \text{c.c.}) \right) \quad (\text{VIII.30})$$

Is there a relation between the  $\beta_{k,j}$ ? In fact, the  $\beta_{k,0}$  are for the standard Kuramoto model easy to compute, combining Eq. (V.44c) and Eq. (V.45c), we get for  $k \geq 2$ ,

$$\begin{aligned} A^k (k(\lambda + i\omega) h_{k,0} + O(|A|^2)) &= \mathcal{N}_k[f] = \frac{K}{2} k (f_{k-1} r_{-1}[f] - f_{k+1} r_{k+1} r_1[f]) \\ &= k \frac{K}{2} A^k \left( h_{k-1,0} \underbrace{r_{-1}[\Psi^*]}_{2\pi} + O(|A|^2) \right) \end{aligned} \quad (\text{VIII.31})$$

where we have used that  $\mathcal{L}_{k \neq 1} = -ik\partial_\theta$ . For  $k = 2$  see Eq. (VIII.15). Thus, by simple recurrence we get

$$\beta_{k,0} = \beta_{1,0}^k \quad (\text{VIII.32a})$$

$$\beta_{1,0} = 2\pi \frac{K}{2} \frac{1}{\lambda + i\omega} \quad (\text{VIII.32b})$$

which is the exact same structure that the OA ansatz! Therefore, the unstable manifold is at its first order expansion belonging to the OA manifold for every  $g$  distribution. What is remarkable is that at this order time is decoupled from natural frequency

$$\alpha_1(t) = A(t) \beta_1(\omega). \quad (\text{VIII.33})$$

Preliminary calculations tend to show that if we consider higher orders, this structure does not hold...

## 4 MATHEMATICAL RESULTS

Results a la Crawford although very powerful do not prove that the built unstable manifold is attractive, which means that we could miss with this technique a large panel of the dynamics. The job of mathematician in the Kuramoto field was to prove rigorously several things. Here are some results obtained

- The nonlinear Landau damping occurs which was proven in a similar spirit than for the Vlasov equation [FGVG16, Die16b]. Due to the simpler structure of the potential and of the equation there is no echo effect that was appearing in the nonlinear Vlasov Landau damping [MV11, Vil10].
- The rigorous reduction and the associated bifurcation in the supercritical case was proven with two different methods [Die16b, CN11].

The demonstration of H. Chiba [CN11] use larger functional spaces the so called "rigged Hilbert spaces". It provides a good framework to deal with the continuous spectrum. The proof of H. Dietert [Die16b] also uses a functional space where there is no continuous spectrum combined with estimates in spatial and velocity Fourier modes. Note that those results deal uniquely with regular<sup>8</sup> monotonic functions, which do not include the subcritical case when  $g''(0) < 0$ . It is to my knowledge the only mathematical theorems concerning bifurcations in a system with a continuous spectrum.

## 5 EVERYTHING FALLS APART: THE KURAMOTO-DAIDO CASE (1992)!

So far, we have only seen the standard Kuramoto case where everything worked out greatly. A suggestion of Crawford in one of his first paper on unstable manifold [Cra94b] tackles the difference in terms of singular/nonsingular coefficient  $c_3$  and Hopf/trapping scaling between the Vlasov and Kuramoto model:

*"This difference in the nonlinear behavior seems noteworthy since the linear dynamics of the model is qualitatively similar to Vlasov although apparently lacking a Hamiltonian structure"*

So is the possibility of exact dimensional reduction/rigorous mathematical results/non singular coefficients/Hopf scaling lies uniquely in the non Hamiltonian nature of the Kuramoto model?

As we will see in this simple extension of the Kuramoto model introduced and discussed by H. Daido [Dai92, Dai94, Dai96], the answer is clearly no. We will very quickly state the main result of the unstable manifold approach for the Kuramoto-Daido model.

The model is defined as

$$\dot{\theta}_i = \omega_i + \frac{K}{N} \sum_j \sin(\theta_j - \theta_i) - \frac{K}{N} \sum_j \chi \sin 2(\theta_j - \theta_i). \quad (\text{VIII.34})$$

It adds a second harmonic to the standard model, which of course can be relevant in the physics of some systems. H. Daido through a self-consistent method predicted that in general at the onset of synchronization the exponent of saturation  $A_\infty \propto \lambda^\iota$  was  $\iota = 1$  and not  $\iota = 1/2$ .

8. In [Chi13] the distribution are either Gaussian or Lorentzian while in [Die16b] they belong to the Sobolev space  $\mathcal{W}^{(n,1)}$  with  $g''(0) > 0$ .

## 5.1 Crawford result (1994)

Once again J.D. Crawford attacked the problem with the unstable manifold technique [Cra95b, CD99] confirming H. Daido's result. He computed the singularities in the coefficients of the dynamical expansion and showed how the saturation scaling was modified in general. He recovers the Daido scaling  $\iota = 1$  and also that the truncation of the dynamical expansion was impossible since every order contributes the same at the saturation level.

The linear problem is the same as before since the most unstable mode is still associated with the first Fourier mode (one can see it easily comparing the dispersion relation for the two modes). At the nonlinear level, we have minimal differences

$$\mathcal{N}_0[f] = \text{Eq. (VIII.13a)}, \quad (\text{VIII.35a})$$

$$\mathcal{N}_1[f] = -2\pi|A|^2 A \frac{K}{2} \left( h_{2,0} + \chi \psi^* \int h_{2,0} d\omega \right), \quad (\text{VIII.35b})$$

$$\mathcal{N}_2[f] = \text{Eq. (VIII.13c)}. \quad (\text{VIII.35c})$$

We can compute  $h_{2,0}$  using the resolvent Eq. (IV.23), to find

$$h_{2,0} = -\chi \psi \int h_{2,0} d\omega + \pi K \frac{\psi}{\lambda + i\omega} \quad \text{and} \quad \int h_{2,0} d\omega = \pi K \frac{\Lambda'(\lambda)}{1 + \chi}. \quad (\text{VIII.36})$$

It eventually gives for the cubic coefficient

$$c_3 = \frac{\pi^2 K^2}{2} \frac{\Lambda_1''(\lambda)}{\Lambda_1'(\lambda)} - \chi (\pi K)^2 \frac{\Lambda_1'(\lambda)}{1 + \chi} \langle \tilde{\psi}, \psi^* \rangle. \quad (\text{VIII.37})$$

As we have previously experienced this type of projection with  $\langle \tilde{\psi}, \psi^* \rangle$  displays pinching singularities. Here a simple computation shows that we have a  $1/\lambda$  singularity. Hence

$$c_3 \sim -\chi \frac{(\pi K)^3}{2\lambda} \frac{g(0)}{1 + \chi}. \quad (\text{VIII.38})$$

The sign of  $\chi$  does play an important role here: for  $\chi > 0$ , the contribution of the second harmonic has an anti-ferromagnetic effect (repulsive), and the transition is always supercritical<sup>9</sup> with a scaling

$$A_\infty \propto \lambda \quad (\text{VIII.39})$$

which recover Daido prediction. So physically this second harmonic repulsion has an effect of slowing down the synchronization growth. On the contrary if  $0 < \chi < 1$  the second harmonic has an attractive effect and the bifurcation is subcritical. For  $\chi \geq 1$  the second harmonic becomes the most unstable mode, so the unstable decomposition on the first harmonic has to be modified. A study of the population of oscillators (via self-consistent method and numerical experiments) reveals that several clusters of oscillators can be formed in presence of a second harmonic [KP13, LMLY14, KP14] and that several bifurcation branches with various stability can exist in the subcritical case. It is not captured in the Crawford analysis where we only see the onset of synchronization when varying the coupling parameter.

9. To be complete we would have to prove that  $\Lambda'(\lambda) > 0$  which is the same discussion as in VIII.3 and Appendix D.3.

## 5.2 Comparison with the Ott-Antonsen ansatz

---

When discovering this Kuramoto-Daido model which very much looks like both the Vlasov case (in terms of singularities) and Kuramoto (in terms of structure), we immediately wondered if the OA ansatz could apply or not. If it was it would open a door to dimensional reduction of infinite dimensional systems with a singular dynamical expansion like the Vlasov equation. However, it does not work. When trying the ansatz on the Kuramoto-Daido case, we end up with two equations producing inconsistencies, one for the first Fourier mode and one that can be factorized for higher Fourier modes

$$\partial_t \alpha + i\omega \alpha + \frac{K}{2} (\alpha^2 r^* - r) - \chi \frac{K}{2} (\alpha^3 r_2^* - r_2 \alpha^*) = 0 \quad k = 1 \quad (\text{VIII.40a})$$

$$\partial_t \alpha + i\omega \alpha + \frac{K}{2} (\alpha^2 r^* - r) - \chi \frac{K}{2} \left( \alpha^3 r_2^* - r_2 \frac{1}{\alpha} \right) = 0 \quad k > 1 \quad (\text{VIII.40b})$$

$$r^*(t) = \int \alpha(\omega, t) g(\omega) d\omega \quad (\text{VIII.40c})$$

$$r_2^*(t) = \int \alpha^2(\omega, t) g(\omega) d\omega. \quad (\text{VIII.40d})$$

It implies

$$\alpha_{-1}(\omega, t) = \alpha^*(\omega, t) = \alpha^{-1}(\omega, t),$$

hence that  $|\alpha_1|(\omega, t) = 1$ . Which can be problem for the convergence of the series Eq. (VIII.21).

Note that the OA ansatz works partially when there is uniquely one non zero harmonic  $k$  ( $k = 1$  being the standard case). It is partial in the sense that is predictive only for the Fourier modes  $n \times k$ . For example, with only non zero  $\sin 3\theta$ , the evolution of  $r_3[f], r_6[f], \dots$  is known but not  $r_1[f], r_2[f]$ .

### Remark VIII.4

The structure  $\beta_{k,0} = \beta_{1,0}^k$  Eq. (VIII.32) a la OA ansatz for the unstable manifold Fourier coefficients  $h_{k,0}$  that was holding in the standard Kuramoto case does not hold with a second harmonic. It is thus tempting to link the OA ansatz failure to this lack of power structure in the unstable manifold. An idea we had was to use the structure of the unstable manifold to guess an ansatz on the full kinetics equation. But so far it has not worked.

## 5.3 The Chiba result (2011)

---

In [CN11] there is a tentative of a mathematical approach to the Kuramoto-Daido problem. Unfortunately, despite rigorous result with the standard Kuramoto case, it seems that in the Daido case the bifurcation analysis is not rigorous. He claims to obtain the dynamics for any coupling function:

*"The dynamics on the manifold is derived for any coupling functions. When the coupling function is  $\sin \theta$ , a bifurcation diagram conjectured by Kuramoto is rigorously obtained. When it is not  $\sin \theta$ , a new type of bifurcation phenomenon is found due to the discontinuity of the projection operator to the center subspace."*

Nevertheless, his result is interesting since he finds for the bifurcation, also a "singular" (in his case discontinuous) projection that does not produce a singularity of the type  $1/\lambda$ , but a

quadratic term that respects the  $\mathcal{SO}(2)$  symmetry

$$\dot{A} = \lambda A - \frac{\chi}{1 + \chi} C |A| A + O(|A|^2 A), \quad (\text{VIII.41})$$

for some  $C > 0$  coefficient. This equation produces the same bifurcations than the Crawford result with a super critical bifurcation with  $\iota = 1$  when  $\chi > 0$  and a subcritical one for  $-1 < \chi < 0$ . The difference is that a priori the higher orders terms will not diverge which may say that locally the reduction is exact. If the claim concerning the rigorousness of this approach as well as the method of derivation remain unclear the idea that a term like  $|A|A$  could remove and contain the singularities at every order is appealing. For Vlasov to get the trapping scaling would require a  $\sqrt{|A|}A$  term. But it would still not be enough to account for the trapping oscillations.

## 5.4 What is the difference?

---

The fundamental difference between the standard Kuramoto model and the Kuramoto-Daido model occurs at the nonlinear level for  $\mathcal{N}_1[f] = \text{Eq. (VIII.35b)}$ . With only a first harmonic,  $f_k$  is nonlinearly coupled with  $f_{k-1}, f_{k+1}$ . However, since  $f_0 = 0$  nothing couples (at every order) positive Fourier modes  $k > 0$  to negative ones  $k < 0$ . Those modes have a free transport evolution  $e^{-ikpt}$  to the "left" for  $k > 0$  and to the "right" for  $k < 0$ . With a second harmonic, the unstable mode  $f_1$  is now coupled also with  $f_3$  and  $f_{-1}$ . In the projection, a la Crawford or a la Chiba it is this negative mode that causes the singularity/discontinuity. In terms of singularities we understand that positive Fourier modes are associated with poles on (with convention of Eq. (V.55)) the upper half plane while negative modes will have their poles on the lower half plane, which eventually causes pinching singularities. For the Ott-Antonsen ansatz this negative mode is also responsible of the failure Eq. (VIII.40). In fact, in the Vlasov case since  $f_0$  is non zero it directly couples positive and negative Fourier modes independently of the presence of a second harmonic. The "proximity" of this coupling seems to produce the most important divergence. On this subject if one takes a Daido like model with a first and third harmonic  $\sin \theta - \chi \sin 3\theta$ ,  $f_1$  is not directly coupled with its opposite  $f_{-1}$  but to  $f_{-2}$ . The consequence is that the cubic coefficient  $c_3$  is nonsingular while the quintic one  $c_5 \propto \lambda^{-2}$  is. It produces a scaling with an exponent  $3/4 \geq \iota < 1$ .

In the result of H. Dietert [Die16b] this positive/negative coupling is also what would cause the failure of the estimates used for the bifurcation analysis.

Hence the standard Kuramoto model with its exact or even rigorous local dimension reduction is an exception in the sea of examples with continuous spectrum and generic coupling function.



---

## KURAMOTO MODEL WITH INERTIA

---

We have seen that in the Vlasov-HMF model (Chapter V), singularities appear in the bifurcation expansion while in the standard Kuramoto model a regular exact dimensional reduction is possible. The former model is purely Hamiltonian whereas the latter follows a first order dynamics. What would give a system interpolating the two models as two limiting cases? Would such a model display singularities only in the Vlasov limit? Or on the contrary be regular only for the standard Kuramoto limit? Or something in between? Such a model already exists and it is called the second order Kuramoto model (or Kuramoto with inertia). It is a second order model with friction  $\gamma$  and inertia  $m$ . We find that some singularities always appear in the vicinity of the bifurcation. These singularities come from the coupling with the zeroth Fourier harmonic term that unlike the original Kuramoto model is not constant in time. In the zero inertia  $m = 0$  limit we get back the standard Kuramoto case with no singularities, while in the frictionless limit  $\gamma = 0$ , we recover the Vlasov Hamiltonian Mean Field model with its characteristic trapping scaling (due to very strong nonlinear effects).

This model was not introduced to serve our questioning but for physical reasons. Inertia was added to the original Kuramoto model to describe the synchronization of a certain fireflies [Erm91], and proved later useful to model coupled Josephson junctions [WCS96, TSS05] and power grids [FNP08, ONBT14, DCB13]. Recently, an inertial model on a complex network was shown to display a new type of "explosive synchronization" [JPM<sup>+</sup>13]. It was quickly recognized [TLO97a, AS98] that inertia could turn the continuous Kuramoto transition into a discontinuous one with hysteresis. At first sight, a natural adaptation of the original clever self-consistent mean-field approach by Kuramoto [Kur75] seems to explain satisfactorily this observation [TLO97a, TLO97b] a sufficiently large inertia induces a bistable dynamical behavior of some oscillators, that translates into a hysteretic dynamics at the collective level. However, Figure IX.1 makes it clear that even a small inertia is enough to trigger a discontinuous transition: this cannot be accounted for by the bistability picture.

Many other generalizations of the standard Kuramoto model have been introduced to better fit modeling needs. Citing just a few contributions: more general coupling than the sole  $\sin \theta$ -

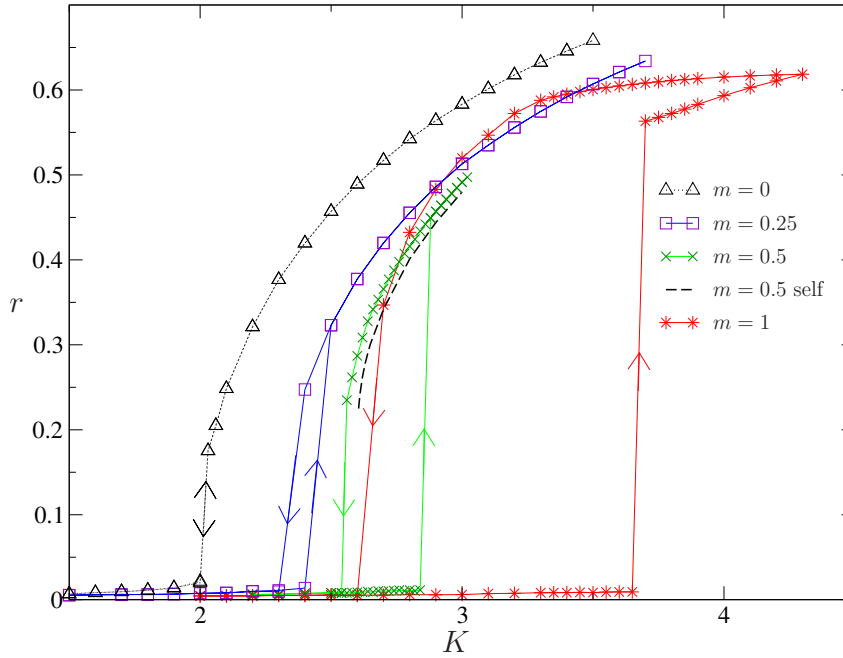


Figure IX.1 – Asymptotic order parameter  $r$  as a function of  $K$  for different  $m$  ( $\alpha = 0$ ). The arrows indicate the direction of the jumps. Without inertia, the transition is continuous, while a hysteresis appears already for small  $m$ . Note the presence of a single branch with  $r \neq 0$  for  $m = 0.25, 0.5$ , while there are two for  $m = 1$ . The dashed line is the partially synchronized solution given by the self-consistent method (see Appendix D.2) for  $m = 0.5$ . The frequency distribution is Lorentzian:  $g_\sigma(\omega) = (\sigma/\pi)/(\sigma^2 + \omega^2)$  with  $\sigma = 1$ .

harmonic [Dai92] (as we have just seen in Section VIII.5), noise [Sak88], phase shifts bringing frustration [SSK88] (that we will use here), delays [YS99, Izh98] (see the next Chapter), or a more realistic interaction topology [SSK87, HCK02].

In the Kuramoto model with inertia the only predictive approach so far was the self-consistent method a la Kuramoto (see the Chapter VIII.1.2 and Appendix D.2). This approach was studied numerically or analytically in the large friction limit [TLO97a, ONBT14]. The Ott-Antonsen ansatz fails immediately. However, in [JPRK14] a tentative is done with no true reduction a la Ott-Antonsen but with some function with fitting parameters. Thus, an unstable manifold approach was lacking to explain the "explosive" transition toward synchronization observed. It will also serve as a bridge between the Vlasov HMF and standard Kuramoto model.

In this Chapter, we prove that any non zero inertia, however small, is able to change the nature of the synchronization transition in Kuramoto-like models, either from continuous to discontinuous, **or from discontinuous to continuous** (this latter case is new to the literature to my knowledge). The bifurcation nature is given again by the sign and scaling of the cubic coefficient in the bifurcation expansion. This original result was published in [BM16]. It is obtained again through an unstable manifold expansion.

We compare our predictions with large-scale numerical simulations (molecular dynamics): using again a GPU (graphics processing unit) architecture allows us to reach a number of oscillators significantly larger than in most previous works; this is crucial to test with a reasonable precision scaling laws in the vicinity of bifurcations.

# 1 THE MODEL

Our starting point is the model introduced by Tanaka et al. [TLO97a], which adds inertia to the original Kuramoto model. It has been since then studied by many authors, often in presence of noise, and we first discuss some of the theoretical results obtained so far. [TLO97a] adapts the original self-consistent Kuramoto method to the presence of inertia, and predicts, consistently with the numerics, that a large enough inertia makes the transition discontinuous. The small inertia case was apparently not studied. In [AS98, ABS00], the authors perform a bifurcation study of the incoherent state in presence of noise, and find a critical inertia beyond which the transition should be discontinuous; their result suggests that a small inertia can make a qualitative difference, but the singular nature of the small-noise limit makes an extrapolation to zero noise difficult. We note that a full "phase diagram" compatible with [AS98, ABS00] is presented in [GCR14, SSK88] (see also [KP14]). In the following, we also add to the model in [TLO97a] a "frustration" parameter  $\alpha$ , as in [SSK88]; this will provide us with a further parameter to make testable predictions. Our resulting model is then the same as [KP14], without noise.

Each of the  $N$  oscillators in the system has a frequency  $v_i$ , with  $i \in 1, \dots, N$  and a phase  $\theta_i \in [0, 2\pi[$ ; it also has a natural frequency  $\omega_i$ , drawn from a frequency distribution  $g$ . We assume that  $g$  is even ( $g(-\omega) = g(\omega)$ ). If there is no coupling between oscillators, the actual frequency  $v_i$  tends to their natural frequency  $\omega_i$  thanks to the friction. The dynamical equations for positions and velocities are

$$\dot{\theta}_i = v_i \quad (\text{IX.1a})$$

$$m \dot{v}_i = \gamma(\omega_i - v_i) + \frac{K}{N} \sum_{j=1}^N \sin(\theta_j - \theta_i - \alpha). \quad (\text{IX.1b})$$

This is the second order Kuramoto model (also referred as Kuramoto with inertia). If the inertia  $m$  tends to 0, one recovers the usual Kuramoto model Eq. (VIII.1) (over damped dynamics). If  $\gamma = 0$ , there is no restoring force towards the natural frequency, and one obtains for  $\alpha = 0$  a Hamiltonian model with an all-to-all coupling and a cosine interaction potential, it is the HMF model Eq. (V.4). We use two rescaled parameters  $\tilde{m} = m/\gamma$ ,  $\tilde{K} = K/\gamma$  as in [BM16] instead of  $K, m, \gamma$ . The Kuramoto limit corresponds to  $\tilde{m} \rightarrow 0$ , and Vlasov limit to  $\tilde{K}, \tilde{m} \rightarrow \infty$  and  $\tilde{K}/\tilde{m} \rightarrow \text{cst}$ . Our parameters now coincide with those of [TLO97a]. Dropping the  $\tilde$  for convenience, In the  $N \rightarrow \infty$  limit, the system Eq. (IX.1) is described by a kinetic equation for the phase space density  $F(\theta, v, \omega, t)$ :

$$\partial_t F + v \partial_\theta F + \frac{K}{2im} (r_1[F] e^{-i\theta} e^{-i\alpha} - r_{-1}[F] e^{i\theta} e^{i\alpha}) \partial_v F - \frac{1}{m} \partial_v ((v - \omega)F) = 0, \quad (\text{IX.2})$$

where the  $r_k$  coefficients representing the different order parameters measuring synchrony are defined as in the first order model Eq. (VIII.9b) with an integration over the extra velocity variable.

The first step of the problem is as always to find the unsynchronized stationary solution  $f^0(v, \omega)$ . It is easy to check that

$$f^0(v, \omega) = g(\omega) \delta(v - \omega) / (2\pi) \quad (\text{IX.3})$$

is indeed a stationary solution of Eq. (IX.2). The first thing to observe is that the velocity distribution in  $v$  lives in a less regular space than usual. Actually, in presence of a Gaussian

noise the stationary solution is a Gaussian [ABS00] and its zero temperature limit coincide with Eq. (IX.3). Increasing the coupling strength  $K$ ,  $f^0$  changes from stable to unstable. Our goal is again to study the dynamics of Eq. (IX.2) in the vicinity of this bifurcation. The linear and a nonlinear decomposition, with  $F = f^0 + f$  gives

$$\partial_t f = \mathcal{L} f + \mathcal{N}[f], \quad (\text{IX.4a})$$

$$\mathcal{L} f = -v \partial_\theta f - \frac{K}{2im} (r_1[f] e^{-i\theta} e^{-i\alpha} - r_{-1}[f] e^{i\theta} e^{i\alpha}) \partial_v f^0 + \frac{1}{m} \partial_v ((v - \omega) f), \quad (\text{IX.4b})$$

$$\mathcal{N}[f] = -\frac{K}{2im} (r_1[f] e^{-i\theta} e^{-i\alpha} - r_{-1}[f] e^{i\theta} e^{i\alpha}) \partial_v f. \quad (\text{IX.4c})$$

In terms of spectrum the perturbation induced by the friction term (last term) is not bounded thus some changes in the continuous spectrum with respect to Vlasov HFM or standard Kuramoto model are possible.

## 2 LINEAR PART

---

### 2.1 Eigenvalue problem

---

Let us solve  $\mathcal{L} \Psi_k = \lambda \Psi_k$  with  $\Psi_k = \psi_k(v, \omega) e^{i\theta}$ . This yields for  $k = 1$  (we remove the index  $\psi_1 = \psi$ )

$$(\lambda + iv)\psi = \frac{1}{m} \partial_v ((v - \omega)\psi) + \frac{K}{2im} e^{i\alpha} g(\omega) \delta'(v - \omega) \int \psi \, dv \, d\omega,$$

where  $\delta'(x)$  stands for the derivative in the distribution sense of the delta Dirac distribution.

The difficult part of the inertia bifurcation problem is first to solve the eigenvalue problem which is neither like standard Kuramoto or Vlasov HMF (without friction) neither like Vlasov-Fokker-Planck (with friction and dissipation). Indeed, in this latter case the functional space was regular enough so Fourier or Bargman expansion in velocity worked well. Moreover, here we have two "velocity variables" the natural frequency  $\omega$  and the velocity  $v$ . The idea (ansatz) is to look for a solution of the form

$$\psi = U_0(\omega) \delta(v - \omega) + U_1(\omega) \delta'(v - \omega). \quad (\text{IX.5})$$

Imposing the normalization  $\int \psi \, dv \, d\omega = 1$ , one finds

$$U_0 = \frac{K}{2m} e^{i\alpha} \frac{g(\omega)}{(\lambda + i\omega)(\lambda + 1/m + i\omega)} \quad (\text{IX.6})$$

$$U_1 = \frac{K}{2im} e^{i\alpha} \frac{g(\omega)}{\lambda + 1/m + i\omega}. \quad (\text{IX.7})$$

where we used the identity  $x \delta^{(n)}(x) = -n \delta^{(n-1)}(x)$  for  $n > 1$  and  $x \delta(x) = 0$ . Expliciting the normalization condition yields the dispersion relation for  $k = \pm 1$ :

$$\Lambda_k(\lambda) = 1 - \frac{K}{2m} e^{ik\alpha} \int \frac{g(\omega)}{(\lambda + ik\omega)(\lambda + 1/m + ik\omega)} \, d\omega = 0. \quad (\text{IX.8})$$

This dispersion relation can be recovered as the noiseless limit of the one in [ABS00], as it should. One can also check that the limit  $m \rightarrow \infty$ ,  $K/m = \text{cst}$  yields the Vlasov dispersion relation<sup>1</sup> with a cosine potential and  $g(\omega)$  as stationary velocity profile  $f^0(v)$ ; the  $m \rightarrow 0$  limit yields the standard Kuramoto dispersion relation.

The effect of the friction operator modified the continuous spectrum. Looking at the singular points in the dispersion relation (or equivalently looking for generalized eigenvector), we do not find one continuous spectrum but many! One is the usual situated on the imaginary axis while the other are placed in the left plane. In fact, if we had chosen  $\psi(v, \omega) = U_n(\omega)\delta^{(n)}(v - \omega)$ , we would have found continuous spectrum on every axis  $\text{Re } \lambda = -n/m$ . Hence  $\sigma_c = \{\lambda / \text{Re } \lambda = -n/m, \forall n \geq 0\}$ . Therefore, the effect<sup>2</sup> of friction (without noise) on the linear operator Kuramoto operator is to split the continuous spectrum in an infinite number of parts situated in the left plane and thus associated with damped oscillations (excepted for  $n = 0$ ). It is interesting the look in [ABS00] at the effect of an additional noise measured by  $D$  (dispersion in velocity as for Vlasov-Fokker-Planck). It has for effect to shift all these spectra further in the left plane, in particular the spectrum in  $n = 0$  is situated in  $\text{Re } \lambda = -D$ . Hence stochastic stability like in Vlasov-Fokker-Planck, Section VII.2.3, does not occur here since the continuous spectrum still exists after the addition of friction and dissipation. Hence the additional natural frequency variable must be responsible for this change.

## 2.2 Adjoint problem

The definition of the scalar product with two frequency variables is straight forward

$$(f_1, f_2) = \int \langle f_1, f_2 \rangle d\theta = \int \int f_1^* f_2 d\omega dv d\theta. \quad (\text{IX.9})$$

The adjoint is thus

$$\mathcal{L}^\dagger q = v\partial_\theta q - \frac{1}{m}(v - \omega)\partial_v q + \frac{K}{2im} (e^{i\alpha} e^{-i\theta} r_1 [q\partial_v f^0] - e^{-i\alpha} e^{i\theta} r_{-1} [q\partial_v f^0]). \quad (\text{IX.10})$$

$\mathcal{L}^\dagger$  is also diagonal when expressed in the Fourier basis with respect to  $\theta$  we thus concentrate on

$$\tilde{\Psi}_k = \frac{\tilde{\psi}_k(v, \omega)}{2\pi} e^{ik\theta}.$$

Then for  $k = 1$

$$(\lambda^* - iv)\tilde{\psi} + \frac{1}{m}(v - \omega)\partial_v \tilde{\psi} = \frac{K}{2im} e^{-i\alpha} \int g(\omega)\partial_v \tilde{\psi}(\omega, \omega) d\omega. \quad (\text{IX.11})$$

It is not obvious how to compute  $\tilde{\psi}$  from the above equation. Nevertheless, taking  $v = \omega$ , one easily extracts  $\tilde{\psi}(\omega, \omega)$ :

$$\tilde{\psi}(\omega, \omega) = \frac{K}{2im} e^{-i\alpha} \frac{C}{\lambda^* - i\omega}$$

with  $C$  a constant to be determined by normalization: we impose  $\int \tilde{\psi}^* \psi dv d\omega = 1$ . Differentiating repeatedly Eq. (IX.11) with respect to  $v$ , and then taking  $v = \omega$ , one can compute

1. Thanks to an integration by parts.

2. Of course a rigorous spectral analysis is needed to really understand this result.

$\tilde{\psi}^{(n)}(\omega) = \partial_v^n [\tilde{\psi}](\omega, \omega)$  for any  $n$ . From Eq. (IX.5), we see that we need to compute up to  $n = 1$  in order to obtain  $C$ ; the result is

$$C = \frac{2im}{K} e^{i\alpha} \frac{1}{\Lambda'(\lambda)^*} \quad (\text{IX.12})$$

which once again links the scalar product  $\langle \tilde{\Psi}, \Psi \rangle$  to the derivative of the dispersion relation. In the following, we will need

$$\tilde{\psi}(\omega, \omega) = \frac{1}{\Lambda'(\lambda)^*} \frac{1}{\lambda^* - i\omega} \quad (\text{IX.13a})$$

$$\tilde{\psi}^{(1)}(\omega) = \frac{i}{\Lambda'(\lambda)^*} \frac{1}{(\lambda^* - i\omega)(\lambda^* - i\omega + 1/m)} \quad (\text{IX.13b})$$

$$\tilde{\psi}^{(2)}(\omega) = \frac{-2}{\Lambda'(\lambda)^*} \times \frac{1}{\prod_{l=0}^2 (\lambda^* - i\omega + l/m)} \quad (\text{IX.13c})$$

$$\tilde{\psi}^{(3)}(\omega) = \frac{-6i}{\Lambda'(\lambda)^*} \times \frac{1}{\prod_{l=0}^3 (\lambda^* - i\omega + l/m)} \quad (\text{IX.13d})$$

### 3 UNSTABLE MANIFOLD EXPANSION

In this Section, we are going to perform the unstable manifold expansion in a very similar fashion than the homogeneous Vlasov case (with or without friction/dissipation).

The dynamics Eq. (IX.2) is symmetric with respect to rotations  $\mathcal{SO}(2)$ ,  $(\theta, v, \omega) = (\theta + \varphi, v, \omega)$ ; if  $\alpha = 0$  and  $g(\omega)$  even, it is in addition symmetric with respect to reflections  $(\theta, v, \omega) = -(\theta, v, \omega)$ . To simplify a bit the calculation we choose here to take  $g$  even, and we restrict to the case of two unstable eigenvectors. This is generically the case when:

- i)  $\alpha \neq 0$ ; in this case, there is a complex unstable eigenvalue  $\lambda$ , and  $\lambda^*$  is also an unstable eigenvalue;
- ii)  $\alpha = 0$ , and  $\lambda$  is real; in this case, it is twice degenerate, associated with two eigenvectors.

Hence in both cases we will build a two-dimensional unstable manifold. We leave for future studies the cases  $\alpha = 0$ ,  $\lambda$  complex, which leads to a four-dimensional unstable manifold [Cra94a], as well as non even  $g(\omega)$  distributions. We decompose the solution on the unstable manifold as before

$$f = A\Psi + A^*\Psi^* + H[A, A^*](\theta, v, \omega). \quad (\text{IX.14})$$

with  $H = O((A, A^*)^2)$ . We expect once again by symmetry to get

$$\begin{aligned} \dot{A} &= \lambda A + c_3 |A|^2 A + O(A^5) \\ H(A, A^*) &= AA^* h_{0,0}(v, \omega) + A^2 h_{2,0}(v, \omega) e^{2i\theta} + c.c. + \dots \end{aligned} \quad (\text{IX.15})$$

where we have used the  $A \leftrightarrow -A$  and translation symmetries. From Eq. (IX.4c) we get for the Fourier components of  $\mathcal{N}[f]$ :

$$(\mathcal{N}[f])_0 = i \frac{2\pi K e^{-i\alpha}}{2m} \sigma \partial_v \psi + c.c. + O(|A|^4) \quad (\text{IX.16})$$

$$(\mathcal{N}[f])_2 = -i \frac{2\pi K e^{i\alpha}}{2m} A^2 \partial_v \psi + O(A^2 |A|^2). \quad (\text{IX.17})$$

Thus, using the time equation as in Eq. (V.44) we have to solve

$$(2\lambda_r - \mathcal{L}_0)h_{0,0} = i\frac{2\pi K e^{-i\alpha}}{2m}\partial_v\psi + \text{c.c.} \quad (\text{IX.18})$$

$$(2\lambda - \mathcal{L}_2)h_{2,0} = -i\frac{2\pi K e^{i\alpha}}{2m}\partial_v\psi. \quad (\text{IX.19})$$

where  $\mathcal{L}_0 \neq 0$  due to the friction term. The  $\mathcal{N}_1[f]$  term gives

$$\dot{A} = \lambda A + A|A|^2\frac{2\pi K}{2im}\left(e^{i\alpha}\langle\tilde{\psi}, \partial_v h_{0,0}\rangle - e^{-i\alpha}\langle\tilde{\psi}, \partial_v h_{2,0}\rangle\right) + \text{O}(A|A|^4). \quad (\text{IX.20})$$

### 3.1 Computation of $h_{0,0}$

We start from Eq. (IX.18). We have  $h_{0,0} = h + \text{c.c.}$ , where  $h$  is the solution of

$$(2\lambda_r - \mathcal{L}_0) \cdot h = i\frac{2\pi K e^{-i\alpha}}{2m}\partial_v\psi. \quad (\text{IX.21})$$

Eq. (IX.21) reads

$$2\lambda_r - \frac{1}{m}\partial_v[(v - \omega)h_{0,0}] = \frac{2\pi K^2}{4im^2}\left(\frac{g\delta'(v - \omega)}{(\lambda^* - i\omega)(\lambda^* - i\omega + 1/m)} + i\frac{g\delta''(v - \omega)}{(\lambda^* - i\omega + 1/m)}\right). \quad (\text{IX.22})$$

We introduce the ansatz:

$$h = W_0(\omega)\delta(v - \omega) + W_1(\omega)\delta'(v - \omega) + W_2(\omega)\delta''(v - \omega).$$

Using the identities

$$\begin{aligned} x\delta'(x) &= -\delta(x) \\ x\delta''(x) &= -2\delta'(x), \end{aligned}$$

we obtain

$$W_0(\omega) = 0 \quad (\text{IX.23})$$

$$W_1(\omega) = \frac{2i\pi(K/2m)^2g(\omega)}{(2\lambda_r + 1/m)(\lambda + i\omega)(\lambda + 1/m + i\omega)} \quad (\text{IX.24})$$

$$W_2(\omega) = \frac{2\pi(K/2m)^2g(\omega)}{2(\lambda_r + 1/m)(\lambda + 1/m + i\omega)}. \quad (\text{IX.25})$$

### 3.2 Computation of $h_{2,0}$

A similar computation starting from Eq. (IX.19) yields  $h_{2,0}$ . We have to solve

$$(2\lambda - \mathcal{L}_2) \cdot h_{2,0} = -i\frac{2\pi K e^{i\alpha}}{2m}\partial_v\psi. \quad (\text{IX.26})$$

Using the ansatz

$$h_{2,0} = X_0\delta(v - \omega) + X_1\delta'(v - \omega) + X_2\delta''(v - \omega),$$

we obtain

$$\begin{aligned} X_0(\omega) &= \frac{iX_1(\omega)}{(\lambda + i\omega)} \\ X_1(\omega) &= \frac{-i(2\pi K e^{i\alpha}/2m)U_0(\omega)}{(2\lambda + 2i\omega + 1/m)} + \frac{4iX_2(\omega)}{(2\lambda + 2i\omega + 1/m)} \\ X_2(\omega) &= \frac{-i(2\pi K e^{i\alpha}/2m)U_1(\omega)}{2(\lambda + i\omega + 1/m)}. \end{aligned}$$

### 3.3 Putting everything together

Inserting the expressions of  $h_{0,0}$  and  $h_{2,0}$  into Eq. (IX.20), we obtain the final reduced equation we were looking for. Let us start with the first contribution, which comes from  $\langle \tilde{\psi}, \partial_v h_{0,0} \rangle$ :

$$\begin{aligned} \langle \tilde{\psi}, \partial_v h_{0,0} \rangle &= \iint \tilde{\psi}^*(v, \omega) [(W_1(\omega) + W_1^*(\omega)) \delta^{(2)}(v - \omega) \\ &\quad + (W_2(\omega) + W_2^*(\omega)) \delta^{(3)}(v - \omega)] dv d\omega \\ &= \int \left[ \tilde{\psi}^{(2)*}(\omega) (W_1(\omega) + W_1^*(\omega)) - \tilde{\psi}^{(3)*}(\omega) (W_2(\omega) + W_2^*(\omega)) \right] d\omega. \end{aligned} \quad (\text{IX.27})$$

We have to compute the above integrals in the limit  $\lambda_r \rightarrow 0^+$ . A pole which moves to the real axis when  $\lambda_r \rightarrow 0^+$  does not create any divergence by itself (see Section V.5.4) although the integral is not well defined a priori, it can be analytically continued. However, divergences may appear through "pinching singularities", see Section V.5.4, that is when two poles approach the real axis, each on one side. From Eq. (IX.13b), Eq. (IX.13c), Eq. (IX.13d) and Eq. (IX.24), Eq. (IX.25) one sees that a pinching singularity appears only in  $\int \tilde{\psi}^{(2)*} W_1^*$ ; hence this provides the leading term:

$$\begin{aligned} \int \tilde{\psi}^{(2)*} W_1^* d\omega &= i\pi \frac{K^2}{m^2} \frac{1}{(1/m)} \frac{1}{\Lambda'(i\lambda_i)} \int \left( \frac{g(\omega)}{(\lambda_r^2 + (\omega + \lambda_i)^2)((\lambda_r + 1/m)^2 + (\omega + \lambda_i)^2)} \times \right. \\ &\quad \left. \frac{1}{(\lambda_r + 2/m + i(\omega + \lambda_i))} \right) d\omega \\ &\sim i\pi \frac{K^2}{m^2} \frac{1}{(1/m)^4} \frac{1}{\Lambda'(i\lambda_i)} \frac{\pi}{2} \frac{g(-\lambda_i)}{\lambda_r}, \end{aligned}$$

where we have used

$$\int \frac{\varphi(x)}{x^2 + \varepsilon^2} \underset{\varepsilon \rightarrow 0^+}{\sim} \pi \frac{\varphi(0)}{\varepsilon}. \quad (\text{IX.28})$$

Let us turn to the second contribution, coming from  $\langle \tilde{\psi}, \partial_v h_{2,0} \rangle$ :

$$\begin{aligned} \langle \tilde{\psi}, \partial_v h_{2,0} \rangle &= \iint \tilde{\psi}^*(v, \omega) \left[ X_0(\omega) \delta'(v - \omega) + X_1(\omega) \delta''(v - \omega) + X_2(\omega) \delta^{(3)}(v - \omega) \right] dv d\omega \\ &= \int \left[ -\tilde{\psi}^{(1)*}(\omega) X_0(\omega) + \tilde{\psi}^{(2)*}(\omega) X_1(\omega) - \tilde{\psi}^{(3)*}(\omega) X_2(\omega) \right] d\omega. \end{aligned} \quad (\text{IX.29})$$

It is not difficult to see that no pinching singularity appears, so that the above term has a finite limit when  $\lambda_r \rightarrow 0$ .

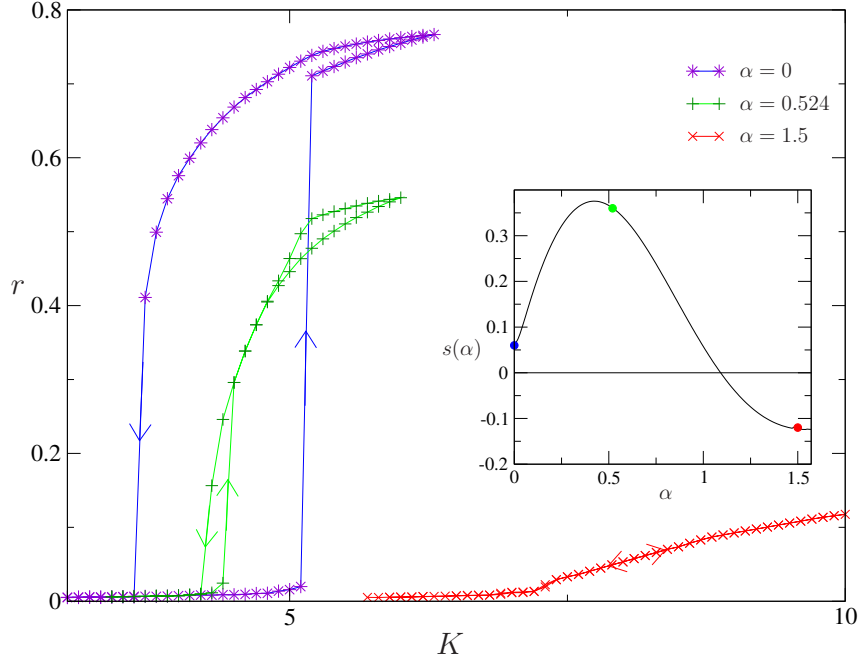


Figure IX.2 –  $r$  (computed in the asymptotic stationary state) as a function of the coupling constant  $K$  for different parameter  $\alpha$ , with  $m = 0.4$  or  $m = 0$ . Arrows indicate the direction of the jumps. The frequency distribution is a Lorentzian Eq. (VIII.25), with  $\sigma = 1$ . The bifurcation is clearly sub-critical for  $\alpha = 1.5, m = 0$ , and supercritical for  $\alpha = 1.5, m = 0.4$ ; here  $r$  is linear with  $K - K_c$  as predicted by Eq. (IX.30). The inset shows  $s(\alpha)$ , which is positive for  $\alpha = 0$  and  $0.524$  and negative for  $\alpha = 1.5$ . The value corresponding to the bifurcation is shown by a point of the same color as the graph.

We conclude that the leading behavior of  $c_3$  for  $m > 0$  is given by:

$$c_3 \sim \frac{\pi^3}{2} m K^3 \frac{e^{i\alpha}}{\Lambda'(i\lambda_i)} \frac{g(-\lambda_i)}{\lambda_r}. \quad (\text{IX.30})$$

In particular, the sign of  $s(\alpha) = \text{Re} \left( \frac{e^{i\alpha}}{\Lambda'(i\lambda_i)} \right)$  determines the type (sub- or super-critical) of the bifurcation. Our hypothesis of a two-dimensional unstable manifold ensures that  $\Lambda'(i\lambda_i) \neq 0$ .

## 4 DISCUSSION

Using the reduced dynamics Eq. (IX.15) truncated at order  $A^3$  provides essential qualitative information: i) The bifurcation is subcritical if and only if  $\text{Re}(c_3) > 0$  ii) In the supercritical case, one obtains the asymptotic order parameter  $|A|_\infty \sim \sqrt{-\lambda_r / \text{Re}(c_3)}$ . From this, the dramatic effect of the inertia  $m$  appears clearly: it introduces into  $c_3$  a contribution diverging like  $1/\lambda_r$ , which is the dominant one: the sign of  $s = \text{Re}(e^{i\alpha}/\Lambda'(i\lambda_i))$  controls the bifurcation type, sub-(resp. super) critical for  $s > 0$  (resp.  $s < 0$ ). For  $m = 0$ , the next order term, which does not diverge when  $\lambda_r \rightarrow 0$ , is needed; the bifurcation is then controlled by  $s^0 =$

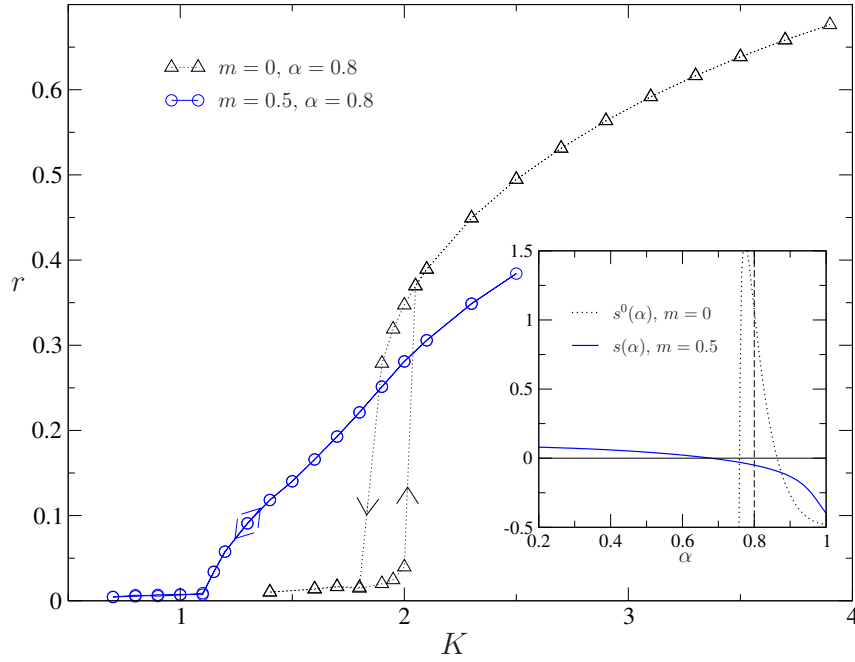


Figure IX.3 – Asymptotic  $r$  as a function of  $K$  for  $\alpha = 0.8$ , with  $m = 0$  or  $m = 0.5$ . The frequency distribution is a superposition of two Lorentzian as in [OW12], figure 3:  $g(\omega) = \tau g_1 + (1 - \tau)g_\delta$ , with  $\tau = 0.8$ ,  $\delta = 0.075$ ; note that  $g$  is unimodal. The inset shows that  $s^0(\alpha = 0.8) > 0$  (hence discontinuous transition at  $m = 0$ ), and  $s(\alpha = 0.8) < 0$  (hence continuous transition as soon as  $m > 0$ ).

$\text{Re}(\Lambda''(i\lambda_i)/\Lambda'(i\lambda_i))$ : sub-(resp. super) critical for  $s_0 > 0$  (resp.  $s_0 < 0$ ) (this generalizes to  $\alpha \neq 0$  a result of [Cra95b], see Appendix D.1.1).

Hence, any small  $m$  may either turn a supercritical bifurcation at  $m = 0$  into a subcritical one, or the other way around, turn a subcritical bifurcation at  $m = 0$  into a supercritical one. While the first direction, illustrated in Figure IX.1, was anticipated in [GCR14, KP14], the second direction is unexpected. Figure IX.3 provides an example with a unimodal  $g(\omega)$  and  $\alpha \neq 0$ . Furthermore, in the supercritical case, we predict the scaling law for the asymptotic order parameter  $|A|_\infty \propto \lambda_r$ , and this is also observed.

If the distribution  $g$  is unimodal we note that  $s(\alpha = 0) > 0$ , so the bifurcation is always subcritical. It means that for the system without frustration parameter  $\alpha = 0$ , we indeed proved that with any inertia  $m$  the bifurcation is discontinuous (we should as in the standard Kuramoto case prove that for generic symmetric  $g$  distribution  $\Lambda'(0) > 0$ , which we are able to do only for unimodal function). Finally, Eq. (VIII.16) makes clear that both the standard first order Kuramoto ( $m = 0, \alpha = 0$ ) and Vlasov ( $m = \infty, K/m = \text{cst}$ , see Appendix D.1.2) limits are singular. In the first case, the divergent term vanishes, and the bifurcation is controlled by the sign of  $s^0$ . One recovers the already known results: for a symmetric unimodal  $g$ ,  $s^0(\alpha = 0) < 0$  and the bifurcation is supercritical, with standard scaling  $|A|_\infty \propto \sqrt{\lambda_r}$ . In the second case, Eq. (VIII.16) diverges when  $m, K \rightarrow \infty$ . Redoing the computations in this limit indeed yields (for  $\alpha = 0$ )  $c_3 \propto -\frac{1}{\lambda_r^3}$ , as found in [Cra95a]. This leads to the trapping scaling  $|A|_\infty \propto \lambda_r^2$ .

## 4.1 Numerics

We present in this Section precise numerical simulations that fully support the above analysis. The Kuramoto codes (with and without inertia) were constructed by myself. The time-evolved system is obtained via GPU parallel implementation of a Runge-Kunta 4 scheme for the equations Eq. (IX.1) [GCR14]. The order parameter is computed by its standard discrete definition [Kur75]. For every simulation, we take  $N = 65536$ , and a time step  $\Delta t = 10^{-3}$ . The asymptotic order parameter  $r$  is the average of  $|r_1|(t)$  for  $t \in [1500, 2000]$ . In order to test our prediction on the type of bifurcation, we start from an unsynchronized state (drawing positions  $\theta_i$  uniformly on a unit circle). The  $\omega_i$  are sampled according to  $g$ , the initial velocities are  $v_i = \omega_i$ . We let the system evolve until  $t = 2000$  and measure the averaged order parameter. Then we vary the coupling constant  $K \rightarrow K + \Delta K$  with  $\Delta K = 0.1$  or  $0.2$  (or smaller close to transitions) and reiterate the procedure; at some point the bifurcation towards synchronization is observed. When  $K$  is large enough we apply the same procedure in the other direction,  $K \rightarrow K - \Delta K$ . Thus, we are able to distinguish clearly a subcritical bifurcation (with a characteristic hysteresis cycle) from a supercritical bifurcation (with no hysteresis). In figure IX.1, we see how the hysteretic cycle depends on the inertia  $m$ . For  $m = 1$ , there are two branches with  $r \neq 0$ : these correspond to the bistable behavior of the single oscillator dynamics in a range of  $\omega$ , see [TLO97a]; for  $m = 0.5$  and  $m = 0.25$ , the single oscillator dynamics is not bistable in the transition region, and, accordingly, there is only one branch with  $r \neq 0$ . The bifurcation remains nevertheless clearly subcritical. Tests varying  $\alpha$  are reported on figure IX.2: we see that the singular term Eq. (VIII.16) again correctly predicts the type of bifurcation (continuous vs discontinuous), as well as the scaling of the saturated state in the continuous case. In figure IX.3 and IX.2, inertia induces a supercritical transition; Eq. (VIII.16) also correctly predicts the linear scaling of the saturated state in this case. Finally, we note that in the subcritical regime, the numerically observed  $K_c$  is sometimes lower than the prediction Eq. (IX.2); this is presumably related to strong finite size effects [HCPT07], especially in presence of inertia [ONBT14].

In conclusion, we have once again successfully constructed an unstable manifold expansion for models of synchronization with inertia and frustration, circumventing the problem of the continuous spectrum on the imaginary axis. The singularities appearing in the expansion control the system's behavior in the vicinity of the bifurcation, and allow useful qualitative and quantitative predictions. In particular, while synchronization models tend to present complicated phase diagrams for which it is difficult to develop an intuition [OW12, KP14], we obtain simple criteria determining the character of the transition. We were also thanks to the cubic coefficient able to predict a case where inertia turns a subcritical bifurcation into a supercritical one, which is new to the literature.

However, to be complete we should look at the higher order terms to check that as previous cases with singular coefficients they produce same order terms when there is saturation ( $\text{Re } c_3 < 0$ ). A surprising result would be that they produce negligible terms at saturation which could be a sign that rigorous dimensional reduction is possible. The bad case would be that those higher order terms are of lower order, which would invalidate this result.

Regarding the guiding thread of this thesis, that is to say the singularities in the unstable manifold expansion, we have also confirmed some ideas. The presence of the zeroth harmonic  $H_0 = |A|^2 h_0$  is crucial to qualitative behavior of the bifurcation. As soon as it is non zero (for  $m \neq 0$ ) it produces a dominating contribution  $\propto 1/\lambda_r$  in the bifurcation expansion. Nevertheless, here its effect is weaker than in the Vlasov case, which is probably due to the friction  $\gamma$ . Indeed, compared to the Vlasov-HMF case we have here  $\mathcal{L}_0 \neq 0$  and a split continuous

spectrum which might weaken the resonance phenomena. To get more insight on what is really happening a development a la Single Wave Model [BS00, BMT13] for the Kuramoto would be very useful. However even consideration in terms of critical layers are not simple in Kuramoto like model since an extra variable  $\omega$  is present.

---

## KURAMOTO MODEL WITH DELAY

---

This Chapter is dedicated to the study of both first and second order Kuramoto model with delayed interaction. The Kuramoto model with delayed interaction was introduced in [Izh98] and studied first in [YS99] by M.K.S. Yeung and S.H. Strogatz (see [CKKH00] for a self-consistent and numerical study). The physical motivation for this model is clear: interactions such as two crickets hearing each other is not instantaneous and always slower than the speed of light. Of course, such example might seem a bit irrelevant but delay could become non-negligible in some electrical network like power grid systems [LC04] or coupled neuron systems [DJM<sup>+</sup>09, DJM<sup>+</sup>09, NUS13, ST15]. Hence what is the effect of delay on the bifurcation in Kuramoto models? Another challenge is to recover the bifurcation diagram of [YS99] Figure 4 which predicts sub/super-critical bifurcation for a varying delay (in what seems to be a periodic pattern). Providing a cubic coefficient with such positive/negative oscillation would give the first theoretical explanation/prediction for this phenomenon.

To answer this question, we will have to introduce quickly the essential features of delayed equation framework. The two main changes are the addition of the delay variable for operators and functions and the modification of the scalar product. We will then apply this formalism to the bifurcation problem in a very similar fashion than the two previous Chapters for Kuramoto system with or without inertia, writing uniquely the crucial steps. In the standard Kuramoto case as a security check we will also compare the unstable manifold result with the one predicted by the OA ansatz (which does work in this case). Moreover, thanks to this broader formalism of delay equations (also called Theory of Functional Differential Equations) we will be able to prove a general result linking the normalization factor (of the projection on the unstable mode) with the derivative of the dispersion relation.

The main result of this Chapter yields is the explicit expression of the cubic coefficient of the unstable manifold expansion for both Kuramoto models with or without inertia. In the former case, the expression is compared with the one obtained with the OA ansatz.

# 1 THEORY OF DELAY DIFFERENTIAL EQUATION

In this Section, we summarize the formalism to study the linear and nonlinear dynamics of delay equations. The main points to accept are

- The distribution studied  $f(t)$  is now a function of the delay  $f_t(\varphi) = f(t+\varphi)$  (for negative  $\varphi$ ).
- The linear and nonlinear operators have a different expression for zero and non-zero delay Eq. (X.10)
- The adjoint operators are defined through a bilinear form acting as the usual inner product.
- This new inner product depends on the delay dependence of the linear operator Eq. (X.11). Its form is motivated by the so-called Lagrange identities [Hal63, BKNG09, Gao13].

## 1.1 Extended functional space and operator

In this Section, we motivate with a brief derivation the form of operators in the delay formalism.

The nonlinear operator  $\mathcal{M}$  acts on functions in some functional space  $f(\theta, \omega, t) \in \mathcal{B}$ , we want to study the evolution equation

$$\frac{\partial}{\partial t} f = \mathcal{M}[f]. \tag{X.1}$$

We can extend the functional space, for a given  $\tau \geq 0$ ,  $\mathcal{B}_\tau = \mathcal{C}^0([-\tau, 0], \mathcal{B})$  denotes the Banach space of continuous mappings from  $[-\tau, 0]$  into  $\mathcal{B}$  equipped with a norm  $\|u\| = \sup_{-\tau \leq \varphi \leq 0} \|u(\varphi)\|_{\mathcal{B}}$  for function  $u \in \mathcal{B}_\tau$ . Now for  $t \geq 0$ ,  $f_t \in \mathcal{B}_\tau$  is defined by  $f_t(\varphi) = f(t + \varphi)$  for  $\varphi \in [-\tau, 0]$ . Hence the problem writes

$$\frac{\partial}{\partial t} f(t) = M[f_t]. \tag{X.2}$$

Operators with delay can be conveniently represented as integral over delay [HL93, GW13]

$$M[f_t] = \int_{-\tau}^0 [d\eta(\varphi)] f_t(\varphi) \tag{X.3}$$

where  $\varphi$  acts as the delay variable and  $\eta$  is an operator with bounded variation depending on the delay parameter. For example, for a discrete time delay  $\tau$  we have

$$\eta(\varphi) = \Theta(\varphi + \tau) \mathcal{L} \tag{X.4}$$

that give  $M[f_t] = \mathcal{L} f_t(-\tau) = \mathcal{L} f(t - \tau)$ .

Let  $f_i(\varphi)$ , for  $-\tau \leq \varphi \leq 0$  define the "initial condition" (which is a function of delay). The solution is given by the nonlinear solution operator  $T(t)$ :

$$f_t(\varphi) = (T(t)F)(\varphi), \quad -\tau \leq \varphi \leq 0. \tag{X.5}$$

The uniqueness is given by the fact that  $T$  has properties of a semi-group

$$T(t + \delta) = T(t)T(\delta) \quad t, \delta \geq 0, \quad T(0) = I \tag{X.6}$$

Thus, we can rewrite

$$\frac{\partial}{\partial t} f_t(\varphi) = (\mathcal{A} f_t)(\varphi), \quad -\tau \leq \varphi \leq 0 \quad (\text{X.7})$$

where  $\mathcal{A}$  is the infinitesimal generator of the operator  $T$  which correspond to

$$(\mathcal{A} f_t)(\varphi) = \lim_{\epsilon \rightarrow 0} \frac{1}{\epsilon} [(T(\epsilon) f_t)(\varphi) - f_t(\varphi)]. \quad (\text{X.8})$$

Thus, we deduce<sup>1</sup> that

$$(\mathcal{A} f_t)(\varphi) = \begin{cases} \frac{d}{d\varphi} f_t(\varphi), & -\tau \leq \varphi \leq 0, \\ M[f_t], & \varphi = 0. \end{cases} \quad (\text{X.9})$$

We split linear and nonlinear part to write

$$(\mathcal{A} f_t)(\varphi) = (\mathcal{D} f_t + \mathcal{F}[f_t])(\varphi) = \begin{cases} \frac{d}{d\varphi} f_t(\varphi) \\ \mathcal{L} f_t(\varphi) \end{cases} + \begin{cases} 0, & -\tau \leq \varphi < 0 \\ \mathcal{N}[f_t], & \varphi = 0. \end{cases} \quad (\text{X.10})$$

The expression of the operator for nonzero delay is the translation of the function to its previous times. We will also need to decompose the linear operator in two parts  $\mathcal{L} = L + R$ , one that does not contain any delay  $L$  term and one with all delayed terms  $R$ .

## 1.2 Dual space

In the space  $\mathcal{B}_\tau$  there is no canonical inner product. However, in 1963 J.K. Hale [Hal63] managed to define a bilinear form acting as the inner product on this space. The method to define it is generic for functional space with no natural inner product (some further motivations are given in Section 1.3 of [Gao13]). In our problem with a discrete delay the scalar product is

$$(g_t, f_t)_\tau = (g_t^*(0) f_t(0)) + \int_{-\tau}^0 (g_t^*(\xi - \tau) R f_t(\xi)) d\xi \quad (\text{X.11})$$

where  $(g, f)$  denotes the usual scalar product on  $\mathcal{B}$  (position and velocity).

The additional terms contains the delay, this integral term often appears in the context of boundary problems (here the boundary is the time). The adjoint operator is then

$$(\mathcal{D}^\dagger g_t)(\vartheta) = \begin{cases} -\frac{d}{d\vartheta} g_t(\vartheta), & 0 < \vartheta \leq \tau \\ \mathcal{L}^\dagger g_t(\vartheta), & \vartheta = 0. \end{cases} \quad (\text{X.12})$$

The minus sign represents the fact that in the adjoint space the variable delay evolves in the positive sense  $0 \rightarrow \tau$  ("future").

1.  $(T(\epsilon) f_t)(\varphi) - f_t(\varphi) = (f_t)(\varphi + \epsilon) - f_t(\varphi)$

### 1.3 Eigenvalue problem

---

With this new formalism, it rather clear how to solve the eigenvalue problem, indeed we still look for unstable eigenmodes as

$$\mathcal{D}p(\varphi) = \lambda p(\varphi) \quad (\text{X.13a})$$

$$\mathcal{D}^\dagger q(\vartheta) = \lambda^* q(\vartheta). \quad (\text{X.13b})$$

For  $\vartheta$  and  $\varphi \neq 0$  the delay dependence is easily extracted to be as

$$p = p(0)e^{\lambda\varphi} = \Psi e^{\lambda\varphi} \quad (\text{X.14a})$$

$$q = q(0)e^{-\lambda^*\vartheta} = \tilde{\Psi} e^{-\lambda^*\vartheta}. \quad (\text{X.14b})$$

From the  $\varphi = 0$  equation we get

$$(\lambda I - \mathcal{L}(e^{\lambda \cdot} I)) \Psi = \left( \lambda I - \int_{-\tau}^0 d\eta(\varphi) e^{\lambda\varphi} I \right) \Psi = 0 \quad (\text{X.15})$$

where  $I$  denotes the identity (we have the same type of equation for the adjoint). Calling

$$\Delta(\lambda) = \lambda I - \int_{-\tau}^0 d\eta(\varphi) e^{\lambda\varphi} I \quad (\text{X.16})$$

we have the dispersion relation as  $\Lambda(\lambda) = \det \Delta(\lambda)$ . We want as usual the normalization  $(q, p)_\tau = 1$ .

$$\begin{aligned} (q, p)_\tau &= \left( \tilde{\Psi}, \Psi \right) - \int_{-\tau}^0 \int_0^\varphi e^{-\lambda(\xi-\varphi)+\lambda\xi} \left( \tilde{\Psi}, d\eta(\varphi) \Psi \right) d\xi = \left( \tilde{\Psi}, \left( I - \int_{-\tau}^0 \varphi e^{\lambda\varphi} d\eta(\varphi) \right) \Psi \right) \\ &= \left( \tilde{\Psi}, \Delta'(\lambda) \Psi \right) = 1. \end{aligned} \quad (\text{X.17})$$

The derivative of the dispersion relation appeared naturally during the computation. When  $\Delta$  is a diagonal operator of scalar equation the  $1/\Lambda'(\lambda)$  is the appropriate normalization. It should prove in a generic fashion, what we have so far always observed Eq. (V.24), Eq. (VI.44), Eq. (VII.22), Eq. (VIII.12b), Eq. (IX.12), that is that the normalization factor of the adjoint eigenvector is proportional to  $1/\Lambda'(\lambda)$ . In particular it shows that if  $\Lambda'(i\lambda_i) = 0$  (like in non-homogeneous Vlasov case with  $\lambda_i = 0$ ) the projection on the adjoint space is singular. Note that the validity of this formal result and its exact formulation is still a bit unclear.

## 2 OTT-ANTONSEN ANSATZ WITH DELAY

---

In this Section, we use the OA ansatz to first reduce the system to an ordinary differential equation with delay. This o.d.e with delay has only one mode thus it is direct to use an unstable manifold reduction with the previous formalism to describe the onset of synchronization.

## 2.1 Settings

The delayed model introduced in [YS99] for the first order Kuramoto model (with a frustration parameter) is

$$\dot{\theta}_i(t) = \omega_i + \frac{K}{N} \sum_{j=1}^N \sin(\theta_j(t - \tau) - \theta_i(t) - \alpha), \quad (\text{X.18})$$

where the delay  $\tau$  represents the time for one oscillator  $i$  to "see" the others. The associated Kuramoto equation is for the evolution of the density  $f(\theta, \omega, t)$ ,

$$\partial_t F(t) + \omega \partial_\omega F(t) + \frac{K}{2i} \partial_\theta \left( (r_1[F](t - \tau) e^{-i\theta - i\alpha} - r_{-1}[F](t - \tau) e^{i\theta + i\alpha}) F(t) \right) = 0. \quad (\text{X.19})$$

### Remark X.1

Thanks to the very generic formalism Eq. (X.4) of delay theory, we could study more complex delay terms. For example, a continuous delay as

$$\lim_{T \rightarrow \infty} \frac{1}{T} \int_{-T}^0 \theta_j(t + \varphi) d\eta(\varphi)$$

for some measure  $d\eta(\tau)$ .

## 2.2 Ott-Antonsen ansatz

As already observed in their original paper [OA08], the Ott-Antonsen ansatz works in the delayed case. For a Lorentzian distribution

$$g_L(\omega) = \frac{\sigma}{\pi} \frac{1}{(\omega - \omega_0)^2 + \sigma^2} \quad (\text{X.20})$$

centered in  $\omega_0$ . The OA ansatz gives for the order parameter

$$\dot{r}(t) = \frac{K}{2} e^{-i\omega_0\tau + i\alpha} r(t - \tau) - \sigma r(t) - \frac{K}{2} e^{i\omega_0\tau - i\alpha} r^*(t - \tau) (r(t))^2. \quad (\text{X.21})$$

The delay ordinary differential equation is simpler than the kinetic equation Eq. (X.19), but still infinite dimensional, because the "initial condition" is a function of delay (and not a finite set of values). The reduction Eq. (X.21) is global in the sense that it describes the system for any  $r$ , however the possible bifurcations are not immediately deduced from the sign of the cubic coefficient because of the delay that may induce changes. Hence, we want to put Eq. (X.21) in a "normal form"<sup>2</sup>, that is the "simplest" equivalent form of a dynamical equation close to a given bifurcation point, see [Mur06, HI10]. Therefore, this will reduce the dimension of the system close to the bifurcation (losing information on the global system).

2. Strictly speaking the final equation will be the true normal form up to a rescaling.

## 2.3 Unstable manifold calculation

### 2.3.a Linear part

We start with

$$\dot{r} = \mathcal{L} r_t + \mathcal{N}[r_t] \quad (\text{X.22})$$

Following the steps of analysis previously stated we define

$$(\mathcal{D}r_t)(\varphi) = \begin{cases} \frac{d}{d\varphi} r_t(\varphi) & -\tau \leq \varphi < 0 \\ \mathcal{L}r_t(\varphi) = Lr_t(0) + Rr_t(-\tau) & \varphi = 0 \end{cases} \quad (\text{X.23})$$

and

$$(\mathcal{F}[r_t])(\varphi) = \begin{cases} 0 & -\tau \leq \varphi < 0 \\ \mathcal{N}[r_t] & \varphi = 0 \end{cases} \quad (\text{X.24})$$

and the adjoint linear operator

$$(\mathcal{D}^\dagger s_t)(\vartheta) = \begin{cases} -\frac{d}{d\vartheta} s_t(\vartheta) & 0 < \vartheta \leq \tau \\ \mathcal{L}^\dagger s_t(\varphi) = L^\dagger s_t(0) + R^\dagger s_t(\tau) & \vartheta = 0 \end{cases} \quad (\text{X.25})$$

with

$$Lr = -\sigma r, \quad (\text{X.26a})$$

$$Rr = \frac{K}{2} e^{i(\alpha - \omega_0 \tau)} r, \quad (\text{X.26b})$$

$$\mathcal{N}[r_t] = -\frac{K}{2} e^{-i(\alpha - \omega_0 \tau)} r_t(-\tau)^* r_t(0)^2. \quad (\text{X.26c})$$

Let's now solve the eigenfunction equation

$$\mathcal{D}p(\varphi) = \lambda p(\varphi) \quad (\text{X.27})$$

for  $-\tau \leq \varphi < 0$ , the solution to Eq. (X.23) gives  $p = p(0)e^{\lambda\varphi}$ , from the  $\varphi = 0$  term we get the dispersion relation

$$\Lambda(\lambda) = \lambda + \sigma - \frac{K}{2} e^{-\lambda\tau + i(\alpha - \omega_0 \tau)}. \quad (\text{X.28})$$

We can fix the initial condition normalization  $p(0) = 1$ . At criticality, we have

$$\frac{K_c}{2} \cos(\alpha - \omega_0 \tau - \lambda_i \tau) = \sigma \quad (\text{X.29a})$$

$$\frac{K_c}{2} \sin(\alpha - \omega_0 \tau - \lambda_i \tau) = \lambda_i. \quad (\text{X.29b})$$

For  $K > K_c$  we could show that only one complex mode (and its conjugate) goes unstable. All other mode will have a negative real part.

#### Remark X.2

This time the o.d.e. Eq. (X.21) is really simple compared to a kinetic equation. For example, we can see from Eq. (X.28) that there is no continuous spectrum. Thus, we do not expect the unstable manifold expansion to be plagued by singular effects coefficients. Moreover, since there is only one unstable mode (and its conjugate) for small  $K - K_c$  the unstable manifold will be attractive [Mur06, GW13, HL93] (thus the local reduction rigorous).

### 2.3.b Adjoint problem

From the adjoint problem we get of course the same dispersion relation and an eigenvector associated with  $\lambda^*$  of the form  $q(\vartheta) = q(0)e^{-\lambda\vartheta}$ . The normalization for  $q$  is chosen such that  $(q, p)_\tau = 1$ , with the expression of the inner product we easily get that

$$q(0) = \frac{1}{\Lambda'(\lambda)} = \frac{1}{1 + \tau \frac{K}{2} e^{-(\lambda+i\omega_0)+i\alpha}}. \quad (\text{X.30})$$

### 2.3.c Nonlinear part

We now seek to expand the dynamic around  $r = 0$  when the asynchronous state is unstable  $K - K_c > 0$ . The unstable manifold expansion is

$$r_t(\varphi) = A(t)p(\varphi) + w_t(\varphi) \quad (\text{X.31})$$

where  $A(t) = (q, r_t)_\tau$  and  $0 = (q, w_t)_\tau$ . The time evolution is

$$\dot{A} = \lambda A + (q, \mathcal{F}[r_t])_\tau = \lambda A + q(0) \mathcal{N}[r_t]. \quad (\text{X.32})$$

Since we require  $w_t = O(A^2)$ , the nonlinear term is of order three, we don't even have to compute the first order of  $w_t$ ,

$$\mathcal{N}[Ap] = -\frac{K}{2} e^{i(\omega_0\tau-\alpha)} p^*(-\tau)p(0)^2 |A|^2 A$$

is enough. We get eventually the normal form of the delayed problem

$$\dot{A} = \lambda A - \frac{K}{2} \frac{e^{(i\omega_0-\lambda^*)\tau-i\alpha}}{1 + \tau \frac{K}{2} e^{-(i\omega_0+\lambda)\tau+i\alpha}} |A|^2 A + O(|A|^4 A). \quad (\text{X.33a})$$

The relevant parameter to study the bifurcation type is given by the sign of the cubic term in the limit  $\lambda_r \rightarrow 0$ ,

$$\text{Re } c_3 = -\frac{K_c}{2} \text{Re} \left( \frac{e^{i(\omega_0+\lambda_i-\alpha)\tau}}{1 + \tau \frac{K_c}{2} e^{-i(\omega_0+\lambda_i-\alpha)\tau}} \right). \quad (\text{X.33b})$$

This result will be analyzed later Section [X.3.5.b](#).

## 3 STANDARD KURAMOTO MODEL WITH DELAY

---

In this Section, the idea and method are exactly the same as before except that we work directly on the delay kinetic system (and not on the OA ansatz). The result obtained for generic  $g$  distribution will be compared in the Lorentzian  $g_L$  case with the previous result Eq. [\(X.33\)](#). Also, as in the Kuramoto case we will observe that the unstable manifold structure at first order is the same as for the OA ansatz for generic distribution  $g$ .

### 3.1 Setting

Let's  $g(\omega)$  be a symmetric distribution centered in  $\omega_0$ . By a change of variable  $\omega \rightarrow \omega - \omega_0$ ,  $\theta \rightarrow \theta - \omega_0\tau$  we now study a symmetric 0-centered distribution with phase lag  $\omega_0\tau$  (in addition to the phase lag  $\alpha$ ). For a perturbation of the incoherent initial state,  $F = g(\omega)/(2\pi) + f$

$$\partial_t f = \mathcal{L} f + \mathcal{N}[f]. \quad (\text{X.34})$$

Following the steps of the previous analysis

$$(\mathcal{D}f_t)(\varphi) = \begin{cases} \frac{d}{d\varphi} f_t(\varphi) & -\tau \leq \varphi < 0 \\ \mathcal{L} f_t(\varphi) = L f_t(0) + R f_t(-\tau) & \varphi = 0 \end{cases} \quad (\text{X.35})$$

and

$$(\mathcal{F}[f_t])(\varphi) = \begin{cases} 0 & -\tau \leq \varphi < 0 \\ \mathcal{N}[f_t] & \varphi = 0 \end{cases} \quad (\text{X.36})$$

and the adjoint linear operator

$$(\mathcal{D}^\dagger g_t)(\vartheta) = \begin{cases} -\frac{d}{d\vartheta} g_t(\vartheta) & 0 < \vartheta \leq \tau \\ \mathcal{L}^\dagger g_t(\varphi) = L^\dagger g_t(0) + R^\dagger g_t(\tau) & \vartheta = 0 \end{cases} \quad (\text{X.37})$$

with

$$L f = -\omega \partial_\theta f, \quad (\text{X.38a})$$

$$R f = -\frac{K}{2i} \frac{g(\omega)}{2\pi} \partial_\theta (r_1[f] e^{-i\theta - i(\alpha - \omega_0\tau)} - r_{-1}[f] e^{i\theta + i(\alpha - \omega_0\tau)}), \quad (\text{X.38b})$$

$$\mathcal{N}[f_t] = -\frac{K}{2i} \partial_\theta ((r_1[f_t](-\tau) e^{-i\theta - i(\alpha - \omega_0\tau)} - r_{-1}[f_t](-\tau) e^{i\theta + i(\alpha - \omega_0\tau)}) f_t(0)). \quad (\text{X.38c})$$

### 3.2 Eigenvalue problem

Let's now solve the eigenfunction equation

$$\mathcal{D}p(\varphi) = \lambda p(\varphi) \quad (\text{X.39})$$

for  $-\tau \leq \varphi < 0$ , the solution of Eq. (X.35) gives  $p = \Psi e^{\lambda\varphi}$ . The  $\varphi = 0$  equation gives

$$\Psi(\theta, \omega) = \psi(\omega) e^{i\theta} = \frac{K}{2} e^{-\lambda\tau + i(\alpha - \omega_0\tau)} \frac{g(\omega)}{\lambda + i\omega} e^{i\theta}. \quad (\text{X.40})$$

We choose to normalize such that  $r_1[\Psi] = 2\pi$ , this yield the dispersion relation

$$\Lambda(\lambda) = 1 - \frac{K}{2} e^{-\lambda\tau + i(\alpha - \omega_0\tau)} \int \frac{g(\omega)}{\lambda + i\omega} d\omega. \quad (\text{X.41})$$

Here we have computed the eigenvector  $p$  and associated eigenvalue  $\lambda$  associated with the  $k = 1$  spatial mode, by the exact same procedure we can show that  $p^*$  is an eigenvector associated with the eigenvalue  $\lambda^*$ . The eigenvalues  $\lambda, \lambda^*$  are both associated with a eigenspace of dimension one because the reflexion symmetry  $\mathcal{O}(2)$  is broken thanks to the phase lag  $\alpha - \omega_0\tau$ .

### 3.3 Adjoint problem

By adjoint computations we get

$$q(\vartheta) = \tilde{\Psi}(\theta, \omega)e^{-\lambda^*\vartheta} = \tilde{\psi}(\omega)\frac{e^{i\theta}}{2\pi}e^{-\lambda^*\vartheta} = \frac{1}{\Lambda'(\lambda)}\frac{1}{\lambda^* - i\omega}\frac{e^{i\theta}}{2\pi}e^{-\lambda^*\vartheta} \quad (\text{X.42})$$

where we have chosen the normalization factor so that  $(q, p)_\tau = 1$ . As expected from the general relation Eq. (X.17), the function  $\Lambda'(\lambda)$  appears, even though the scalar product choice was non-intuitive.

### 3.4 Unstable manifold calculation

We now decompose the perturbed solution  $f_t$  along the two unstable eigenvectors and the unstable manifold

$$f_t(\varphi) = A(t)p(\varphi) + A^*(t)p^*(\varphi) + w_t(\varphi) \quad (\text{X.43})$$

with  $A(t) = (q, f_t)_\tau$ ,  $(q, p^*)_\tau = 0$  and  $(q, w_t)_\tau = 0$ . The time evolution equation is hence rewritten as

$$\dot{A}p + \text{c.c.} + \dot{w}_t = A\mathcal{D}p + \text{c.c.} + \mathcal{D}w_t + \mathcal{F}[f_t]. \quad (\text{X.44})$$

After projections, it reads:

$$\dot{A} = \lambda A + (q, \mathcal{F}[f_t]) = \lambda A + (q(0), \mathcal{N}[f_t]) = \lambda A + \left\langle \tilde{\psi}, \mathcal{N}_1[f_t] \right\rangle \quad (\text{X.45a})$$

$$\dot{w}_t = \mathcal{D}w_t + \mathcal{F}[w_t] - \left\langle \tilde{\psi}, \mathcal{N}_1[f_t] \right\rangle p - \left\langle \tilde{\psi}^*, \mathcal{N}_1[f_t] \right\rangle p^*. \quad (\text{X.45b})$$

The 0<sup>th</sup> Fourier mode is zero as in the standard Kuramoto case, so only the second harmonic term  $(w_t)_{2,0}$  will contribute to the cubic coefficient. The Fourier terms of the nonlinear operator is

$$\mathcal{N}_1[f_t] = -A|A|^2\frac{K}{2}r_1[p^*(-\tau)]e^{-i(\alpha-\omega_0\tau)}(w_t)_{2,0}(0) + \text{O}(|A|^4) \quad (\text{X.46a})$$

$$\mathcal{N}_2[f_t] = A^2Kr_{-1}[p(-\tau)]e^{i(\alpha-\omega_0\tau)}p(0) + \text{O}(|A|^2) \quad (\text{X.46b})$$

where we can obtain at first order

$$(w_t)_{2,0}(\varphi) = h_{2,0}e^{2\lambda\varphi} \quad (\text{X.47a})$$

$$(h_t)_{2,0} = \frac{\pi K^2}{2} \frac{g(\omega)}{(\lambda + i\omega)^2} e^{2i(\alpha-\omega_0\tau)} e^{-2\lambda\tau}. \quad (\text{X.47b})$$

In this computation with time derivative one should not get confused by the presence of a delay variable that is considered separately. The delay dependence is obtained again through equation Eq. (X.35) for nonzero delay.

The cubic coefficient is then obtained thanks to Eq. (X.45a) and Eq. (X.46a)

$$\begin{aligned}
 c_3 &= -\frac{\pi^2 K^3}{2} \frac{e^{-2\lambda\tau - \lambda^*\tau + i(\alpha - \omega_0\tau)}}{\Lambda'(\lambda)} \int \frac{g(\omega)}{(\lambda + i\omega)^3} d\omega \\
 &= -\pi^2 K^2 e^{-2\lambda_r\tau} \frac{\int \frac{g(\omega)}{(\lambda + i\omega)^3}}{\int \frac{g(\omega)}{(\lambda + i\omega)^2} + \tau \int \frac{g(\omega)}{(\lambda + i\omega)}} \quad (\text{X.48}) \\
 c_3 &= -\pi^2 K^2 e^{-2\lambda_r\tau} \frac{\int \frac{g(\omega)}{(\lambda + i\omega)^3}}{\int \frac{g(\omega)}{(\lambda + i\omega)^2} + \tau \frac{2}{K} e^{\lambda\tau - i(\alpha - \omega_0\tau)}}
 \end{aligned}$$

where we have used that  $\lambda$  is an eigenvalue of the dispersion relation to obtain the last line. This yields the main result of this Section. The sign of  $\text{Re } c_3$  in the  $\lambda_r \rightarrow 0$  limit gives the nature of the bifurcation. The delay adds an oscillating term in the coefficient  $c_3$ , in addition to modifying the eigenvalue. For a fixed  $\omega_0$  and varying delay  $\tau$  one can plot the sign of  $c_3$  computing at the criticality  $K = K_c(\tau)$  and  $\lambda = \lambda(\tau)$ , see Figure X.1.

### Remark X.3

As in the standard Kuramoto case no divergence appears within the unstable manifold approach thus the one dimensional local reduction should be rigorous. Once again, we link this success with the fact that we have despite the delay a constant zeroth harmonic  $f_0$  ( $\mathcal{N}_0 = \mathcal{L}_0 = 0$ ) and no coupling between positive  $f_{k>0}$  and negative modes  $f_{k<0}$ , see Section VIII.5.4. Moreover, the unstable manifold lies at its first order on the OA manifold as in the standard Kuramoto case (see Section VIII.5.2). Indeed, its coefficients have the OA ansatz form:  $(w_t)_{k,0} = \beta_t^k$  for some  $\beta_t$ .

## 3.5 Application

---

### 3.5.a Centered distribution $\omega_0 = 0$

Can a delay affect the bifurcation of symmetric centered distribution  $g$  with no frustration parameter? Letting  $\lambda_r \rightarrow 0$  in Eq. (X.48) and Eq. (X.41) we get that with  $\alpha, \omega_0 = 0$ ,  $\lambda_i = 0$  and  $K_c = (K_c)_{\text{Kuramoto}}$

$$c_3 = \frac{\pi^3 K_c^2}{2} \frac{g''(0)}{-\text{PV} \int (g'(\omega)/\omega) + 2\tau/K_c}. \quad (\text{X.49})$$

Therefore, for a unimodal function we see that the sign of the coefficient is unchanged compared to the standard Kuramoto case since both denominator terms are positive. If  $g(\omega)$  is for example bimodal with real eigenvalue the sign of the denominator is unchanged (see Appendix D.3). Remember that the case of a symmetric distribution with complex eigenvalue is possible but requires a four-dimensional unstable manifold that this result does not cover. In conclusion for "standard" (at least unimodal and bimodal where we could prove the sign of the denominator) distribution with real eigenvalue, delay does not affect the nature of the bifurcation nor the critical coupling.

### 3.5.b Lorentzian distribution

For a Lorentzian  $g_L(\omega) = \frac{\sigma}{\pi}(\omega^2 + \sigma^2)^{-1}$  the integral in Eq. (X.48) are easy to compute with

$$\int \frac{g_L(\omega)}{(\lambda + i\omega)^n} = (\lambda + \sigma)^{-n}$$

and so is the dispersion relation, that gives the same expression as in the OA case Eq. (X.28). The cubic coefficient is then

$$(c_L)_3 = -(2\pi)^2 \frac{K}{2} \frac{e^{-\lambda^* \tau} e^{-i(\alpha - \omega_0 \tau)}}{1 + \tau \frac{K}{2} e^{-\lambda \tau + i(\alpha - \omega_0 \tau)}} \quad (\text{X.50})$$

which is the exact same coefficient (up to the change  $r \sim 2\pi A$ ) as with the OA ansatz Eq. (X.33a) which confirms both results.

A direct application is to recover the numerical observation of [YS99] Figure 4 which predicts for a Lorentzian (with  $\sigma = 0.1$  and  $\omega_0 = 3$ ) the critical coupling constant line with respect to delay  $K_c(\tau)$ . Moreover, in this article simulations were performed for  $\tau = 1$  and  $2$  and show respectively a subcritical and supercritical bifurcation. These observations agree fully with Figure X.1; our plot of  $\text{Re } c_3$  is indeed positive for  $\tau = 1$  and negative for  $\tau = 2$ . Furthermore, thanks to this theoretical expression Eq. (X.48) we can do simple predictions. As observed in [YS99] for Lorentzian Eq. (X.20)

- $K_c$  is minimum for every  $\omega_0 \tau = 2n\pi$  with associated  $K_c = 2\sigma$  and  $\lambda_i = 0$ . Thus, in these points

$$\text{Re } c_3 = -\frac{1}{1 + \sigma\tau} < 0.$$

- $K_c$  is a local maximum for  $\omega_0 \tau = (2n + 1)\pi$ .

It is possible to show<sup>3</sup> with Eq. (X.41) that for  $\tau \rightarrow \infty$ ,  $\lambda_i \tau \rightarrow \pi^-$  and  $K_c \rightarrow 2\sigma$ . So above some critical delay  $\tau_c$ , we always have  $\text{Re } c_3 < 0$ .

Hence we have given for the first time (to my knowledge) a theoretical support for the numerical observations of [YS99]. Moreover, we could predict that for large delay the bifurcation is always supercritical. Of course, this demonstration holds only for Lorentzian distribution Eq. (X.20) but thanks to our generic results Eq. (X.41), Eq. (X.48) one could also study other distributions  $g(\omega)$ .

---

## 4 KURAMOTO MODEL WITH INERTIA AND DELAY

---

As we have motivated in the introduction, in some electric systems (like power grid or neural systems) delay could play a non-negligible part. Some of those system requires a second order description including an inertial dynamics. It is thus natural (now that we have all the tools) to study the Kuramoto model with inertia. The method is very similar to the previous Section and the Chapter IX on inertia so we will jump some identical steps.

---

3. Doing the demonstration for the local maximum  $\omega_0 \tau = (2n + 1)\pi$ .

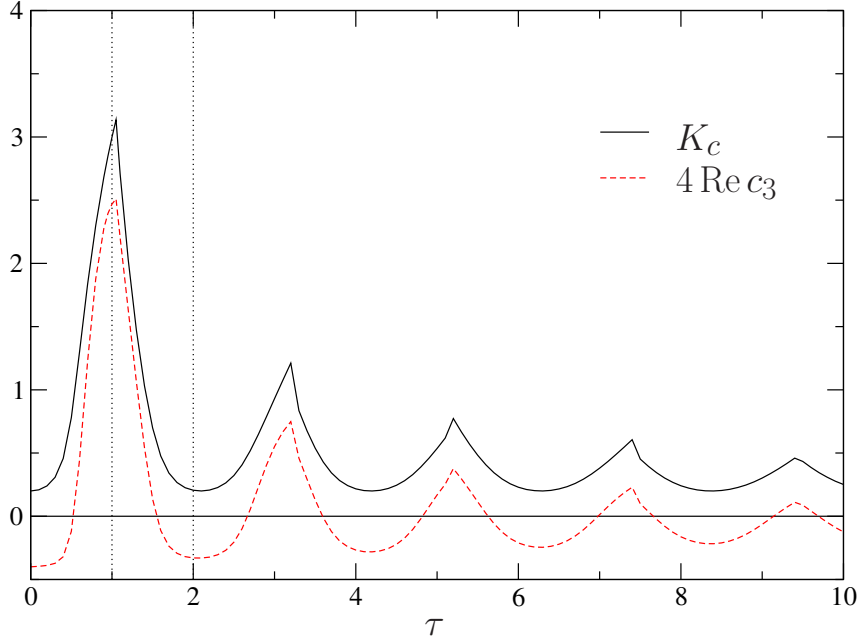


Figure X.1 – Stability region of the incoherent state for Lorentzian  $g_L(\omega) = \text{Eq. (X.20)}$  with  $\sigma = 0.1$  and  $\omega_0 = 3$ . The solid line shows the critical line  $K_c(\tau)$  (for  $K > K_c$  the system is unstable). The red dashed line shows the associated  $4 \text{Re } c_3$  at criticality (it has been multiplied by four to be visible). Its sign determines the super/sub-critical nature of the bifurcation. Vertical dotted lines  $\tau = 1$  and  $2$  show where the bifurcation simulations were performed in Figure 4 of [YS99].

## 4.1 Settings

The microscopic model is

$$\dot{\theta}_i(t) = v_i(t) \quad (\text{X.51a})$$

$$m\dot{v}_i(t) = (\omega_i - v_i(t)) + \frac{K}{N} \sum_{j=1}^N \sin(\theta_j(t - \tau) - \theta_i(t) - \alpha). \quad (\text{X.51b})$$

While the kinetic equation (in rescaled parameters) for the phase space density  $F(\theta, v, \omega, t)$  is

$$\begin{aligned} \partial_t F(t) + v \partial_\theta F(t) + \frac{K}{2im} (r_1[F](t - \tau) e^{-i(\theta + \alpha)} - r_{-1}[F](t - \tau) e^{i(\theta + \alpha)}) \partial_v F(t) \\ - \frac{1}{m} \partial_v ((v - \omega) F(t)) = 0, \end{aligned} \quad (\text{X.52})$$

where we have only written the time dependence, the order parameter definition is unchanged Eq. (VIII.9b). The incoherent stationary solution is still  $F(\theta, v, \omega, t) = f^0(v, \omega) = g(\omega) \delta(v - \omega) / (2\pi)$ . We write Eq. Eq. (X.52) as a sum of a linear and a nonlinear part, with  $F = f^0 + f$ :

$$\frac{df_t}{dt} = \mathcal{D}f_t + \mathcal{F}[f_t], \quad (\text{X.53})$$

with the delay operators  $\mathcal{D}$ ,  $\mathcal{F}$  and the adjoint  $\mathcal{D}^\dagger$  defined as in Eq. (X.35) and Eq. (X.37) with

$$Lf = -v\partial_\theta + \frac{1}{m}\partial_v((v-\omega)f), \quad (\text{X.54a})$$

$$Rf = -\frac{K}{2im}(r_1[f]e^{-i\theta}e^{-i(\alpha-\omega_0\tau)} - r_{-1}[f]e^{i\theta}e^{i(\alpha-\omega_0\tau)})\partial_v f^0, \quad (\text{X.54b})$$

$$\mathcal{N}[f_t] = -\frac{K}{2im}(r_1[f_t](-\tau)e^{-i\theta}e^{-i\alpha} - r_{-1}[f_t](-\tau)e^{i\theta}e^{i\alpha})\partial_v f(0). \quad (\text{X.54c})$$

## 4.2 Eigenvalue problem

Similarly the eigenvalue problem

$$\mathcal{D}p = \lambda p \quad (\text{X.55})$$

is straightforward, with  $p(\varphi) = \Psi e^{\lambda\varphi} = \psi e^{i\theta} e^{\lambda\varphi}$ . For  $\varphi = 0$ , looking for a solution in the form

$$\psi = U_0(\omega)\delta(v-\omega) + U_1(\omega)\delta'(v-\omega) \quad (\text{X.56})$$

and imposing the normalization  $\int \psi dv d\omega = 1$ , one finds

$$U_0 = \frac{K}{2m}e^{i(\alpha-\omega_0\tau)}e^{-\lambda\tau}\frac{g(\omega)}{(\lambda+i\omega)(\lambda+1/m+i\omega)} \quad (\text{X.57})$$

$$U_1 = \frac{K}{2im}e^{i(\alpha-\omega_0\tau)}e^{-\lambda\tau}\frac{g(\omega)}{\lambda+1/m+i\omega}. \quad (\text{X.58})$$

Expliciting the normalization condition yields the dispersion relation:

$$\Lambda(\lambda) = 1 - \frac{K}{2m}e^{i(\alpha-\omega_0\tau)}e^{-\lambda\tau}\int\frac{g(\omega)}{(\lambda+i\omega)(\lambda+1/m+i\omega)}d\omega = 0. \quad (\text{X.59})$$

Hence, if  $\lambda$  is an eigenvalue of  $\mathcal{D}_1$ ,  $\lambda^*$  is an eigenvalue of  $\mathcal{D}_{-1}$ , as expected from the rotation symmetry.

We compute the adjoint eigenvector as  $q(\vartheta) = \tilde{\Psi}e^{-\lambda^*\vartheta} = \tilde{\psi}\frac{e^{i\theta}}{2\pi}e^{-\lambda^*\vartheta}$ , through

$$(\lambda^* - iv)\tilde{\psi} + \frac{1}{m}(v-\omega)\partial_v\tilde{\psi} = \frac{K}{2im}e^{-i(\alpha-\omega_0\tau)}e^{-\lambda^*\tau}\int g(\omega)\partial_v\tilde{\psi}(\omega,\omega)d\omega. \quad (\text{X.60})$$

Again the normalization with  $1/\Lambda'(\lambda)$  will play an important role. The expression of the  $\tilde{\psi}^{(n)}(\omega,\omega)$  terms is formally the same as in Eq. (IX.13).

## 4.3 Unstable manifold

The decomposition on the center manifold is again

$$f_t(\varphi) = A(t)p(\varphi) + A^*(t)p^*(\varphi) + H[A, A^*](\varphi) \quad (\text{X.61})$$

with  $A(t) = (q, f_t)$ ,  $(q, p^*) = 0$  and  $(q, H) = 0$  with the same time evolution equations Eq. (X.45). The dynamical expansion gives

$$\dot{A} = \lambda A + A|A|^2\frac{2\pi K}{2im}\left(e^{i(\alpha-\omega_0\tau)}e^{-\lambda\tau}\langle\tilde{\psi}, \partial_v h_{0,0}\rangle - e^{-i(\alpha-\omega_0\tau)}e^{-\lambda^*\tau}\langle\tilde{\psi}, \partial_v h_{2,0}\rangle\right) + O(|A|^4). \quad (\text{X.62})$$

The Fourier component of the unstable manifold can be computed as before for  $\varphi \neq 0$  ( $w_t)_{0,0}(\varphi) = h_{0,0}e^{2\lambda_r\varphi}$ ,  $(w_t)_{2,0}(\varphi) = h_{2,0}e^{2\lambda\varphi}$  and with the "boundary condition"  $\varphi = 0$

$$(2\lambda_r - \mathcal{L}_0) \cdot h_{0,0} = i \frac{2\pi K}{2m} e^{-i(\alpha - \omega_0\tau)} e^{-\lambda^*\tau} \partial_v \psi + \text{c.c.} \quad (\text{X.63})$$

$$(2\lambda - \mathcal{L}_2) \cdot h_{2,0} = -i \frac{2\pi K}{2m} e^{i(\alpha - \omega_0\tau)} e^{-\lambda\tau} \partial_v \psi. \quad (\text{X.64})$$

#### 4.3.a Computation of $h_{0,0}$

We start from Eq. (X.63). We have  $h_{0,0} = h + \text{c.c.}$ , where  $h$  is the solution of

$$(2\lambda_r - \mathcal{L}_0) \cdot h = i \frac{2\pi K}{2m} e^{-i(\alpha - \omega_0\tau)} e^{-\lambda^*\tau} \partial_v \psi. \quad (\text{X.65})$$

Eq. (X.65) reads

$$2\lambda_r h_{0,0} - \frac{1}{m} \partial_v [(v - \omega) h_{0,0}] = \frac{2\pi K^2}{4im^2} e^{-2\lambda_r\tau} \left( \frac{g\delta'(v - \omega)}{(\lambda^* - i\omega)(\lambda^* - i\omega + 1/m)} + i \frac{g\delta''(v - \omega)}{(\lambda^* - i\omega + 1/m)} \right). \quad (\text{X.66})$$

We introduce the ansatz:

$$h = W_0(\omega)\delta(v - \omega) + W_1(\omega)\delta'(v - \omega) + W_2(\omega)\delta''(v - \omega).$$

to get

$$W_0(\omega) = 0 \quad (\text{X.67})$$

$$W_1(\omega) = \frac{2i\pi(K/2m)^2 e^{-2\lambda_r\tau} g(\omega)}{(2\lambda_r + 1/m)(\lambda + i\omega)(\lambda + 1/m + i\omega)} \quad (\text{X.68})$$

$$W_2(\omega) = \frac{2\pi(K/2m)^2 e^{-2\lambda_r\tau} g(\omega)}{2(\lambda_r + 1/m)(\lambda + 1/m + i\omega)}. \quad (\text{X.69})$$

#### 4.3.b Computation of $h_{2,0}$

A similar computation starting from Eq. (X.64) yields  $h_{2,0}$ . We have to solve

$$(2\lambda - \mathcal{L}_2) \cdot h_{2,0} = -i \frac{2\pi K}{2m} e^{i(\alpha - \omega_0\tau)} e^{-\lambda\tau} \partial_v \psi. \quad (\text{X.70})$$

Using the ansatz

$$h_{2,0} = X_0\delta(v - \omega) + X_1\delta'(v - \omega) + X_2\delta''(v - \omega),$$

we obtain

$$\begin{aligned} X_0(\omega) &= \frac{iX_1(\omega)}{(\lambda + i\omega)} \\ X_1(\omega) &= \frac{-i(2\pi K e^{i(\alpha - \omega_0\tau)} e^{-\lambda\tau} / 2m) U_0(\omega)}{(2\lambda + 2i\omega + 1/m)} + \frac{4iX_2(\omega)}{(2\lambda + 2i\omega + 1/m)} \\ X_2(\omega) &= \frac{-i(2\pi K e^{i(\alpha - \omega_0\tau)} e^{-\lambda\tau} / 2m) U_1(\omega)}{2(\lambda + i\omega + 1/m)}. \end{aligned}$$

### 4.3.c Putting everything together

As in IX.3.3 one can insure that the only diverging term will come from  $\int \tilde{\psi}^{(2)*} W_1^*$ ; thus the leading term is

$$\int \tilde{\psi}^{(2)*} W_1^* d\omega \sim i\pi \frac{K^2}{m^2} \frac{e^{-2\lambda_r \tau}}{(1/m)^4} \frac{1}{\Lambda'(i\lambda_i)} \frac{\pi}{2} \frac{g(-\lambda_i)}{\lambda_r}, \quad (\text{X.71})$$

We conclude that the leading behavior of  $c_3$  for  $m > 0$  is given by:

$$c_3 \sim \frac{\pi^3}{2} m K^3 \frac{e^{i(\alpha - (\omega_0 + \lambda_i)\tau)}}{\Lambda'(i\lambda_i)} \frac{g(-\lambda_i)}{\lambda_r}. \quad (\text{X.72})$$

In particular, the sign of  $s(\tau) = \text{Re} \left( \frac{e^{i(\alpha - (\omega_0 + \lambda_i)\tau)}}{\Lambda'(i\lambda_i)} \right)$  determines the type (sub- or super-critical) of the bifurcation.

#### Remark X.4

As we have seen the second order Kuramoto model links the Vlasov-HMF model with the standard Kuramoto model. Thus, here without really paying attention we have also studied the delayed Vlasov-HMF model (one should take the frictionless limit as shown in D.1.2 for the non-delay equation). In this limit, we also expect the delay to change periodically the super/sub-critical nature of the bifurcation.

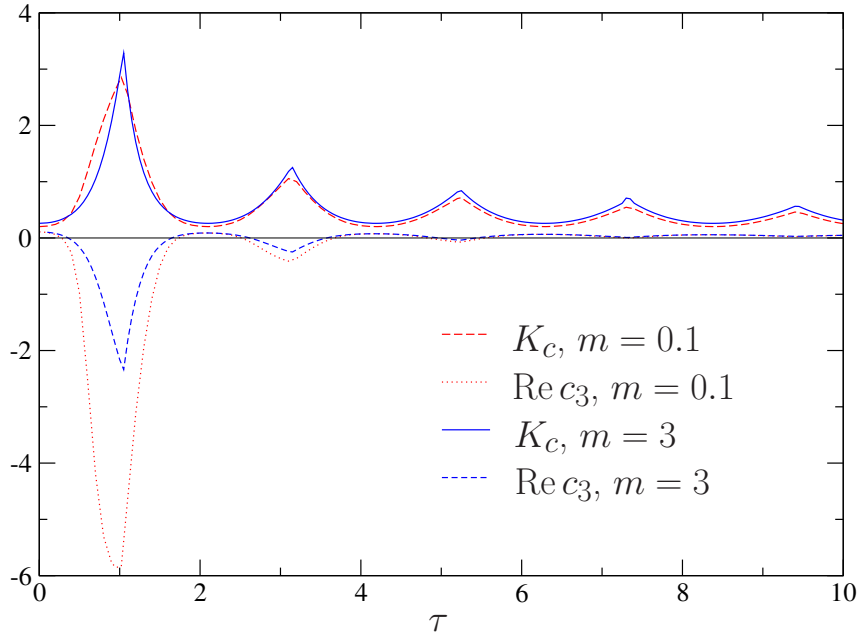


Figure X.2 – Stability region of the incoherent state for Lorentzian  $g_L(\omega) = \text{Eq. (X.20)}$  with  $\sigma = 0.1$  and  $\omega_0 = 3$ . We show the  $K_c(\tau)$  and  $\text{Re } c_3(\tau)$  for  $m = 0.1$  and 3. The signs of  $\text{Re } c_3(\tau)$  determines the super/sub-critical nature of the bifurcation.

## 4.4 Application to a Lorentzian distribution

---

To get some insight of what is the effect of inertia in a delay system we once again do a Lorentzian application. The dispersion relation gives Eq. (X.59) at criticality

$$\frac{K_c}{2} = (\sigma + m\sigma^2 - m\lambda_i^2) \csc((\omega_0 + \lambda_i)\tau) \quad (\text{X.73a})$$

$$\frac{\lambda_i(1 + 2\sigma m)}{\sigma + m\sigma^2 - m\lambda_i^2} = -\tan((\omega_0 + \lambda_i)\tau). \quad (\text{X.73b})$$

A full demonstration on the behavior of  $K_c(\tau)$  and  $\lambda_i(\tau)$  is more tedious than in the standard Kuramoto case but is in principle doable. The sign of the cubic coefficient is given for a Lorentzian by

$$s(\tau) = \text{Re} \left( \frac{(\sigma + i\lambda_i)^2(1 + m(\sigma + i\lambda_i))^2}{m(1 + (\sigma + i\lambda_i)(\tau + m(i\lambda_i\tau + \sigma\tau + 2)))} \right). \quad (\text{X.74})$$

We plot on Figure X.2  $K_c$  and  $\text{Re } c_3$  with respect to the delay for two different inertia  $m = 0.1$  and 3 for the same Lorentzian distribution than in Figure X.1. As before we see that the inertia makes  $\text{Re } c_3$  positive when there is no delay  $\tau = 0$ . Moreover, as before the delay induces some "oscillations" in the sign of  $\text{Re } c_3$ . Therefore, we predict that systems with inertia and a delay  $\tau \sim 1$  display a supercritical bifurcation toward synchronization. Moreover at large  $\tau$  it seems clear that  $K_c(\tau) \xrightarrow{\tau \rightarrow \infty} K_c(0)$  and  $\text{Re } c_3(\tau) \xrightarrow{\tau \rightarrow \infty} \text{Re } c_3(0) > 0$ .

---

## REMARKS, CONJECTURES, CONCLUSION & PERSPECTIVES

---

To conclude Part [Two](#), we dedicate this Chapter to a summary of the results obtained with the various bifurcation analyses we performed.

We have studied multiple collisionless kinetics equations accounting for different physical situations. Each time, the goal was to describe the dynamics of these equations (of infinite dimension) close to unstable steady state. We wanted to obtain a dimensional reduction of the problem to get a simple description of the bifurcation. This dimensional reduction often yields a one-dimensional (or two-dimensional if the order parameter is complex) regular differential equation.

Each system had its own difficulties inherent with its physical specificities. Nevertheless, in each situation we managed to perform the Unstable Manifold expansion: we provided the expression of the cubic coefficient (or quadratic for the Vlasov non homogeneous case) and thus the qualitative nature of the bifurcation. Every numerical test done was fully supporting of our analytical findings (scaling, nature of the bifurcation, parameters dependence). Thus, despite the singular nature of the unstable manifold reduction when neutral modes (or a continuum of neutral modes) are present, it made every time right predictions. Its general formalism makes it suitable for very generic problems (delay, dissipation/friction, ...). Our results should then establish further the singular expansions a la Crawford as a method of choice to understand the qualitative behavior of collisionless models.

*Difficulties and Specificities*

- Vlasov around non homogeneous state (VNH) with non oscillating perturbation  $\lambda \in \mathbb{R}$ :  
**Technically** We need the angle-action variables to deal with the linear problem. Computation of the Fourier coefficients of the HMF potential in angle-action variable.  
**Numerically** The GPU semi-Lagrangian HMF-Vlasov solver was generously provided by T. R. Filho [RF13]. Small modifications were necessary to handle the initial conditions and the output data. Our study required careful choices of parameters (grid size and maximum velocity  $p_{\max}$ ) close to the bifurcations. The other numerical work hidden in this manuscript is related to the precise evaluation of the theoretical expressions e.g. roots of the dispersion relation for the eigenvalue  $\lambda$ , determination of the equilibrium parameters  $(M_0, \mu_0)$ , angle-action functions  $(\Omega(J), c_m(J), \dots)$ , Triple Zero coefficients, ... This was whole done using the software Mathematica [Inc].  
**Physically** Weaker resonances that allow a three-dimensional reduction of the bifurcation, reproducing well the simulations. This reduction could be very generic.
- Vlasov-Fokker-Planck (VFP):  
**Technically** Velocity Fourier description of the problem, asymptotic behavior of integrals with special functions.  
**Physically** Interplay between two small parameters leading to different types of critical layer dominating in different regimes at the bifurcation.
- Kuramoto with inertia (KuI):  
**Technically** Three variables  $(\theta, v, \omega)$ ; the eigenvalue problem is solved with distributions.  
**Numerically** The GPU codes used for the numerical part were developed during the thesis using standard schemes [GCR14]. We also evaluated via Mathematica [Inc], all the wanted quantities e.g.  $K_c, c_3(\alpha), \dots$   
**Physically** Singular contributions controlling the bifurcation nature even for small inertia.
- Kuramoto with delay (KuD) with and without inertia:  
**Technically** Functional differential equations.  
**Physically** Delay does not bring any singularities but it changes the sub/super-critical nature of the bifurcation periodically up to some critical delay.

We summarize further the main characteristic of each case treated in Table XI.1.

- The symbol ♠ stands for cases treated originally by J.D. Crawford.
- $\mathcal{H}$  means Hamiltonian system.
- $k \lesseqgtr 0$  means presence of nonlinear mixing of positive and negative Fourier modes.
- CS means continuous spectrum.
- H.O.T. stands for the higher order terms.
- Reduction asks if a dimensional reduction was found. It is not definitive, it only specifies the current state of the art.

So far only four of these systems have (or are believed to have) exhibited a dimensional reduction. The first one is the standard Kuramoto model where a global reduction (valid for any order parameter) of the dynamics is achievable thanks to the Ott-Antonsen (OA) ansatz. Moreover for this systems strong mathematical results were obtained. The second system is the Kuramoto with delay model where the OA ansatz yields an infinite dimensional delayed ordinary differential equation. This latter equation can be studied locally via standard bifurcation techniques (e.g. center manifold for delayed equations). The third system is the VNH model with  $\lambda \in \mathbb{R}$  (non oscillating perturbation) where a three-dimensional reduction through the Triple Zero nor-

mal form was done. In this case we believe that weak resonance effect could allow a rigorous regular reduction using the center manifold method. The fourth model where dimensional reduction is expected is the Vlasov-Fokker-Planck system with "large" friction ( $\lambda \ll \gamma^{1/3}$ ). This is quite standard for dissipative systems. Numerical test would probably help to better understand the interplay between the friction  $\gamma$  and instability rate  $\lambda$ .

What makes these cases (Ku, KuD, VNH) so unique? Remember that at the linear level all the eight cases display more or less the same characteristics with the Landau damping (through phase mixing in velocity) while differences emerge at the nonlinear level. For the standard and delay Kuramoto model it seems that the non mixing of Fourier modes is the biggest difference, while for VNH the weak resonance of particles around the separatrix with the unstable wave is the key ingredient. Could these two phenomena be somehow related? In the Kuramoto case there seems to be strong resonances but since there is no real velocity variable ("overdamped oscillators" with their own natural frequency), it is difficult to be definitive. In the VNH case there is mixing between negative and positive Fourier modes, nevertheless terms that usually produce pinching singularities due to this mixing are strongly attenuated.

How are the resonances linked with the mixing of Fourier modes?

	$\mathcal{H}?$	$k \leq 0$	CS	$\Lambda'(0^+)$	$c_k$	H.O.T.	Reduction
♠ VH	Yes	Yes	Yes	$\neq 0$	$c_3 \sim \lambda^{-3}$	=	No
VNH	Yes	Yes	Yes depends on $V_{int}, f^0$ +weak resonances	0	$c_2 \propto \lambda^{-1}$	=	Yes? TZ?
VFP	No	Yes	No	$\neq 0$	$c_3 \propto \begin{cases} \text{i) } \lambda^{-3} \\ \text{ii) } \lambda \gamma^{-4/3} \\ \text{iii) } O(1) \end{cases}$	$\begin{cases} = ? \\ \ll ? \\ \ll ? \end{cases}$	$\begin{cases} \text{No?} \\ \text{Yes?} \\ \text{Yes?} \end{cases}$
♠ Ku	No	No	Yes	$\neq 0$	$c_3 \propto O(1)$	$\ll$	Yes O.A. ansatz Math results
♠ Ku <sup>2nd</sup>	No	Yes	Yes	$\neq 0$	$c_3 \propto \lambda^{-1}$	=	No
KuI	No	Yes	Yes split	$\neq 0$	$c_3 \propto \lambda^{-1}$	= ?	No
KuD	No	Yes	Yes	$\neq 0$	$c_3 \propto O(1)$	$\ll$	Yes O.A. ansatz
KuID	No	Yes	Yes split	$\neq 0$	$c_3 \propto \lambda^{-1}$	= ?	No

Table XI.1 – Comparison between the various kinetic models studied. VH: Vlasov homogeneous; VNH: Vlasov non homogeneous (with  $\lambda \in \mathbb{R}$ ); VFP: Vlasov-Fokker-Planck; Ku: Standard Kuramoto; Ku<sup>2nd</sup>: Kuramoto-Daido; KuI: Kuramoto with inertia; KuD: Kuramoto with delay; KuID: Kuramoto with inertia and delay; TZ: Triple Zero.

# 1 CONJECTURES

---

---

Since many directions have been evoked to understand the possibility of a dimensional reduction we listed ideas and conjectures on the topic.

## **Conjecture XI.1**

If the unstable manifold approach can be performed without singular coefficients, then the bifurcation description is exact close to the criticality.

A stronger version that could be applied to the VFP system.

## **Conjecture XI.2**

When the bifurcation is supercritical and higher order terms of the unstable manifold are negligible at the saturation level, then the reduction can be made exact close the criticality.

As we have seen we know that the opposite implication is false: indeed if the expansion has the same order coefficient it does not mean that there are no possibilities to obtain a dimensional reduction. For example, in the finite dimensional case Section IV.1, the one dimensional unstable manifold was singular while a two-dimensional model (in this case the full model) was not. Moreover, it seems that the same thing happens with VNH where the unstable manifold is singular and a three-dimensional description is not.

Is there any case where the unstable manifold expansion fails? Why does it has always provided (so far) the right scaling and bifurcation nature via the  $c_3$  sign, with the right parameters dependence (as tested for example in KuI and KuD by varying the frustration or delay parameter)? Is there a way to show mathematically that this is true? We can risk the following conjecture:

## **Conjecture XI.3**

The unstable manifold always yields the right sub/super-critical behavior of the bifurcation. In the supercritical case, it also provides the right saturation scaling.

## ***Continuous Spectrum***

The continuous spectrum (CS) and in general the infinite dimensional structure of neutral modes in these kinetic equations were being pointed as necessarily responsible of singularities in the unstable manifold expansion. Additionally, dimensional reduction looked hopeless with this structure, though we saw in the standard Kuramoto model and up to a certain extent in the VNH model (with  $\lambda$  real) that this was in general false.

However even if the CS does not necessary imply singular coefficients with respect to  $\lambda$  we might conjecture that:

## **Conjecture XI.4**

To get a singular unstable manifold expansion, one needs a slow manifold of dimension strictly larger than the unstable manifold. This slow manifold is associated with eigenvalues  $\nu_k$  (or a continuum of neutral modes) that are of the same order (or smaller) than the unstable mode  $0 \leq |\operatorname{Re} \nu_k| \lesssim \operatorname{Re} \lambda$ .

Since the unstable manifold close to the criticality is always included in the slow manifold, it follows that as soon as an additional slow mode is added the unstable manifold will be singular.

In the VNH unstable description we also have a non empty slow manifold: in addition to unstable eigenvalue  $\lambda \rightarrow 0^+$  there is the stable one approaching the imaginary axis from the left  $-\lambda \rightarrow 0^-$ .

### ***Resonances***

Regarding the resonances, we have seen their crucial role in the VNH case: due to very weak effects the system behaves like a finite dimensional system with a Jordan block. This phenomenon was translated by  $(\tilde{\Psi}_\lambda, \Psi_\lambda) \propto \Lambda'(\lambda) \xrightarrow{\lambda \rightarrow 0} 0$  (where we explicit the normalization factor for this scalar product). With strong resonances, the same limit was non zero. In the VNH case this zero limit required to extend the eigenbasis at criticality from one to three (and not two because of the additional eigenvalue in 0). For VH the unstable manifold was of dimension two (due to symmetry) but at criticality it did not turn to four as it is expected for finite dimensional systems. We can thus try the following conjecture

#### **Conjecture XI.5**

If at criticality  $\Lambda'(0^+ \pm \lambda_i) = 0$  then center manifold expansion can be done thanks to generalized eigenvectors and will provide a non singular dimensional reduction of the bifurcation.

This means that such systems could behave as finite dimensional ones, thus implying that along all the infinite dimensional effects of a Vlasov/Kuramoto like equation, one of the most essential could be the resonance effect (and removing it would change greatly the bifurcation dimension).

Nevertheless, does it mean that models with  $\Lambda'(0^+ \pm \lambda_i) \neq 0$  cannot be reduced? No, because in the standard Kuramoto exact reduction exists (Section VIII.3 and VIII.4 or [OA08, CN11, Die16b]) although  $\Lambda'(0^+ \pm \lambda_i) \neq 0$ . Hence there must be another (related?) mechanism.

### ***Nonlinear spatial Fourier mixing***

#### **Conjecture XI.6**

In an unstable manifold expansion with neutral modes (or continuum of neutral modes), the zeroth harmonic always gives the most singular (or equally singular) contribution (except if it is zero) to the bifurcation equation.

In the Kuramoto standard case there is a constant zeroth harmonic while in Vlasov systems (and probably in generic Hamiltonian systems) this is not the case.

### *Single Wave Model*

The Single Wave Model (SWM) [dCN98a, dCN98b, BMT13] is an infinite dimensional normal form of the VH model. This normal form is shared with many Hamiltonian systems like Euler 2D and the XY model. The Kuramoto model and its relatives (Ku<sup>2nd</sup>, KuI, KuD, KuID, ...) are non Hamiltonian, hence this specific SWM will not apply in these cases. Nevertheless, it is fair, looking at the similarities of these systems, to expect normal forms a la SWM for Kuramoto like models. A first attempt was made in the standard Kuramoto case in [BS00].

For the KuI model this normal form would, in the Kuramoto limit, reduce to the finite Ott-Antonsen reduction while in the Vlasov limit it should reduce to the SWM. Similarly, is it possible to obtain a normal form for the first order Kuramoto model with generic coupling [Dai92, CD99] (that would also reduce to the OA reduction with one harmonic)?

Another direction concerning this topic: since inviscid fluids and pure Vlasov model share the same SWM normal form, is it possible that they also share a more general normal form with dissipation and friction? Indeed, we have seen that the different regimes and scaling predicted in this work were similar<sup>1</sup> to the ones found for viscous fluid [CS87, CS95, CS96].

---

## 2 FURTHER WORK TO DO

---

As we just saw, while we answered many questions we also raised many others (and set aside some technical proof). Answering them all would certainly take quite some time. Thus, for now we will just list the most directly related questions that we hope to answer:

- The Triple Zero reduction of the VNH problem will be explored and tested. We hope that it will be able to predict the different behaviors observed in Figure VI.5 insets. A decisive step would be to compute the different coefficients of the normal form for the  $G_\mu^0 = \text{Eq. (VI.37b)}$  and  $F_\mu^0 = \text{Eq. (VI.37a)}$ . Then by plugging them into the normal form we could check if the behavior is consistent with the numerics. It would certainly establish further the validity of this reduction.
- What happens when the unstable eigenvalues of the VNH model are complex? We expect that the resonance phenomenon is important in this case as for VH. Hence what produces an unstable manifold calculation? Is the center manifold reduction to a normal form possible? Or will the Single Wave Model be the infinite dimensional normal form of this bifurcation (like in VH)? Or neither?
- We plan to do some numerical simulation for the Vlasov-Fokker-Planck system to check the various predicted regimes. We also plan to estimate the higher order terms.
- Does the Kuramoto model with inertia and dissipation displays such interplay between dissipation and instability?
- For the delayed Kuramoto models I will soon start a collaboration with S. Gupta to explore further these results (and probably other directions). Moreover, numerics are still lacking to support fully the preliminary predictions. In the inertialess case we managed to avoid numerical simulations since we used the ones of [YS99]. However, we predicted that there exists some critical delay  $\tau_c$  for which the bifurcation is always supercritical (for a Lorentzian). Results on generic distribution should be obtained.

---

1. The intermediate regime was slightly different but it could be due to the forcing added in the fluid system.

- Another interesting related problem would be to study the bifurcation in Kuramoto models around partially synchronized states where the stable case was recently treated in [DFGV16].



# **APPENDIXES**



---

# MAGNETO-OPTICAL-TRAP COLLABORATION

---

## 1 STRUCTURE FACTOR AND DIFFRACTED INTENSITY

---

### Dipole equations

---

In this section, we link the structure factor with an experimental observable, the diffracted intensity  $I$ . Probing the cloud with a laser of wavenumber  $k_L$  excites atoms so that they emit a field that we can measure. In linear regime and one dimension [BPK12, RSB<sup>+</sup>14] (neglecting the Doppler effect terms), atoms are considered as dipoles. The coupled equations for their amplitudes  $\beta_i$  are

$$\dot{\beta}_i = \left[ -\frac{\Gamma_d}{2} + i\delta \right] \beta_i - \frac{id_p}{\hbar} E_{\text{in}}(\vec{r}_i) + \frac{i\Gamma_d}{2} \sum_{j \neq i} V_{ij} \beta_j \quad (\text{A.1})$$

where  $V_{ij}(t) = c \frac{e^{-ik_L|\vec{r}_i - \vec{r}_j|}}{\omega_{\text{atom}}|\vec{r}_i - \vec{r}_j|}$ ,  $E_{\text{in}}$  is the shape of the monochromatic incident beam (typically plane or Gaussian wave) of pulsation  $\omega_L$  in direction  $\vec{e}_z$ ,  $d_p$  is electric dipole matrix element and  $\Gamma_d$  is the natural width of the transition. At equilibrium, one get

$$\vec{\beta} = -\frac{id_p}{\hbar} M^{-1} \vec{E}_{\text{in}} \quad (\text{A.2})$$

with

$$M = \begin{pmatrix} i\delta - \frac{\Gamma_d}{2} & & & & \\ & \ddots & & \frac{i\Gamma_d}{2} V_{ij} & \\ & & \ddots & & \\ & & & \ddots & \\ \frac{i\Gamma_d}{2} V_{ij} & & & & \\ & & & & \ddots \\ & & & & & i\delta - \frac{\Gamma_d}{2} \end{pmatrix}. \quad (\text{A.3})$$

Off diagonal terms correspond to multiple scattering. The order of magnitude of these effects are measured by the optical thickness  $b$ . In experiments  $b(\delta) \sim 1$  so it is not clear whether the effects of multiple scattering will be strong or not. In the simulations presented in Chapter II and III, we are forced to get a very small  $b \sim 4 \cdot 10^{-2}$  to achieve a cloud with a step like profile and with small correlations (like the expected experimental regime). Thus, no multiple scattering effects can be seen. A larger  $b$  would require a larger number of particles in the simulation.

In next Section, we will test on an example with larger  $b$  (but a Gaussian like density profile) the effect of multiple scattering in the diffraction profile.

## Scattered intensity

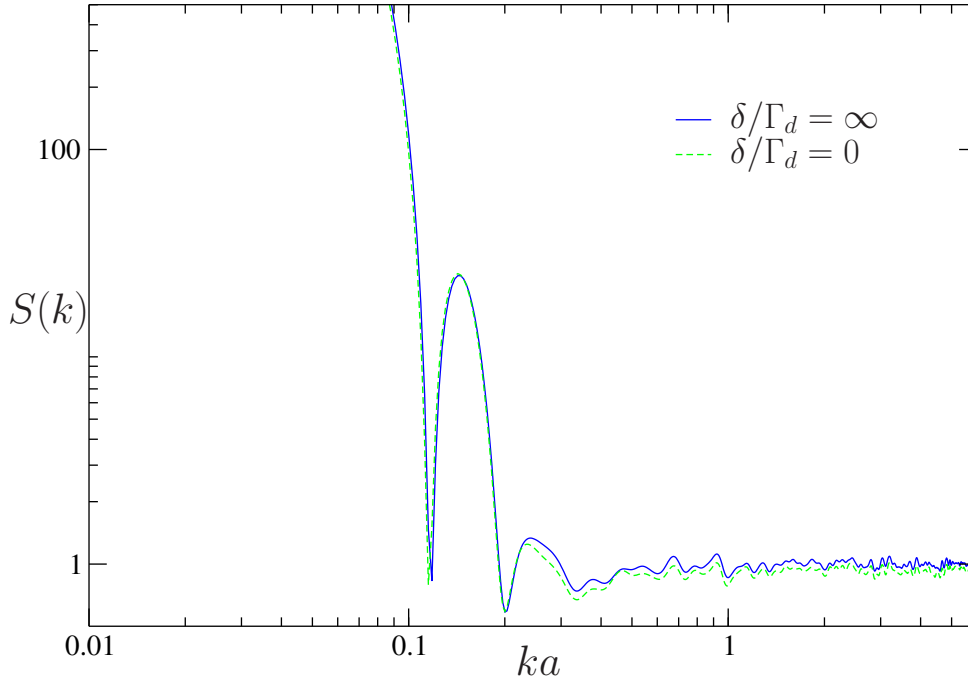


Figure A.1 – MD simulations of the structure factor  $S(k)$ ,  $T = 4$ ,  $\omega_0 = 10$ ,  $C = 0.001$ ,  $b_0 = 0.769$ .

The incident Laser intensity  $I$  is scattered in direction  $\vec{k}_f = k_L(\cos \varphi_k \sin \theta_k, \sin \varphi_k \sin \theta_k, \cos \theta_k)$ ,

see Figure II.6. For elastic scattering ( $|\vec{k}_f| = |\vec{k}_i| = k_L|\vec{e}_z|$ ), thus we have

$$I(\theta_k, \varphi_k) = \left| \left( \exp(-i\vec{k}_f \cdot \vec{r}_1), \dots, \exp(-i\vec{k}_f \cdot \vec{r}_i), \dots, \exp(-i\vec{k}_f \cdot \vec{r}_N) \right) \vec{\beta} \right|^2, \quad (\text{A.4})$$

in spherical coordinate.

In Figure A.1 we show two structure factors for the same cloud, one is obtained uniquely via simple scattering (corresponding to  $\delta/\Gamma_d = \infty$ ), and one obtained via multiple scattering (we choose to be at resonance  $\delta = 0$  where multiple scattering effects are the strongest). The optical thickness at resonance is about the one used in experiment at working regime  $b = 0.769 \sim b_{\text{exp}} \sim 1$ . The difference between the two structure factor is very thin. Thus, since the effects we seek are much bigger we can only look at the single scattering effects for a first exploration.

## 2 THEORETICAL DENSITY PROFILE

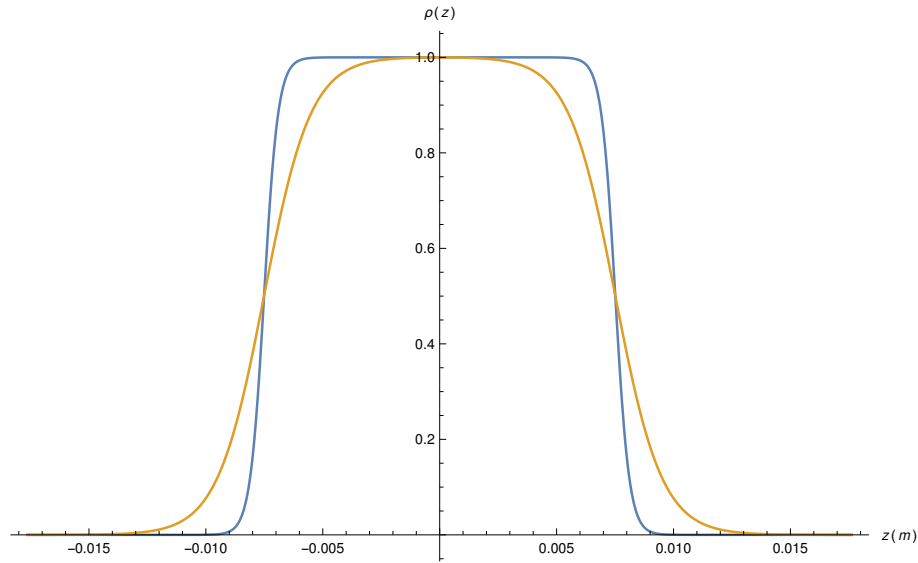


Figure A.2 – Longitudinal density  $\rho(z)$  with  $\lambda = 300 \mu\text{m}$  (blue),  $\lambda = 1 \text{ mm}$  (orange) and  $L = 7.36 \text{ mm}$  (as in the experiments)

In Section III.2.3.b we have studied an over simplified step function density profile section III.2.3.b to get a simple view of the two diffraction regimes Raman-Nath/Bragg. Here we explicit a more realistic shape (with smooth borders). We used this "realistic" density to obtain the theoretical curve in Figure III.6 that is consistent with the experimental data.

We choose on the longitudinal direction a symmetrized Fermi function Eq. (A.5). It is a step profile with a parameter  $\lambda$  controlling the smoothness of the step ( $\lambda/L$  going to 0 gives a Heaviside profile). In the perpendicular direction, we simply use a Gaussian shape with waist  $w$ . Indeed, in the experiment the probing Laser has a Gaussian shape with a width much smaller than the cloud ( $w \ll L_{\perp}$ ), thus border effects of the real density should be small in this

perpendicular plane. The mathematical expression of the symmetrized Fermi function is

$$\rho(z, r_{\perp}, L, \lambda, w) = \frac{\lambda}{L} \frac{\sinh\left(\frac{L}{\lambda}\right)}{\cosh\left(\frac{L}{\lambda}\right) + \cosh\left(\frac{z}{\lambda}\right)} \exp\left(-\frac{2r_{\perp}^2}{w^2}\right) / (\pi w^2) \quad (\text{A.5})$$

Its 3D Fourier transform can be done separately for the Gaussian and the longitudinal parts. The Fourier transform of the symmetrized Fermi function is provided in [SM97]. The result is

$$\rho(k_z, k_{\perp}) = \lambda \frac{e^{-\frac{w^2}{8} k_{\perp}^2} \pi \sin(k_z L)}{2L \sinh(\pi \lambda k_z)}. \quad (\text{A.6})$$

As an illustration, we plot, Figure A.2, the longitudinal density profiles for experimental parameters  $w = 2.2$  mm,  $L = 7.51$  mm ( $L$  is the radius of the distribution, so the FWHM is a bit larger than that, here it is around 1 cm like in the experiment). We compare two different parameter  $\lambda$  that measure the stiffness of the step.

---

# VLASOV NON HOMOGENEOUS

---

## 1 ANGLE ACTION VARIABLES

---

In this Section, we derive the explicit expression for the Fourier coefficients of the potential  $(\cos q, \sin q)$ . The Fourier coefficients are defined through

$$\mathbb{C}_m(k) = \frac{1}{2\pi} \int_{-\pi}^{\pi} \cos(q(\theta, \kappa)) e^{-im\theta}, \quad (\text{B.1a})$$

$$\mathbb{S}_m(\kappa) = \frac{1}{2\pi} \int_{-\pi}^{\pi} \sin(q(\theta, \kappa)) e^{-im\theta}. \quad (\text{B.1b})$$

We can write  $\cos q$  and  $\sin q$  explicitly in angle action variables [Oga13]:

$$\cos(q(\theta, \kappa)) = \begin{cases} 1 - 2\kappa^2 \operatorname{sn}^2\left(\frac{2K(\kappa)}{\pi}\theta, \kappa\right), & \kappa < 1 \\ 1 - 2 \operatorname{sn}^2\left(\frac{K(1/\kappa)}{\pi}\theta, \frac{1}{\kappa}\right), & \kappa > 1. \end{cases} \quad (\text{B.2a})$$

$$\sin(q(\theta, \kappa)) = \begin{cases} 2\kappa \operatorname{sn}\left(\frac{2K(\kappa)}{\pi}\theta, \kappa\right) \operatorname{dn}\left(\frac{2K(\kappa)}{\pi}\theta, \kappa\right), & \kappa < 1 \\ 2 \operatorname{sn}\left(\frac{K(1/\kappa)}{\pi}\theta, \frac{1}{\kappa}\right) \operatorname{cn}\left(\frac{K(1/\kappa)}{\pi}\theta, \frac{1}{\kappa}\right), & \kappa > 1, \quad p > 0 \\ -2 \operatorname{sn}\left(\frac{K(1/\kappa)}{\pi}\theta, \frac{1}{\kappa}\right) \operatorname{cn}\left(\frac{K(1/\kappa)}{\pi}\theta, \frac{1}{\kappa}\right), & \kappa > 1, \quad p < 0, \end{cases} \quad (\text{B.2b})$$

where definition of the complete elliptic integral of the first  $K(\kappa)$  and second kind  $E(\kappa)$  and the Jacobi elliptic functions  $\operatorname{sn}$  are given through the incomplete elliptic integral of the first and

second kind [WW96]

$$F(\phi, \kappa) = \int_0^\phi \frac{dt}{\sqrt{1 - \kappa^2 \sin^2 t}} \quad (\text{B.3a})$$

$$K(\kappa) = F(\pi/2, \kappa) \quad (\text{B.3b})$$

$$\text{sn}(F(\phi, \kappa)) = \sin \phi \quad (\text{B.3c})$$

$$E(\phi, \kappa) = \int_0^\phi \sqrt{1 - \kappa^2 \sin^2 t} dt \quad (\text{B.3d})$$

$$E(\kappa) = E(\pi/2, \kappa), \quad (\text{B.3e})$$

$$(\text{B.3f})$$

with  $K(0) = E(0) = 1$  and  $K(1^-)$  diverges. Injecting Eq. (B.2b) in Eq. (B.1b) and using reference [Mil02] for the Fourier expansion of  $\text{sn}^2$ ,  $\text{sn} \times \text{cn}$ ,  $\text{sn} \times \text{dn}$  gives the coefficients. We find

$$\mathbb{C}_0(\kappa) = \begin{cases} \frac{2E(\kappa)}{K(\kappa)} - 1, & \kappa < 1 \\ \frac{2\kappa^2 E(1/\kappa)}{K(1/\kappa)} + 1 - 2\kappa^2, & \kappa > 1 \end{cases} \quad (\text{B.4a})$$

$$\mathbb{C}_{2m}(\kappa) = \frac{2\pi^2}{K(\kappa)^2} \frac{mq(\kappa)^m}{1 - q(\kappa)^{2m}} \quad \kappa < 1 \quad (\text{B.4b})$$

$$\mathbb{C}_{2m+1}(\kappa) = 0 \quad \kappa < 1 \quad (\text{B.4c})$$

$$\mathbb{C}_m(\kappa) = \frac{2\pi^2 \kappa^2}{K(1/\kappa)^2} \frac{mq(1/\kappa)^m}{1 - q(1/\kappa)^{2m}} \quad \kappa > 1 \quad (\text{B.4d})$$

and

$$\mathbb{S}_0(\kappa) = 0 \quad (\text{B.5a})$$

$$\mathbb{S}_{2m}(\kappa) = 0 \quad \kappa < 1 \quad (\text{B.5b})$$

$$\mathbb{S}_{2m-1}(\kappa) = -i \text{sign}(m) \frac{\pi^2}{K(\kappa)^2} \frac{(2m-1)q(\kappa)^{m-1/2}}{1 + q(\kappa)^{2m-1}} \quad \kappa < 1 \quad (\text{B.5c})$$

$$\mathbb{S}_m(\kappa) = -i \text{sign}(m) \frac{2\pi^2 \kappa^2}{K(1/\kappa)^2} \frac{mq(1/\kappa)^m}{1 + q(1/\kappa)^{2m}} \quad \kappa > 1, \quad p > 0 \quad (\text{B.5d})$$

$$\mathbb{S}_m(\kappa) = i \text{sign}(m) \frac{2\pi^2 \kappa^2}{K(1/\kappa)^2} \frac{mq(1/\kappa)^m}{1 + q(1/\kappa)^{2m}} \quad \kappa > 1, \quad p < 0 \quad (\text{B.5e})$$

where the  $q$ -function is defined as

$$q(\kappa) = \exp\left(-\pi K(\sqrt{1 - \kappa^2})/K(\kappa)\right).$$

These explicit expressions are essential to manipulate the dispersion relation (for its roots or resonances). For example, thanks to the fast convergence although of the  $(\mathbb{C}_m, \mathbb{S}_m)$  coefficients, one can for numerical applications truncate safely and even estimate error. We provide the expression of  $\Lambda(\lambda)$  used to compute  $\lambda$  in Figure VI.5,

$$\Lambda(\lambda) = 1 + 4\pi \left( \sum_{n=1}^{n_M} \int_0^1 \frac{4n^2 [\mathbb{C}_{2n} \Omega \partial_\kappa \bar{f}^0](\kappa)}{\lambda^2 + 4n^2 \Omega(\kappa)^2} + 2 \sum_{m=1}^{2n_M} \int_1^\infty \frac{m^2 [\mathbb{C}_m \Omega \partial_\kappa \bar{f}^0](\kappa)}{\lambda^2 + m^2 \Omega(\kappa)^2} \right), \quad (\text{B.6a})$$

where typically  $n_M = 9$  ( $n_M = 7$ ) for  $F_\mu^0$  the Fermi distribution Eq. (VI.37a) ( $G_\mu^0$  Eq. (VI.37b)) is enough to compute  $\lambda$  with six-digit accuracy.

## 2 COMPUTATIONS AT HIGHER ORDERS

Since the effect of resonant particles was weaker than for homogeneous case (and Landau damping algebraic for long time), we expected nonlinearities to also be weaker. Are they weak enough for  $c_3 A_{\text{sat}}^3 = o(c_2 A_{\text{sat}}^2)$ ? We explain here how to compute the higher order terms. While the structure is standard, the effective computations are intricate. The first paragraph is valid for a general potential, but in order to explicitly work out the order of magnitude of  $c_3$ , we restrict to the cosine potential. We then show that  $c_3 \sim C/\lambda^3$ , as  $\lambda \rightarrow 0^+$ .

### 2.1 Structure of the computation for a general potential

Let us parameterize the unstable manifold of  $f^0$  as

$$g = \sum_{k \geq 1} H_k A^k, \quad H_1 = \Psi_c. \quad (\text{B.7})$$

Since the nonlinear part  $N[g]$  of the Vlasov equation,  $\partial_t g = \mathcal{L}g + N[g]$ , is bilinear, we write it as

$$N[g] = B(g, g), \quad \text{with } B(g, h) = \partial_J g \partial_\theta \phi[g] - \partial_\theta g \partial_J \phi[h].$$

Recalling that the reduced dynamics on the unstable manifold is

$$\dot{A} = \sum_{k \geq 1} c_k A^k, \quad c_1 = \lambda, \quad (\text{B.8})$$

our goal is to provide a formal expression for  $c_k$ . This requires computing at the same time the  $H_k$ 's. We write the time evolution equation for  $g$  in two ways:

$$\begin{aligned} \partial_t g &= \sum_{k \geq 1} \sum_{l \geq 1} A^{k+l-1} k c_l H_k \\ &= \sum_{k \geq 1} A^k \mathcal{L} H_k + \sum_{k \geq 1} \sum_{l \geq 1} A^{k+l} B(H_k, H_l), \end{aligned} \quad (\text{B.9})$$

where we have used Eq. (B.8). Picking up the terms order by order, we have for any  $k$

$$(k c_1 - \mathcal{L}) H_k = \sum_{l=1}^{k-1} [B(H_{k-l}, H_l) - (k-l) c_{l+1} H_{k-l}]. \quad (\text{B.10})$$

This equation for  $k = 1$  is simply  $\mathcal{L} \Psi_c = \lambda \Psi_c$ , and we focus on  $k \geq 2$ .

We now project these equations onto  $\text{span}\{\Psi_c\}$  and  $\text{span}\{\Psi_c\}^\perp$ ; we note the corresponding projection operators  $\Pi$  and  $\Pi^\perp = \mathbb{I} - \Pi$ , where  $\mathbb{I}$  is the identity. The projection operators work as

$$\begin{aligned} (\Pi \circ \mathcal{L}) \Psi_c &= \lambda \Psi_c, & (\Pi^\perp \circ \mathcal{L}) \Psi_c &= 0, \\ (\Pi \circ \mathcal{L}) H_k &= 0, & (\Pi^\perp \circ \mathcal{L}) H_k &= \mathcal{L} H_k, \quad k \geq 2. \end{aligned} \quad (\text{B.11})$$

The projection operator  $\Pi$  induces

$$c_k \Psi_c = \sum_{l=1}^{k-1} \Pi \circ B(H_{k-l}, H_l), \quad (\text{B.12})$$

and  $\Pi^\perp$  yields

$$(k\lambda - L)H_k = \sum_{l=1}^{k-1} \Pi^\perp \circ B(H_{k-l}, H_l) - \sum_{l=1}^{k-2} (k-l)c_{l+1}H_{k-l}. \quad (\text{B.13})$$

Equation Eq. (B.12) determines  $c_k$  from  $H_l$ , and Eq. (B.13)  $H_k$  from  $H_l$  and  $c_l$  with  $l \in \{1, \dots, k-1\}$ .

## 2.2 Cosine potential - Order of magnitude of $c_3$

---

We now specialize to the cosine potential and focus on the third order coefficient  $c_3$ .

Calling  $G_k$  the r.h.s. of Eq. Eq. (B.13), we have

$$H_k = R(k\lambda) G_k, \quad (\text{B.14})$$

where  $R(z) = (z - \mathcal{L})^{-1}$  is the resolvent of  $L$ . Our first task is to determine the  $\lambda$  dependence of  $R(k\lambda) G_k$ . Let us then consider the equation

$$(z - \mathcal{L})X = G,$$

and solve for  $X(\theta, J)$ . Denoting the  $m$ -th Fourier component of  $X$  in  $\theta$  as  $X_m$ , we find after some computations, for all  $m \in \mathbb{Z}$ :

$$X_m = \frac{G_m}{z + im\Omega(J)} - C(z) \frac{imc_m \partial_J F^0(J)}{z + im\Omega(J)} \quad (\text{B.15})$$

where

$$C(z) = \frac{2\pi \sum_l \int \frac{G_l c_l^*}{z + il\Omega(J')} dJ'}{\Lambda(z)}. \quad (\text{B.16})$$

Taking  $z = 2\lambda$  in Eq. (B.15), we see that  $\Lambda(2\lambda)^{-1}$  introduces a  $1/\lambda^2$  divergence, and that the  $m = 0$  term in the sum yields an extra  $1/\lambda$  divergence, unless  $G_{m=0} = 0$ . Thus, the  $C$  factor Eq. (B.16) gives the leading singularity.

Now, recalling Eq. (B.13), we have to apply the resolvent to  $G = \Pi^\perp B(\Psi_c, \Psi_c)$ . Using the definition of  $c_2$ , we have

$$H_2 = R(2\lambda) B(\Psi_c, \Psi_c) - c_2 R(2\lambda) \Psi_c. \quad (\text{B.17})$$

We first note that  $B(\Psi_c, \Psi_c)_{m=0} = 0$  ( $B$  contains two terms, each containing a derivative with respect to  $\theta$ ; hence the zeroth Fourier mode vanishes) and that  $\Psi_{\lambda, m=0} = 0$ . Hence the possible divergence related to  $m = 0$  in Eq. (B.15) does not exist, and the resolvent introduces only a  $1/\lambda^2$  divergence. We conclude that in the r.h.s. of Eq. (B.17), the first term is  $O(\lambda^{-2})$ . The second is a priori  $O(\lambda^{-3})$ , since  $c_2 \propto 1/\lambda$ , but we show now it is actually also  $O(\lambda^{-2})$ . The

$C$  factor Eq. (B.16) for  $(R(2\lambda)\Psi_c)_m$  is

$$\begin{aligned}
 C &= \frac{2\pi \sum_m \int \frac{\Psi_m c_m^*}{2\lambda + im\Omega(J)} dJ}{\Lambda(2\lambda)} \\
 &= \frac{2\pi}{\Lambda(2\lambda)} \sum_m \int im \frac{\partial_J F^0(J) |c_m|^2}{(\lambda + im\Omega)(2\lambda + im\Omega(J))} dJ \\
 &= \frac{2\pi}{\Lambda(2\lambda)} 6\lambda \sum_{m>0} \int m^2 \frac{\partial_J F^0(J) |c_m|^2}{|\lambda + im\Omega|^2 |2\lambda + im\Omega|^2} dJ \\
 &\sim \frac{3}{2} \frac{\Lambda'(\lambda)}{\Lambda(2\lambda)} = O(1/\lambda)
 \end{aligned}$$

where the last line is for  $\lambda \rightarrow 0^+$ . Hence, the second term in the r.h.s. of Eq. (B.17) is  $O(\lambda^{-2})$ , and so is  $H_2$ . From Eq. (B.12)

$$c_3 \Psi_c = \Pi \circ [B(H_2, \Psi_c) + B(\Psi_c, H_2)], \quad (\text{B.18})$$

where the r.h.s. is  $\Pi$  applied to a  $O(\lambda^{-2})$ . Now, the projection  $\Pi$  contains a diverging  $1/\lambda$  factor, coming from the normalization factor  $1/\Lambda'(\lambda)$ , needed in  $\tilde{\Psi}_c$  to ensure that  $\langle \tilde{\Psi}_c, \Psi_c \rangle = 1$ . Hence, except for a restricted set of functions  $\varphi$  such that  $\langle \tilde{\Psi}_c, \varphi \rangle = O(1)$ , we have (for  $\varphi$  independent of  $\lambda$ ):  $\Pi\varphi \propto \frac{1}{\lambda}$ . The exceptional  $\varphi$  such that the projection  $\Pi$  does not introduce a diverging  $1/\lambda$  factor lie close to the kernels of  $\Pi$  and  $\Pi^\perp$  (the latter is just  $\text{Span}(\Psi_c)$ ). With this in mind, it is not difficult to conclude that  $c_3 \propto 1/\lambda^3$ . This is the same divergence strength as the one which appears in the homogeneous case [Cra94a], although the mechanism inducing the divergence is different.



---

## VLASOV-FOKKER-PLANCK

---

In this Appendix, we compute in details the dependence on the friction  $\gamma$  and instability parameter  $\lambda$ , of the cubic coefficient  $c_3$ . Since the calculations are done for a small friction, the limit  $\gamma = 1/y \rightarrow 0$  will always be considered. In fact, as it is possible to check directly, in the case where  $\gamma$  is a nonzero finite constant no divergence appears.

We still use the notation  $\gamma = 1/y$  and  $a = y^2 + \lambda y$  in all this appendix, as well as  $\gamma/2 = 1/y_2$  and  $a_2 = 4y^2 + 2\lambda y$ .

The strategy of all estimation is to express the integrals in exponential form

$$\iiint e^{y^2 p(x,u,s)} ds du dx.$$

For a standard integral one would use Laplace method determining the maximum (independent of  $y$ ) and expanding around it and then make  $y \rightarrow \infty$ . We apply a similar procedure here but our maximum depends on  $y$  and in general goes toward one integration bound with  $y$ . So, we estimate the maximum  $p$  first according to  $s$ , then expand around this maximum  $s^*$  and compute the integral. Then we repeat the procedure for each integral. We can check then that neglected terms are indeed negligible around those maximum, for example if  $x^* \sim y^{-1}$ , we can safely neglect  $(\lambda y + 1)x$  in front of  $x^2 y^2$  in the exponential. It results in having a  $(1 + O(\lambda, y^{-1}))$  term for the whole integral.

# 1 ZEROTH HARMONIC CONTRIBUTION

As it can be expected from the frictionless case and for example [CS87], the divergence will come uniquely from the zeroth harmonic term. We had from Eq. (VII.30),

$$c_3^{(h_0)} = \frac{\pi^2 K^3}{4\Lambda'(\lambda)} \lambda y^2 \int_{-y}^0 \eta^{1-2\lambda y} (1 + \eta/y)^{a-1} e^{-y\eta} \int_0^\eta t^{2\lambda y} (d(a^*, y^2 - yt) - d(a, y^2 + yt)) dt d\eta. \quad (\text{C.1})$$

After changing variables in both integrals  $x = -\eta/y$  and  $u = -t/(xy)$

$$c_3^{(h_0)} = -\frac{\pi^2 K^3}{4\Lambda'(\lambda)} \lambda y^5 \int_0^1 x^2 (1-x)^{a-1} e^{y^2 x} \int_0^1 u^{2\lambda y} (d(a, y^2(1+ux)) - d(a, y^2(1-ux))) du dx. \quad (\text{C.2})$$

## 1.1 Diverging term

We will use the expression of  $d(a, x)$  as an integral over  $[0, 1]$  Eq. (VII.10). We first look at the left term that will diverge:

$$B^{(1)} = -\frac{\pi^2 K^3}{4\Lambda'(\lambda)} \lambda y^5 \int_0^1 \int_0^1 \int_0^1 x^2 e^{y^2 p(x,u,s)} ds du dx, \quad (\text{C.3})$$

were

$$p(x, u, s) = x + (1 + ux)s + \ln(1 - x) + \ln(1 - s) + \frac{\lambda}{y} (2 \ln u + \ln(1 - x) + \ln(1 - s)) - \frac{1}{y^2} (\ln(1 - x) + \ln(1 - s)). \quad (\text{C.4})$$

The goal of this formulation in the spirit of the Laplace approach, find the maximum and expand around it. For  $\lambda \gg y^{-1/3}$  we will prove self consistently that  $x^* \sim (\lambda y)^{-1}$  and for  $\lambda \ll y^{-1/3}$ ,  $x^* \sim y^{-2/3}$ .

Here we develop the expression first for small  $s$ , assuming  $1 - u$  small, which will be self consistently proved.

$$p_s(x, u, s) = \left( ux - \frac{\lambda}{y} + \frac{1}{y^2} \right) s - \frac{s^2}{2} + O\left(\frac{\lambda}{y} s^2, \frac{1}{y^2} s^2\right) = ux s - \frac{s^2}{2} + O\left(\frac{\lambda}{y} s, \frac{1}{y^2} s\right) \quad (\text{C.5})$$

where the last maximum was obtained using the scaling of  $x^*$  (terms like  $x^\infty y$  will always go to infinity). So, it gives for the integral over  $s$ ,

$$B^{(1)} = -2\sqrt{\frac{\pi}{2}} \frac{\pi^2 K^3}{4\Lambda'(\lambda)} \lambda y^4 \int_0^1 \int_0^1 x^2 \exp(y^2 p_u(x, u)) \left(1 + O\left(\frac{\lambda}{y}, \frac{1}{y^2}\right)\right) ds du dx, \quad (\text{C.6})$$

with

$$p_u(x, u) = \frac{x^2 u^2}{2} + 2 \frac{\lambda}{y} \ln u + x + \ln(1-x) + \frac{\lambda}{y} \ln(1-x) + \frac{1}{y^2} \ln(1-x). \quad (\text{C.7})$$

As stated before the maximum in  $u$  is situated near  $u = 1$  so we can expand as  $\delta u = 1 - u \ll 1$ ,

$$p_u(x, u) = - \left( x^2 + 2 \frac{\lambda}{y} \right) \delta u + \frac{x^2}{2} + \text{O}(\delta u^2) + x + \ln(1-x) + \frac{\lambda}{y} \ln(1-x) + \frac{1}{y^2} \ln(1-x). \quad (\text{C.8})$$

So, we can integrate

$$B^{(1)} = -2 \sqrt{\frac{\pi}{2}} \frac{\pi^2 K^3}{4\Lambda'(\lambda)} \lambda y^4 \int_0^1 \frac{\exp(y^2 p_x(x))}{y^2 x^2 + 2\lambda y} \left( 1 + \text{O}\left(\frac{\lambda}{y}, \frac{1}{y^2}\right) \right) ds du dx, \quad (\text{C.9})$$

where

$$p_x(x) = \frac{x^2}{2} + x + \ln(1-x) + \frac{\lambda}{y} \ln(1-x) + \frac{1}{y^2} \ln(1-x) + 2 \ln x. \quad (\text{C.10})$$

Again, expanding for small  $x$  where the maximum is situated, we have

$$p_x(x) = - \left( \frac{\lambda}{y} + \frac{1}{y^2} \right) x - \frac{x^3}{3} + 2 \ln x. \quad (\text{C.11})$$

This gives

$$B^{(1)} = -2 \sqrt{\frac{\pi}{2}} \frac{\pi^2 K^3}{4\Lambda'(\lambda)} \lambda y^4 \int_0^1 x^2 \frac{\exp\left(- (2\lambda y - 1)x - y^2 \frac{x^3}{3}\right)}{y^2 x^2 + 2\lambda y} \left( 1 + \text{O}\left(\frac{\lambda}{y}, \frac{1}{y^2}\right) \right) dx. \quad (\text{C.12})$$

The maximum  $x^*$  depends on which of the two terms  $(x^*)^2 y^2$ ,  $\lambda y$  dominate. We find as already formulated that  $x^* \sim (\lambda y)^{-1}$  and for  $\lambda \ll y^{-1/3}$ ,  $x^* \sim y^{-2/3}$ . So  $(x^*)^2 y^2 \ll \lambda y$  for  $\lambda \gg y^{-1/3}$  and  $(x^*)^2 y^2 \gg \lambda y$  for  $\lambda \ll y^{-1/3}$ .

— It gives for  $\lambda \gg y^{-1/3}$ ,

$$B^{(1)} \sim -2 \sqrt{\frac{\pi}{2}} \frac{\pi^2 K^3}{4\Lambda'(\lambda)} \frac{1}{4\lambda^3} = -\pi^2 K^2 \frac{1}{4\lambda^3}. \quad (\text{C.13})$$

It is exactly as in [V.54](#).

— For  $\lambda \ll y^{-1/3}$ ,

$$B^{(1)} \sim -2 \sqrt{\frac{\pi}{2}} \frac{\pi^2 K^3}{4\Lambda'(\lambda)} \frac{\lambda y^{4/3} \Gamma\left(\frac{1}{3}\right)}{3^{2/3}}, \quad (\text{C.14})$$

so, when  $\lambda \ll \gamma^{4/3}$   $B^{(1)}$  does not diverge and is a priori of order 1.

## 1.2 Non diverging term

---

The second term is non divergent as we will quickly see

$$B^{(2)} = \frac{\pi^2 K^3}{4\Lambda'(\lambda)} \lambda y^5 \int_0^1 \int_0^1 \int_0^1 x^2 e^{y^2 p(x,u,s)} ds du dx, \quad (\text{C.15})$$

were

$$p(x, u, s) = x + (1 - ux)s + \ln(1 - x) + \ln(1 - s) + \frac{\lambda}{y}(2 \ln u + \ln(1 - x) + \ln(1 - s)) - \frac{1}{y^2}(\ln(1 - x) + \ln(1 - s)). \quad (\text{C.16})$$

The maximum is still close to zero so we expand

$$p_s(x, u, s) = \left(-ux - \frac{\lambda}{y} + \frac{1}{y^2}\right)s - \frac{s^2}{2} + O\left(\frac{\lambda}{y}s^2, \frac{1}{y^2}s^2\right) = uxs - \frac{s^2}{2} + O\left(\frac{\lambda}{y}s, \frac{1}{y^2}s\right). \quad (\text{C.17})$$

The difference here is the minus sign in front of  $ux$  which makes the maximum negative  $s^* < 0$ . It means that the maximum on this  $s \in [0, 1]$  interval is reached at  $s = 0$  for large  $y$  assuming  $u^* x^* \gg \frac{\lambda}{y}, \frac{1}{y^2}$  (which we will check thereafter). The implication is that we can use the Laplace formula for a maximum situated at a boundary [Avr00] (which says that instead of integrating  $p''(s^*s)s^2/2$  we integrate  $p'(s^*)s$ ). In our formalism, we consider  $uxs \gg s^2$ .

$$B^{(2)} = \frac{\pi^2 K^3}{4\Lambda'(\lambda)} \lambda y^3 \int_0^1 \int_0^1 \int_0^1 \frac{x}{u} u^{2\lambda y} e^{y^2 p_x(x)} du dx, \quad (\text{C.18})$$

with

$$p_x(x) = x + \ln(1 - x) + \frac{\lambda}{y} \ln(1 - x) + \frac{1}{y^2} \ln(1 - x). \quad (\text{C.19})$$

The integration over  $u$  is in fact immediate and produce a  $(\lambda y)^{-1}$  factor, thus

$$B^{(2)} = \frac{\pi^2 K^3}{4\Lambda'(\lambda)} y^2 \int_0^1 \int_0^1 \int_0^1 x e^{y^2 p_x(x)} dx, \quad (\text{C.20})$$

$$p_x(x) + \ln x = y^{-2} \ln x - \frac{x^2}{2} - \left(\frac{\lambda}{y} + \frac{1}{y^2}\right)x + O\left(x^3, \frac{\lambda}{y}x^2, \frac{1}{y^2}x^2\right) \quad (\text{C.21})$$

the quadratic term always dominates, the maximum is  $x^* \sim 1/y$ . The remaining integral is

$$\propto \int x e^{\frac{y^2 x^2}{2}} dx.$$

It cancels the last  $y^2$  prefactor thus the whole  $B^{(2)}$  coefficient is finite. It is easy to check self consistently that neglected terms are indeed small.

## 2 SECOND HARMONIC CONTRIBUTION

We use the notation  $\gamma/2 = 1/y_2$  and  $a_2 = 4y^2 + 2\lambda y$ . So  $y_2 = 2y$ . We have

$$\widehat{h}_{2,0}(\eta) = -\frac{K^2}{8}\sqrt{2\pi}e^{-\eta^2/2}\frac{e^{\eta y_2}}{2}\left(1+\frac{\eta}{y_2}\right)^{-a_2}\int_{-y_2}^{\eta}te^{-y_2t}(1+t/y_2)^{a_2-1}(1-\lambda yd(a,y^2+yt))dt. \quad (\text{C.22})$$

The associated cubic coefficient is

$$c_3^{(h_2)} = \frac{\pi^2 K^3}{8\Lambda'(\lambda)}\int_{-y}^0\eta e^{-\eta y}\left(1+\frac{\eta}{y}\right)^{a-1}e^{\eta y_2}\left(1+\frac{\eta}{y_2}\right)^{-a_2}\times \int_{-y_2}^{\eta}te^{-y_2t}(1+t/y_2)^{a_2-1}(1-\lambda yd(a,y^2+yt))dtd\eta. \quad (\text{C.23})$$

Here  $-2y \geq t \geq 0$  So the term

$$\begin{aligned} \lambda yd(a,y^2+yt) &= \lambda y\int_0^1e^{(y^2+yt)s}(1-s)^{a-1}ds \leq \lambda y\int_0^1e^{y^2s}(1-s)^{a-1}ds \\ &= \lambda ye^{y^2}y^{-2a}\gamma(a,y^2) \sim \lambda\sqrt{\frac{\pi}{2}} \rightarrow 0 \end{aligned} \quad (\text{C.24})$$

where we used known equivalent of the lower incomplete Gamma function [Par02] for the situation  $\text{Re}(y^2 - a) \geq 0$  and  $\text{Re}(y^2 - a)/y \rightarrow 0$ .

So

$$|c_3^{(h_2)}| \leq \left|\frac{\pi^2 K^3}{8\Lambda'(\lambda)}\int_{-y}^0\frac{e^{\eta y_2}}{2}\left(1+\frac{\eta}{y_2}\right)^{-a_2}\int_{-y_2}^{\eta}te^{-y_2t}(1+t/y_2)^{a_2-1}dtd\eta\right|. \quad (\text{C.25})$$

The integral over  $t$  can be re-expressed with the  $d(a, x)$  function as

$$|c_3^{(h_2)}| \leq \left|\frac{\pi^2 K^3}{8\Lambda'(\lambda)}\int_{-y}^0\eta e^{-\eta y}\left(1+\frac{\eta}{y}\right)^{a-1}\left(1-\lambda y_2d(a_2,y_2^2+y_2\eta)\right)d\eta\right|. \quad (\text{C.26})$$

Once again, the terms

$$2\lambda yd(a_2,y_2^2+y_2\eta) \leq \lambda ye^{4y^2}(2y)^{-2a_2}\gamma(a_2,4y^2) \sim \lambda\sqrt{\frac{\pi}{2}},$$

so we can bound further the coefficient

$$|c_3^{(h_2)}| \leq \left|\frac{\pi^2 K^3}{8\Lambda'(\lambda)}\int_{-y}^0\eta e^{-\eta y}\left(1+\frac{\eta}{y}\right)^{a-1}d\eta\right|. \quad (\text{C.27})$$

The integrand can be written as an exponential  $e^{y^2p(x)}$ ,

$$\int_{-y}^0\eta e^{-\eta y}\left(1+\frac{\eta}{y}\right)^{a-1}d\eta = -y^2\int_0^1e^{y^2(x+\ln(1-x))+\ln x+(\lambda y-1)\ln(1-x)}dx \quad (\text{C.28})$$

which give a maximum  $x^* \sim y^{-1}$  so the exponent can be safely expanded for small  $x$ . So

$$\begin{aligned} -y^2 \int_0^1 e^{y^2(x+\ln(1-x))+\ln x+(\lambda y-1)\ln(1-x)} dx &= -y^2 \int_0^1 x e^{y^2 \frac{x^2}{2}} (1 + O(\lambda, y^{-1})) dx \\ &= -1 - O(\lambda, y^{-1}). \end{aligned} \quad (\text{C.29})$$

Which conclude that  $c_3^{(h_2)}$  does not display any divergences. It is also easy to observe with Eq. (C.23) that  $c_3^{(h_2)} < 0$ .

---

# THE KURAMOTO MODELS

---

## 1 KURAMOTO WITH INERTIA

---

In this Section we show how to recover Vlasov and standard Kuramoto limit from the Kuramoto with inertia model.

### 1.1 Standard Kuramoto limit, $m \rightarrow 0$

---

We have to take first the limit  $m \rightarrow 0$ , before  $\lambda_R \rightarrow 0$ . Counting the powers of  $m$  in Eq. (IX.28) shows that the whole contribution of  $h_{0,0}$  vanishes in this limit, even taking into account the overall  $1/m$  factor in front of the  $O(A^3)$  term, see Eq. (IX.20). Similarly, the  $X_1$  and  $X_2$  terms in Eq. (IX.29) give a vanishing contribution in the  $m \rightarrow 0$  limit. Let us estimate the  $X_0$  term:

$$\int -\tilde{\psi}^{(1)*}(\omega) X_0(\omega) d\omega \underset{m \rightarrow 0^+}{\sim} \frac{im e^{2i\alpha}}{\Lambda'(\lambda)} \frac{\pi K^2}{2} \int \frac{g(\omega)}{(\lambda + i\omega)^3} d\omega.$$

One may then take the  $\lambda_R \rightarrow 0^+$  limit, and this yields the following result

$$\lim_{\lambda_R \rightarrow 0^+} c_3 = \frac{\pi^2 K^2}{2} \frac{\Lambda''(i\lambda_I)}{\Lambda'(i\lambda_I)}, \quad (\text{D.1})$$

where we have used the expression for  $\Lambda$  in the limit  $m \rightarrow 0$ :

$$\Lambda(\lambda) = 1 - \frac{K}{2} e^{i\alpha} \int \frac{g(\omega)}{\lambda + i\omega} d\omega.$$

This recovers the expression for the standard Kuramoto model, see Eq.(139) in [Cra94a]. In particular, the sign of  $s^0(\alpha) = \text{Re} \left( \frac{\Lambda''(i\lambda_I)}{\Lambda'(i\lambda_I)} \right)$  determines the type of the bifurcation:  $s^0 > 0$  (resp.  $s^0 < 0$ ) corresponds to a subcritical (resp. supercritical) bifurcation.

## 1.2 Hamiltonian (Vlasov) limit, $\alpha = 0$ , $m \rightarrow \infty$ , $K \rightarrow \infty$ , $K/m = \text{cst}$

---

The Vlasov limit consists in taking  $m \rightarrow \infty$ ,  $K \rightarrow \infty$  while keeping  $K/m = \text{cst}$  (this cancels the friction and the natural frequency driving), and  $\alpha = 0$  (no shift between oscillator). As in the general case the  $h_{2,0}$  term does not give any pinching singularity. Here as in [Cra95a] we use a fraction decomposition to get

$$\begin{aligned}
 & \int \left( \tilde{\psi}^{(2)*}(W_1^* + W_1) - \tilde{\psi}^{(3)*}(W_2^* + W_2) \right) d\omega = \\
 & \frac{-2i\pi}{\lambda_R \Lambda'(\lambda)} \left( \frac{K}{2m} \right)^2 \int \frac{g(\omega) (3\lambda^* - \lambda - 4i\omega)}{(\lambda + i\omega)^4 (\lambda^* - i\omega)^2} d\omega + O(\lambda_R^{-1}) \\
 & = \frac{2i\pi}{\Lambda'(\lambda)} \left( \frac{K}{2m} \right)^2 \int \left( \frac{-1}{8\lambda_R^4 (\lambda + i\omega)^2} + \frac{1}{8\lambda_R^4 (\lambda^* - i\omega)^2} \right. \\
 & \quad \left. - \frac{1}{2\lambda_R^3 (\lambda + i\omega)^3} \right) g(\omega) d\omega + O(\lambda_R^{-2}) \\
 & = \frac{i\pi}{\Lambda'(\lambda)} \frac{K}{2m} \left( \frac{\Lambda(\lambda) - 1 - \Lambda(\lambda^*) + 1}{4\lambda_R^4} - \frac{\Lambda'(\lambda)}{2\lambda_R^3} \right) + O(\lambda_R^{-2}) \\
 & = -\frac{i\pi}{4\lambda_R^3} \frac{K}{m} + O(\lambda_R^{-2}),
 \end{aligned} \tag{D.2}$$

where we have used  $\Lambda(\lambda) = \Lambda(\lambda^*) = 0$ . Finally, in the limit  $\lambda_R \rightarrow 0^+$

$$c_3 \sim -\frac{\pi^2 K^2}{4m^2} \frac{1}{\lambda_R^3}. \tag{D.3}$$

It is the exact same result (with  $K = 1$ ) than Eq.(V.54). As noted by Crawford this result does not depend on the initial velocity distribution. The  $1/\lambda_R^3$  divergence yields the well know trapping scaling for the instability's saturation amplitude  $|A|_\infty \propto \lambda_R^2$ .

## 2 THE SELF-CONSISTENT MEAN-FIELD METHOD, AND BISTABLE BEHAVIOR

---

The self-consistent method (introduced in the original Kuramoto article [Kur75], and later adapted to the case with inertia [TLO97a, TLO97b]) is a standard tool to understand qualitatively Kuramoto-like models. We show here that:

i) The bistability of single oscillators pointed out in [TLO97a, TLO97b] as the origin of the hysteretic behavior at large inertia cannot explain the results at small mass presented in figure IX.1 of the main article.

ii) Nevertheless, the self-consistent method does predict a discontinuous transition for the parameters of figure 1, although it is difficult to make a general statement.

The basis of the method is to assume a constant value for the order parameter  $r$ . Then, considering the dynamics of the single oscillators with this  $r$ , one may evaluate the contribution of each oscillator to the order parameter, and write a self-consistent equation.

## 2.1 Bistable behavior

---

We assume that  $r$  is fixed, and take its phase to be 0 without loss of generality. The dynamics for a single oscillator with intrinsic frequency  $\omega$  is (in rescaled parameters)

$$m\ddot{\theta} + \dot{\theta} = \omega - Kr \sin \theta. \quad (\text{D.4})$$

Through the change of variable  $t = Ts$  with  $T = 1/Kr$ , the dynamics reduces to (keeping the notation  $\theta$ )

$$M \frac{d^2\theta}{ds^2} + \frac{d\theta}{ds} = \Omega - \sin \theta, \quad (\text{D.5})$$

with  $M = mKr$  and  $\Omega = \omega/Kr$ . When  $M = 0$ , Eq. (D.5) has a single attractive fixed point for small  $\Omega$  (corresponding to phase locked oscillators); this fixed point collides with an unstable one for  $\Omega = 1$ , and the dynamics becomes periodic (drifting oscillators). This behavior persists for small enough  $M$ . However, a qualitative change occurs for  $M = M_{\text{crit}} \simeq 0.83$ . Beyond this point, there is a range of values for  $\Omega$  where the stable fixed point coexists with an attractive periodic orbit: the dynamics Eq. (D.5) is bistable.

Notice that the curves presented on Figure IX.1 for  $m = 0.25$  and  $m = 0.5$  feature in the transition region  $K < 3$  and  $r < 0.5$ ; thus, the reduced mass  $M < M_{\text{crit}}$ , and bistability of the single oscillator dynamics cannot explain the discontinuous transition.

Nevertheless, it is possible that the self-consistent mean-field method predict a discontinuous transition, even without bistability of the single oscillator dynamics.

## 2.2 Self-consistent equation

---

We compute now the self-consistent equation "à la Kuramoto" for the parameters of figure 1,  $m = 0.5$ ; the starting point is Eq. (D.4). We have seen that there is no bistability for individual oscillators (at least in the transition region). Thus, the self-consistent equation simply reads as the sum of the contributions of locked and drifting oscillators:

$$r = r_{\text{locked}} + r_{\text{drift}}. \quad (\text{D.6})$$

The locked part is [TLO97a]

$$r_{\text{locked}} = Kr \int_{-\pi/2}^{\pi/2} \cos^2 \theta g(Kr \sin \theta) d\theta. \quad (\text{D.7})$$

The drifting part is more involved:

$$r_{\text{drift}} = 2 \int_{\omega > Kr} \frac{g(\omega)}{T(\omega)} \int_{-\pi}^{\pi} \frac{\cos \theta}{V_{\omega}(\theta)} d\theta, \quad (\text{D.8})$$

where  $(\theta, V_\omega(\theta))$  is the attractive periodic orbit for an oscillator with intrinsic frequency  $\omega$ , and  $T(\omega)$  is the period of this orbit. The factor 2 in front comes from the  $\omega \rightarrow -\omega$  symmetry. Eq. (D.8) is usually computed in the large  $m$  regime (or rather large  $M$ ), which is of no interest to us. It would be possible to perform a small  $M$  expansion. The results presented on Figure IX.1 rely instead on a direct numerical estimation of Eq. (D.7) and Eq. (VIII.6). For small  $K$ , Eq. (D.6) has a single solution,  $r = 0$ . Increasing  $K$ , two new solutions appear  $r_<$  and  $r_>$ , at finite distance from 0. On figure , we have plotted the  $r_>$  solution as soon as it appears, although the  $r = 0$  solution may still be stable. We see that this self-consistent method i) does predict a discontinuous transition for these parameters, and is in fair quantitative agreement with the numerical data ii) does not easily provide general statements about the transition, for different values of the parameters, and different frequency distributions.

### 3 SIGN OF DISPERSION RELATION DERIVATIVE

---

#### 3.1 Standard Kuramoto model

---

The standard Kuramoto model has an  $\mathcal{O}(2)$  symmetry (reflection and rotation invariance) when the distribution of natural frequencies  $g$  is symmetric. In this situation when  $K > K_c$  the system becomes linearly unstable and unstable eigenvalue(s) are

- i) One real eigenvalue  $\lambda$  with an associated eigenspace of dimension 2. Thus, the unstable manifold is also of dimension two.  $g$  is even.
- ii) Two complex conjugate eigenvalues  $\lambda, \lambda^*$  with where each are associated to an eigenspace of dimension 2. This yields an unstable manifold of dimension 4.  $g$  is even.

If the  $\mathcal{O}(2)$  symmetry is broken, situation iii), eigenvalues are always complex conjugate with an associated eigenspace of dimension 1. This yields an unstable manifold of dimension 2.

In this Ph.D. thesis, we focused on unstable manifold of dimension 1 or 2 to avoid more intricate computation. For an example treated by J.D. Crawford see [Cra94a]. Hence, we want to avoid case ii).

In case i) the final result of the unstable manifold was

$$c_3 = \frac{\pi^2 K^2}{2} \frac{\Lambda''(\lambda)}{\Lambda'(\lambda)} \xrightarrow{\lambda \rightarrow 0} \frac{\pi^3 K_c^2}{4} \frac{g''(0)}{-\text{PV} \int (g'(\omega)/\omega) d\omega} \quad (\text{D.9})$$

where we used

$$\Lambda'(0) = -\frac{K_c}{2} \text{PV} \int \frac{g'(\omega)}{\omega} d\omega \quad (\text{D.10a})$$

$$\Lambda''(0) = \frac{K_c}{2} \frac{\pi g''(0)}{2}. \quad (\text{D.10b})$$

The conclusion was that the sub/super-critical behavior of the transition was given by the sign  $g''(0)$ . But what if  $\Lambda'(0)$  was negative? Can this happen for some well-chosen distribution?

In this Section, we conjecture that in case i)  $\Lambda'(0) > 0$ . In fact, we also conjecture that the transition between case i) and ii) is given by  $\Lambda''(0) = 0$ .

We are able to demonstrate this claim only for unimodal and bimodal distribution (and bimodal like distribution).

### Unimodal distribution

Unimodal functions are functions with  $g'(\omega) \leq 0$  for  $\omega > 0$ . In this case the demonstration is direct since we always have  $\Lambda'(0) > 0$ .

### Bimodal distribution

Bimodal functions are function one local maximum for  $\omega > 0$  and  $g''(0) > 0$ . At the criticality  $K = K_c$  the dispersion relation Eq. (VIII.12c) satisfies in case i) and ii) (complex or real eigenvalue)

$$\begin{cases} \text{PV} \int \frac{g(\omega - \lambda_i)}{\omega} d\omega = 0 \\ \frac{2}{K_c(\lambda_i)} = \pi g(\lambda_i). \end{cases} \quad (\text{D.11})$$

The first equation gives the admissible values for  $\lambda_i$ , while the second give the associated  $K_c$ .

We define

$$\begin{cases} d(\lambda) = \text{PV} \int \frac{g(\omega - \lambda)}{\omega} d\omega = \int_0^\infty \frac{g(\omega - \lambda) - g(\omega + \lambda)}{\omega} d\omega \\ d'(\lambda) = - \int_0^\infty \frac{g'(\omega - \lambda) + g'(\omega + \lambda)}{\omega} d\omega. \end{cases} \quad (\text{D.12})$$

Note that  $d(0) = 0$  for every (symmetric)  $g$ . Hence, we want to show:

$d'(0) < 0 \Rightarrow \exists \lambda_i > 0$  such that  $d(\lambda_i) = 0$  and  $g(\lambda_i) > g(0)$  (which directly implies that  $K_c(\lambda_i) < K_c(0)$ ).

It says that if  $\Lambda'(0) < 0$  is negative then, there exists a pair of complex eigenvalue, and these complex eigenvalues go unstable first and thus drive the instability, this is case ii).

To prove the first implication, we just need to prove  $d(\lambda) \xrightarrow{\lambda \rightarrow \infty} 0^+$ . Indeed since  $d(0) = 0$  and we assumed  $d'(0) < 0$ ,  $d$  is negative for small  $\lambda$  and if it has a positive limit by continuity, there must exist at least one root  $\lambda_i$ . If we call the integrand of  $d$

$$s(\omega) = \frac{g(\omega - \lambda) - g(\omega + \lambda)}{\omega} \quad (\text{D.13})$$

we have  $s(0) = -2g'(\lambda)$  and  $s'(0) = -2g''(\lambda)$ ,  $s(\infty) = 0^+$  because we chose  $g$  to decrease monotonically at infinity.

To prove the second part the idea is to prove that  $\lambda_i \in ]0, \lambda_{\max}]$  where  $\lambda_{\max}$  is the position of the maximum. In this case  $g(\lambda_i) > g(0)$  We proceed with a proof by contradiction Suppose  $\lambda_i \in [\lambda_{\max}, +\infty[$ . Then  $s_{\lambda_i}(\omega) \geq 0$  (since in this interval of a binomial function we have  $g'(\omega) \leq 0$ ). Hence  $d(\lambda_i) > 0$  and  $\lambda_i$  is not a root of  $d$ . Absurd!

Thus if  $\lambda_i$  exists  $\lambda_i \in [0, \lambda_{\max}[$  with  $K_c(\lambda_i) < K_c(0)$ .

This reasoning can be applied to slightly more generic bimodal-like distributions but no general results has been found so far. One can check explicitly that for a bi-Lorentzian distribution Eq. (VIII.28) the criteria from case i) to case ii) (partial synchronized state to standing wave [Cra94a, MBS<sup>+</sup>09]) corresponds to  $\Lambda'(0) = 0$ .

### 3.2 Kuramoto with inertia

---

In the case with inertia the relations given by the dispersion relation Eq. (IX.8) at criticality are more difficult to analyze and looking at  $g(0)$  and  $g(\lambda_i)$  is not enough.

---

## BIBLIOGRAPHY

---

- [ABS00] J. A. Acebrón, L. L. Bonilla, and R. Spigler. Synchronization in populations of globally coupled oscillators with inertial effects. Physical Review E, 62(3):3437–3454, September 2000. - Cited 3 times: pages 167, 168 and 169 -
- [AEM<sup>+</sup>95] Mike H Anderson, Jason R Ensher, Michael R Matthews, Carl E Wieman, and Eric A Cornell. Observation of Bose-Einstein condensation in a dilute atomic vapor. science, 269(5221):198, 1995. - Cited 1 time: page 27 -
- [AR95] Mickael Antoni and Stefano Ruffo. Clustering and relaxation in Hamiltonian long-range dynamics. Physical Review E, 52(3):2361–2374, September 1995. - Cited 1 time: page 91 -
- [AS98] J. A. Acebrón and R. Spigler. Adaptive Frequency Model for Phase-Frequency Synchronization in Large Populations of Globally Coupled Nonlinear Oscillators. Physical Review Letters, 81(11):2229–2232, September 1998. - Cited 2 times: pages 165 and 167 -
- [Avr00] Ivan Avramidi. Lecture notes on asymptotic expansion. University lectures, 2000. - Cited 1 time: page 216 -
- [Bal99] NJ Balmforth. Shear instability in shallow water. J. Fluid Mech., 387:99–127, 1999. - Cited 2 times: pages 142 and 148 -
- [BBDR05] Julien Barré, Freddy Bouchet, Thierry Dauxois, and Stefano Ruffo. Large Deviation Techniques Applied to Systems with Long-Range Interactions. Journal of Statistical Physics, 119(3-4):677–713, May 2005. - Cited 1 time: page 18 -
- [BGK57] Ira B. Bernstein, John M. Greene, and Martin D. Kruskal. Exact Nonlinear Plasma Oscillations. Physical Review, 108(3):546–550, November 1957. - Cited 1 time: page 77 -
- [BH77] W. Braun and K. Hepp. The Vlasov dynamics and its fluctuations in the 1/N limit of interacting classical particles. Communications in Mathematical Physics, 56(2):101–113, June 1977. - Cited 1 time: page 20 -

- [BH80] Marc Baus and Jean-Pierre Hansen. Statistical mechanics of simple coulomb systems. Physics Reports, 59(1):1–94, March 1980. - Cited 1 time: page 48 -
- [BH07] A. J. Brizard and T. S. Hahm. Foundations of nonlinear gyrokinetic theory. Reviews of Modern Physics, 79(2):421–468, April 2007. - Cited 1 time: page 21 -
- [BKNG09] Balakumar Balachandran, Tamás Kalmár-Nagy, and David E. Gilsinn. Delay Differential Equations: Recent Advances and New Directions. Springer Science & Business Media, April 2009. - Cited 1 time: page 178 -
- [BL08] Jean-Michel Bismut and Gilles Lebeau. The Hypoelliptic Laplacian and Ray-Singer Metrics. (AM-167). Princeton University Press, August 2008. - Cited 2 times: pages 139 and 142 -
- [BM16] J. Barré and D. Métivier. Bifurcations and Singularities for Coupled Oscillators with Inertia and Frustration. Physical Review Letters, 117(21):214102, November 2016. - Cited 2 times: pages 166 and 167 -
- [BM17a] Julien Barré and David Métivier. Unstable manifold expansion for Vlasov-Fokker-Planck equation. [arXiv:1703.01668 \[cond-mat, physics:math-ph\]](https://arxiv.org/abs/1703.01668), March 2017. arXiv: 1703.01668. - Cited 3 times: pages 139, 142 and 145 -
- [BM17b] F. P. C. Benetti and B. Marcos. Collisional relaxation in the inhomogeneous Hamiltonian mean-field model: Diffusion coefficients. Physical Review E, 95(2):022111, February 2017. - Cited 1 time: page 116 -
- [BMT13] N. J. Balmforth, P. J. Morrison, and J.-L. Thiffeault. Pattern formation in Hamiltonian systems with continuous spectra; a normal-form single-wave model. [arXiv:1303.0065 \[cond-mat, physics:math-ph, physics:nlin\]](https://arxiv.org/abs/1303.0065), February 2013. arXiv: 1303.0065. - Cited 10 times: pages 85, 89, 95, 107, 116, 117, 130, 148, 176 and 198 -
- [BMW14] J. Barré, B. Marcos, and D. Wilkowski. Nonequilibrium Phase Transition with Gravitational-like Interaction in a Cloud of Cold Atoms. Physical Review Letters, 112(13):133001, March 2014. - Cited 1 time: page 36 -
- [BMWZ85] C. Burnap, M. Miklavcic, B. L. Willis, and P. F. Zweifel. Single-mode saturation of a linearly unstable plasma. The Physics of Fluids, 28(1):110–115, January 1985. - Cited 1 time: page 88 -
- [BMY16] J. Barré, D. Métivier, and Y. Y. Yamaguchi. Trapping scaling for bifurcations in the Vlasov systems. Physical Review E, 93(4):042207, April 2016. - Cited 4 times: pages 89, 92, 111 and 124 -
- [Bog75] R. I. Bogdanov. Versal deformations of a singular point of a vector field on the plane in the case of zero eigenvalues. Functional Analysis and Its Applications, 9(2):144–145, April 1975. - Cited 1 time: page 134 -
- [BOY10] Julien Barré, Alain Olivetti, and Yoshiyuki Y. Yamaguchi. Dynamics of perturbations around inhomogeneous backgrounds in the HMF model. Journal of Statistical Mechanics: Theory and Experiment, 2010(08):P08002, 2010. - Cited 2 times: pages 114 and 116 -

- 
- [BOY11] Julien Barré, Alain Olivetti, and Yoshiyuki Y. Yamaguchi. Algebraic damping in the one-dimensional Vlasov equation. Journal of Physics A: Mathematical and Theoretical, 44(40):405502, 2011. - Cited 1 time: page 116 -
- [BPK12] Tom Bienaimé, Nicola Piovella, and Robin Kaiser. Controlled Dicke Subradiance from a Large Cloud of Two-Level Systems. Physical Review Letters, 108(12):123602, March 2012. - Cited 1 time: page 203 -
- [Bra98] Marco Brambilla. Kinetic theory of plasma waves: homogeneous plasmas. Oxford University Press, 1998. - Cited 1 time: page 95 -
- [BS00] Neil J Balmforth and Roberto Sassi. A shocking display of synchrony. Physica D: Nonlinear Phenomena, 143(1):21–55, September 2000. - Cited 3 times: pages 156, 176 and 198 -
- [BT11] James Binney and Scott Tremaine. Galactic Dynamics: (Second Edition). Princeton University Press, October 2011. - Cited 5 times: pages 60, 77, 113, 130 and 137 -
- [BY15] Julien Barré and Yoshiyuki Y Yamaguchi. On the neighborhood of an inhomogeneous stable stationary solution of the Vlasov equation—Case of an attractive cosine potential. Journal of Mathematical Physics, 56(8):081502, 2015. - Cited 1 time: page 128 -
- [Cas59] K. M Case. Plasma oscillations. Annals of Physics, 7(3):349–364, July 1959. - Cited 3 times: pages 95, 97 and 100 -
- [CD99] John D. Crawford and K. T. R. Davies. Synchronization of globally coupled phase oscillators: singularities and scaling for general couplings. Physica D: Nonlinear Phenomena, 125(1):1–46, January 1999. - Cited 2 times: pages 161 and 198 -
- [CDR09] Alessandro Campa, Thierry Dauxois, and Stefano Ruffo. Statistical mechanics and dynamics of solvable models with long-range interactions. Physics Reports, 480(3–6):57–159, September 2009. - Cited 1 time: page 18 -
- [CGM14] John Cheng, Max Grossman, and Ty McKercher. Professional CUDA C Programming. John Wiley & Sons, September 2014. Google-Books-ID: q3DvBQAAQBAJ. - Cited 1 time: page 49 -
- [CGML08] Alessandro Campa, Andrea Giansanti, Giovanna Morigi, and Francesco Sylos Labini. Dynamics and Thermodynamics of systems with long range interactions: theory and experiments. In Dynamics and Thermodynamics of Systems with Long Range Interactions: Theory and Experiments, volume 970, 2008. - Cited 1 time: page 18 -
- [CH89] John David Crawford and Peter D Hislop. Application of the method of spectral deformation to the Vlasov-poisson system. Annals of Physics, 189(2):265–317, February 1989. - Cited 7 times: pages 22, 87, 89, 95, 97, 101 and 131 -
- [Cha13] Pierre-Henri Chavanis. Initial value problem for the linearized mean field Kramers equation with long-range interactions. The European Physical Journal Plus, 128(9):106, September 2013. - Cited 1 time: page 142 -
-

- [CHB<sup>+</sup>14] R. Chang, A. L. Hoendervanger, Q. Bouton, Y. Fang, T. Klafka, K. Audo, A. Aspect, C. I. Westbrook, and D. Clément. Three-dimensional laser cooling at the Doppler limit. Physical Review A, 90(6):063407, December 2014.  
- Cited 2 times: pages 34 and 37 -
- [Chi13] Hayato Chiba. A proof of the Kuramoto conjecture for a bifurcation structure of the infinite-dimensional Kuramoto model. Ergodic Theory and Dynamical Systems, 35(03):762–834, 2013.  
- Cited 3 times: pages 87, 148 and 160 -
- [CK76] C. Z Cheng and Georg Knorr. The integration of the vlasov equation in configuration space. Journal of Computational Physics, 22(3):330–351, November 1976.  
- Cited 1 time: page 88 -
- [CKKH00] M. Y. Choi, H. J. Kim, D. Kim, and H. Hong. Synchronization in a system of globally coupled oscillators with time delay. Physical Review E, 61(1):371–381, January 2000.  
- Cited 1 time: page 177 -
- [CKL14] A. Camara, R. Kaiser, and G. Labeyrie. Scaling behavior of a very large magneto-optical trap. Physical Review A, 90(6):063404, December 2014.  
- Cited 7 times: pages 27, 28, 36, 38, 41, 48 and 72 -
- [CMM90] Alexandre Joel Chorin, Jerrold E Marsden, and Jerrold E Marsden. A mathematical introduction to fluid mechanics, volume 3. Springer, 1990.  
- Cited 1 time: page 101 -
- [CN11] Hayato Chiba and Isao Nishikawa. Center manifold reduction for large populations of globally coupled phase oscillators. Chaos: An Interdisciplinary Journal of Nonlinear Science, 21(4):043103, October 2011.  
- Cited 4 times: pages 87, 160, 162 and 197 -
- [CP70] R. P. H. Chang and M. Porkolab. Experimental Observation of Nonlinear Landau Damping of Plasma Waves in a Magnetic Field. Physical Review Letters, 25(18):1262–1266, November 1970.  
- Cited 1 time: page 88 -
- [Cra91a] John David Crawford. Amplitude Equations on Unstable Manifolds: singular behavior from neutral modes. In Prof William Greenberg and Dr Jacek Polewczak, editors, Modern Mathematical Methods in Transport Theory, number 51 in Operator Theory: Advances and Applications, pages 97–108. Birkhäuser Basel, 1991. DOI: 10.1007/978-3-0348-5675-1\_9.  
- Cited 1 time: page 78 -
- [Cra91b] John David Crawford. Introduction to bifurcation theory. Reviews of Modern Physics, 63(4):991–1037, October 1991.  
- Cited 2 times: pages 78 and 79 -
- [Cra94a] John David Crawford. Amplitude expansions for instabilities in populations of globally-coupled oscillators. Journal of Statistical Physics, 74(5-6):1047–1084, March 1994.  
- Cited 11 times: pages 22, 89, 92, 105, 106, 148, 170, 211, 220, 222 and 223 -
- [Cra94b] John David Crawford. Universal Trapping Scaling on the Unstable Manifold for a Collisionless Electrostatic Mode. Physical Review Letters, 73(5):656–659, August 1994.  
- Cited 4 times: pages 22, 100, 147 and 160 -

- 
- [Cra95a] John David Crawford. Amplitude equations for electrostatic waves: universal singular behavior in the limit of weak instability. Physics of Plasmas, 2(1):97–128, 1995. - Cited 9 times: pages 22, 92, 100, 116, 147, 148, 156, 174 and 220 -
- [Cra95b] John David Crawford. Scaling and Singularities in the Entrainment of Globally Coupled Oscillators. Physical Review Letters, 74(21):4341–4344, May 1995. - Cited 4 times: pages 22, 148, 161 and 174 -
- [CS87] S. M. Churilov and I. G. Shukhman. Note on weakly nonlinear stability theory of a free mixing layer. Proceedings of the Royal Society of London Series A, 409:351–367, February 1987. - Cited 5 times: pages 138, 147, 154, 198 and 214 -
- [CS95] S. M. Churilov and I. G. Shukhman. Critical layer and nonlinear evolution of disturbances in weakly supercritical shear flows. Oceanographic Literature Review, 31(4):185, 1995. - Cited 3 times: pages 138, 147 and 198 -
- [CS96] S.M. Churilov and I.G. Shukhman. The nonlinear critical layer resulting from the spatial or temporal evolution of weakly unstable disturbances in shear flows. Journal of Fluid Mechanics, 318:189–221, 1996. - Cited 2 times: pages 147 and 198 -
- [CT98] Claude N. Cohen-Tannoudji. Nobel Lecture: Manipulating atoms with photons. Reviews of Modern Physics, 70(3):707–719, July 1998. - Cited 1 time: page 28 -
- [DAC<sup>+</sup>00] Y Dancheva, G Alzetta, S Cartaleva, M Taslakov, and Ch Andreeva. Coherent effects on the Zeeman sublevels of hyperfine states in optical pumping of Rb by monomode diode laser. Optics Communications, 178(1–3):103–110, May 2000. - Cited 1 time: page 37 -
- [Dai92] Hiroaki Daido. Order Function and Macroscopic Mutual Entrainment in Uniformly Coupled Limit-Cycle Oscillators. Progress of Theoretical Physics, 88(6):1213–1218, December 1992. - Cited 3 times: pages 160, 166 and 198 -
- [Dai94] Hiroaki Daido. Generic scaling at the onset of macroscopic mutual entrainment in limit-cycle oscillators with uniform all-to-all coupling. Physical Review Letters, 73(5):760–763, August 1994. - Cited 1 time: page 160 -
- [Dai96] Hiroaki Daido. Onset of cooperative entrainment in limit-cycle oscillators with uniform all-to-all interactions: bifurcation of the order function. Physica D: Nonlinear Phenomena, 91(1):24–66, March 1996. - Cited 1 time: page 160 -
- [Dal88] J. Dalibard. Laser cooling of an optically thick gas: The simplest radiation pressure trap? Optics Communications, 68(3):203–208, October 1988. - Cited 2 times: pages 28 and 35 -
- [Dal14] Jean Dalibard. Une brève histoire des atomes froids, 2014. - Cited 4 times: pages 28, 31, 33 and 34 -
- [DCB13] Florian Dörfler, Michael Chertkov, and Francesco Bullo. Synchronization in complex oscillator networks and smart grids. Proceedings of the National Academy of Sciences, 110(6):2005–2010, February 2013. - Cited 1 time: page 165 -
-

## BIBLIOGRAPHY

---

- [dCN98a] D. del Castillo-Negrete. Nonlinear evolution of perturbations in marginally stable plasmas. Physics Letters A, 241(1):99–104, April 1998. - Cited 3 times: pages 89, 107 and 198 -
- [dCN98b] D. del Castillo-Negrete. Weakly nonlinear dynamics of electrostatic perturbations in marginally stable plasmas. Physics of Plasmas, 5(11):3886–3900, October 1998. - Cited 4 times: pages 89, 107, 148 and 198 -
- [DCT89] J. Dalibard and C. Cohen-Tannoudji. Laser cooling below the Doppler limit by polarization gradients: simple theoretical models. JOSA B, 6(11):2023–2045, November 1989. - Cited 1 time: page 37 -
- [Deg86] Pierre Degond. Spectral Theory of the Linearized Vlasov-Poisson Equation. Transactions of the American Mathematical Society, 294(2):435–453, 1986. - Cited 1 time: page 93 -
- [Den85] J. Denavit. Simulations of the single-mode, bump-on-tail instability. The Physics of fluids, 28(9):2773–2777, 1985. - Cited 1 time: page 88 -
- [Dew73] R. L. Dewar. Saturation of kinetic plasma instabilities by particle trapping. The Physics of Fluids, 16(3):431–435, March 1973. - Cited 1 time: page 88 -
- [DFGV16] Helge Dietert, Bastien Fernandez, and David Gérard-Varet. Landau damping to partially locked states in the Kuramoto model. arXiv:1606.04470 [math-ph, physics:nlin], June 2016. arXiv: 1606.04470. - Cited 1 time: page 199 -
- [Die16a] Helge Dietert. Contributions to mixing and hypocoercivity in kinetic models. Thesis, Cambridge Centre for Analysis (CCA), Centre for Mathematical Sciences, University of Cambridge, July 2016. DOI: 10.17863/CAM.7765. - Cited 1 time: page 98 -
- [Die16b] Helge Dietert. Stability and bifurcation for the Kuramoto model. Journal de Mathématiques Pures et Appliquées, 105(4):451–489, 2016. - Cited 5 times: pages 87, 148, 160, 163 and 197 -
- [DJM<sup>+</sup>09] Gustavo Deco, Viktor Jirsa, A. R. McIntosh, Olaf Sporns, and Rolf Kötter. Key role of coupling, delay, and noise in resting brain fluctuations. Proceedings of the National Academy of Sciences, 106(25):10302–10307, June 2009. - Cited 1 time: page 177 -
- [DLN<sup>+</sup>94] M. Drewsen, Ph Laurent, A. Nadir, G. Santarelli, A. Clairon, Y. Castin, D. Grison, and C. Salomon. Investigation of sub-Doppler cooling effects in a cesium magneto-optical trap. Applied Physics B, 59(3):283–298, September 1994. - Cited 1 time: page 37 -
- [DMF88] C. F. Driscoll, J. H. Malmberg, and K. S. Fine. Observation of transport to thermal equilibrium in pure electron plasmas. Physical Review Letters, 60(13):1290–1293, March 1988. - Cited 1 time: page 39 -
- [DO99] Daniel H. E. Dubin and T. M. O’Neil. Trapped nonneutral plasmas, liquids, and crystals (the thermal equilibrium states). Reviews of Modern Physics, 71(1):87–172, January 1999. - Cited 1 time: page 39 -

- 
- [Dob79] R. L. Dobrushin. Vlasov equations. Functional Analysis and Its Applications, 13(2):115–123, April 1979. - Cited 1 time: page 20 -
- [DRAW02] Thierry Dauxois, Stefano Ruffo, Ennio Arimondo, and Martin Wilkens. Dynamics and Thermodynamics of Systems with Long Range Interactions. Springer Science & Business Media, December 2002. - Cited 1 time: page 18 -
- [Dro16] Alexis Drouot. Pollicott-Ruelle resonances via kinetic Brownian motion. arXiv:1607.03841 [math], July 2016. arXiv: 1607.03841. - Cited 1 time: page 142 -
- [DZ15] Semyon Dyatlov and Maciej Zworski. Stochastic stability of Pollicott–Ruelle resonances. Nonlinearity, 28(10):3511, 2015. - Cited 1 time: page 142 -
- [EE02] Y. Elskens and D. F. Escande. Microscopic Dynamics of Plasmas and Chaos. CRC Press, October 2002. - Cited 1 time: page 18 -
- [Erm91] B. Ermentrout. An adaptive model for synchrony in the firefly *Pteroptyx malaccae*. Journal of Mathematical Biology, 29(6):571–585, June 1991. - Cited 1 time: page 165 -
- [FGRLA02] E. Freire, E. Gamero, A. J. Rodríguez-Luis, and A. Algaba. A note on the triple-zero linear degeneracy: normal forms, dynamical and bifurcation behaviors of an unfolding. International Journal of Bifurcation and Chaos, 12(12):2799–2820, December 2002. - Cited 1 time: page 132 -
- [FGVG16] Bastien Fernandez, David Gérard-Varet, and Giambattista Giacomini. Landau Damping in the Kuramoto Model. Annales Henri Poincaré, 17(7):1793–1823, July 2016. - Cited 2 times: pages 148 and 160 -
- [FNP08] G. Filatrella, A. H. Nielsen, and N. F. Pedersen. Analysis of a power grid using a Kuramoto-like model. The European Physical Journal B, 61(4):485–491, February 2008. - Cited 1 time: page 165 -
- [GA80] J. P. Gordon and A. Ashkin. Motion of atoms in a radiation trap. Physical Review A, 21(5):1606–1617, May 1980. - Cited 1 time: page 34 -
- [Gao13] David Yang Gao. Duality Principles in Nonconvex Systems: Theory, Methods and Applications. Springer Science & Business Media, March 2013. - Cited 2 times: pages 178 and 179 -
- [Gat08] Giovanni Luca Gattobigio. Manipulation of a Large Magneto-Optical Trap: application to Four-Wave Mixing. phdthesis, Università degli studi di Ferrara ; Université Nice Sophia Antipolis, February 2008. - Cited 1 time: page 38 -
- [GCR14] Shamik Gupta, Alessandro Campa, and Stefano Ruffo. Nonequilibrium first-order phase transition in coupled oscillator systems with inertia and noise. Physical Review E, 89(2):022123, February 2014. - Cited 4 times: pages 167, 174, 175 and 194 -
- [GFRL<sup>+</sup>99] E. Gamero, E. Freire, A. J. Rodríguez-Luis, E. Ponce, and A. Algaba. Hypernormal form calculation for triple-zero degeneracies. Bulletin of the Belgian Mathematical Society - Simon Stevin, 6(3):357–368, 1999. - Cited 1 time: page 132 -
-

- [GH88] M. E. Goldstein and Lennart S. Hultgren. Nonlinear spatial evolution of an externally excited instability wave in a free shear layer. Journal of Fluid Mechanics, 197:295–330, December 1988. - Cited 1 time: page 148 -
- [GH13] John Guckenheimer and P. J. Holmes. Nonlinear Oscillations, Dynamical Systems, and Bifurcations of Vector Fields. Springer Science & Business Media, November 2013. - Cited 1 time: page 79 -
- [GPLK10] G. L. Gattobigio, T. Pohl, G. Labeyrie, and R. Kaiser. Scaling laws for large magneto-optical traps. Physica Scripta, 81(2):025301, 2010. - Cited 3 times: pages 28, 36 and 38 -
- [GSW<sup>+</sup>08] A. M. Ghez, S. Salim, N. N. Weinberg, J. R. Lu, T. Do, J. K. Dunn, K. Matthews, M. R. Morris, S. Yelda, E. E. Becklin, T. Kremenek, M. Milosavljevic, and J. Naiman. Measuring Distance and Properties of the Milky Way’s Central Supermassive Black Hole with Stellar Orbits. The Astrophysical Journal, 689(2):1044, 2008. - Cited 1 time: page 131 -
- [GW13] Shangjiang Guo and Jianhong Wu. Bifurcation Theory of Functional Differential Equations. Springer Science & Business Media, July 2013. - Cited 2 times: pages 178 and 182 -
- [Hal63] J. K. Hale. Linear functional-differential equations with constant coefficients. NASA; United States, January 1963. - Cited 2 times: pages 178 and 179 -
- [HC89] P. D. Hislop and J. D. Crawford. Application of spectral deformation to the Vlasov-Poisson system. II. Mathematical results. Journal of mathematical physics, 30(12):2819–2837, 1989. - Cited 3 times: pages 22, 97 and 101 -
- [HCK02] H. Hong, M. Y. Choi, and Beom Jun Kim. Synchronization on small-world networks. Physical Review E, 65(2):026139, January 2002. - Cited 1 time: page 166 -
- [HCPT07] Hyunsuk Hong, Hugues Chaté, Hyunggyu Park, and Lei-Han Tang. Entrainment Transition in Populations of Random Frequency Oscillators. Physical Review Letters, 99(18):184101, October 2007. - Cited 1 time: page 175 -
- [HD23] E Hückel and P Debye. The theory of electrolytes: I. lowering of freezing point and related phenomena. Phys. Z., 24:185–206, 1923. - Cited 1 time: page 42 -
- [HI10] Mariana Haragus and Gérard Iooss. Local Bifurcations, Center Manifolds, and Normal Forms in Infinite-Dimensional Dynamical Systems. Springer Science & Business Media, November 2010. - Cited 2 times: pages 80 and 181 -
- [HK91] Jack K. Hale and Hüseyin Kocak. Dynamics and Bifurcations. Springer Science & Business Media, 1991. - Cited 1 time: page 134 -
- [HKO<sup>+</sup>13] Kenichi Hirosawa, Seiichi Kittaka, Yu Oishi, Fumihiko Kannari, and Takayuki Yanagisawa. Phase locking in a Nd:YVO<sub>4</sub> waveguide laser array using Talbot cavity. Optics Express, 21(21):24952–24961, October 2013. - Cited 1 time: page 149 -
- [HL93] Jack K. Hale and Sjoerd M. Verduyn Lunel. Introduction to Functional Differential Equations. Springer Science & Business Media, 1993. - Cited 2 times: pages 178 and 182 -

- 
- [HM06] Jean-Pierre Hansen and Ian R McDonald. Theory of simple liquids (Third Edition). Elsevier, 2006. *- Cited 1 time: page 52 -*
- [HM13] G. I. Hagstrom and P. J. Morrison. Continuum Hamiltonian Hopf Bifurcation II. arXiv:1308.6161 [math-ph, physics:physics], August 2013. arXiv: 1308.6161. *- Cited 3 times: pages 22, 89 and 136 -*
- [HS75] T. W. Hänsch and A. L. Schawlow. Cooling of gases by laser radiation. Optics Communications, 13(1):68–69, January 1975. *- Cited 1 time: page 30 -*
- [Ich82] Setsuo Ichimaru. Strongly coupled plasmas: high-density classical plasmas and degenerate electron liquids. Reviews of Modern Physics, 54(4):1017–1059, October 1982. *- Cited 1 time: page 39 -*
- [ICT16] ICTP. Conference on Long-Range-Interacting Many Body Systems: from Atomic to Astrophysical Scales, 2016. *- Cited 1 time: page 18 -*
- [Inc] Wolfram Research, Inc. Mathematica, Version 11.2. Champaign, IL, 2017. *- Cited 2 times: pages 128 and 194 -*
- [ISP10] J. A. Izaguirre, C. R. Sweet, and V. S. Pande. Multiscale Dynamics of Macromolecules Using Normal Mode Langevin. Pacific Symposium on Biocomputing. Pacific Symposium on Biocomputing, pages 240–251, 2010. *- Cited 1 time: page 49 -*
- [Izh98] Eugene M. Izhikevich. Phase models with explicit time delays. Physical Review E, 58(1):905–908, July 1998. *- Cited 2 times: pages 166 and 177 -*
- [Jea02] James H Jeans. The stability of a spherical nebula. Philosophical Transactions of the Royal Society of London. Series A, Containing Papers of a Mathematical or Physical Character, 199:1–53, 1902. *- Cited 1 time: page 60 -*
- [JH11] Pierre-Emmanuel Jabin and Maxime Hauray. Particles approximations of Vlasov equations with singular forces : Propagation of chaos. arXiv:1107.3821 [math], July 2011. arXiv: 1107.3821. *- Cited 1 time: page 20 -*
- [JPM<sup>+</sup>13] Peng Ji, Thomas K. DM. Peron, Peter J. Menck, Francisco A. Rodrigues, and Jürgen Kurths. Cluster Explosive Synchronization in Complex Networks. Physical Review Letters, 110(21):218701, May 2013. *- Cited 1 time: page 165 -*
- [JPRK14] Peng Ji, Thomas K. D. M. Peron, Francisco A. Rodrigues, and Jürgen Kurths. Low-dimensional behavior of Kuramoto model with inertia in complex networks. Scientific Reports, 4:srep04783, May 2014. *- Cited 1 time: page 166 -*
- [JR81] Peter A. E. M. Janssen and J. Juul Rasmussen. Limit cycle behavior of the bump-on-tail instability. The Physics of Fluids, 24(2):268–273, 1981. *- Cited 1 time: page 88 -*
- [Kan98] Henry E. Kandrup. Violent Relaxation, Phase Mixing, and Gravitational Landau Damping. The Astrophysical Journal, 500(1):120, 1998. *- Cited 1 time: page 88 -*
- [Kat95] Tosio Kato. Perturbation theory for linear operators, volume 132. Springer Science & Business Media, 1995. *- Cited 1 time: page 93 -*
-

- [KC67] W. R. Klein and B. D. Cook. Unified Approach to Ultrasonic Light Diffraction. IEEE Transactions on Sonics and Ultrasonics, 14(3):123–134, July 1967. - Cited 1 time: page 65 -
- [KHS<sup>+</sup>16] Ole Kock, Wei He, Dariusz Swierad, Lyndsie Smith, Joshua Hughes, Kai Bongs, and Yeshpal Singh. Laser controlled atom source for optical clocks. Scientific Reports, 6:srep37321, November 2016. - Cited 1 time: page 27 -
- [KP13] Maxim Komarov and Arkady Pikovsky. Multiplicity of Singular Synchronous States in the Kuramoto Model of Coupled Oscillators. Physical Review Letters, 111(20):204101, November 2013. - Cited 1 time: page 161 -
- [KP14] M. Komarov and A. Pikovsky. The Kuramoto model of coupled oscillators with a bi-harmonic coupling function. Physica D: Nonlinear Phenomena, 289:18–31, December 2014. - Cited 4 times: pages 161, 167, 174 and 175 -
- [Kub66] R. Kubo. The fluctuation-dissipation theorem. Reports on Progress in Physics, 29(1):255, 1966. - Cited 1 time: page 18 -
- [Kur75] Yoshiki Kuramoto. Self-entrainment of a population of coupled non-linear oscillators. In International Symposium on Mathematical Problems in Theoretical Physics, pages 420–422. Springer, Berlin, Heidelberg, 1975. DOI: 10.1007/BFb0013365. - Cited 5 times: pages 148, 151, 165, 175 and 220 -
- [Kur84] Yoshiki Kuramoto. Cooperative Dynamics of Oscillator Community A Study Based on Lattice of Rings. Progress of Theoretical Physics Supplement, 79:223–240, February 1984. - Cited 1 time: page 151 -
- [Kur15] Y. Kuramoto. Kuramoto talks about the Kuramoto model <https://www.youtube.com/watch?v=lac4txwybog>, 2015. - Cited 1 time: page 149 -
- [Kuz04] Yuri A. Kuznetsov. Elements of Applied Bifurcation Theory. Springer Science & Business Media, April 2004. - Cited 1 time: page 134 -
- [Kuz05] Yu. A. Kuznetsov. Practical computation of normal forms on center manifolds at degenerate bogdanov–takens bifurcations. International Journal of Bifurcation and Chaos, 15(11):3535–3546, November 2005. - Cited 1 time: page 134 -
- [KZH02] István Z. Kiss, Yumei Zhai, and John L. Hudson. Emerging Coherence in a Population of Chemical Oscillators. Science, 296(5573):1676–1678, May 2002. - Cited 1 time: page 149 -
- [Lan46] L Landau. On the vibrations of the electronic plasma. Akad. Nauk SSSR. Zhurnal Eksper. Teoret. Fiz., 16:574–586, 1946. - Cited 2 times: pages 20 and 88 -
- [LB58] A. Lenard and Ira B. Bernstein. Plasma Oscillations with Diffusion in Velocity Space. Physical Review, 112(5):1456–1459, December 1958. - Cited 1 time: page 139 -
- [LB99] D. Lynden-Bell. Negative specific heat in astronomy, physics and chemistry. Physica A: Statistical Mechanics and its Applications, 263(1):293–304, February 1999. - Cited 1 time: page 18 -

- 
- [LC04] Chunguang Li and Guanrong Chen. Synchronization in general complex dynamical networks with coupling delays. Physica A: Statistical Mechanics and its Applications, 343:263–278, November 2004. - Cited 1 time: page 177 -
- [LLP81] Lev Davidovich Landau, EM Lifshitz, and LP Pitaevskij. Course of theoretical physics. vol. 10: Physical kinetics. Oxford, 1981. - Cited 1 time: page 137 -
- [LMK06] G. Labeyrie, F. Michaud, and R. Kaiser. Self-Sustained Oscillations in a Large Magneto-Optical Trap. Physical Review Letters, 96(2):023003, January 2006. - Cited 1 time: page 38 -
- [LMLY14] Keren Li, Shen Ma, Haihong Li, and Junzhong Yang. Transition to synchronization in a Kuramoto model with the first- and second-order interaction terms. Physical Review E, 89(3):032917, March 2014. - Cited 1 time: page 161 -
- [LPR<sup>+</sup>89] P. D. Lett, W. D. Phillips, S. L. Rolston, C. E. Tanner, R. N. Watts, and C. I. Westbrook. Optical molasses. JOSA B, 6(11):2084–2107, November 1989. - Cited 1 time: page 37 -
- [Man97] Giovanni Manfredi. Long-Time Behavior of Nonlinear Landau Damping. Physical Review Letters, 79(15):2815–2818, October 1997. - Cited 1 time: page 88 -
- [MBS<sup>+</sup>09] E. A. Martens, E. Barreto, S. H. Strogatz, E. Ott, P. So, and T. M. Antonsen. Exact results for the Kuramoto model with a bimodal frequency distribution. Physical Review E, 79(2):026204, February 2009. - Cited 3 times: pages 157, 158 and 223 -
- [MDB<sup>+</sup>88] JH Malmberg, CF Driscoll, B Beck, DL Eggleston, J Fajans, K Fine, X-P Huang, AW Hyatt, CW Roberson, and C Fred Driscoll. Experiments with pure electron plasmas. In AIP Conference Proceedings, volume 175, pages 28–74. AIP, 1988. - Cited 1 time: page 39 -
- [MH13] Philip J. Morrison and George I. Hagstrom. Continuum Hamiltonian Hopf Bifurcation I. arXiv:1308.3807 [math-ph, physics:nlin, physics:physics], August 2013. arXiv: 1308.3807. - Cited 3 times: pages 22, 89 and 136 -
- [Mie92] Alexander Mielke. On nonlinear problems of mixed type: A qualitative theory using infinite-dimensional center manifolds. Journal of Dynamics and Differential Equations, 4(3):419–443, July 1992. - Cited 1 time: page 85 -
- [Mil90] Jonathan Miller. Statistical mechanics of Euler equations in two dimensions. Physical Review Letters, 65(17):2137–2140, October 1990. - Cited 1 time: page 18 -
- [Mil02] Stephen C. Milne. Infinite Families of Exact Sums of Squares Formulas, Jacobi Elliptic Functions, Continued Fractions, and Schur Functions. The Ramanujan Journal, 6(1):7–149, March 2002. - Cited 3 times: pages 116, 123 and 208 -
- [MMS09] Seth A. Marvel, Renato E. Mirollo, and Steven H. Strogatz. Identical phase oscillators with global sinusoidal coupling evolve by Möbius group action. Chaos: An Interdisciplinary Journal of Nonlinear Science, 19(4):043104, October 2009. - Cited 1 time: page 158 -
-

- [Mol69] B. R. Mollow. Power Spectrum of Light Scattered by Two-Level Systems. Physical Review, 188(5):1969–1975, December 1969. - Cited 2 times: pages 37 and 72 -
- [Mon16] Pierre Monmarché. Ergodicity and propagation of chaos for mean field kinetic particles. [arXiv:1603.03179 \[math\]](https://arxiv.org/abs/1603.03179), March 2016. arXiv: 1603.03179. - Cited 1 time: page 21 -
- [Mor00] Philip J. Morrison. Hamiltonian description of Vlasov dynamics: Action-angle variables for the continuous spectrum. Transport Theory and Statistical Physics, 29(3-5):397–414, April 2000. - Cited 1 time: page 20 -
- [MS79] VG Minogin and OT Serimaa. Resonant light pressure forces in a strong standing laser wave. Optics Communications, 30(3):373–379, 1979. - Cited 1 time: page 37 -
- [MTFH13] Erik Andreas Martens, Shashi Thutupalli, Antoine Fourrière, and Oskar Halatschek. Chimera states in mechanical oscillator networks. Proceedings of the National Academy of Sciences, 110(26):10563–10567, June 2013. - Cited 1 time: page 149 -
- [Mur06] James Murdock. Normal Forms and Unfoldings for Local Dynamical Systems. Springer Science & Business Media, April 2006. - Cited 2 times: pages 181 and 182 -
- [MV11] Clément Mouhot and Cédric Villani. On Landau damping. Acta Mathematica, 207(1):29–201, September 2011. - Cited 4 times: pages 20, 88, 99 and 160 -
- [MW64] J. H. Malmberg and C. B. Wharton. Collisionless Damping of Electrostatic Plasma Waves. Physical Review Letters, 13(6):184–186, August 1964. - Cited 2 times: pages 88 and 107 -
- [MWGO68] J. H. Malmberg, C. B. Wharton, R. W. Gould, and T. M. O’Neil. Plasma Wave Echo Experiment. Physical Review Letters, 20(3):95–97, January 1968. - Cited 1 time: page 77 -
- [MYMB10] J. J. McFerran, L. Yi, S. Mejri, and S. Bize. Sub-Doppler cooling of fermionic Hg isotopes in a magneto-optical trap. Optics Letters, 35(18):3078–3080, September 2010. - Cited 3 times: pages 34, 37 and 38 -
- [NBS99] C. S. Ng, A. Bhattacharjee, and F. Skiff. Kinetic Eigenmodes and Discrete Spectrum of Plasma Oscillations in a Weakly Collisional Plasma. Physical Review Letters, 83(10):1974–1977, September 1999. - Cited 1 time: page 139 -
- [NBS04] C. S. Ng, A. Bhattacharjee, and F. Skiff. Complete Spectrum of Kinetic Eigenmodes for Plasma Oscillations in a Weakly Collisional Plasma. Physical Review Letters, 92(6):065002, February 2004. - Cited 2 times: pages 141 and 143 -
- [NRV<sup>+</sup>00] Z. Nédá, E. Ravasz, T. Vicsek, Y. Brechet, and A. L. Barabási. Physics of the rhythmic applause. Physical Review E, 61(6):6987–6992, June 2000. - Cited 1 time: page 149 -
- [NUS13] Anders Nordenfelt, Javier Used, and Miguel A. F. Sanjuán. Bursting frequency versus phase synchronization in time-delayed neuron networks. Physical Review E, 87(5):052903, May 2013. - Cited 1 time: page 177 -

- [NW80] H Neunzert and J Wick. The convergence of simulation methods in plasma physics. Mathematical methods of plasmaphysics (Oberwolfach, 1979), 20:271–286, 1980. - Cited 1 time: page 20 -
- [OA08] Edward Ott and Thomas M. Antonsen. Low dimensional behavior of large systems of globally coupled oscillators. Chaos: An Interdisciplinary Journal of Nonlinear Science, 18(3):037113, September 2008. - Cited 5 times: pages 149, 156, 157, 181 and 197 -
- [OA09] Edward Ott and Thomas M. Antonsen. Long time evolution of phase oscillator systems. Chaos: An Interdisciplinary Journal of Nonlinear Science, 19(2):023117, May 2009. - Cited 1 time: page 158 -
- [ODL<sup>+</sup>14] F.W. Olver, Olde Daalhuis, D.W. Lozier, B.I. Schneider, R.F. Boisvert, C.W. Clark, B.R. Miller, and B.V. Saunders. NIST Digital Library of Mathematical Functions <http://dlmf.nist.gov/8.2#E1>, January 2014. - Cited 1 time: page 141 -
- [Oga13] Shun Ogawa. Spectral and formal stability criteria of spatially inhomogeneous stationary solutions to the Vlasov equation for the Hamiltonian mean-field model. Physical Review E, 87(6):062107, June 2013. - Cited 4 times: pages 94, 120, 122 and 207 -
- [OHA11] Edward Ott, Brian R. Hunt, and Thomas M. Antonsen. Comment on “Long time evolution of phase oscillator systems” [Chaos 19, 023117 (2009)]. Chaos: An Interdisciplinary Journal of Nonlinear Science, 21(2):025112, June 2011. - Cited 1 time: page 158 -
- [OM15] Henrique M. Oliveira and Luís V. Melo. Huygens synchronization of two clocks. Scientific Reports, 5:11548, July 2015. - Cited 1 time: page 150 -
- [ONBT14] Simona Olmi, Adrian Navas, Stefano Boccaletti, and Alessandro Torcini. Hysteretic transitions in the Kuramoto model with inertia. Physical Review E, 90(4):042905, October 2014. - Cited 3 times: pages 165, 166 and 175 -
- [OW12] Oleh E. Omel’chenko and Matthias Wolfrum. Nonuniversal Transitions to Synchrony in the Sakaguchi-Kuramoto Model. Physical Review Letters, 109(16):164101, October 2012. - Cited 2 times: pages 174 and 175 -
- [OWM71] T. M. O’Neil, J. H. Winfrey, and J. H. Malmberg. Nonlinear Interaction of a Small Cold Beam and a Plasma. The Physics of Fluids, 14(6):1204–1212, June 1971. - Cited 2 times: pages 88 and 107 -
- [Pal94] P. L. Palmer. Stability of Collisionless Stellar Systems: Mechanisms for the Dynamical Structure of Galaxies, volume 185 of Astrophysics and Space Science Library. Springer Science & Business Media, 1994. - Cited 1 time: page 130 -
- [Par02] R. B. Paris. A uniform asymptotic expansion for the incomplete gamma function. Journal of Computational and Applied Mathematics, 148(2):323–339, November 2002. - Cited 1 time: page 217 -
- [PCMM15] Francesco Pegoraro, Francesco Califano, Giovanni Manfredi, and Philip J. Morrison. Theory and applications of the Vlasov equation. The European Physical Journal D, 69(3):68, March 2015. - Cited 1 time: page 88 -

## BIBLIOGRAPHY

---

- [Per06] Jérôme Perez. Gravity, dimension, equilibrium, and thermodynamics. Comptes Rendus Physique, 7(3):406–413, April 2006. - Cited 1 time: page 18 -
- [PPA90] P. L. Palmer, J. Papaloizou, and A. J. Allen. Neighbouring equilibria to radially anisotropic spheres: possible end-states for violently relaxed stellar systems. Monthly Notices of the Royal Astronomical Society, 246(3):415–432, 1990. - Cited 2 times: pages 130 and 131 -
- [PQ02] R. L. Pego and J. R. Quintero. A Host of Traveling Waves in a Model of Three-Dimensional Water-Wave Dynamics. Journal of Nonlinear Science, 12(1):59–83, April 2002. - Cited 1 time: page 85 -
- [PR08] Arkady Pikovsky and Michael Rosenblum. Partially Integrable Dynamics of Hierarchical Populations of Coupled Oscillators. Physical Review Letters, 101(26):264103, December 2008. - Cited 1 time: page 158 -
- [PRK01] Arkady Pikovsky, Michael Rosenblum, and Jürgen Kurths. Synchronization: A Universal Concept in Nonlinear Sciences. Cambridge University Press, 2001. - Cited 1 time: page 150 -
- [Pru12] Laurence Pruvost. Coulomb-like force induced by radiation trapping in a cold atom cloud. In AIP Conference Proceedings, volume 1421, pages 80–92. AIP, 2012. - Cited 1 time: page 38 -
- [PSDJ00] Laurence Pruvost, Isabelle Serre, Hong Tuan Duong, and Joshua Jortner. Expansion and cooling of a bright rubidium three-dimensional optical molasses. Physical Review A, 61(5):053408, 2000. - Cited 1 time: page 38 -
- [PTA<sup>+</sup>01] Pat Dallard, Tony Fitzpatrick, Anthony Flint, Angus Low, Roger Ridsdill Smith, Michael Willford, and Mark Roche. London Millennium Bridge: Pedestrian-Induced Lateral Vibration. Journal of Bridge Engineering, 6(6):412–417, December 2001. - Cited 1 time: page 149 -
- [RF13] Tarcísio M. Rocha Filho. Solving the Vlasov equation for one-dimensional models with long range interactions on a GPU. Computer Physics Communications, 184(1):34–39, January 2013. - Cited 2 times: pages 127 and 194 -
- [RHV11] R. Romain, D. Hennequin, and P. Verkerk. Phase-space description of the magneto-optical trap. The European Physical Journal D, 61(1):171–180, January 2011. - Cited 2 times: pages 37 and 40 -
- [Ris89] Hannes Risken. The Fokker-Planck equation. Springer Series in Synergetics, 18, 1989. - Cited 1 time: page 139 -
- [RPC<sup>+</sup>87] E. L. Raab, M. Prentiss, Alex Cable, Steven Chu, and D. E. Pritchard. Trapping of Neutral Sodium Atoms with Radiation Pressure. Physical Review Letters, 59(23):2631–2634, December 1987. - Cited 4 times: pages 31, 38, 44 and 73 -
- [RS80] Michael Reed and Barry Simon. Methods of modern mathematical physics. vol. 1. Functional analysis. Academic, 1980. - Cited 1 time: page 85 -

- 
- [RS91] R. Robert and J. Sommeria. Statistical equilibrium states for two-dimensional flows. Journal of Fluid Mechanics, 229:291–310, August 1991. - Cited 1 time: page 18 -
- [RSB<sup>+</sup>14] Mohamed-Taha Rouabah, Marina Samoylova, Romain Bachelard, Philippe W. Courteille, Robin Kaiser, and Nicola Piovella. Coherence effects in scattering order expansion of light by atomic clouds. JOSA A, 31(5):1031–1039, May 2014. - Cited 1 time: page 203 -
- [RTBPL14] Ana C. Ribeiro-Teixeira, Fernanda P. C. Benetti, Renato Pakter, and Yan Levin. Ergodicity breaking and quasistationary states in systems with long-range interactions. Physical Review E, 89(2):022130, February 2014. - Cited 1 time: page 18 -
- [Sak88] Hidetsugu Sakaguchi. Cooperative Phenomena in Coupled Oscillator Systems under External Fields. Progress of Theoretical Physics, 79(1):39–46, January 1988. - Cited 1 time: page 166 -
- [SCF92] A. M. Steane, M. Chowdhury, and C. J. Foot. Radiation force in the magneto-optical trap. JOSA B, 9(12):2142–2158, December 1992. - Cited 1 time: page 37 -
- [SF91] A. M. Steane and C. J. Foot. Laser Cooling below the Doppler Limit in a Magneto-Optical Trap. EPL (Europhysics Letters), 14(3):231, 1991. - Cited 1 time: page 38 -
- [SJM15] Stefan Schütz, Simon B. Jäger, and Giovanna Morigi. Thermodynamics and dynamics of atomic self-organization in an optical cavity. Physical Review A, 92(6):063808, December 2015. - Cited 2 times: pages 18 and 92 -
- [SM91] Steven H. Strogatz and Renato E. Mirollo. Stability of incoherence in a population of coupled oscillators. Journal of Statistical Physics, 63(3-4):613–635, May 1991. - Cited 2 times: pages 153 and 154 -
- [SM97] D. W. L. Sprung and J. Martorell. The symmetrized Fermi function and its transforms. Journal of Physics A: Mathematical and General, 30(18):6525, 1997. - Cited 1 time: page 206 -
- [SOG<sup>+</sup>02] R. Schödel, T. Ott, R. Genzel, R. Hofmann, M. Lehnert, A. Eckart, N. Mouawad, T. Alexander, M. J. Reid, R. Lenzen, M. Hartung, F. Lacombe, D. Rouan, E. Gendron, G. Rousset, A.-M. Lagrange, W. Brandner, N. Ageorges, C. Lidman, A. F. M. Moorwood, J. Spyromilio, N. Hubin, and K. M. Menten. A star in a 15.2-year orbit around the supermassive black hole at the centre of the Milky Way. Nature, 419(6908):694–696, October 2002. - Cited 1 time: page 131 -
- [Spr05] Volker Springel. The cosmological simulation code gadget-2. Monthly Notices of the Royal Astronomical Society, 364(4):1105–1134, December 2005. - Cited 1 time: page 49 -
- [SR76] Albert Simon and Marshall N. Rosenbluth. Single-mode saturation of the bump-on-tail instability: Immobile ions. The Physics of Fluids, 19(10):1567–1580, October 1976. - Cited 1 time: page 88 -
-

- [SR00] L. Saint-Raymond. The gyrokinetic approximation for the vlasov–poisson system. Mathematical Models and Methods in Applied Sciences, 10(09):1305–1332, December 2000. - Cited 1 time: page 21 -
- [SRS88] Albert Simon, Shelden Radin, and Robert W. Short. Long-time simulation of the single-mode bump-on-tail instability. The Physics of Fluids, 31(12):3649–3659, December 1988. - Cited 1 time: page 88 -
- [SS02] R. W. Short and A. Simon. Damping of perturbations in weakly collisional plasmas. Physics of Plasmas, 9(8):3245–3253, July 2002. - Cited 4 times: pages 137, 138, 139 and 141 -
- [SSK87] Hidetsugu Sakaguchi, Shigeru Shinomoto, and Yoshiki Kuramoto. Local and Grobal Self-Entrainments in Oscillator Lattices. Progress of Theoretical Physics, 77(5):1005–1010, May 1987. - Cited 1 time: page 166 -
- [SSK88] Hidetsugu Sakaguchi, Shigeru Shinomoto, and Yoshiki Kuramoto. Mutual Entrainment in Oscillator Lattices with Nonvariational Type Interaction. Progress of Theoretical Physics, 79(5):1069–1079, May 1988. - Cited 2 times: pages 166 and 167 -
- [ST15] Maximilian Sadilek and Stefan Thurner. Physiologically motivated multiplex Kuramoto model describes phase diagram of cortical activity. Scientific Reports, 5:srep10015, May 2015. - Cited 1 time: page 177 -
- [ST16] S. Sridhar and Jihad R. Touma. Stellar Dynamics around a Massive Black Hole I: Secular Collisionless Theory. Monthly Notices of the Royal Astronomical Society, 458(4):4129–4142, June 2016. arXiv: 1509.02397. - Cited 1 time: page 131 -
- [Ste96] George Serman. Partons, Factorization and Resummation, TASI95. arXiv:hep-ph/9606312, June 1996. arXiv: hep-ph/9606312. - Cited 1 time: page 106 -
- [Ste01] Daniel A Steck. Rubidium 87 D line data, 2001. - Cited 4 times: pages 28, 34, 37 and 45 -
- [Str00] Steven H. Strogatz. From Kuramoto to Crawford: exploring the onset of synchronization in populations of coupled oscillators. Physica D: Nonlinear Phenomena, 143(1):1–20, September 2000. - Cited 1 time: page 154 -
- [SVH<sup>+</sup>04] Bernard Smith, John Vasut, T Hyde, L Matthews, Jerry Reay, Mike Cook, and Jimmy Schmoke. Dusty plasma correlation function experiment. Advances in Space Research, 34(11):2379–2383, 2004. - Cited 1 time: page 48 -
- [SW51] R. S Spencer and R. M Wiley. The mixing of very viscous liquids. Journal of Colloid Science, 6(2):133–145, April 1951. - Cited 1 time: page 85 -
- [Szn91] Alain-Sol Sznitman. Topics in propagation of chaos. In Ecole d’Eté de Probabilités de Saint-Flour XIX — 1989, pages 165–251. Springer, Berlin, Heidelberg, 1991. DOI: 10.1007/BFb0085169. - Cited 1 time: page 21 -
- [Tak74] Floris Takens. Singularities of vector fields. Publications Mathématiques de l’IHÉS, 43:47–100, 1974. - Cited 1 time: page 134 -

- 
- [TDM87] S. I. Tsunoda, F. Doveil, and J. H. Malmberg. Nonlinear Interaction between a Warm Electron Beam and a Single Wave. Physical Review Letters, 59(24):2752–2755, December 1987. - Cited 1 time: page 88 -
- [TLB99] M. N. Tamashiro, Yan Levin, and Marcia C. Barbosa. The one-component plasma: a conceptual approach. Physica A: Statistical Mechanics and its Applications, 268(1–2):24–49, June 1999. - Cited 1 time: page 39 -
- [TLO97a] Hisa-Aki Tanaka, Allan J. Lichtenberg, and Shin’ichi Oishi. First Order Phase Transition Resulting from Finite Inertia in Coupled Oscillator Systems. Physical Review Letters, 78(11):2104–2107, March 1997. - Cited 6 times: pages 165, 166, 167, 175, 220 and 221 -
- [TLO97b] Hisa-Aki Tanaka, Allan J. Lichtenberg, and Shin’ichi Oishi. Self-synchronization of coupled oscillators with hysteretic responses. Physica D: Nonlinear Phenomena, 100(3):279–300, February 1997. - Cited 2 times: pages 165 and 220 -
- [TMK10] H. Terças, J. T. Mendonça, and R. Kaiser. Driven collective instabilities in magneto-optical traps: A fluid-dynamical approach. EPL (Europhysics Letters), 89(5):53001, 2010. - Cited 1 time: page 38 -
- [Tro86] M. Trocheris. On the derivation of the one dimensional Vlasov equation. Transport Theory and Statistical Physics, 15(5):597–628, August 1986. - Cited 1 time: page 20 -
- [TSS05] B. R. Trees, V. Saranathan, and D. Stroud. Synchronization in disordered Josephson junction arrays: Small-world connections and the Kuramoto model. Physical Review E, 71(1):016215, January 2005. - Cited 1 time: page 165 -
- [TZT<sup>+</sup>12] Amirkhan A. Temirbayev, Zeinulla Zh. Zhanabaev, Stanislav B. Tarasov, Vladimir I. Ponomarenko, and Michael Rosenblum. Experiments on oscillator ensembles with global nonlinear coupling. Physical Review E, 85(1):015204, January 2012. - Cited 1 time: page 149 -
- [Van89] A. Vanderbauwhede. Centre Manifolds, Normal Forms and Elementary Bifurcations. In Dynamics Reported, Dynamics Reported, pages 89–169. Vieweg+Teubner Verlag, Wiesbaden, 1989. DOI: 10.1007/978-3-322-96657-5\_4. - Cited 1 time: page 87 -
- [VDMvdM85] Jan-Cees Van Der Meer and Jan-Cees van der Meer. The hamiltonian Hopf bifurcation. Springer, 1985. - Cited 1 time: page 101 -
- [VI92] A. Vanderbauwhede and G. Iooss. Center Manifold Theory in Infinite Dimensions. In Dynamics Reported, Dynamics Reported, pages 125–163. Springer, Berlin, Heidelberg, 1992. DOI: 10.1007/978-3-642-61243-5\_4. - Cited 1 time: page 87 -
- [Vil10] C. Villani. Landau damping, Notes for a course given in Cotonou, Benin, and in CIRM, Luminy, 2010. - Cited 3 times: pages 85, 88 and 160 -
-

## BIBLIOGRAPHY

---

- [VK55] N. G. Van Kampen. On the theory of stationary waves in plasmas. Physica, 21(6):949–963, January 1955. - Cited 2 times: pages 95 and 100 -
- [Vla68] A. A. Vlasov. The Vibrational Properties of an Electron Gas. Soviet Physics Uspekhi, 10(6):721, 1968. - Cited 1 time: page 88 -
- [Wal69] T J Walker. Acoustic synchrony: two mechanisms in the snowy tree cricket. Science, 166(3907):891–894, 1969. - Cited 1 time: page 149 -
- [WCS96] Kurt Wiesenfeld, Pere Colet, and Steven H. Strogatz. Synchronization Transitions in a Disordered Josephson Series Array. Physical Review Letters, 76(3):404–407, January 1996. - Cited 1 time: page 165 -
- [WD75] D Wineland and Hans Dehmelt. Proposed  $10^{14} \Delta \nu / \nu$  laser fluorescence spectroscopy on  $\text{Ti}^+$  mono-ion oscillator III. In Bulletin of the American Physical Society, volume 20, pages 637–637. Amer Inst Physics Circulation Fulfillment, 1975. - Cited 1 time: page 30 -
- [Win67] Arthur T. Winfree. Biological rhythms and the behavior of populations of coupled oscillators. Journal of Theoretical Biology, 16(1):15–42, July 1967. - Cited 1 time: page 150 -
- [Win80] Arthur T. Winfree. The Geometry of Biological Time. Springer, New York, 1980. - Cited 1 time: page 150 -
- [WS93] Shinya Watanabe and Steven H. Strogatz. Integrability of a globally coupled oscillator array. Physical Review Letters, 70(16):2391–2394, April 1993. - Cited 1 time: page 158 -
- [WSW90] Thad Walker, David Sesko, and Carl Wieman. Collective behavior of optically trapped neutral atoms. Physical Review Letters, 64(4):408–411, January 1990. - Cited 4 times: pages 28, 36, 57 and 59 -
- [WW96] E. T. Whittaker and G. N. Watson. A Course of Modern Analysis. Cambridge University Press, September 1996. Google-Books-ID: ULVdGZmi9VcC. - Cited 1 time: page 208 -
- [XVF<sup>+</sup>15] G. Xu, D. Vocke, D. Faccio, J. Garnier, T. Roger, S. Trillo, and A. Picozzi. From coherent shocklets to giant collective incoherent shock waves in nonlocal turbulent flows. Nature Communications, 6:ncomms9131, September 2015. - Cited 1 time: page 18 -
- [XVS08] D. Xenides, D. S. Vlachos, and T. E. Simos. Synchronization in complex systems following a decision based queuing process: rhythmic applause as a test case. Journal of Statistical Mechanics: Theory and Experiment, 2008(07):P07017, 2008. - Cited 1 time: page 149 -
- [YS99] M. K. Stephen Yeung and Steven H. Strogatz. Time Delay in the Kuramoto Model of Coupled Oscillators. Physical Review Letters, 82(3):648–651, January 1999. - Cited 6 times: pages 166, 177, 181, 187, 188 and 198 -

- [ZGS01] Tie Zhou, Yan Guo, and Chi-Wang Shu. Numerical study on Landau damping. Physica D: Nonlinear Phenomena, 157(4):322–333, October 2001. *- Cited 1 time: page 88 -*
- [Zwo15] Maciej Zworski. Scattering resonances as viscosity limits. arXiv:1505.00721 [math-ph], May 2015. arXiv: 1505.00721. *- Cited 1 time: page 142 -*



# RÉSUMÉ

---

Les systèmes en interaction à longue portée sont connus pour avoir des propriétés statistiques et dynamiques particulières. Pour décrire leur évolution dynamique, on utilise des équations cinétiques décrivant leur densité dans l'espace des phases. Ce manuscrit est divisé en deux parties indépendantes. La première traite de notre collaboration avec une équipe expérimentale sur un Piège Magnéto-Optique. Ce dispositif à grand nombre d'atomes présente des interactions coulombiennes effectives provenant de la rediffusion des photons. Nous avons proposé des tests expérimentaux pour mettre en évidence l'analogie d'une longueur de Debye, et son influence sur la réponse du système. Les expériences réalisées ne permettent pour l'instant pas de conclure de façon définitive. Dans la deuxième partie, nous avons analysé les modèles cinétiques de Vlasov et de Kuramoto. Pour étudier leur dynamique de dimension infinie, nous avons examiné les bifurcations autour des états stationnaires instables, l'objectif étant d'obtenir des équations réduites décrivant la dynamique de ces états. Nous avons réalisé des développements en variété instable sur cinq systèmes différents. Ces réductions sont parsemées de singularités, mais prédisent correctement la nature de la bifurcation, que nous avons testée numériquement. Nous avons conjecturé une réduction exacte (obtenue via la forme normale Triple Zero) autour des états inhomogènes de l'équation de Vlasov. Ces résultats génériques pourraient être pertinents dans un contexte astrophysique. Les autres résultats s'appliquent aux phénomènes de synchronisation du modèle de Kuramoto pour les oscillateurs avec inertie et/ou interactions retardées.

**Mots-clés :** Dynamique, Réduction Dimensionnelle, Non Linéaire, Hors d'Équilibre, Interactions à Longue Portée, Équation Cinétique Sans Collisions, Vlasov, Fokker-Planck, Triple Zero, Oscillateurs Couplés, Synchronisation, Kuramoto, Piège Magnéto-Optique, Atomes Froids, Longueur de Debye

## ABSTRACT

---

Long-range interacting systems are known to display particular statistical and dynamical properties. To describe their dynamical evolution, we can use kinetic equations describing their density in the phase space. This PhD thesis is divided into two distinct parts. The first part concerns our collaboration with an experimental team on a Magneto-Optical Trap. The physics of this widely-used device, operating with a large number of atoms, is supposed to display effective Coulomb interactions coming from photon rescattering. We have proposed experimental tests to highlight the analog of a Debye length, and its influence on the system response. The experimental realizations do not allow yet a definitive conclusion. In the second part, we analyzed the Vlasov and Kuramoto kinetic models. To study their infinite dimensional dynamics, we looked at bifurcations around unstable steady states. The goal was to obtain reduced equations describing the dynamical evolution. We performed unstable manifold expansions on five different kinetic systems. These reductions are in general not exact and plagued by singularities, yet they predict correctly the nature and scaling of the bifurcation, which we tested numerically. We conjectured an exact dimensional reduction (obtained using the Triple Zero normal form) around the inhomogeneous states of the Vlasov equation. These results are expected to be very generic and could be relevant in an astrophysical context. Other results apply to synchronization phenomena through the Kuramoto model for oscillators with inertia and/or delayed interactions.

**Keywords:** Dynamics, Dimensional Reduction, Nonlinear, Out-of-Equilibrium, Long-Range Interactions, Collisionless Kinetics Equations, Vlasov, Fokker-Planck, Triple Zero, Coupled Oscillators, Synchronization, Kuramoto, Magneto-Optical Trap, Cold Atoms, Debye Length